# PROTEIN ARGININE METHYLTRANSFERASE 5 (PRMT5) IS AN ESSENTIAL REGULATOR OF THE CELLULAR RESPONSE TO IONIZING RADIATION AND A THERAPEUTIC TARGET TO ENHANCE RADIATION THERAPY FOR PROSTATE CANCER TREATMENT

by

**Jake L. Owens**

**A Dissertation**

*Submitted to the Faculty of Purdue University*

*In Partial Fulfillment of the Requirements for the degree of*

**Doctor of Philosophy**


Department of Medicinal Chemistry and Molecular Pharmacology

West Lafayette, Indiana

August 2020

# THE PURDUE UNIVERSITY GRADUATE SCHOOL
# STATEMENT OF COMMITTEE APPROVAL

**Dr. Chang-Deng Hu, Chair**

Department of Medicinal Chemistry and Molecular Pharmacology

**Dr. Emily C. Dykhuizen**

Department of Medicinal Chemistry and Molecular Pharmacology

**Dr. Ourania M. Andrisani**

Department of Basic Medical Sciences

**Dr. Vincent Jo Davisson**

Department of Medicinal Chemistry and Molecular Pharmacology

**Approved by:**

Dr. Andy Hudmon

*To my Mom (Gail), Dad (Steve), sister (Emily), and brother (Zack)*
*for their unconditional love and support*

# ACKNOWLEDGEMENTS

Professional acknowledgements:

Studies in this dissertation were partially supported by grants from U.S. Army Medical Research Acquisition Activity, Prostate Cancer Research Program (PC11190, PC120512, PC150697) and NCI RO1CA212403, and Purdue University Center for Cancer Research Small Grants. Primary RNA-seq analysis and TCGA data analysis were performed by the Collaborative Core for Cancer Bioinformatics ($C^3B$) shared by Indiana University Simon Cancer Center (P30CA082709) and Purdue University Center for Cancer Research (P30CA023168) with support from the Walther Cancer Foundation. DNA sequencing was conducted by the Genomic Core Facility supported by NCI CCSG CA23168 to Purdue University Center for Cancer Research. We would like to thank Indiana University Precision Health Initiative.

Most of my thesis research was from when I was a recipient of the Indiana Clinical and Translational Sciences Institute (CTSI) Pre-Doctoral Fellowship, which was made possible with partial support from Grant Numbers TL1 TR001107, TL1 TR002531, UL1 TR001108, and UL1 TR002529 (A. Shekhar, PI) from the National Institutes of Health, National Center for Advancing Translational Sciences, Clinical and Translational Sciences Award. I would also like to thank Dr. Liang Cheng and Dr. Jeannie Poulson Plantenga for mentoring me as part of the CTSI Fellowship. I was also a recipient of the Ross Award Graduate Student fellowship and Bilsland Dissertation Fellowship provided by Purdue University.

Personal acknowledgements

My years at Purdue University for my thesis study were the most difficult years of my life. I couldn't have completed my dissertation and got my Ph.D. without the help of the diverse community of colleagues, labmates, professors, teammates, friends, family, and even my pets.

I would first like to thank the Hu lab. I extend my gratitude to my PI, Dr. Chang-Deng Hu, for always seeing my potential and believing that I have what it takes to be a great scientist. I want to thank Xuehong, our lab manager, and all the members of the Hu lab. Special thanks to the Hu lab graduate students Elena Wild (Beketova), Andrew Asberry, and Samantha Tinsley for their intellectual contribution and aid throughout my thesis study. I am grateful for the genuine, life-long friendships we have formed, and I am excited to continue collaborating in the future. I would

also like to recognize Dr. Jun Wan for the incredible job he and his team do collaborating with our lab on bioinformatics projects. Our research could not have the same clinical impact without you. Additionally, a special thank you to my dissertation committee, Dr. Emily C. Dykhuizen, Dr. Ourania M. Andrisani, and Dr. Vincent Jo Davisson for the productive scientific discussions and the support in my career pursuits.

I would like to thank my professors from Monmouth College who laid the foundation for my success at Purdue University. Each professor played an essential role in my development. I would like to recognize Dr. Crystal Walline specifically. Dr. Walline got her Ph.D. from Purdue University in the PULSe program and did her thesis study in an MCMP lab. Although she arrived at Monmouth College during my senior year, she was the most influential professor I had. For example, she gave me the opportunity to teach one of her cell biology lectures as preparation for teaching as a graduate student. I really appreciate her mentorship and how she would challenge me above and beyond to prepare me for my Ph.D. study.

A special thanks to all of my soccer friends. Soccer has always been one of my biggest passions. I played soccer since I can remember and even played for my undergraduate college. I did not play soccer during the beginning of my thesis study (2014-2017) and something felt missing from my life. Then an old friend, Jeremy, moved to Purdue in the summer of 2017 and we found a soccer league to play in. Since then, I played for the Old Lions soccer team and they became a family to me. I also had the privilege of playing for two other teams in the local Hispanic league (La liga de fútbol Lafayette/Lafayette fútbol la gran familia). I would like to thank Nain for introducing me this league and recruiting me to play for Parra FC. I would also like to thank Jose for recruiting me for his team Gaskin FC (my current team). I really appreciate how welcoming and friendly everyone in the league is. Playing soccer was critical for keeping me happy, healthy, and sane. No matter how stressful things in the lab were, I could always look forward to soccer with my friends every week.

I would like to thank the new friends I have met at Purdue (the Lab Savages crew). It is truly a blessing to have this tight-knit group during my thesis study. Thanks so much for the help with many tasks such as prelim, posters, presentations, publications, fellowship applications, job search, job applications, interviews, and thesis. I also really appreciate those trips to Lavazza to get coffee, lunches at PMU, hangouts, movie nights, game nights, study dates, captain crunches, and so on. My life wouldn’t be the same without your friendship. When looking back at my thesis

study, I can guarantee I will remember the times spent with you all more than the hours on the bench (Although I will never forget preparing samples to run over 10,000 qPCR reactions). I would also like to thank my best friends from high school (the Naperville crew). I am so glad we routinely keep in touch and can still hang out years after graduating from Neuqua Valley High School. Thanks for always being encouraging and supportive to me even during the most difficult times.

Big thanks to Kole for the love and support during my final two years of thesis study, even when 9,000 miles away! It amazes me how you remain calm when life is so uncertain. You have helped me tremendously, especially when writing my dissertation, and will continue to help me with the transition from thesis study to beginning my career.

Last but not least, I would like to give my biggest thank you to my family including my two cats: Sgt Pepper (Sarge) and Cayenne Pepper (Cai Cai). I could honestly write a whole thesis about how influential my family has been (and will be) on my life. My family supported my faith in God and allowed me to grow into the person I am today. My parents were also a huge influence on my love for science. Interestingly enough, my parents always told me that when I grow up, I should either solve the energy crisis or cure cancer. And as it turns out, I ended up doing cancer research for my Ph.D. study. Although I cannot list my entire family, I have to give my biggest thanks to my Mom (Gail Owens), Dad (Steve Owens) and sister (Emily Owens). At the beginning of March 2020, I went to visit their house for a weekend. However, I was stranded there because of the 'stay-at-home' orders for the COVID19 pandemic. I ended up staying there throughout the duration of writing my dissertation and my family was the biggest help to keeping me happy and healthy both physically and mentally.

# TABLE OF CONTENTS

# LIST OF FIGURES

# LIST OF ABBREVIATIONS

***53BP1*:** p53-binding protein

***ACTS*:** Association for Clinical and Translational Science

***aDMA*:** Asymmetric dimethylarginine

***AdoMet/SAM*:** S-adenosylmethionine

***ADT*:** Androgen deprivation therapy

***AKT*:** Protein kinase B (PKB)

***alt-NHEJ*:** Alternative-non-homologous end joining (see also MMEJ)

***APAF1*:** Apoptotic protease-activating factor 1

***AR*:** Androgen receptor

***ASCL1*:** Achaete-Scute Family BHLH Transcription Factor 1

***ASK1*:** Apoptosis signal-regulating kinase 1

***ATAC*:** Assay for Transposase-Accessible Chromatin

***ATCC*:** American Type Culture Collection

***ATF2*:** Activating transcription factor 2

***ATF4*:** Activating transcription factor 4

***ATM*:** Ataxia-telangiectasia mutated serine/threonine kinase

***BAX*:** BCL2 associated X protein, BCL2 associated X, apoptosis regulator

***BCL2*:** B-cell lymphoma 2 apoptosis regulator

***BED*:** Biologically effective dose

***BER*:** Base excision repair

***BiFC*:** Bimolecular fluorescence complementation

***BL21 bacterial cells*:** Competent *E. coli* strain

***BLL3.3*:** PRMT5 inhibitor

| | |
|---|---|
| ***bp*:** | Base pair |
| ***BRCA1*:** | Breast cancer type 1 susceptibility protein |
| ***BRCA2*:** | Breast cancer type 2 susceptibility protein |
| ***C2C12*:** | mouse myoblast cell line |
| ***cAMP***: | Cyclic adenosine monophosphate |
| ***CARM1/PRMT4*:** | Coactivator-associated arginine methyltransferase 1,protein arginine methyltransferase 4 |
| ***cATF2***: | cytoplasmic ATF2 |
| ***CBP-1*:** | CREB-binding protein 1, *C. elegans* ortholog of human p300/CBP |
| ***CCNB2*:** | G2/mitotic-specific cyclin-B2 |
| ***CCNE1*:** | G1/S-specific cyclin-E1 |
| ***CDC20*:** | Cell-division cycle protein 20 |
| ***CDC25C*:** | Cell-division cycle protein 25C, M-phase inducer phosphatase 3 |
| ***CDK1/CDC2*:** | Cyclin-dependent kinase 1, cell division cycle protein 2 homolog |
| ***CDK2*:** | Cyclin-dependent kinase 2, cell division protein kinase 2 |
| ***CDK4*:** | Cyclin-dependent kinase 4, cell division protein kinase 4 |
| ***CDK6*:** | Cyclin-dependent kinase 6, cell division protein kinase 6 |
| ***CDKN2A*:** | Cyclin-dependent kinase inhibitor 2A gene, p16INK4a) and p14arf protein |
| ***CEP-1*:** | *C. elegans* p53-like protein 1, *C. elegans* homologue of human p53 |
| ***CFP*:** | Cerulean florescent protein |
| ***CgA*:** | Chromogranin A |
| ***ChIP*:** | Chromatin immunoprecipitation |
| ***CHIP*:** | C-terminus of Hsc70-interacting protein E3 ubiquitin-protein ligase |
| ***ChIP-qPCR*:** | Chromatin immunoprecipitation quantitative real-time polymerase chain reaction (ChIP-qPCR) |
| ***ChIP-seq*:** | Chromatin immunoprecipitation sequencing |

***Chk1*:** Checkpoint kinase 1

***CHX***: Cycloheximide

***c-Jun*:** AP-1 transcription factor subunit c-Jun

***c-NHEJ***: Canonical-non-homologous end joining

***COPR5/COPRS*:** Coordinator of protein arginine methyltransferase 5 and differentiation stimulator

***CPT***: Camptothecin

***CREB*:** cAMP response element-binding protein transcription factor

***CRPC*:** Castration-resistant prostate cancer

***Cryo-EM*:** Cryo-electron microscopy

***$C_T$ value*:** Threshold cycle (cycle number when fluorescent signal crosses threshold)

***CtIP*:** C-terminal binding protein

***CTSI:*** Clinical and Translational Science Institute

***Cut&Run*:** Cleavage Under Targets and Release Using Nuclease

***DAPI*:** 4,6-diamidino-2-phenylindole

***dCas8*:** Catalytically inactive form of Cas9

***DDR*:** DNA damage response

***DDR*:** DNA damage response

***DEG*:** Differentially expressed genes

***DI*:** Detained-intron

***DISC*:** Death-inducing signaling complex

***DMSO*:** Dimethyl sulfoxide

***DNA*:** Deoxyribonucleic acid

***DNAPKcs/PRKDC*:** A DNA-dependent protein kinase, catalytic subunit

***Dox*:** Doxycycline

***DR4*:** Death receptor 4

| | |
|---|---|
| ***DSB*:** | Double-strand break |
| ***DTT*:** | Dithiothreitol |
| ***DU145 cells*:** | Androgen-insensitive human prostate cancer cells |
| ***E2F*:** | E2 transcription factor family |
| ***E2F1*:** | E2 transcription factor1 |
| ***EDTA*:** | Ethylenediaminetetraacetic acid |
| ***EGFR*:** | Epidermal growth factor receptor |
| ***eIF2α*:** | Eukaryotic Initiation Factor 2α |
| ***eIF4E*:** | Eukaryotic Translation Initiation Factor 4E |
| ***enChIP*:** | Engineered DNA-binding molecule-mediated chromatin immunoprecipitation |
| ***EZH2*:** | Enhancer of zeste homolog 2, enzymatic component of the Polycomb Repressive Complex 2 (PRC2) |
| ***FANCA*:** | Fanconi anaemia, complementation group A gene |
| ***FANCG*:** | Fanconi anaemia, complementation group G gene |
| ***FC*:** | Fold-change |
| ***FDR*:** | False discovery rate |
| ***FEN1*:** | Flap structure-specific endonuclease 1 |
| ***FIR*:** | Fractionated ionizing radiation |
| ***FIR-*:** | Non-irradiated |
| ***FIR+*:** | Irradiated with fractionated ionizing radiation |
| ***FITC*:** | Fluorescein isothiocyanate |
| ***FOXA2*:** | Forkhead Box A2 transcription factor |
| ***GADD45*:** | Growth Arrest and DNA Damage gene |
| ***Gas1*:** | Growth arrest-specific protein 1 |
| ***GATA*:** | GATA-binding factor transcription factor |

| | |
|---|---|
| ***GEO*:** | Gene Expression Omnibus |
| ***Gli1*:** | Glioma-associated oncogene, Zinc finger protein GLI1 |
| ***GO*:** | Gene Ontology |
| ***GRG motif*:** | Glycine-arginine-glycine motif |
| ***gRNA*:** | Guide RNA |
| ***Gy*:** | Gray, unit for ionizing radiation dose |
| ***H&E*:** | Hematoxylin and eosin |
| ***h*:** | Hour |
| ***H2AR3me2s*:** | Symmetrical dimethylation of histone H2AR3 |
| ***H3K9Ac*:** | Acetylated Histone 3 lysine 9 |
| ***H3K9me3*:** | Methylated Histone 3 lysine 9 |
| ***H3R2me2s*:** | Symmetrical dimethylation of histone H3R2 |
| ***H3R8me2s*:** | Symmetrical dimethylation of histone H3R8 |
| ***H4K16Ac*:** | Acetylation of histone H4K16 |
| ***H4R3me2s*:** | Symmetric dimethylation of histones H4R3 |
| ***HCl*:** | Hydrochloric acid |
| ***HEK293T cells*:** | Human embryonic kidney cells that express a mutant version of the SV40 large T antigen |
| ***HeLa cells*:** | Cervical cancer cells |
| ***HR*:** | Homologous recombination |
| ***HRP*:** | Horseradish peroxidase |
| ***Hsl7*:** | Protein arginine N-methyltransferase HSL7, yeast homologue of human PRMT5 |
| ***IBUR*:** | Indiana society of Basic Urological Research |
| ***ICC*:** | Immunocytochemistry |
| ***IgG*:** | Immunoglobulin G |

***IHC*:** Immunohistochemistry

***IKK*:** IκB kinase

***INO80*:** Chromatin-remodeling ATPase INO80

***INSM1*:** Insulinoma-associated protein 1

***IP*:** Immunoprecipitation

***IPA*:** Ingenuity pathway analysis

***IP-MS*:** Immunoprecipitation followed by mass-spectrometry

***IR*:** Ionizing radiation

***IR-*:** Non-irradiated

***IR+*:** Irradiated with a single dose of ionizing radiation

***IRR*:** Isolated IR-resistant

***IVL*:** Involucrin gene

***KEGG*:** Kyoto Encyclopedia of Genes and Genomes

***KIX domain*:** Kinase-inducible domain (KID) interacting domain), CREB binding domain

***KLF4*:** Kruppel Like Factor 4, SP1-like transcription factor

***KO*:** Knockout

***Ku70/XRCC5*:** 70 KDa subunit Of Ku antigen, X-ray repair complementing defective repair in Chinese hamster cells 6

***Ku80/XRCC5*:** 80 KDa subunit Of Ku antigen, X-ray repair complementing defective repair in Chinese hamster cells 5

***LKB1/STK11*:** Liver kinase B1, Serine/threonine kinase 11

***LNCaP cells*:** Androgen-sensitive human prostate cancer cells

***LP-BER*:** Long patch base excision repair pathway

***m*:** Minute

***MCF7 cells*:** Luminal breast adenocarcinoma cells

***MCMP*:** Medicinal Chemistry and Molecular Pharmacology (department at Purdue University)

***Menin/MEN1*:** Multiple endocrine neoplasia type 1

***MEP50/WDR77*:** Methylosome protein 50, WD repeat-containing protein 77

***MG132*:** Proteasome inhibitor

***miRNA/miR*:** microRNA

***MMEJ*:** Microhomology-mediated end joining (see also alt-NHEJ)

***MMM*:** Mono-methylarginine

***MMS*:** Methyl methanesulfonate

***MRI*:** Magnetic resonance imaging

***MRN*:** Mre11, Rad50 and Nbs1 complex

***mRNA*:** Messenger RNA

***MS*:** Mass spectrometry

***MTA*:** 5'-methylthioadenosine

***MTAP*:** S-methyl-5'-thioadenosine phosphorylase

***mTOR*:** Mammalian target of rapamycin, mechanistic target of rapamycin

***MTT (assay)*:** 3-(4,5-dimethylthiazol-2-yl)-2,5-diphenyltetrazolium bromide (assay)

***MUTYH*:** MutY DNA glycosylase

***MYOG*:** Myogenin transcription factor

***N:B ratio*:** Neurite:body ratio

***N:C ratio*:** Nuclear:cytoplasmic ratio

***nATF2*:** Nuclear localized ATF2

***NCAM1*:** Neural cell adhesion molecule

***NE*:** Neuroendocrine

***NED*:** Neuroendocrine differentiation

***NEPC*:** Neuroendocrine prostate cancer

| | |
|---|---|
| ***NER*:** | Nucleotide-excision repair |
| ***NFYA*:** | Nuclear transcription factor Y subunit alpha |
| ***NFYB*:** | Nuclear transcription factor Y subunit beta |
| ***NFYC*:** | Nuclear transcription factor Y subunit gamma |
| ***NF-κB*:** | Nuclear factor kappa-light-chain-enhancer of activated B cells, transcription factor |
| ***NHEJ*:** | Non-homologous end joining |
| ***NHEJ1/XLF*:** | Non-homologous end-joining factor 1, XRCC4-like factor |
| ***NIH 3T3 cells*:** | Mouse embryonic fibroblast cells |
| ***NIH*:** | National Institutes of Health |
| ***NLS*:** | Nuclear localization signal |
| ***NM23*:** | Nonmetastatic 23 |
| ***NRG (mice)*:** | NOD-Rag1$^{null}$, IL2rg$^{null}$, NOD rag gamma mice |
| ***NSE*:** | Neuron-specific enolase |
| ***NTC*:** | Non-template controls |
| ***N-terminal*:** | Amino-terminal (end of a peptide) |
| ***OGG1*:** | 8-Oxoguanine DNA Glycosylase |
| ***p21*:** | Cyclin-dependent kinase inhibitor 1 or CDK-interacting protein 1 |
| ***p300/CBP*:** | CREB-binding protein |
| ***p53*:** | Tumor protein p53 |
| ***PACUC*:** | Purdue Animal Care and Use Committee |
| ***PBS*:** | Phosphate buffered saline |
| ***PC3 cells*:** | Androgen-insensitive human prostate cancer cells |
| ***PCNA*:** | Proliferating cell nuclear antigen |
| ***PCR*:** | Polymerase chain reaction |

***pCREB*:** Phosphorylated CREB

***PDCD4*:** Programmed cell death protein 4

***PI*:** Propidium Iodide

***PI3K*:** Phosphoinositide 3-kinase

***pICln/CLNS1A*:** Methylosome subunit, chloride conductance regulatory protein, chloride nucleotide-sensitive channel 1A

***PMSF*:** Phenylmethylsulfonyl fluoride

***PPI*:** Protein-protein interaction

***PRMT4*:** Protein arginine methyltransferase 4

***PRMT5*:** Protein arginine methyltransferase 5

***PRMT7*:** Protein arginine methyltransferase 7

***PRMTs*:** Protein arginine methyltransferases

***PROTAC*:** Proteolysis targeting chimera

***PSA*:** Prostate-specific androgen

***PTEN*:** Phosphatase and tensin homolog

***PTM*:** Post-translational modification

***PULSe*:** Purdue University Interdisciplinary Life Science Program

***qPCR*:** Quantitative real-time polymerase chain reaction

***RA*:** Resistance acquisition (phase of fractionated ionizing radiation-induced neuroendocrine differentiation)

***RAD51*:** Radiation protein 51, DNA repair protein 51, recombinase 51

***RAD51AP1*:** RAD51 Associated Protein 1

***RAD51D*:** RAD51 paralog D

***RAD52*:** Radiation protein 52, DNA repair protein 52

***RAD9*:** Radiation protein 9, Cell cycle checkpoint control protein 9

***Rb*:** Retinoblastoma protein

***REST*:** RE1-Silencing Transcription factor

***RGG/RG motifs*:** Arginine-glycine-glycine or Arginine-glycine motifs

***RGRER motif*:** Arginine-glycine-arginine-glutamic acid-arginine motif

***RIN*:** RNA integrity number

**RioK1:** Rio serine/threonine-protein kinase

***RIPA (buffer)*:** Radioimmunoprecipitation assay *buffer*

***RNA*:** Ribonucleic acid

***RNA-seq*:** Ribonucleic acid sequencing

***ROI*:** Regions of interest

***RT*:** Radiation therapy, radiotherapy

***RTEL1*:** Regulator of telomere elongation helicase 1

***RT-qPCR*:** Reverse transcriptase quantitative real-time polymerase chain reaction

***RuvBL1*:** RuvB Like AAA ATPase 1, pontin

***RuvBL2*:** RuvB Like AAA ATPase 2

***RWPE-1 cells*:** Immortalized (carrying HPV-18 gene) normal prostate cells

***SBUR*:** Society of Basic Urological Research

***SC*:** Scramble control

***SCR*:** SCARECROW, *Arabidopsis* transcription factor

***sDMA*:** Symmetric dimethylarginine

***SDS-PAGE*:** Sodium dodecyl sulfate (containing) polyacrylamide gel

***sf9 insect cells*:** Competent *Spodoptera frugiperda* pupal ovarian tissue

***SHARPIN*:** SHANK Associated RH Domain Interactor

***SHR*:** SHORTROOT, *Arabidopsis* transcription factor

***SKB1*:** Protein arginine N-methyltransferase SKB1, *Arabidopsis* homologue of human PRMT5

***Sm*:** Sm RNA-binding protein

| | |
|---|---|
| ***SOX2*:** | Sex determining region Y (SRY)-box 2 transcription factor |
| ***SP1*:** | Specificity Protein 1 transcription factor |
| ***SPDEF*:** | SAM pointed domain containing ETS transcription factor |
| ***SRCAP*:** | Snf2 Related CREBBP Activator Protein |
| ***SRRM4*:** | Serine/Arginine Repetitive Matrix 4 |
| ***SSA*:** | Single strand annealing |
| ***SSB*:** | Single strand break |
| ***ST7*:** | Suppressor of tumorigenicity |
| ***SYBR Green*:** | Nucleic acid stain (asymmetrical cyanine dye) used for qPCR |
| ***SYP*:** | Synaptophysin |
| ***TCGA*:** | The Cancer Genome Atlas |
| ***TDP1*:** | Tyrosyl-DNA Phosphodiesterase 1 |
| ***Tip60/KAT5*:** | Tat Interacting Protein 60kDa, histone lysine acetyltransferase 5 |
| ***TMM*:** | Trimmed mean of M value |
| ***TNF*:** | Tumor necrosis factor |
| ***Top1*:** | DNA topoisomerase 1 |
| ***Top1cc*:** | Top1 cleavage complex |
| ***TRAIL*:** | Tumor necrosis factor-related apoptosis-inducing ligand |
| ***TRUS*:** | Transrectal ultrasound |
| ***U2OS cells*:** | Osteosarcoma cells |
| ***U87MG cells*:** | Glioblastoma astrocytoma cells |
| ***UV*:** | Ultraviolet (electromagnetic radiation) |
| ***VHL*:** | Von Hippel-Lindau Tumor Suppressor, E3 Ubiquitin Protein Ligase |
| ***WEE1*:** | WEE1 $G_2$ checkpoint kinase, mitosis inhibitor protein kinase |
| ***wt*:** | Wild-type |

***XRCC4*:** X-ray repair cross-complementing protein 4

***β-Actin*:** Beta-actin, non-muscle cytoskeletal actin

***γH2AX*:** Phosphorylated serine S139 form of histone H2AX

# ABSTRACT

Prostate cancer is one of the most frequently diagnosed cancers and failure to manage localized disease contributes to the majority of deaths. Radiation therapy (RT) is a common treatment for localized prostate cancer and uses ionizing radiation (IR) to damage DNA. Although RT is potentially curative, tumors often recur and progress to terminal disease. The cellular response to RT is multidimensional. For example, cells respond to a single dose of IR by activating the DNA damage response (DDR) to repair the DNA. Targeting proteins involved in the DDR is an effective clinical strategy to sensitize cancer cells to RT. However, multiple radiation treatments, as in fractionated ionizing radiation (FIR), can promote neuroendocrine differentiation (NED). FIR-induced NED is an emerging resistance mechanism to RT and tumors that undergo NED are highly aggressive and remain incurable.

Currently, the only clinical approach that improves RT for prostate cancer treatment is androgen deprivation therapy (ADT). ADT blocks androgen receptor (AR) signaling which inhibits the repair of DNA damage. In 2017, my lab reported that targeting Protein arginine methyltransferase 5 (PRMT5) blocks AR protein expression. Therefore, targeting PRMT5 may also sensitize prostate cancer cells to RT via a novel mechanism of action.

This dissertation focuses on the role of PRMT5 in the cellular response to IR and the goal of my work is to validate PRMT5 as a therapeutic target to enhance RT for prostate cancer treatment. I demonstrate that PRMT5 has several roles in the cellular response to IR. Upon a single dose of IR, PRMT5 cooperates with pICln to function as a master epigenetic activator of DDR genes and efficiently repair IR-induced DNA damage. There is an assumption in the field that the methyltransferase activity and epigenetic function of PRMT5 is dependent on the cofactor MEP50. I demonstrate that PRMT5 can function independently of MEP50 and identify pICln as a novel epigenetic cofactor of PRMT5. During FIR, PRMT5, along with both cofactors MEP50 and pICln, are essential for initiation of NED, maintenance of NED, and cell survival. Targeting PRMT5 also sensitizes prostate cancer xenograft tumors in mice to RT, significantly reduces and delays tumor recurrence, and prolongs overall survival. Incredibly, while 100% of control mice died due to tumor burden, targeting PRMT5 effectively cured ~85% of mice from their xenograft tumor. Overall, this work provides strong evidence for PRMT5 as a therapeutic target and suggests that targeting PRMT5 during RT should be assessed clinically.

# CHAPTER 1. INTRODUCTION

The following chapter was not published at the time of dissertation deposit. However, parts of this chapter was reproduced and modified with permission from[1]:

Owens, J. L. et al. PRMT5 Cooperates with pICln to Function as a Master Epigenetic Activator of DNA Double-Strand Break Repair Genes. iScience 23, 100750 (2020).

## 1.1 Prostate cancer

### 1.1.1 *Prostate cancer diagnosis*

Prostate cancer is a male-specific cancer that affects about 1 in 9 men in the United States during their lifetime[2]. The two biggest risk factors are age and family history. According to the American Cancer Society, the average age at diagnosis is ~66 and ~60% of cases are diagnosed in men who are 65 years of age or older. Additionally, men whose father or brother was diagnosed with prostate cancer have more than double the likelihood of being diagnosed with prostate cancer themselves. This suggests that inherited genetics may play a role in prostate cancer risk. However, the only well-established genetic link to prostate cancer is mutations in the BRCA1 or BRCA2 gene[3,4]. Men of African ancestry are more likely to get prostate cancer while men of Asian, Hispanic, or Latinx ancestry are less likely to get prostate cancer. Like most other cancers, general poor health such as obesity and poor diet also increase the risk. Overall, most risk factors for prostate cancer are not extremely strong.

There are several symptoms associated with prostate cancer including difficulty urinating, painful urinating, changes in urination frequency, loss of bladder control, blood in urine or semen, and sexual dysfunction. Symptoms are typically different for each patient and every symptom has other potential causes. Patients with early stage disease commonly do not display symptoms. Therefore, diagnostic tests are important to diagnose prostate cancer at the earliest possible stages and before symptoms arise.

Many healthcare professionals opt for routine screening involving either prostate-specific androgen (PSA) tests or digital rectal exams. PSA is a protein made by prostate cells and can be detected in the blood. Elevated PSA in the blood is associated with prostate cancer. According to the American Cancer Society, an individual with a blood [PSA] over 10 ng/mL has over a 50% chance of having prostate cancer. However, it remains controversial if increasing blood PSA levels

is a better predictor of prostate cancer than absolute PSA levels[5]. Imaging tests with MRI (especially multiparametric MRI) or transrectal ultrasound (TRUS) may also be used particularly if PSA tests or digital rectal exams suggest the presence of prostate cancer. Lastly, biopsies are used to confirm the presence of prostate cancer.

### 1.1.2 *Prostate cancer statistics*

For men in the United States, prostate cancer remains the second most diagnosed cancer behind skin cancer and the second leading cause of cancer death behind lung cancer[2]. Additionally, prostate cancer is the third most common cancer overall with an estimated 191,930 new cases in 2020[2]. About 1 in 9 men in the United States during their lifetime will be diagnosed with prostate cancer[2]. It is worth noting that transgender women can be diagnosed with prostate cancer which is an area of increasing study[6,7]. Fortunately, prostate cancer is largely manageable with a five-year relative survival rate of ~98%[2]. According to the American Cancer Society, 3.1 million men in the United States either have been cured or are currently living with prostate cancer today (~2% of the entire male population). However, with the high incidence of prostate cancer, an estimated 33,300 people will die from prostate cancer in 2020[2].

### 1.1.3 *Treatment options for prostate cancer*

Treatment options for prostate cancer depend on several factors, particularly the clinical stage and grade. The clinical stage ranges from I-IV and describe the spread of the tumor. Stages I-III are localized to either a portion of the prostate, the entire prostate, or the prostate and adjacent sites. Stage IV has widespread local and/or metastatic invasion. Prostate cancer biopsies are used to assess the grade. The grade is largely based on Gleason score which assesses the cell morphology and differentiation of the tumor. Tumors are also classified as low-, intermediate-, or high-risk which describes the likelihood of the disease spreading or recurring after treatment. Additional factors that are considered include age, expected life span, other health conditions, side-effects, blood PSA levels, and if the treatment is potentially curative or not.

Surgery and radiation therapy (RT) are the only curative treatments for prostate cancer patients and can be used for localized disease. Given that ~78% of current patients have localized disease[2] and ~96-97% of patients present with localized disease upon diagnosis[8], RT remains a

viable treatment option for the majority of current and newly diagnosed prostate cancer patients. Additional treatments for localized disease are under study but remain largely unused clinically[9,10]. Failure to manage localized prostate cancer eventually leads to disease progression and contributes to the majority of prostate cancer deaths.

Androgen deprivation therapy (ADT), which targets androgen receptor (AR) signaling, has been a mainstay to manage late-stage prostate cancer since the discovery in 1941 that prostate cancer cells rely on androgens[11]. However, ADT is limited mainly to patients with high-risk disease due to associated adverse effects[12–14]. Despite initial positive response for the majority of patients, ADT eventually fails within 1-2 years resulting in the development of castration-resistant prostate cancer (CRPC)[15]. CRPC readily metastasizes and is ultimately fatal. Therefore, future studies may focus on improving treatment for localized prostate cancer when it is still curable.

## 1.2 Radiation therapy (RT) is a potential curative treatment for prostate cancer

### 1.2.1 *Radiation therapy (RT) is a common treatment option for localized prostate cancer*

According to the American Cancer Society, over half of all cancer patients receive RT. For prostate cancer specifically, a study in 2010 demonstrated that above 25% of prostate cancer patients elect RT for their definitive treatment[16]. Results from recent clinical trials promote the use of RT as the standard of care for prostate cancer treatment[17–19]. Therefore, it is likely that even more prostate cancer patients will receive RT in the near future.

### 1.2.2 *Radiation therapy (RT) kills cells by inducing double-strand breaks (DSBs) in DNA*

RT is a potentially curative treatment because it can kill cancer cells. RT uses high-energy photons or particles, termed ionizing radiation (IR), which cause breaks in DNA, called DNA damage. IR can induce both single-strand breaks (SSBs) and double-strand breaks (DSBs) in DNA. DSBs are the most cytotoxic DNA lesion and are lethal to cells if not repaired. IR induces ~25 times more SSBs than DSBs[20,21]. During replication, these SSBs can be converted into DSBs when replication machinery interacts with the DNA damage. Because cancer cells grow and divide more quickly than normal cells, the effective DSBs induced by IR is typically higher in cancer cells than normal cells.

In general, most cells are able to survive a single IR treatment by repairing the DNA via DSB repair. Cells are able to repair almost all IR-induced DSBs within 24 h following a single dose of IR treatment[1]. However, because some DSBs remain unrepaired after 24 h, it is reasonable to suspect that multiple doses of IR would cause accumulation of DSBs. RT protocols utilize fractionated ionizing radiation (FIR) to administer multiple fractions of IR over a longer time period. FIR in RT is able to kill the cancer cells by inducing DSBs in DNA that cannot be repaired.

### 1.2.3 *Calculation of biologically effective dose (BED) allows for the comparison of different radiation therapy (RT) protocols*

RT protocols utilize different doses per fraction, cumulative doses, or overall treatment time. Biologically effective dose (BED) is used clinically to facilitate a better comparison of RT protocols. The calculation of BED utilizes an α/β ratio which is determined by the cell survival vs. dose curve. The α/β ratio represents the dose where the linear component (α) and quadratic component (β) of the curve are equal. The α/β ratio is inherently different for each normal tissue and each cancer. Tissues with higher α/β ratios have more linear survival curves and their survival depends more on the total cumulative dose of radiation as opposed to the dose in each individual fraction. Tissues with lower α/β ratios have more curved survival curves demonstrating increased survival at lower radiation doses and decreased survival at higher doses. It is classically assumed that prostate cancer has an α/β ratio of ~1.5[22], however recent reviews suggest it may be higher at ~2.7-4.9[23–26]. Nonetheless, most RT protocols use a BED between 98-200 Gy[27].

### 1.2.4 *Advances in technology promote the use of radiation therapy (RT) as the standard care for localized prostate cancer*

Meta-analysis of several RT clinical trials demonstrated that increases in BED significantly correlate with better outcomes but do not associate with adverse effects to a significant extent[27]. Instead, other factors are better predictors of adverse effects than BED and increases in BED are typically well-tolerated[28]. Advances in RT technology such as better image guiding technology, robot assistance, hydrogel spacers that separate the prostate from other organs, and proton therapy can further increase the tolerability of RT[29–31]. Continued improvement in RT will allow more patients to use RT as a potentially curative treatment for prostate cancer.

### 1.2.5 *Prostate cancer can become resistant to radiation therapy (RT)*

Although RT is potentially curative, evidence of tumors recurrence is observed within 5 years of RT completion for ~10-15% of prostate cancer patients with low-risk disease and ~50-60% of patients with high-risk disease[32–35]. Additionally, ~20-30% of patients with high-risk prostate cancer die within 10 years[33,36–38]. Therefore, resistance to RT promotes tumor recurrence and contributes greatly to prostate cancer mortality.

Currently, the only clinical approach to improve RT is ADT. ADT blocks AR signaling to decrease the efficiency of DSB repair[39–46]. Future studies may assess the feasibility of targeting additional pathways to enhance RT including (1) the DNA damage response (DDR), particularly DSB repair, (2) tumor hypoxia, and (3) abnormal cell signaling pathways (including PTEN/PI3K/AKT/mTOR, EGFR, and immune checkpoint)[47]. Although enhanced DDR should promote resistance to RT, it is unknown if prostate cancer cells commonly have more robust DDR compared to normal cells. It also remains unknown if increased AR signaling, tumor hypoxia, or additional signaling pathways associated with prostate cancer promote resistance to RT.

In 2008, our lab identified a novel potential mechanism of resistance to RT. In this study and a subsequent study, we reported that that prostate cancer cells undergo neuroendocrine differentiation (NED) in response to FIR[48,49]. Accumulating evidence suggests that NED is a clinically-relevant, emerging mechanism of resistance to RT[50].

## 1.3 Neuroendocrine differentiation (NED) is an emerging mechanism of treatment resistance in prostate cancer

### 1.3.1 *Normal prostate neuroendocrine (NE) cells*

Normal neuroendocrine (NE) cells are present in several tissues throughout the body including the prostate. Akin to their name, these NE cells share similar features with neural cells (synthesis and storage of monoamines and morphology such as neurite projections and presence of dense core granules) and endocrine cells (synthesis and secretion of peptide hormones)[51,52]. Specifically, NE cells express and secrete specific NE-associated proteins (such as neuron-specific enolase (NSE), chromogranin A (CgA), or synaptophysin (SYP)) and display NE-like morphology (such as presence of long, neurite projections)[50,53–56]. While NE-like morphology is easily visible for cells *in vitro* using bright field microscopy, NE-like morphology cannot be easily detected in the prostate gland *in vivo* even by using conventional hematoxylin and eosin (H&E) staining.

Electron microscopy can be used to identify normal prostate NE cells *in vivo* by the presence of neurite projections, similar to those seen *in vitro*, or microvilli extending into the lumen of the prostate gland[57]. Immunohistochemistry (IHC) is also used to identify normal prostate NE cells by staining for NE-associated proteins.

The prostate consists of several prostate glands (between 30-50). Prostate glands are formed by epithelial cells which are surrounded by stromal cells. Basal epithelial cells separate the glands from the stroma and luminal epithelial cells line the inside of the gland. Less than 1% of normal prostate epithelial cells are NE cells[57]. Normal prostate NE cells are randomly dispersed among the luminal and basal cells[58]. There are two different types of normal prostate NE cells that are defined by their morphology and location: (1) open-type cells which possess the aforementioned microvilli and (2) closed-type cells which possess the aforementioned neurite projections[57]. Based upon their morphology and location, normal prostate NE cells likely play a role in prostate growth, differentiation, and secretion[59]. However, these functions have not been well-studied and the biological role of normal prostate NE cells remains largely unknown[60].

### 1.3.2 *Neuroendocrine differentiation (NED) is associated with prostate cancer development*

Neuroendocrine differentiation (NED) is a process that describes how prostate cancer cells can transdifferentiate into NE-like cells. NE-like prostate cancer cells share some similar characteristics as normal prostate NE cells. NE-like prostate cancer cells secrete signaling molecules[61–63], as well as express high levels of ion channels to facilitate intracellular and extracellular signaling pathways[64–68]. This suggests NE-like prostate cancer cells communicate with other surrounding cells. One compelling study assessed if NE-like prostate cancer cells can participate in long-distance endocrine signaling in mice by implanting allograft NE-10 tumors (mice NE prostate cancer derived from the prostate lobe of transgenic 12T-10 mice[69]) into one flank and generating LNCaP tumors (human prostate adenocarcinoma) in the other flank. Indeed, while ADT inhibits LNCaP xenograft growth, the presence of the NE-10 tumor was able to rescue the growth of LNCaP tumors upon ADT[70]. This supports a model where NE-like cells can secrete factors into the bloodstream and participate in long-distance endocrine signaling to promote the growth and proliferation of other cancer cells. NE-like prostate cancer cells are also negative for AR and PSA[71], suggesting they do not require AR signaling. They are also negative for Ki-67[71]

and are resistant to apoptosis[72]. Overall NE-like prostate cancer cells are durable and support the growth, proliferation, and survival of the overall prostate cancer tumor.

Although NE cells constitute <1% of epithelial cells in the prostate gland[57], the proportion of NE-like cells is elevated in nearly all prostate cancer tumors[50,57,73–75]. Typically NE-like cells constitute ~1-5% of the overall tumor mass and tumors with more than 5% NE-like cells are typically defined as neuroendocrine prostate cancer (NEPC)[73,76]. There is still debate over how NE-like prostate cancer cells arise: either normal prostate NE cells mutate to become oncogenic (*de novo* NE-like prostate cancer cells) or other epithelial cells first become oncogenic and then transdifferentiate into NE-like prostate cancer cells (induced NE-like prostate cancer cells). Similarly, although some studies suggest that *de novo* NE-like prostate cancer cells are different in both morphology and behavior, they are understudied largely due to limited clinical distinction between *de novo* and induced NE-like prostate cancer cells[77,78]. Commonly, prostate cancer tumors have small areas of NE-like cells typically defined as 'prostate adenocarcinoma with focal NED'. Conversely, pure NE prostate cancer tumors, comprised of only oncogenic NE cells without evidence of adenocarcinoma, are rare[57,79,80]. This would suggest that in the majority of cases, transdifferentiation explains the increase in NE-like cells in prostate cancer tumors.

Several studies have shown that prostate cancer cells can transdifferentiate into NE-like cells and have termed this process neuroendocrine differentiation (NED)[50,81–83]. Molecular mechanisms of NED have been reviewed recently[60,80,81]. For example, NE-like cells utilize cAMP signaling and activation of CREB[61,84,85]. Furthermore, transient expression of a constitutively activated, nuclear- localized mutant of CREB alone induces NED[48]. Although it has been demonstrated that NE-like prostate cancer cells can promote growth of other prostate cancer cells via long-distance endocrine signaling [70,86], it will be interesting to see if they can also promote NED. However, what causes prostate cancer cells to undergo NED remains an area of study.

### 1.3.3 *Clinical treatment of prostate cancer can promote neuroendocrine differentiation (NED)*

Because NE-like prostate cancer cells are resistant to apoptosis, much research has assessed if they confer resistance to treatment. Although the proportion of NE-like cells is elevated in nearly all prostate cancer tumors, the proportion is even higher in CRPC tumors[87] After this finding, many studies demonstrated that NED is an emerging mechanism of resistance to several cancer

treatments[50,60,77,81,83,88–91]. Clinically, the presence of NE-like cells also correlates with poor prognosis and treatment-resistance[53,56,75,92].

Most studies on treatment-induced NED have focused on ADT. Selection pressure by ADT can promote focal NED[81] as well as NEPC. Between 10-20% of CRPC tumors are also NEPC[93–95]. Although there are many studies characterizing ADT-induced NED, it is worth noting a recent review which developed a 12-gene signature of NEPC[96]. This gene list was created by analysis of both literature and the Beltran NEPC dataset[89] which assessed patients with CRPC tumors. Therefore these 12 genes are likely representative of ADT-induced NE-like prostate cancer cells. In general, the role of the proteins encoded by these genes in NED has been well-studied. Despite recent advances in the field, therapeutic targets involved in ADT-induced NED remain elusive and NEPC remains incurable.

In 2008, our lab reported that prostate cancer cells also undergo NED in response to FIR, as performed in RT[48,49]. Unfortunately, because tumor biopsies following long-term RT treatment are difficult to obtain, confirmation that RT induces NED clinically is lacking. However, we and others have observed that blood CgA levels are elevated in a subset of prostate cancer patients treated with RT[49,97]. Isolated IR-resistant (IRR) NE-like prostate cells are also cross-resistant to other prostate cancer treatments including ADT[48,49]. Collectively, these studies suggest NED likely contributes significantly to the incidence of tumor recurrence following RT.

There are several potential mechanisms that contribute to FIR-induced NED[50]. For example, we reported that CREB is a transcriptional activator of NED while ATF2 is a transcriptional repressor of NED, and that FIR alters the subcellular localization of CREB and ATF2 to promote differentiation[85]. Compared to ADT-induced NED, FIR-induced NED less studied. For example, to our knowledge, RNA-seq analysis on FIR-induced NE-like prostate cancer cells has not been performed. Therefore, functional studies to identify mechanisms of FIR-induced NED are lacking. Future studies that identify therapeutic targets involved in FIR-induced NED will likely improve the cure rate of RT and improve survival of prostate cancer patients.

## 1.4 Protein arginine methyltransferase (PRMT5)

### 1.4.1 *The epigenetic regulation of gene expression is an emerging field in cancer research*

The epigenetic regulation of genes is cell type, temporal, and context dependent. Recent studies have demonstrated that the epigenetic regulation of gene expression mediates the development, progression, and therapeutic response of cancer[98,99]. DNA methylation was the first epigenetic mechanism to be linked to cancer while histone modification was the most recent[100]. Most studies have focused on histone lysine methylation; however, histone arginine methylation has emerged as an important regulatory event in cancer.

### 1.4.2 *Arginine methylation and protein arginine methyltransferases (PRMTs)*

Histone arginine methylation plays a key role in the epigenetic regulation of gene expression[101,102] among several other biological roles. Protein arginine methyltransferases (PRMTs) are a family of enzymes that facilitate the methylation of arginine residues on proteins by transferring donor methyl groups from S-adenosylmethionine (AdoMet or SAM) onto the guanidine nitrogen[102]. Arginine residues are commonly located on the surface of proteins where the hydrophilic head group (containing nitrogen and a positive charge) can interact with other molecules via salt bridge formation or hydrogen bonding. Methylation of arginine increases steric bulk, increases the hydrophobicity, and diffuses the localization of the positive charge[103]. Thus, arginine methylation is a common regulatory event that modulates the biological function of the protein substrate.

There are 9 PRMTs that can be classified into 3 types based upon the final product formed[104,105]: All PRMTs can catalyze the formation of mono-methylarginine (MMM). Type I (PRMT1, PRMT2, PRMT3, PRMT4, PRMT6, and PRMT8) form asymmetric dimethylarginine (aDMA). Type II (PRMT5 and PRMT9) form symmetric dimethylarginine (sDMA). Type III (PRMT7) can only catalyze MMA. PRMT7 is the only known type III PRMT and is only shown to methylate histones[106].

The biological role for PRMTs depends on the substrate. PRMTs can methylate both histone and non-histone substrates. Methylation by PRMTs can alter many processes including gene expression, RNA processing, splicing, protein stability, protein-protein interactions, and

signaling. Given the diverse array of substrates, the biological roles of PRMTs has been extensively studied including the role of arginine methylation in the DDR[107] and cell cycle[108].

### 1.4.3 *Biochemical function and roles of Protein arginine methyltransferase 5 (PRMT5)*

PRMT5 is a type II PRMT that can catalyze monomethylation and symmetric dimethylation of both histone and non-histone substrates. Human PRMT5 was discovered around two decades ago in 1999[109], and although the first decade focused on the biochemical characterization of PRMT5, recent studies have focused on the biological roles of PRMT5 such as cell proliferation, differentiation, and cell cycle progression[110,111]. PRMT5 regulates these processes by modulating gene expression, splicing, protein stability, protein-protein interactions, and signaling[110,111].

PRMT5 is an emerging epigenetic enzyme that regulate genes expression. PRMT5 regulates these changes in gene expression via symmetrical dimethylation of arginine residues in histones H4R3 (H4R3me2s), H3R2 (H3R2me2s), H3R8 (H3R8me2s), and H2AR3 (H2AR3me2s)[105,110–112]. Methylation of histones is well-established as an important mechanism to regulate gene expression. For example, PRMT5-catalyzed H4R3me2s represents one of the most repressive methylations in CD4+ T cells among the 20 histone methylations examined[113]. While PRMT5 is generally considered an epigenetic repressor [105,110–112], recent evidence from our lab and others demonstrate that PRMT5 also functions as an epigenetic activator [1,114,115]. PRMT5 can also regulate other processes though post-translational regulation of non-histone substrates[110]. For example, PRMT5 methylates and regulates several proteins and signaling molecules including NF-κB[116], HOXA9[117], and EGFR[118]. Collectively, PRMT5 has diverse biological roles and regulates cellular processes by methylation of histone and non-histone substrates.

PRMT5 is overexpressed in nearly all cancer types and promotes cancer cell growth[105,110–112,119–129]. Mechanistic studies have suggested that PRMT5 may promote cancer growth through the repression of tumor suppressor genes, repression of cell cycle checkpoint genes, or post-translational regulation of signaling molecules. PRMT5 has been demonstrated to play several biological roles in cancer including proliferation, differentiation, invasion, and migration[120]. Thus, PRMT5 has been proposed as a potential therapeutic target for cancer treatment[119].

### 1.4.4 *Protein arginine methyltransferase 5 (PRMT5) functions as an epigenetic activator of the androgen receptor (AR) to promote prostate cancer cell growth*

AR signaling is a hallmark of prostate cancer[130,131]. Many studies focus on developing novel therapeutics that inhibit AR signaling by blocking either production of androgens or AR itself[132–134]. A novel approach to target AR signaling is to block transcription of AR, thus preventing AR from being expressed at the protein level. The epigenetic regulation of AR transcription has been studied as early as 2000 when it was demonstrated that the level of DNA methylation at the AR promotor negatively correlates with the level of AR expression[135]. Since then, studies have shown that histone methylation and expression of non-coding RNAs also contribute to the regulation of AR expression[136]. Additionally, epigenetic mechanisms that mediate both activation and repression of AR transcription have been identified[136].

In 2017, our lab reported that PRMT5 epigenetically activates AR transcription in hormone-naïve prostate cancer cells[114]. Mechanistically, PRMT5 is recruited to the AR promoter to activate AR transcription through H4R3me2s in prostate cancer cells[114]. Specifically, PRMT5 is recruited to the AR promotor by SP1, the major transcriptional activator of AR expression[137,138], where it forms a complex with BRG1, an ATP-dependent chromatin remodeler involved in cancer[139]. Targeting PRMT5 causes a downregulation of AR at the mRNA and protein level[114]. Functionally, targeting PRMT5 inhibits growth of prostate cancer cells in an AR-dependent manner and prevents growth of xenograft tumors in mice[114]. PRMT5 is overexpressed in ~60% of intermediate- and high-risk prostate cancer tumors and the expression of PRMT5 positively correlates with the expression of AR at both the mRNA and protein level[114]. Collectively, this study demonstrated that PRMT5 is a novel epigenetic activator of AR transcription in prostate cancer cells and raised the possibility that targeting PRMT5 may block AR protein expression and be an effective approach to treat prostate cancer.

### 1.4.5 *Protein arginine methyltransferase 5 (PRMT5) activity is regulated by interaction with cofactors including MEP50 and pICln*

PRMT5 requires the interaction with other proteins to facilitate its biological role. These proteins are often termed cofactors and are generally associated with a subset of cellular processes regulated by PRMT5. For example, a protein may specifically be an epigenetic cofactor of PRMT5. Cofactors of PRMT5 include MEP50, pICln, RioK1, Menin/MEN1, and COPR5[110]. Overall,

cofactors can alter the methyltransferase activity, substrate specificity, or subcellular localization of PRMT5.

There is a long-standing view in the field that the cofactor MEP50 is required for PRMT5 methyltransferase activity and epigenetic function[110,111,140,141]. In solution, PRMT5 can exist as a homodimer or homotetramer. With MEP50, PRMT5 forms a hetero-octameric complex ($PRMT5_4$:$MEP50_4$)[142]. Consistent with these structural studies, biochemical studies have provided evidence that purified PRMT5:MEP50 complex can catalyze dimethylation of various substrates such as H4R3[140,143]. Although PRMT5-catalyzed histone methylation is predominantly repressive[110], recent studies show that PRMT5 can function as an activator of gene expression[114,141,144]. Activation or repression is not likely dependent solely on PRMT5-catalyzed histone methylation as H4R3me2s has been shown to be both a repressive[141] and active chromatin mark[114]. Therefore, additional factors are required to mediate the positive or negative epigenetic regulation by PRMT5.

PRMT5 does not contain a DNA binding domain and additional proteins that recruit PRMT5 to sites on the genome may play a role in mediating the epigenetic function of PRMT5. For example, biochemical assays demonstrate that PRMT5 requires MEP50 for methyltransferase activity. Additionally, a previous report also demonstrated that titration of pICln decreased H3 and H4 methylation by PRMT5 in an *in vitro* methylation assay[145]. This suggests that pICln may alter PRMT5 substrate specificity and inhibit the interaction with histones. However, as PRMT5 functions in a larger complex, this *in vitro* assay using proteins from a bacterial expression system might not recapitulate the biochemical and cellular conditions required for histone methylation *in vivo*. Therefore, it is possible that the epigenetic role of PRMT5 is not always dependent on MEP50 and may instead utilize other cofactors. Future studies may provide an answer to this such as (1) further biochemical assays of PRMT5 with other cofactors in the presence of in-tact nucleosomes to assess the effect of cofactors on PRMT5 histone methyltransferase activity, (2) structural analysis of the PRMT5 complex at the promoter of target genes to elucidate cofactors involved in the regulation of specific genes, and (3) genome-wide analyses such as ChIP-seq and ATAC-seq to identify putative PRMT5 target genes that are regulated by specific cofactors.

Menin/MEN1 is another protein that may modulate the epigenetic function of PRMT5. Three related reports in 2013 demonstrate that PRMT5 interacts with Menin/MEN1[146–148], a scaffold protein of lysine methyltransferase complexes that mediate epigenetic regulation of

transcription[149]. Menin/MEN1 can recruit PRMT5 to the promoters of the Gas1 and Gli1 genes to facilitate H4R3me2s and subsequent transcriptional repression (Gas1[147] and Gli1[148]). Menin/MEN1 is commonly inactivated by mutations in cancer. Analysis using the cBioPortal database[150,151] shows that Menin/MEN1 point mutations are common particularly in NE tumors (~35-50% of pancreatic NE tumors) but not common in prostate cancer tumors (~0%). Interestingly, these Menin/MEN1 point mutations decrease the interaction between Menin/MEN1 and PRMT5 as well as decrease histone methyltransferase activity towards histone H4 in an *in vitro* methylation assay[147]. Therefore, it is possible that Menin/MEN1 is an epigenetic cofactor of PRMT5 that aids in transcriptional repression in a subset of PRMT5 target genes.

COPR5 is another protein that may modulate the epigenetic function of PRMT5. Two reports from the same lab demonstrate that PRMT5 interactions with COPR5[152,153]. At least in U2OS osteosarcoma cells, COPR5 can recruit PRMT5 to the promoter of CCNE1 to facilitate transcriptional repression[152]. Interestingly, an interaction with COPR5 favored PRMT5 histone methyltransferase activity towards histone H4 over H3 in an *in vitro* methylation assay[152]. This is likely explained by the binding of COPR5 to the N-terminus of histone H4 and recruitment of PRMT5[152]. Furthermore, at least in C2C12 myoblast cells, COPR5 can recruit PRMT5 to the promoter of p21 and MYOG[153]. Therefore, COPR5 is involved in muscle cell differentiation by mediating the recruitment of PRMT5 to the promoter of genes involved in both cell cycle and differentiation. Similar to Menin/MEN1, it is possible that COPR5 is also an epigenetic cofactor of PRMT5 that aids in transcriptional repression in a subset of PRMT5 target genes

PRMT5 cofactors modulate cellular processes additional to epigenetic regulation. The cofactor pICln has been shown to enhance the splicing activity of PRMT5. Early studies on PRMT5 demonstrated that PRMT5 functions in a complex with MEP50 and pICln to methylate Sm proteins which promotes formation of the spliceosome[154–156]. Functionally, recent studies demonstrate that PRMT5 is required for appropriate splicing by preventing intron retention and exon skipping[157,158]. pICln interacts with the N-terminal domain of PRMT5 which can also be occupied by RioK1[159]. pICln and RioK1 likely compete for PRMT5 binding which may alter substrate specificity[159]. While RioK1 is a cytoplasmic protein, pICln can be found in either the cytoplasm or nucleus. As splicing takes place in the nucleus during or directly following transcription, it is likely nuclear PRMT5 interacts with pICln to promote splicing. The subcellular

localization of pICln leaves the possibility that pICln also modulates the epigenetic regulation of a subset of PRMT5 target genes.

In 2016, 3 studies performed genome-wide screens to identify potential therapeutic targets that would be effective for cancers with deletion of the S-methyl-5'-thioadenosine phosphorylase (MTAP) gene[160–162] which occurs in ~15% of all cancers. Analysis using the cBioPortal database[150,151] shows that MTAP deletions are common in cancers such as in glioblastoma (~41%) or pancreatic cancer (~22-23%), and less common in prostate cancer (~5%). This study identified PRMT5 and cofactors MEP50, pICln, and RioK1[160–162] as therapeutic targets that would synergize with MTAP deletion. Because MTAP cleaves a molecule called 5'-methylthioadenosine (MTA), deletion of MTAP in cancer causes an increase in the cellular MTA concentration. MTA acts as a competitive inhibitor of PRMT5 by binding to the AdoMet/SAM binding pocket[162]. Therefore, PRMT5 may be upregulated or activated via alternative mechanisms in MTAP-deleted cancers to compensate for MTA-mediated enzymatic inhibition. Because MEP50, pICln, and RioK1 were identified in these screens, it is likely these cofactors are the most important to PRMT5 activity.

## 1.5 Protein arginine methyltransferase (PRMT5) plays several roles in the DNA damage response (DDR)

### 1.5.1 *An overview of the DNA damage response (DDR) and double-strand break (DSB) repair*

The human genome is constantly exposed to both endogenous and environmental stresses that cause damage to DNA. Proper repair of DNA is critical for cell survival and to prevent mutations from being passed on to daughter cells. Incorrect or incomplete repair of DNA can lead to somatic mutations and promote cancer development. Extensive DNA damage, as is the case in cancer cells treated with RT, can cause cells to undergo apoptosis. Therefore, the biological mechanisms activated in response to DNA damage has broad applications including RT for cancer treatment.

The DNA damage response (DDR), not to be confused with *Dance Dance Revolution*, is an evolutionarily conserved cellular reaction to these genotoxic stresses that coordinates cell cycle arrest, inhibition of cell division, and DNA repair. Although the name “the DDR” would suggest a singular cellular process, there are different alterations of the DDR depending on which phase of the cell cycle the damage occurred in as well as the type and severity of DNA damage. DNA double-stranded breaks (DSBs) are well-recognized as the most lethal form of DNA damage. The

repair of DSBs occurs in three phases: (1) recognition of DSBs via sensor proteins, (2) initiation of repair by repair proteins, and (3) resolution of repair[163]. Proteins involved in DSB repair are typically expressed at lower basal levels. When sensor proteins recognize DSBs, repair proteins (such as RAD51, BRCA1, and BRCA2) are transiently upregulated at the protein level to facilitate DSB repair[164–166]. This upregulation allows for efficient repair without the need for these proteins to constantly be expressed at a high level. Although the recruitment and action of sensor and repair proteins is well-studied, new studies are focusing on how post-translational modifications contribute to their role in the DDR, particularly the repair of DSBs.

DSBs are mainly repaired via homologous recombination (HR) or non-homologous end joining (NHEJ)/canonical-NHEJ (c-NHEJ). However, alternative forms of DSB repair exist and recent studies have revealed two other common forms of DSB repair: alternative NHEJ (alt-NHEJ)/microhomology-mediated end joining (MMEJ), and single strand annealing (SSA). Pathway choice affects the speed and accuracy of the repair. However, DSBs can be efficiently repaired regardless of pathway choice. Here, we define the efficiency of repair as the ability to complete repair, independent of repair mechanism or if the DNA is repaired correctly. Therefore assays such as γH2AX foci analysis[167] and comet assay[168] can assess the efficiency of DSB repair regardless of which pathway was used to repair the DSB.

### 1.5.2 *An introduction of Protein arginine methyltransferase 5 (PRMT5) in the DNA damage response (DDR)*

In 2008, PRMT5 was shown to methylate p53 to alter its function in response to DNA damage[169]. This study marked the first report of PRMT5's direct involvement in the DDR. Since then, there has been significant progress describing how PRMT5 regulates various DDR processes and pathways. Most initial reports analyzed the role of PRMT5 in the repair of DNA damage at the base or single-strand level. However, studies in the past 2-3 years have established PRMT5 as a key regulator of DSB repair. Studies also demonstrate that PRMT5 is a conserved, essential regulator in the repair of DNA damage across evolution. Lastly, PRMT5 may be an effective therapeutic target for cancer treatment particularly in combination with RT or other DNA damaging treatments.

### 1.5.3 *Protein arginine methyltransferase 5 (PRMT5) regulates DNA Double-Strand Break (DSB) repair choice*

DSBs can be efficiently repaired regardless of pathway choice. However, pathway choice affects the speed and accuracy of the repair. For example, NHEJ has much faster kinetics than HR. This would suggest NHEJ would be the first choice DSB repair mechanism. However, NHEJ can be mutagenic. HR is the only error-free DSB repair mechanism. Alt-NHEJ is inaccurate and can cause insertions and deletions. SSA is inaccurate and can cause large deletions. Lastly, NHEJ is fairly accurate (if the overhangs of the DSB ends are compatible or the ends of the DSBs are blunt without other lesions present, the ends can be ligated without loss of nucleotides) but can cause 1-4 nucleotide deletions. Overall, DSB repair pathway choice is tightly regulated and has been the focus of several recent reviews[170–173], although much of the mechanism remains to be determined.

Pathway choice is dependent on the cell cycle. NHEJ can occur at any point during the cell cycle but is mainly employed during $G_1$ phase. Following DNA replication in S phase, chromosomes have been duplicated which allows for homology-based repair. HR utilizes this identical sequence as a template for repair and thus is the major DSB repair mechanism in late S phase and $G_2$ phase. Although alt-NHEJ and SSA can occur in S and $G_2$ phase, HR is the preferred mechanism given that it is accurate.

The most important biological process that determines DSB repair pathway choice is DSB end resection. In general, if DNA is not resected, DSBs are repaired via NHEJ. If ends are resected, DSBs are repaired via the homology-based repair mechanisms HR, alt-NHEJ, or SSA. Competition of binding proteins, often termed accessory factors, to the DSB can dictate DSB end resection and pathway choice. The most prominent competition is the balance between 53BP1 (which blocks DSB end resection and promotes NHEJ) and BRCA1 (which initiates DSB end resection and promotes other repair mechanisms). If BRCA1 binds, it can form a complex with CtIP and the MRN complex to promote DSB end resection to favor HR. The binding of 53BP1 blocks recruitment of CtIP so DSB end resection is inhibited. The expression and/or activity of these proteins fluctuates during the cell cycle which facilitates pathway choice. DSB end resection is promoted during S/$G_2$ phase. BRCA1 is significantly upregulated in $G_2$/M phase compared to $G_1$ phase[174], which may contribute to the cell cycle-dependent 53BP1/BRCA1 competition.

Post-translational modifications also play a particularly important role in DSB repair choice. One important modification is acetylation of histone H4K16 (H4K16Ac) which is

catalyzed by Tip60. Upon DNA damage, the chromodomain of Tip60 can interact with methylated Histone 3 lysine 9 (H3K9me3) at the DSB site, which activates acetyltransferase activity and promotes acetylation of histone H4K16[175]. H4K16Ac disrupts the salt bridge between H4K16 and the Tudor domain of 53BP1 to facilitate displacement of 53P1 from DSB sites[175,176]. This allows for BRCA1 binding, promotes RPA filament formation, promotes DSB end resection, and promotes subsequent repair via HR.

Recently, it was discovered that PRMT5 regulates members of the Tip60 complex via splicing of Tip60 and methylation of RuvBL1. In 2017, *Clarke et al.* reported that PRMT5 promotes HR through methylation of the Tip60 cofactor RuvBL1[177]. RuvBL1 and its binding partner RuvBL2 exist in several complexes including several involved in the DDR through interactions with Tip60, INO80, and SRCAP[178]. However, PRMT5-catalyzed methylation of RuvBL1 likely does not alter the activity of INO80 or SRCAP complexes[177]. Instead, it promotes Tip60-dependent acetylation of H4K16 specifically to inhibit 53BP1 binding to DSB sites[177]. Thus, a previous report where the presence of RuvBL1 favors RAD51 formation and subsequent HR[179] is likely dependent on PRMT5-catalyzed methylation of RuvBL1. Methylation of RUVBL1 does not affect acetylation of H4K5, H4K12, or H2AK5 and does not prevent Tip60-facilitated activation of ATM[177]. Additionally, methylation of RuvBL1 is increased by IR treatment[177]. Collectively, arginine methylation of RuvBL1 by PRMT5 selectively affects the DSB repair choice function of Tip60.

One year later, *Hamard et al.* reported that PRMT5 regulates Tip60 acetyltransferase activity through splicing of Tip60 at least in hematopoietic cells[180]. There are two spliced isoforms of Tip60: Full-length (Tip60α) and one where exon 5 is skipped (Tip60ΔEx5 or Tip60β). Tip60β has decreased acetylation activity at least towards H4K16[180]. PRMT5 knockout (KO) cells had significantly reduced Tip60α protein levels while Tip60β levels remained unchanged which resulted in decreased H4K16Ac levels[180]. Thus, PRMT5 promotes expression of full-length Tip60 (by preventing exon 5 skipping) which has greater acetyltransferase activity and promotes DSB end resection and HR[180]. Although alt-NHEJ or SSA were not assessed directly in either report, as PRMT5-catalyzed methylation of RuvBL1 and appropriate splicing of Tip60 inhibits binding of 53BP1, DSB end resection is activated and could promote DSB repair via any homology-based repair mechanism. Nevertheless, PRMT5 regulates DSB repair pathway choice via alteration of the Tip60 complex.

### 1.5.4 *Protein arginine methyltransferase 5 (PRMT5) regulates the spicing of DNA repair genes*

PRMT5 can also regulate protein expression via splicing and two recent studies identified PRMT5 splicing targets involved in the DDR[157,158]. In 2017, *Braun et al.* reported that, at least in malignant glioma cells, PRMT5 post-transcriptionally regulates the splicing out of detained-introns (DIs) of genes to modulate gene expression and/or levels of functional protein[157]. Additionally, in 2019 *Tan et al.* reported that, at least in hematopoietic stem cells, PRMT5 is required for appropriate splicing and that targeting PRMT5 causes increased intron retention and exon skipping events[158]. It is possible that PRMT5 may regulate the expression of genes critical to the repair of DSBs via splicing. In fact, both groups performed functional enrichment analysis on alternative splicing events upon PRMT5 knockdown and identified genes associated with "DNA repair" and "cell cycle progression" [157,158] (Appendix A). For example, PRMT5 is required to maintain appropriate expression of functional RAD52[158], and recent reports demonstrate the importance of RAD52 to HR[181–183]. Future studies may determine if PRMT5-associated splicing directly affects the repair of IR-induced DSBs, as occurs in response to RT, as well as other DNA damages in prostate cancer cells.

### 1.5.5 *Protein arginine methyltransferase 5 (PRMT5) regulates other DNA damages*

Several studies suggest PRMT5 may play a versatile regulatory role in the repair of other DNA damages. PRMT5 has been shown to methylate and post-translationally regulate several proteins involved in DDR: p53[169,184–186], E2F1[187–189], FEN1[190,191], RAD9[192], KLF4[193], and TDP1[194]. In general, DNA damage (such as induced by etoposide, hydroxyurea, doxorubicin, or UV treatment) induces methylation of these proteins which alters their biological function. However, it remains to be determined if methylation of these proteins directly affects the repair of DNA damage. Given the vast array of proteins methylated by PRMT5, it is likely that there are also unknown PRMT5 substrates involved in DDR. As PRMT5 is an epigenetic regulator, PRMT5 may also regulate the repair of other DNA damages by regulating the expression of DDR proteins. Future studies may determine if PRMT5-catalyzed methylation of these proteins as well as epigenetic regulation of target genes directly affects the repair of other DNA damages.

Protein arginine methyltransferase 5 (PRMT5) and p53

p53 was the first protein involved in DDR shown to be methylated by PRMT5. PRMT5-catlyzed methylation of p53 alters the biological function of p53 (promoting cell cycle arrest and inhibiting apoptosis) through changing the binding of p53 to its target genes[169]. A year later, it was demonstrated that PRMT5 also promotes p53 protein synthesis through the regulation of eIF4E, a protein involved in the mRNA-ribosome-binding step of protein synthesis [184]. Future studies revealed that PRMT5 epigenetically activates transcription of eIF4E likely though H4R3me2s and/or H3R8me2s[125]. In response to DNA damage, PRMT5 can ensure sufficient p53 levels by activating eIF4E expression. However, none of these studies directly addressed the effect of PRMT5-catalyzed methylation of p53 on the repair of DNA damage.

Protein arginine methyltransferase 5 (PRMT5) and FEN1

Two years following the pioneer study of PRMT5 and p53, PRMT5 was shown to regulate FEN1. FEN1 is a structure-specific endonuclease that participates in DNA replication, DNA repair, and apoptotic DNA fragmentation. Functionally, methylation of FEN1 is required for efficient DNA replication, specifically Okazaki Fragment maturation[190]. During DNA replication, DNA polymerases require short RNA fragments to serve as primers. These primers are removed by FEN1 which also nicks the DNA. DNA ligase I seals the nick to prevent DNA damage. During S phase of the cell cycle, FEN1 is recruited to DNA replication loci via an interaction with PCNA[195] which is likely dependent on PRMT5-catalyzed methylation[190]. After cleavage is complete, FEN1 is demethylated and subsequently phosphorylated, likely by CDK2-Cyclin E[190]. Phosphorylation of FEN1 (1) causes dissociation from PCNA, (2) prevents continuous binding of the FEN1:PCNA complex to DNA, (3) promotes localization of FEN1 to the cytoplasm, and (4) allows DNA ligase I to resolve the nick[190]. Defects in either Okazaki fragment maturation or ligation during DNA repair can lead to DSBs[196]. Therefore, decreased methylation of FEN1 may promote the formation of endogenous DSBs. Indeed, cells expressing non-methylatable FEN1 are also more prone to spontaneous mutations (rate is 32-fold greater than wt)[190]. Interestingly, analysis using the cBioPortal database[150,151] demonstrates that FEN1 is not highly mutated in cancer in general. However, there is a tubular stomach adenocarcinoma patient with a FEN1(R192Q) missense mutation who had a particularly high number of mutations compared to other stomach

adenocarcinoma patients (28th out of 435 cases). It is also interesting that she was the only tubular stomach adenocarcinoma patient with a mutation in PRMT5.

FEN1 also plays a role in base excision repair (BER)[197]. Oxidative stress can promote the oxidation of bases in DNA. Oxidized bases are removed leaving abasic sites which are repaired by BER. In the long patch BER pathway (LP-BER), newly polymerized DNA replaces the damaged DNA while the strand that contains the abasic site is excised by FEN1[197]. Oxidative stress (as generated by $H_2O_2$) induces PRMT5-mediated methylation of FEN1 which increases the rate of LP-BER[190]. However, whether methylation of FEN1 is required to complete LP-BER and how methylation of FEN1 regulates LP-BER remains unknown.

Protein arginine methyltransferase 5 (PRMT5) and RAD9

RAD9, a versatile DDR protein with various roles in cell cycle checkpoint control and DNA repair is methylated by PRMT5 which contributes to DNA damage-induced $G_2$ arrest and Chk1 activation[192]. As phosphorylation of RAD9 also influences the role of RAD9 upon DNA damaging treatment[198–200], it is feasible that there is crosstalk between arginine methylation and phosphorylation to determine the biological function of RAD9 upon DNA damage. RAD9 is also essential for repair of DSBs during $G_2$ phase, likely by promoting HR directly, independently of inducing $G_2$ arrest[201]. It is possible PRMT5-catalyzed methylation of RAD9 might regulate HR. However, a direct role in the repair of any DNA damage was not studied[192]. Interestingly, PRMT5-catalyzed methylation of RAD9 is essential for cell sensitivity to hydroxyurea[192] (a small molecule inhibitor of ribonucleotide reductase which functionally inhibits DNA replication and causes DSBs near replication forks) but does not significantly affect sensitivity to IR. It should be noted that recent studies suggest that cytotoxic effect of hydroxyurea might be mainly due to oxidative stress and mitotic arrest (in cytokinesis phase) as opposed to DSBs[202]. Thus PRMT5-catalyzed methylation of RAD9 may not be critical to the role of RAD9 in HR. Because RAD9 is required for several forms of DNA repair as reviewed[203], including BER as part of the 9-1-1 complex[204], mismatch repair[205], and nucleotide-excision repair (NER)[206], future research may assess if PRMT5-catalyzed methylation of RAD9 affects these forms of DNA damage.

Protein arginine methyltransferase 5 (PRMT5) and E2F1

PRMT5 also post-translationally methylates E2F1[187]. E2F1 is a transcription factor, similar to p53, that is upregulated upon DNA damage to regulate target genes involved in cell cycle arrest and apoptosis[207]. Arginine methylation of E2F1 by PRMT5 likely reduces both E2F1 stability and DNA-binding activity to inhibit transcriptional activation of at least a subset of E2F1 target genes[187]. Functionally, methylation of E2F1 likely promotes cell growth by inhibiting the cell cycle arrest function of E2F1. PRMT5 and PRMT1 battle in a biochemical antagonism to regulate E2F1: symmetric dimethylation by PRMT5 suppresses E2F1 while asymmetric dimethylation by PRMT1 activates E2F1[188]. Upon DNA damage, PRMT1 out competes PRMT5 to regulate E2F1 in a cyclin A-dependent manner[188]. Therefore, methylation of E2F1 is reduced upon DNA damage[187] and unmethylated E2F1 is able to either induce cell cycle arrest or apoptosis.

Protein arginine methyltransferase 5 (PRMT5) and KLF4

PRMT5 also methylates the transcription factor KLF4 which has a similar biological effect as methylation of p53. KLF4 is rapidly turned over by VHL-mediated ubiquitination and proteasomal degradation[208]. KLF4 expression is upregulated upon DNA damage which promotes p21 protein expression[209,210]. If the DNA damage is too extensive, KLF4 will be downregulated which leads to expression of BAX and subsequent activation of apoptosis[209,210]. PRMT5-mediated arginine methylation of KLF4 (1) inhibits VHL-mediated ubiquitination, (2) reduces KLF4 degradation, (3) elevates KLF4 protein levels, (4) increases the transcription of the KLF4-activated gene p21, (5) reduces the transcription of the KLF4-repressed gene BAX, and (6) reduces apoptosis[193]. Therefore PRMT5-mediates upregulation of KLF4 protein, promotes cell cycle arrest, promotes DNA repair, and repress apoptosis.

Protein arginine methyltransferase 5 (PRMT5) and TDP1

Most recently, PRMT5 was shown to methylate TDP1[194], an enzyme which prevents the formation of a specific subset of DSBs which can occur when relaxing supercoiled DNA. Because high tension in the DNA double helix can interfere with DNA metabolic processes, DNA supercoiling must be relaxed. To relax DNA supercoils, DNA topoisomerase 1 (Top1) first nicks one DNA strand to induce a SSB[211]. Top1 then covalently binds to the 3'-terminus of the SSB to

form a Top1 cleavage complex (Top1cc)[212]. After the torsional stress is released, TDP1 hydrolyzes the Top1:DNA bond[211] which frees the 3'-terminus of the SSB allowing it to be resealed and restore double-stranded DNA[213]. If Top1 is trapped, the Top1cc cannot be resolved and the SSBs can be converted to Top1-associated DSBs upon collision with replication machinery, transcription machinery, or DNA damage[211,214]. Several cancer treatments (e.g. camptothecin (CPT), topotecan, and irinotecan) also trap the Top1cc which increases the likelihood of DSB formation[211]. PRMT5 methylates TDP1 which is induced by DNA damage[194].

Arginine methylation directly stimulates TDP1 catalytic activity which enhances the resolution of the Top1cc and prevents DSB formation[194]. CPT treatment induces chromatin binding of PRMT5 and promotes PRMT5 foci formation at the site of DSBs[194]. It is possible that PRMT5 performs additional functions to repair Top1cc-specific DSBs. Expression of a non-methylatable TDP1 mutant inhibits repair of CPT-induced DSBs[194]. However, it remains unknown if cells can resolve endogenous top1cc-specific DSBs independently of PRMT5. Analysis using the cBioPortal database[150,151] demonstrates that out of 44,347 cancer patients, only 1 patient had a TDP1(R361) or (R586) mutation (Head and Neck Squamous Cell Carcinoma patient with a R586W mutation) suggesting that arginine methylation of TDP1 does not have a large effect on genomic stability. Instead, inhibitors of PRMT5-catalyzed methylation of TDP might sensitize cancer cells to CPT-like anticancer drugs.

### 1.5.6 *Protein arginine methyltransferase 5 (PRMT5) regulates the cell cycle and apoptosis*

Protein arginine methyltransferase 5 (PRMT5) is an activator of cell cycle progression

The cell cycle describes cellular events from the replication of DNA to the partition of duplicated DNA to daughter cells during cell division. In general, PRMT5 functions as an activator of the cell cycle. The regulation of the cell cycle by arginine methylation, including PRMT5, was recently reviewed[108]. In most cell lines, PRMT5 knockdown induces $G_1$ arrest which suggests PRMT5 is an activator of $G_1$ progression to promote cell cycling and cell proliferation[126,184,215,216]. Additionally, overexpression of PRMT5 in NIH 3T3 cells (mouse embryonic fibroblast) caused increased cell growth[217]. However, targeting PRMT5 may induce $G_2$ arrest in some cell lines such as U87MG (glioblastoma astrocytoma)[157]. Also cell cycle profiles were the same in HeLa-shCTRL

and shPRMT5 stable cell lines[177]. Future studies such as genomic profiling and transcriptomic analysis may explain how PRMT5 can regulate either $G_1$ or $G_2$ progression in different cell types.

Although the studies above suggest PRMT5 acts as an activator of proliferation, in some instances PRMT5 overexpression can induce cell cycle arrest: In U2OS (p53 +/+) cells (osteosarcoma), ectopic PRMT5 caused $G_1$ arrest[169]. Additionally, overexpression of PRMT5 in MCF7 cells (luminal breast adenocarcinoma) alone had no effect on proliferation[184]. These results must be taken with potential criticism of protein overexpression: (1) overexpression of a single protein may not generate the necessary context to assess the biological role of a protein, (2) the level of overexpression can vary greatly and depends on overexpression method and target proteins used, and (3) overexpression may exhaust cellular resources. Nonetheless, PRMT5 may regulate the cell cycle differently in each cell type.

Protein arginine methyltransferase 5 (PRMT5) promotes cell growth, proliferation, and anchorage-independent growth

There are several potential mechanisms through which PRMT5 might promote cell growth, proliferation, and anchorage-independent growth. One of the first studies demonstrating the role of PRMT5 as an epigenetic regulator detailed how PRMT5 represses the tumor suppressors 'suppressor of tumorigenicity (ST7)' and 'nonmetastatic 23 (NM23)[217]. PRMT5 expression also positively correlates with the expression of CDK4, CDK6, and cyclins D1, D2, E1, as well as the phosphorylation and inactivation of retinoblastoma protein (Rb)[126], although it remains to be determined if any of these are primary target genes of PRMT5. It is possible PRMT5 regulates Rb phosphorylation through a physical interaction with CDK4 to regulate cell cycle progression: (1) PRMT5 binding to CDK4 can displace CDKN2A to free up CDK4, (2) CDK4 can phosphorylate Rb, (3) pRb can activate E2F transcription factors to promote $G_1$-S progression[215]. Clinically PRMT5 expression positively correlates with cyclin D1 and inversely correlates with p16/CDKN2A at least in oropharyngeal squamous cell carcinomas[218] which may further explain the activation of Rb associated with PRMT5.

Protein arginine methyltransferase 5 (PRMT5) regulates DNA damage-induced cell cycle arrest

In the context of DNA damage, PRMT5 plays a different role in the regulation of the cell cycle. Upon DNA damage, cells undergo cell cycle arrest to allow for more time for repair and to

prevent unrepaired or misrepaired DNA from being replicated or passed on to daughter cells. PRMT5 regulates $G_2$ arrest via methylation of RAD9[192] and accumulation of KLF4[193]. PRMT5 also regulates $G_1$ arrest via methylation of p53[169]. Upon DNA damage, PRMT5 methylates R333, R335, and R337 on p53[169]. A mass spectrometry study also determined that R110, R209 and R213 are methylated by an undetermined mechanism[219]. Analysis using the cBioPortal database[150,151] shows that R213 mutations are one of the most common point mutations across cancer (4$^{th}$ most frequently mutated residue of p53 with 356 mutations) and R213 mutations may represent a way in which cancer cells bypass $G_1$ checkpoint to promote cell cycling and cell proliferation. A study also suggested that methylation of p53 on R213 may be required for efficient downstream expression of p21 and subsequent induction of $G_1$ arrest[220], however it remains to be determined if DNA damage also induces methylation of p53 on R213 to promote $G_1$ arrest. Nonetheless, it is likely that PRMT5 can regulate either DNA damage-induced $G_1$ or $G_2$ arrest depending on different contexts (such as intensity or type of DNA damage) or in different cell types.

Protein arginine methyltransferase 5 (PRMT5) regulates apoptosis

As described above, PRMT5-catalyzed methylation often modulates the role of proteins to promote cell cycle while suppressing apoptosis. For example, methylation of p53 promotes cell cycle arrest and inhibits apoptosis[169]. Consistent with this, PRMT5 knockdown alone can induce apoptosis (at least in U1242 and U251 glioblastoma cell lines)[128]. However, there are other PRMT5 targets that are directly involved in apoptosis.

PRMT5 interacts with death receptor 4 (DR4)[221], a cell surface receptor that interacts with tumor necrosis factor (TNF)-related apoptosis-inducing ligand (TRAIL) as part of the death-inducing signaling complex (DISC) which initiates apoptosis of tumor cells specifically. Functionally, PRMT5 inhibits TRAIL-induced apoptosis[221]. Their study suggested that although PRMT5 interacts with DR4, it may not methylate DR4 and did not disrupt DISC formation[221]. Instead, PRMT5 inhibits apoptosis by activating NF-κB signaling and associated induction of NF-κB target genes[221]. PRMT5 was later shown to methylate NF-κB directly[116,222] which may also explain PRMT5-mediated NF-κB activation[221]. PRMT5 also activates IKK activity which likely phosphorylates and activates NF-κB[221]. Thus, PRMT5 may inhibit cancer-associated TRAIL-induced apoptosis via multiple mechanisms.

PRMT5 was also demonstrated to methylate Apoptosis signal-regulating kinase 1 (ASK1)[223], a kinase involved in oxidative stress-induced apoptosis[224]. Phosphorylation of ASK1 by serine/threonine kinases such as Akt1 can inhibit its role in apoptosis[225]. Arginine methylation of ASK1 by PRMT5 promotes its interaction with Akt leading to phosphorylation and subsequent inhibition of apoptosis[223]. PRMT5 also inhibits $H_2O_2$-induced ASK1-mediated apoptosis.

It is important to note that although PRMT5 is shown to methylate the N-terminal region of Programmed cell death protein 4 (PDCD4)[226], a suppressor of apoptosis via inhibition of procaspase-3 mRNA translation into protein[227], a potential effect on apoptosis was not identified. Instead, PRMT5 was shown to switch the role of PDCD4 from a tumor suppressor to an activator of tumor growth (only in the context of a tumor and not in cell culture)[226].

### 1.5.7 *The role of Protein arginine methyltransferase 5 (PRMT5) in the DNA damage response (DDR) is likely evolutionarily conserved*

Studies in several organisms suggest that PRMT5 likely plays an evolutionarily conserved role in the DDR. However, as we see in human cells, PRMT5 may have different mechanisms in various cell types or under specific contexts such as type and severity of DNA damage. The same may hold true when comparing the role of PRMT5 in different species. Nonetheless, evidence suggests PRMT5 plays an important role in DDR throughout eukaryotic cells and is conserved throughout evolution.

Protein arginine methyltransferase 5 (PRMT5) and the p53 homologue in *C. elegans*

In 2009, Yang et al. demonstrated that PRMT5 also regulates the DDR in *C. elegans* via its interaction with the p53 homologue CEP-1 and the p300/CBP ortholog CBP-1[228]. Functionally, the PRMT5 homologue suppresses DNA damage-induced apoptosis[228]. Yang et al. identified homologues for PRMT1-PRMT6 and targeting PRMT5 specifically, increased IR-induced cell death[228]. Biochemically, PRMT5 forms a complex with both the p53 homologue CEP-1 and the p300/CBP ortholog CBP-1 and PRMT5 methylates CBP-1[228]. It is possible that human PRMT5 may also methylate and regulate p300/CBP (ortholog *C. elegans* CEP-1), and the GRG motif of CEP-1 that is methylated by PRMT5 in *C. elegans* is conserved in the N-terminal domain of mammalian p300/CBP. Like in humans, the CEP-1:p53 complex is a key modulator of IR-induced apoptosis in the germ cells of *C. elegans*[229]. Future studies may determine if PRMT5 methylates

p300/CBP as an additional mechanism to mediate apoptosis in mammalian/human cells. Unlike human PRMT5, the *C. elegans* PRMT5 homologue did not methylate the p53 homologue CEP-1 which is likely because CEP-1 does not contain the same RGRER motif as found in human p53[169]. Thus, PRMT5 in humans may regulate p53-mediated apoptosis via alternative or additional mechanisms than in *C. elegans*.

Protein arginine methyltransferase 5 (PRMT5) and the WEE1 homologue

In various yeast species, the PRMT5 homologue Hsl7 was shown to interact with and promote degradation of WEE1 homologues to promote $G_2$ progression independently of its methyltransferase activity [230–232]. PRMT5 may also interact with WEE1 protein in human cells. It remains unknown if PRMT5 methylates WEE1 in any species. Upon DNA damage in human cells, WEE1 is upregulated and is able to induce $G_2$ arrest[233]. It is possible PRMT5 may also promote DNA damage-induced upregulation of WEE1 (which we evaluated in chapter 2)[1]. This would suggest opposing regulation of WEE1 expression by PRMT5: Under normal conditions, PRMT5 physically interacts (and potential methylates) WEE1 to promote degradation which facilitates $G_2$ progression. Upon DNA damage, PRMT5 activates transcription of WEE1 which facilitates $G_2$ arrest. In support, the PRMT5-medaited $G_2$ progression in the Xenopus egg is independent of transcription because Xenopus egg extracts can cycle without *de novo* mRNA transcription [232]. This opposing regulation of WEE1 potentially be explained by modulation of PRMT5 methyltransferase activity, substrate specificity, and/or the absence or presence of DNA damage.

Protein arginine methyltransferase 5 (PRMT5) in *Arabidopsis*

In plants (at least *Arabidopsis*), the PRMT5 homologue SKB1 is essential to maintain genome stability in root stem cells[234]. Plant root stem cells are undifferentiated cells located in the meristems that serve as precursors to differentiated tissues. Given their location, these root stem cells are often exposed to environmental stresses that can induce DNA damage[235]. Plant root stem cells may be particularly sensitive to DNA damage or at the very least undergo apoptotic cell death upon physiological levels of DSBs[235], which prevents mutations from being passed on to the growing underground tissues. The plant DDR, including differences to the human DDR, was recently reviewed[236], and it is important to note that homologues of human p53 and some

downstream proteins involved in apoptosis (including APAF1, BCL2, and caspases) have not been identified in plants[237]. Despite that, just like in humans the PRMT5 homologue SKB1 regulates both cell cycle arrest and apoptosis in plant root stem cells[234]. Root stem cells in SKB1 mutant *Arabidopsis* were more sensitive to DNA damage via both Methyl methanesulfonate (MMS, a radiomimetic compound that induces DSBs[238]) and hydroxyurea[234]. Elevated levels of γH2AX were found in SKB1 mutant plants in the absence of treatment[234], indicating that the PRMT5 homologue SKB1 is also required to prevent the formation of endogenous DSBs or the repair of endogenous DSBs in plants.

Little is known about the molecular mechanisms for the PRMT5 homologue SKB1 in both $G_2$ arrest and apoptosis in *Arabidopsis*. PRMT5 may post translationally regulate proteins. For example, there are two key transcription factors involved in plant stem cell maintenance: SHORTROOT (SHR) and SCARECROW (SCR)[239]. In response to DNA damage, the PRMT5 homologue SKB1 regulates the protein expression and localization of SHR to inhibit plant stem cell death[234]. This was likely a post-translational regulation because SHR expression was not affected at the transcriptional level. In contrast, the PRMT5 homologue SKB1 likely does not regulate SCR expression and localization upon DNA damage in plant stem cells. It is also possible that the PRMT5 homologue SKB1 epigenetically activates transcription of genes involved in DDR. For example, WEE1 and RAD51 are upregulated in response to IR at the mRNA level[240].

## 1.6 Clinical targeting of Protein arginine methyltransferase 5 (PRMT5)

### 1.6.1 *Protein arginine methyltransferase 5 (PRMT5) inhibitors for cancer treatment*

PRMT5 is overexpressed in several cancers, promotes cancer cell growth, and is associated with poor prognosis[105,110–112,119–129]. Thus, PRMT5 has been proposed as a potential therapeutic target for cancer treatment[119]. As of June 2020, there were 6 clinical trials for the use of 5 different PRMT5 inhibitors for cancer treatment (clinicaltrials.gov). The inhibitors in these clinical trials include two studies with GSK3326595 and one study with JNJ-64619178, PF-06939999, PRT543, and PRT811. The advances in PRMT5 inhibitor development have been updated recently[241–243]. Clinical trial and drug information is outlined in Appendix B.

PRMT5 inhibitors may be particularly effective for prostate cancer. AR signaling drives prostate cancer growth and is a therapeutic target for prostate cancer treatment[130,131]. Many studies

focus on developing therapeutics that inhibit AR signaling by blocking either production of androgens or AR itself[132–134]. In 2017, our lab reported that PRMT5 epigenetically activates AR transcription in hormone-naïve prostate cancer cells[114]. Targeting PRMT5 downregulated AR at the mRNA and protein level, inhibited growth of prostate cancer cells in an AR-dependent manner, and completely suppressed growth of xenograft tumors in mice. PRMT5 is overexpressed in ~60% of intermediate- and high-risk prostate cancer cases and PRMT5 expression also positively correlates with AR expression at both the mRNA and protein level in prostate cancer tissues clinically. Therefore, targeting PRMT5 may block AR protein expression and be an effective treatment method for prostate cancer.

PRMT5 inhibitors may be particularly effective for cancers with MTAP deletion. Recently, 3 studies performed genome-wide screens to identify potential therapeutic targets that would synergize with cancers with MTAP deletions[160–162]. PRMT5 and cofactors MEP50, pICln, and RioK1 were all identified suggesting that targeting PRMT5 inhibits growth of MTAP-deleted cancers. Mechanistically, MTAP deletion causes elevation of MTA which acts as a competitive inhibitor of PRMT5 by binging to the AdoMet/SAM binding pocket of PRMT5[162]. To compensate, cancer cells may upregulate PRMT5 expression or increase PRMT5 activity. Consequently, MTAP-deleted cancers are more reliant on PRMT5 signaling. MTAP is deleted in ~15% of all cancers and pre-screening for MTAP deletions may improve potential clinical use of PRMT5-targeting drugs.

### 1.6.2 *Approaches for targeting PRMT5*

There are several approaches for targeting PRMT5[241–243]. Current PRMT5 inhibitors are either SAM uncompetitive inhibitors or SAM competitive inhibitors. In brief, SAM uncompetitive inhibitors bind to the peptide binding pocket in the presence of SAM to inhibit PRMT5 methyltransferase activity. SAM competitive inhibitors are typically nucleosides that bind to the SAM binding pocket to prevent SAM from donating the methyl group involved in the enzymatic reaction. However, non-nucleoside SAM competitive small molecule PRMT5 inhibitors were recently published[244].

Another approach is targeting PRMT5 expression. This can be effectively achieved through proteolysis targeting chimera (PROTAC) technology which was first described in 2001[245]. PROTAC contains a molecule that binds to an E3 ubiquitin ligase covalently linked to another

molecule that binds the protein targeted for degradation. This brings the target protein into close proximity to the E3 ligase to promote degradation. However, this approach has not been applied to targeting PRMT5 clinically.

Targeted delivery could be applied to PRMT5 inhibitors including PROTAC inhibitors to limit the adverse effects. For prostate cancer, targeted delivery has already been achieved through PSMA-based delivery[246]. Future studies may identify delivery targets for different stages of the disease such as specific cell surface markers for prostate cancer NE-like cells.

A novel approach would be to target the protein-protein interaction with cofactors. Because the function of PRMT5 is modulated by several cofactors, protein-protein interaction inhibitors may increase specificity/selectivity towards specific contexts. For example, given that MEP50 is involved in the epigenetic activation of AR, a PRMT5:MEP50 protein-protein interaction inhibitor may be more effective in AR-expressing prostate cancer cells.

## 1.7 Conclusions and scope of dissertation

Prostate cancer is one of the most frequently diagnosed cancers in the world. Failure to manage localized disease contributes to the majority of prostate cancer deaths. RT is a potentially curative treatment used for over half of all cancer patients and is a common treatment option for localized prostate cancer. However, tumors recur and progress to a deadly disease for a significant portion of prostate cancer patients. Mechanistic studies detailing how cancer cells respond to RT may reveal novel therapeutic targets to enhance RT for prostate cancer treatment.

The cellular response to RT is multidimensional. For example, cells respond to a single dose of IR by activating the DDR to repair the DNA. Targeting proteins involved in the DDR is an effective clinical strategy to sensitize cancer cells to RT. However, multiple radiation treatments/FIR, can promote NED. FIR-induced NED is an emerging resistance mechanism to RT and tumors that undergo NED are highly aggressive and remain incurable. Therefore, mechanistic studies on RT should focus on both a single dose and multiple doses of IR.

Currently, the only clinical approach to improve RT for prostate cancer treatment is ADT. ADT blocks androgen receptor (AR) signaling which inhibits the repair of DNA damage. In 2017, our lab reported that PRMT5 epigenetically activates AR transcription and targeting PRMT5 downregulates AR at the mRNA and protein level. Clinically, PRMT5 is overexpressed in ~60% of intermediate- and high-risk prostate cancer cases and PRMT5 expression also positively

correlates with AR expression in prostate cancer tissues. Therefore, targeting PRMT5 may block AR protein expression to mimic ADT and sensitize prostate cancer cells to RT.

Because PRMT5 appears to be a promising therapeutic target, we analyzed the role of PRMT5 in the cellular response to IR. This dissertation focuses on the role of PRMT5 in both the DDR following a single dose of IR and in FIR-induced NED. Our goal is to validate PRMT5 as a therapeutic target to enhance RT for prostate cancer treatment. We demonstrate that PRMT5 has several roles in the cellular response to IR. Upon a single dose of IR, PRMT5 cooperates with pICln to function as a master epigenetic activator of DDR genes. During FIR, PRMT5, along with cofactors MEP50 and pICln, are essential for initiation of NED, maintenance of NED, and cell survival. Overall, this work provides strong evidence for PRMT5 as a therapeutic target. As several PRMT5 inhibitors are already in clinical trials, our work also suggests that targeting PRMT5 during RT should be assessed clinically.

# CHAPTER 2. PRMT5 FUNCTIONS AS A MASTER EPIGENETIC ACTIVATOR OF DNA DOUBLE-STRAND BREAK REPAIR GENES

The following chapter was reproduced and modified with permission from[1]:

Owens, J. L. et al. PRMT5 Cooperates with pICln to Function as a Master Epigenetic Activator of DNA Double-Strand Break Repair Genes. iScience 23, 100750 (2020).

## 2.1 Summary

DNA double-strand break (DSB) repair is critical for cell survival and genome integrity. Upon recognition of DSBs, repair proteins are transiently upregulated to facilitate repair through homologous recombination (HR) or non-homologous end joining (NHEJ). We present evidence that PRMT5 functions as a master epigenetic activator of DNA damage response (DDR) genes involved in HR, NHEJ, and $G_2$ arrest (including RAD51, BRCA1, and BRCA2). PRMT5 is required to maintain basal expression of DDR genes as well as facilitates the transient upregulation of DDR genes upon DNA damage. Targeting PRMT5 hinders repair of DSBs in multiple cancer cell lines, and PRMT5 expression positively correlates with DDR genes across 32 clinical cancer data sets encompassing cancers throughout the entire body. Thus, targeting PRMT5 may be explored in combination with radiation or chemotherapy for cancer treatment.

## 2.2 Introduction

Repair of DNA double-strand breaks (DSBs), the most lethal DNA damage, is critical for cell survival and maintenance of genome integrity[247]. DSBs can be induced both endogenously as well as exogenously through DNA damaging agents or ionizing radiation (IR). Upon recognition of extensive DSBs, repair proteins are upregulated[164–166] and recruited to the sites of damage to facilitate repair through either homologous recombination (HR) or non-homologous end joining (NHEJ)[163]. Although the highly regulated recruitment and action of repair proteins are well-characterized, little is known about how their expression is induced upon DNA damage.

Protein arginine methyltransferase 5 (PRMT5) is an emerging epigenetic enzyme that regulates cellular processes including cell proliferation, differentiation, and cell cycle progression[110,111]. PRMT5 regulates these cellular processes through changes in gene expression via symmetrical dimethylation of arginine residues in histones H4R3 (H4R3me2s), H3R2

(H3R2me2s), H3R8 (H3R8me2s), and H2AR3 (H2AR3me2s), and post-translational regulation of non-histone substrates[110]. Accumulating evidence suggests that PRMT5 may act as an oncogene to promote cancer cell growth[110,111]. Consistent with this, PRMT5 is overexpressed in several cancers and its elevated expression correlates with disease progression and poor prognosis[105,110,111]. Thus, PRMT5 has been proposed as a potential therapeutic target for cancer treatment[119].

We have recently reported that PRMT5 is overexpressed in ~60% of intermediate- and high-risk prostate cancer cases and that PRMT5 expression in prostate cancer tissues positively correlates with androgen receptor (AR) expression[114]. Mechanistically, PRMT5 is recruited to the AR promoter to activate AR transcription through H4R3me2s in prostate cancer cells[114]. Because AR drives prostate cancer development and progression, targeting AR signaling through androgen deprivation therapy (ADT) is a standard of care to treat metastatic prostate cancer[248]. ADT is also used as a radiosensitization approach to enhance radiation therapy (RT) for localized prostate cancer patients[42]. Our finding that PRMT5 activates AR transcription raised the possibility that PRMT5 may be a therapeutic target for prostate cancer radiosensitization.

Contrary to our expectation, we observed that targeting PRMT5 sensitized prostate cancer cells to IR independently of AR expression. Here, we present evidence that PRMT5 functions as a master epigenetic activator of DNA damage response (DDR) genes in various cell types. Upon DNA damage, PRMT5 upregulates target genes that encode proteins involved in HR (RAD51, RAD51D, RAD51AP1, BRCA1, and BRCA2), NHEJ (NHEJ1/XLF and DNAPKcs), and $G_2$ arrest (WEE1). Targeting PRMT5 decreases expression of these DDR genes and hinders repair of DSBs in multiple cancer cell lines suggesting that PRMT5 may play a conserved role in DDR. Thus, targeting PRMT5 may be explored as a monotherapy or in combination with radiation or chemotherapy for cancer treatment. Significantly, PRMT5 expression positively correlates with the expression of these target genes across most of the 32 clinical cancer data sets analyzed. Although PRMT5 primarily functions as an epigenetic repressor, our results demonstrate that PRMT5 can activate gene expression and provide a potential mechanism for the transient upregulation of repair proteins upon DNA damage.

## 2.3 Results

### 2.3.1 *Targeting PRMT5 sensitizes prostate cancer cells to IR in an AR-independent manner*

ADT is the only approved clinical radiosensitization approach for prostate cancer treatment[42]. Because we recently identified PRMT5 as a novel epigenetic activator of AR[114], we tested whether targeting PRMT5 can mimic ADT to sensitize prostate cancer cells to IR. To this end, we established lentivirally infected stable pools with doxycycline (Dox)-inducible PRMT5 knockdown and observed that knockdown of PRMT5 sensitized AR-expressing LNCaP prostate cancer cells (LNCaP-shPRMT5 pool) to IR when compared to scramble control cell lines (LNCaP-shSC) (Figure 2.1A). Likewise, inhibition of PRMT5 by our inhibitor BLL3.3[114,249] also sensitized LNCaP cells to IR (Figure 2.1B). Consistent with previous findings that AR regulates several target genes involved in NHEJ[43,45,46], pharmacological inhibition of PRMT5 with BLL3.3 in irradiated LNCaP cells indeed caused a decrease in AR expression and a concomitant decrease in the expression of Ku80/XRCC5, XRCC4, and DNAPKcs/PRKDC at the mRNA level (Figure 2.1C). Contrary to our expectation, knockdown of PRMT5 also sensitized AR-negative prostate cancer cell lines PC3 and DU145 to IR when similar Dox-inducible knockdown stable cell lines (PC3-shPRMT5 pool and DU145-shPRMT5 pool) were used (Figures 2.1D and 2.1E). However, BLL3.3 treatment had little to no effect on the expression of AR-target genes involved in NHEJ in irradiated AR negative DU145 cells (Figure 2.1F). Given these results, we isolated single-cell-derived clones to develop Dox-inducible knockdown stable cell lines (LNCaP-shPRMT5 and LNCaP-shPRMT5 #2) for all subsequent studies. Dox-induced PRMT5 knockdown is shown in Figures S2.3B-S2.3F and is reported previously[114]. These results suggest that the radiosensitization effect of PRMT5 targeting in prostate cancer cells is likely mediated through both AR-dependent and -independent mechanisms.

### 2.3.2 *PRMT5 regulates the repair of DNA double-strand breaks (DSBs) in prostate cancer cells independently of AR expression*

Next, we determined if the radiosensitization effect of PRMT5 targeting was due to defects in the repair of IR-induced DSBs. We first treated LNCaP cells with IR and quantified DSBs via γH2AX foci analysis to assess the formation and repair of IR-induced DSBs. The majority of DSBs were repaired within 2-6 h following IR treatment (Figures 2.2A and 2.2B). To assess if PRMT5 is required for efficient repair of IR-induced DSBs, we analyzed γH2AX foci 6 h following IR in

more detail. Cells with PRMT5 knockdown retained significantly more DSBs 6 h following IR treatment than cells without knockdown, indicating a defect in DSB repair (Figures 2.2C and 2.2D). Nearly identical results were obtained using a different PRMT5-targeting shRNA (LNCaP-shPRMT5 #2) (Figures 2.2E and 2.2F). Treatment of LNCaP cells with BLL3.3 conferred the same effect as PRMT5 knockdown (Figures 2.2G and 2.2H) while Dox-induced expression of scramble control (SC) shRNA in LNCaP-shSC cells had no effect (Figures 2.2I and 2.2J). Cells with PRMT5 knockdown retained significantly more γH2AX foci even 24 h following IR treatment than cells without knockdown (Figures 2.2K and 2.2L), indicating a prolonged defect in DSB repair. The defects in DSB repair upon PRMT5 knockdown were unlikely an artifact of crosstalk between histone posttranslational modifications as we observed similar results when quantifying DNA damage directly via comet assay (Figures S2.1A-S2.1D). Furthermore, knockdown of PRMT5 also hinders repair of etoposide-induced DSBs (Figures S2.2A-S2.2F) which differ in their mechanism of DSB generation and are replication-dependent[250–252], suggesting that PRMT5 may be required for repair of DSBs independently of how they are formed. Thus, the radiosensitization effect of PRMT5 targeting in prostate cancer cells is likely due to defects in the repair of IR-induced DSBs.

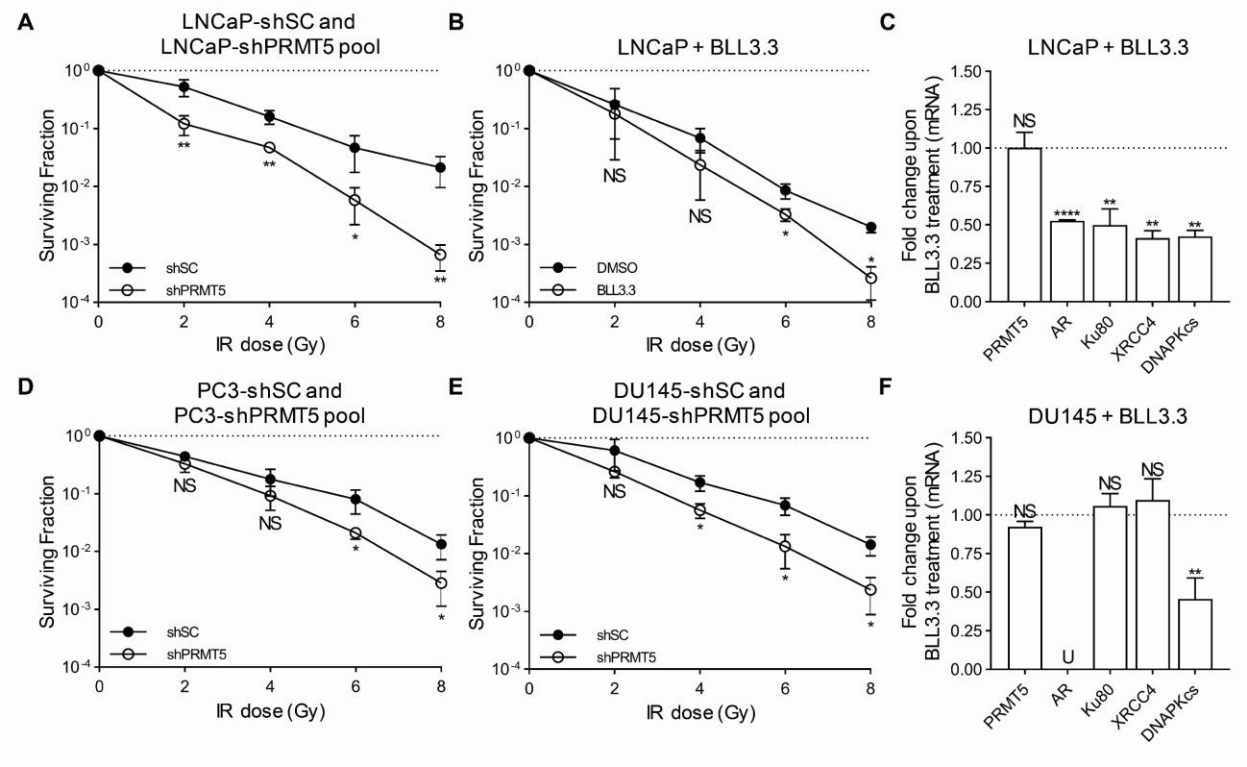


**Figure 2.1: Targeting PRMT5 sensitizes prostate cancer cells to IR in an AR-independent manner**

**(A**, **B**, **D**, and **E)** Quantification of the surviving fraction via clonogenic assay immediately following the indicated dose of IR in the indicated cell lines. Dox treatment was used to express PRMT5-targeting shRNA (shPRMT5) or scramble control-targeting shRNA (shSC). BLL3.3 treatment was used to inhibit PRMT5 activity (**A:** LNCaP-shPRMT5/shSC, **B**: LNCaP + DMSO/BLL3.3, **D**: PC3-shPRMT5/shSC **E**: DU145-shPRMT5/shSC).
**(C** and **F)**, Quantification of mRNA via RT-qPCR 24 h post 2 Gy IR in LNCaP (**C**) and DU145 (**F**) cells. For each biological replicate, the value for BLL3.3 was normalized to the value for DMSO to calculate the fold change in mRNA expression upon PRMT5 inhibition.

Points in **A**, **B**, **D**, and **E** are the mean ± s.d. of 3 independent experiments. Bars in **C** and **F** are the mean ± s.d. of 3 independent experiments. Statistical analysis for **A**, **B**, **D**, and **E** comparing experimental to the control ('shSC' or 'DMSO') was performed using Welch's *t*-test of log-transformed data while statistical analysis for **C** and **F** comparing experimental to the control ('DMSO') was performed using Welch's *t*-test (* $P \leq 0.05$; ** $P \leq 0.01$, *** $P \leq 0.001$, **** $P \leq 0.0001$, NS $P > 0.05$, U = undetected).

To further confirm that PRMT5 also regulates the repair of IR-induced DSBs independently of AR, we performed rescue experiments. Although exogenously expressed AR in Dox-treated LNCaP-shPRMT5 cells fully rescued AR protein levels (Figures 2.2M and 2.2N), the repair of IR-induced DSBs was only partially rescued (Figures 2.2O and 2.2P). Thus, PRMT5 can also regulate repair of IR-induced DSBs through an AR-independent mechanism.

### 2.3.3 *PRMT5 regulates NHEJ, HR, and $G_2$ arrest in response to IR*

The ability to repair DSBs is mainly dependent on NHEJ and HR as well as $G_1$ and $G_2$ cell cycle arrest. We next analyzed IR-induced Ku70 and RAD51 foci formation to examine if PRMT5 knockdown would affect NHEJ or HR repair, respectively. Consistent with the finding that targeting PRMT5 causes a decrease in AR-target genes involved in NHEJ, PRMT5 knockdown decreased IR-induced Ku70 foci formation (Figures 2.3A and 2.3B) indicating that PRMT5 regulates NHEJ. Interestingly, PRMT5 knockdown also decreased IR-induced RAD51 foci formation (Figures 2.3C and 2.3D) confirming that PRMT5 regulates HR repair of IR-induced DSBs as well.

We next investigated whether PRMT5 knockdown has any effect on cell cycle. Consistent with previous findings[126,184,215,216], cells with PRMT5 knockdown had an increase in the $G_1$ population and a concomitant decrease in the S population in the absence of IR (Figure 2.3E) indicative of $G_1$ arrest. Upon IR treatment, cells with PRMT5 knockdown retained the ability to undergo IR-induced $G_1$ arrest (or already arrested in $G_1$ phase due to PRMT5 knockdown prior to IR) yet failed to arrest at $G_2$ (Figure 2.3F). This result suggests that PRMT5 regulates IR-induced $G_2$ arrest but may not be required for IR-induced $G_1$ arrest. Overall, our findings that PRMT5 can regulate repair of IR-induced DSBs through an AR-independent mechanism and that targeting PRMT5 sensitizes prostate cancer cells to IR independently of AR expression are likely due to the regulation of multiple DDR pathways by PRMT5.

### 2.3.4 *PRMT5 regulates DNA damage response (DDR) pathways*

Because PRMT5 is an emerging epigenetic regulator[110,111], we reasoned that PRMT5 may regulate the expression of genes involved in the repair of DSBs. We performed RNA-seq analysis of both non-irradiated (IR-) and irradiated (IR+) LNCaP-shPRMT5 cells with PRMT5 knockdown (Dox+) and without PRMT5 knockdown (Dox-). We identified 2,036 differentially expressed genes (DEGs) upon PRMT5 knockdown in IR- cells and 1,710 DEGs in IR+ cells (Figure 2.4A). Comparing the IR- and IR+ data sets, we determined that 886 genes were differentially regulated only in IR+ cells, of which 563 were downregulated (Figure 2.4B). Consistent with our functional studies, multiple genes encoding repair proteins in HR and NHEJ, and genes involved in $G_2$ arrest were identified as DEGs. Using Gene Ontology (GO) analysis, we identified several GO functions

and KEGG pathways associated with DDR such as 'DNA damage repair' and 'cell cycle regulation' that were significantly over-represented in IR+ only DEGs (Figure 2.4C). Ingenuity pathway analysis (IPA) of the IR+ only DEGs conferred similar outcomes as GO analysis and further revealed that PRMT5 likely regulates genes involved in $G_2$ arrest as well as repair proteins such as BRCA1 and BRCA2 (Figure 2.4D). Results from our RNA-seq analysis suggest PRMT5 regulates expression of DDR genes in response to IR.

**Figure 2.2: PRMT5 regulates the repair of DNA double-strand breaks (DSBs) in prostate cancer cells independently of AR expression**

**(A)** Time-course of the formation and repair of DSBs (γH2AX foci) at the indicated minutes (m) or hours (h) post 2 Gy IR in LNCaP cells.
**(B)** Quantification of DSBs in each individual cell from **A**: 'average' indicates the average number of DSBs in each cell and '0 foci' indicates the percentage of cells that do not contain any DSBs.
**(C**, **E**, **G**, **I**, and **K)** DSBs 6 h or 24 h post 2 Gy IR in the indicated cells (**C**: LNCaP-shPRMT5, **E**: LNCaP-shPRMT5 #2, **G**: LNCaP, **I**: LNCaP-shSC, **K**: LNCaP-shPRMT5) with (Dox+) and without (Dox-) PRMT5 knockdown/scramble control (SC) knockdown or with (BLL3.3) and without (DMSO) PRMT5 inhibition.
**(D**, **F**, **H**, **J**, and **L)** Quantification of DSBs from **C**, **E**, **G**, **I**, and **K** as described above.
**(M)** LNCaP-shPRMT5 cells were co-transfected with plasmids encoding Flag-AR (AR) or empty vector (EV) and a plasmid encoding cerulean fluorescent protein (CFP). Fluorescence images acquired 6 h post 2 Gy IR are representative immunocytochemistry images in 3D where each peak is a cell and the height of each peak is the intensity of signal. Blue peaks represent transfected CFP-expressing cells (CFP+). Colors are indicated as follows: endogenous PRMT5 (red), endogenous and exogenous AR (green), and exogenous CFP (cerulean).
**(N)** Quantification of protein intensity from **M** in untransfected (CFP-) and transfected (CFP+) cells. For each biological replicate, values were normalized to the value for 'Dox- / EV' to calculate the fold change in protein expression upon treatment.
**(O)** DSBs at 6 h post 2 Gy IR in LNCaP-shPRMT5 cells where AR expression was rescued via co-transfection with plasmids encoding Flag-AR (AR) or empty vector (EV) and a plasmid encoding Cerulean fluorescent protein (CFP) as a transfection control.
**(P)** Quantification of DSBs in transfected cells (defined as CFP+) from **O** as described above.

Fluorescence images in **A**, **C**, **E**, **G**, **I**, and **K** are representative immunocytochemistry images (blue = DAPI, green = γH2AX, red = PRMT5). Fluorescence images in **M** are representative immunocytochemistry images (red = PRMT5, green = AR, and blue = CFP). Fluorescence images in **O** are representative immunocytochemistry images (blue = DAPI, green = γH2AX, red = AR, Cerulean = CFP). All bars are the mean ± s.d. of 4 independent experiments. Statistical analysis for **B**, **N**, and **P** comparing experimental to the control ('IR-', 'Dox-', 'DMSO', or 'Dox-,EV') was performed using Brown-Forsythe and Welch ANOVA followed by Dunnett's T3 multiple comparisons test while statistical analysis for **D**, **F**, **H**, **J**, and **L** comparing experimental to the control ('Dox-' or 'DMSO') was performed using Welch's *t*-test (* $P \leq 0.05$; ** $P \leq 0.01$, *** $P \leq 0.001$, **** $P \leq 0.0001$, NS $P > 0.05$).

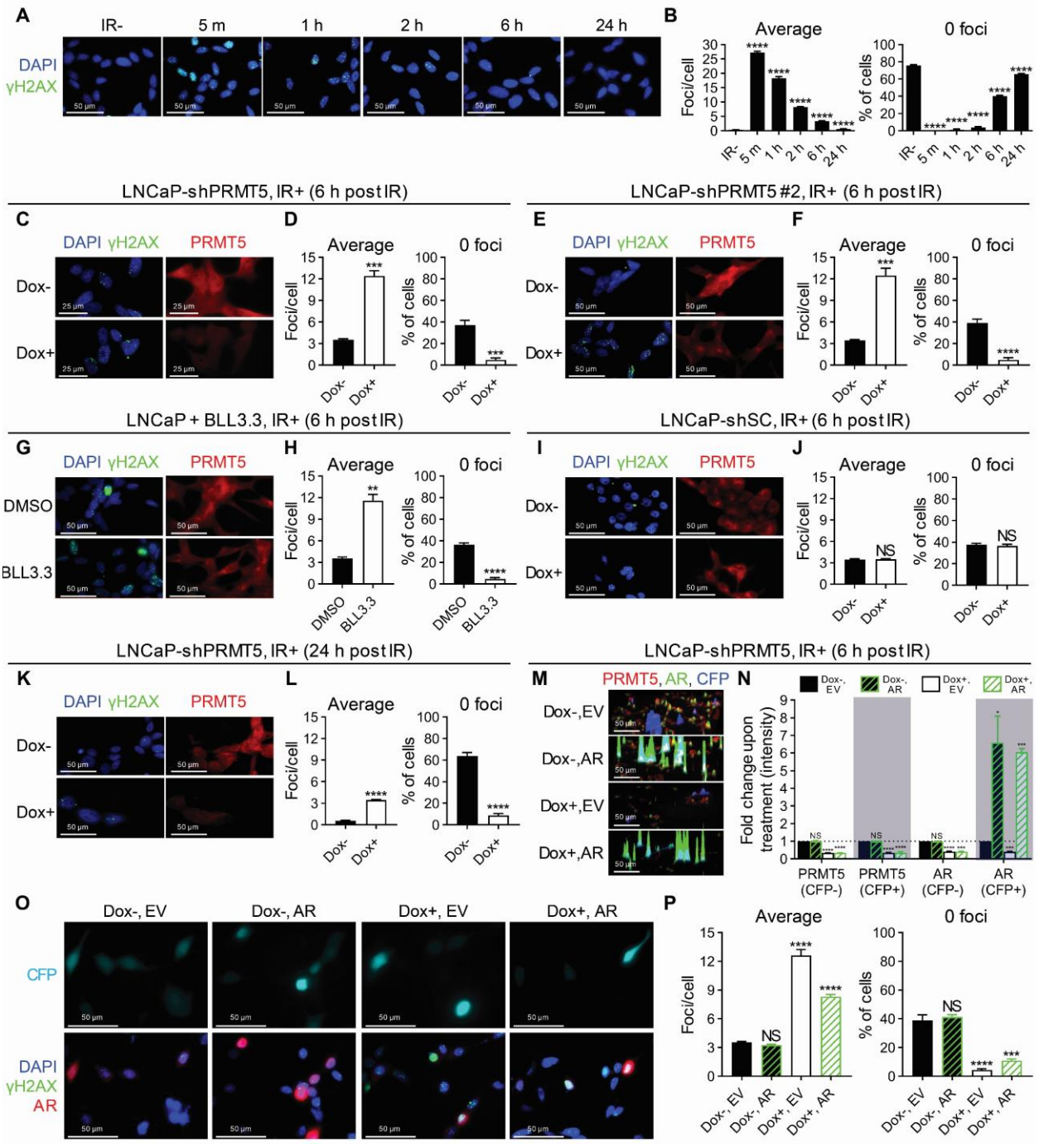
A
IR-
5 m
1 h
2 h
6 h
24 h
DAPI
γH2AX
B
Average
0 foci
Foci/cell
% of cells
LNCaP-shPRMT5, IR+ (6 h post IR)
LNCaP-shPRMT5 #2, IR+ (6 h post IR)
C
D
E
F
DAPI γH2AX PRMT5
Dox-
Dox+
LNCaP + BLL3.3, IR+ (6 h post IR)
LNCaP-shSC, IR+ (6 h post IR)
G
H
I
J
DMSO
BLL3.3
NS
LNCaP-shPRMT5, IR+ (24 h post IR)
LNCaP-shPRMT5, IR+ (6 h post IR)
K
L
M
N
PRMT5, AR, CFP
Dox-,EV
Dox-,AR
Dox+,EV
Dox+,AR
Fold change upon treatment (intensity)
PRMT5 (CFP-)
PRMT5 (CFP+)
AR (CFP-)
AR (CFP+)
O
Dox-, EV
Dox-, AR
Dox+, EV
Dox+, AR
CFP
DAPI
γH2AX
AR
P

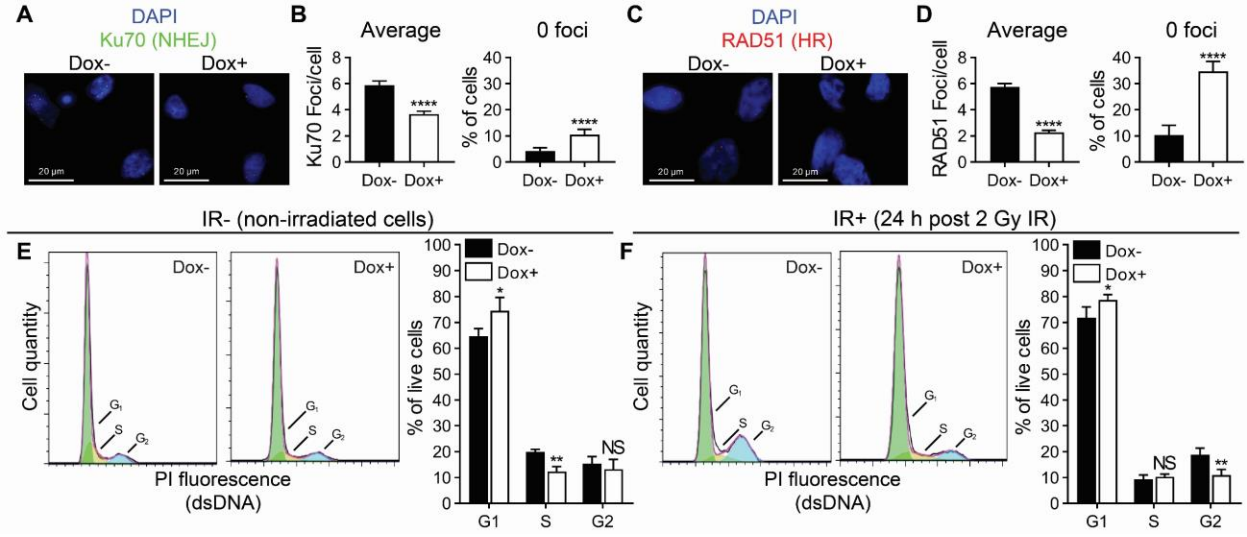


**Figure 2.3: PRMT5 regulates NHEJ, HR, and $G_2$ arrest in response to IR**

**(A)** NHEJ repair foci (Ku70) 1 h post 2 Gy IR in LNCaP-shPRMT5 cells with (Dox+) and without (Dox-) PRMT5 knockdown.
**(B)** Quantification of Ku70 foci from **A** as described in **Figure 2.2B**.
**(C)** HR repair foci (RAD51) 1 h post 2 Gy IR in LNCaP-shPRMT5 cells with (Dox+) and without (Dox-) PRMT5 knockdown.
**(D)** Quantification of RAD51 foci from **C** as described in **Figure 2.2B**.
**(E)** Cell cycle analysis via flow cytometry of propidium iodide (PI) stained LNCaP-shPRMT5 cells with (Dox+) and without (Dox-) PRMT5 knockdown.
**(F)** Cell cycle analysis via flow cytometry of PI stained LNCaP-shPRMT5 cells 24 h post 2 Gy IR, with (Dox+) and without (Dox-) PRMT5 knockdown.

Fluorescence images in **A** and **C** are representative immunocytochemistry images (blue = DAPI, green = Ku70, red = RAD51). Bars in **B** and **D** are the mean ± s.d. of 3 independent experiments while bars in **E** and **F** are the mean ± s.d. of 4 independent experiments. Graphs in **E** and **F** are representative flow traces of cells in various cell cycle stages (green = $G_1$, orange = S, blue = $G_2$). Statistical analysis comparing experimental to the control ('Dox-') was performed using Welch's *t*-test (* $P \leq 0.05$; ** $P \leq 0.01$, *** $P \leq 0.001$, **** $P \leq 0.0001$, NS $P > 0.05$).

### 2.3.5 *PRMT5 activates transcription of genes that encode proteins involved in the repair of DNA double-strand breaks (DSBs)*

Next, we sought to validate a potential role for PRMT5 in regulating the transcription of genes required for DSB repair. Notably, we identified 6 DEGs that encode repair proteins (RAD51, RAD51D, RAD51AP1, BRCA1, BRCA2, and NHEJ1/XLF) and the regulation of these genes by PRMT5 in both irradiated and non-irradiated cells was verified by reverse transcriptase quantitative real-time PCR (RT-qPCR) (Figures 2.5A and S2.3A) and western blot (Figures S2.3B-S2.3F) (additional genes were also individually verified at the mRNA level in Figure S2.3G). IR induces the expression of these genes at both the mRNA (Figure 2.5B) and protein level (Figures S2.3B-S2.3F) on a timescale consistent with the repair of IR-induced DSBs, suggesting that

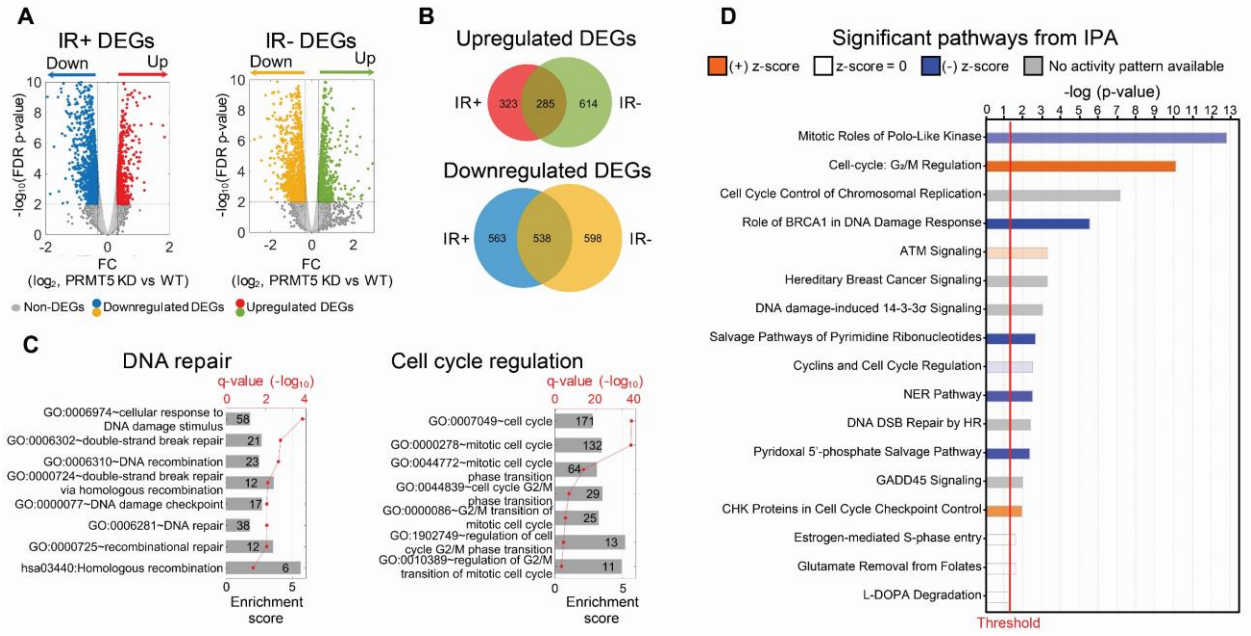


**Figure 2.4: PRMT5 regulates DNA damage response (DDR) pathways**

**(A)** RNA-seq analysis to identify DEGs upon PRMT5 knockdown in LNCaP cells. Gene expression was compared 1 h post 2 Gy IR in irradiated (IR+) and non-irradiated (IR-) LNCaP-shPRMT5 cells with (Dox+) and without (Dox-) PRMT5 knockdown. The volcano plot shows genes based on statistical significance (false discovery rate, FDR-corrected p-values) vs fold change (FC, in logarithm scale with base 2) between PRMT5 knockdown and WT in IR+ and IR- cells, respectively. Upregulated DEGs (red or green) and downregulated DEGs (blue or yellow) are indicated in color.
**(B)** Venn diagram indicating the overlap of DEGs between IR+ (red or blue) and IR- (green or yellow) samples.
**(C)** Gene ontology (GO) enrichment analysis of IR+ only DEGs that were downregulated upon PRMT5 knockdown. Groups of GO terms related to DNA repair and cell cycle regulation were identified to be significantly over-represented in the DEG set. The height of each bar represents the enrichment score for the GO term, while the q-value (FDR-corrected p-value) in red indicates the significance of enrichment. The number in the bar indicates the number of DEGs associated with the corresponding GO annotation.
**(D)** IPA analysis of IR+ only DEGs that were downregulated upon PRMT5 knockdown. The pathways with the highest significance are shown and the bars represent the degree of significance in terms of -log (*p*-value). Pathways shown in blue (negative z-score) are inhibited upon PRMT5 knockdown while pathways in orange (positive z-score) are activated upon PRMT5 knockdown.

PRMT5-mediated upregulation of these genes upon IR is critical for DSB repair. The regulation of positive control genes by PRMT5 was also confirmed: knockdown of PRMT5 prevented repression of IVL expression[253] and prevented activation of AR expression[114] (Figures 2.5A and S2.3G). As expected, IR did not affect expression of IVL or AR at the mRNA level (data not shown).

Chromatin immunoprecipitation (ChIP)-qPCR assays using LNCaP-shSC and LNCaP-shPRMT5 cell lines confirmed that PRMT5 indeed bound to the proximal promoter regions of these 6 genes that encode for repair proteins (Figures 2.5C and S2.4A). IR treatment further

increased the binding of PRMT5 at a time point prior to the upregulation of these genes (Figures 2.5C and S2.4A). Consistent with potential epigenetic activation of these genes by PRMT5, the promoter regions of these genes were selectively enriched with PRMT5-catalyzed H4R3me2s (but not H3R2me2s, H3R8me2s, or H2AR3me2s) as well as the activating histone modification H3K9ac, both of which were induced by IR (Figures 2.5D, 2.5E, and S2.4B-S2.4F). Consistent with our previous finding[114], PRMT5 binding and the enrichment of H4R3me2s and H3K9ac at the proximal promoter region, but not a distal region, of the AR gene were also confirmed (Figures 2.5C-2.5E and S2.4A-S2.4F). To confirm the specificity of our ChIP experiments, we repeated experiments after knocking down PRMT5. PRMT5 knockdown decreased both PRMT5 binding and enrichment of H4R3me2s and H3K9ac at the proximal promoter regions further supporting the specificity of our ChIP assays and suggesting that PRMT5 contributes to transcriptional activation of these genes via methylation of H4R3 (Figures S2.4A-S2.4F). Collectively, these data demonstrate that PRMT5 is required to maintain basal expression of DDR genes, and PRMT5 facilitates the IR-induced transient upregulation of DDR genes by activating their transcription.

Given that PRMT5 was required for IR-induced $G_2$ arrest, we also sought to validate putative PRMT5 target genes involved in the regulation of $G_2$/M transition (DEGs: CCNB2, CDC20, CDC25C, CDK1, and WEE1). RT-qPCR analysis demonstrated that PRMT5 knockdown decreased their expression in both non-irradiated and irradiated cells (Figures 2.5F and S2.3G). Interestingly, ChIP-qPCR assay results suggest that out of the 5 putative target genes, WEE1 may be the only direct target gene of PRMT5 (Figures 2.5G-2.5I and S2.4A-S2.4F). Since CCNB2, CDC20, CDC25C, and CDK1 are typically activators of $G_2$ progression and WEE1 is an activator of $G_2$ arrest, it is possible that PRMT5 actively regulated WEE1 expression while the changes in CCNB2, CDC20, CDC25C, and CDK1 expression were a secondary effect. Therefore, although positive and negative regulators of $G_2$ arrest were downregulated at the mRNA level upon PRMT5 knockdown, the net phenotypic effect is impaired IR-induced $G_2$ arrest.

### 2.3.6 *The transcriptional regulation of double-strand break (DSB) repair genes by PRMT5 is not dependent on RuvBL1 or Tip60*

While this study was ongoing, *Clarke et al.* reported that PRMT5 participates in the DSB repair choice process and promotes HR through methylation of RuvBL1: Methylation of RuvBL1 by PRMT5 alters the RuvBL1:Tip60 complex, promotes Tip60-mediated acetylation of histone

H4K16, demotes 53BP1 binding to DSBs, and initiates DSB repair via HR[177]. We sought to confirm that the mechanism we describe here is independent of RuvBL1 and Tip60. We determined that knockdown of RuvBL1 did not affect expression of PRMT5, RAD51, RAD51D, RAD51AP1, NHEJ1, and Tip60 at the protein level (Figures S2.5A and S2.5B), nor did it affect the efficiency of repair of IR-induced DSBs in LNCaP cells (Figures S2.5C and S2.5D). This is consistent with another study reporting that knockdown of RuvBL1 had no effect on IR-induced 53BP1 foci in hematopoietic cells[180]. Therefore, methylation of RuvBL1 by PRMT5 likely affects DSB repair choice (favoring HR over NHEJ) but not the overall efficiency of repair, whereas the transcriptional activation of DDR genes by PRMT5 is likely required for repair of DSBs.

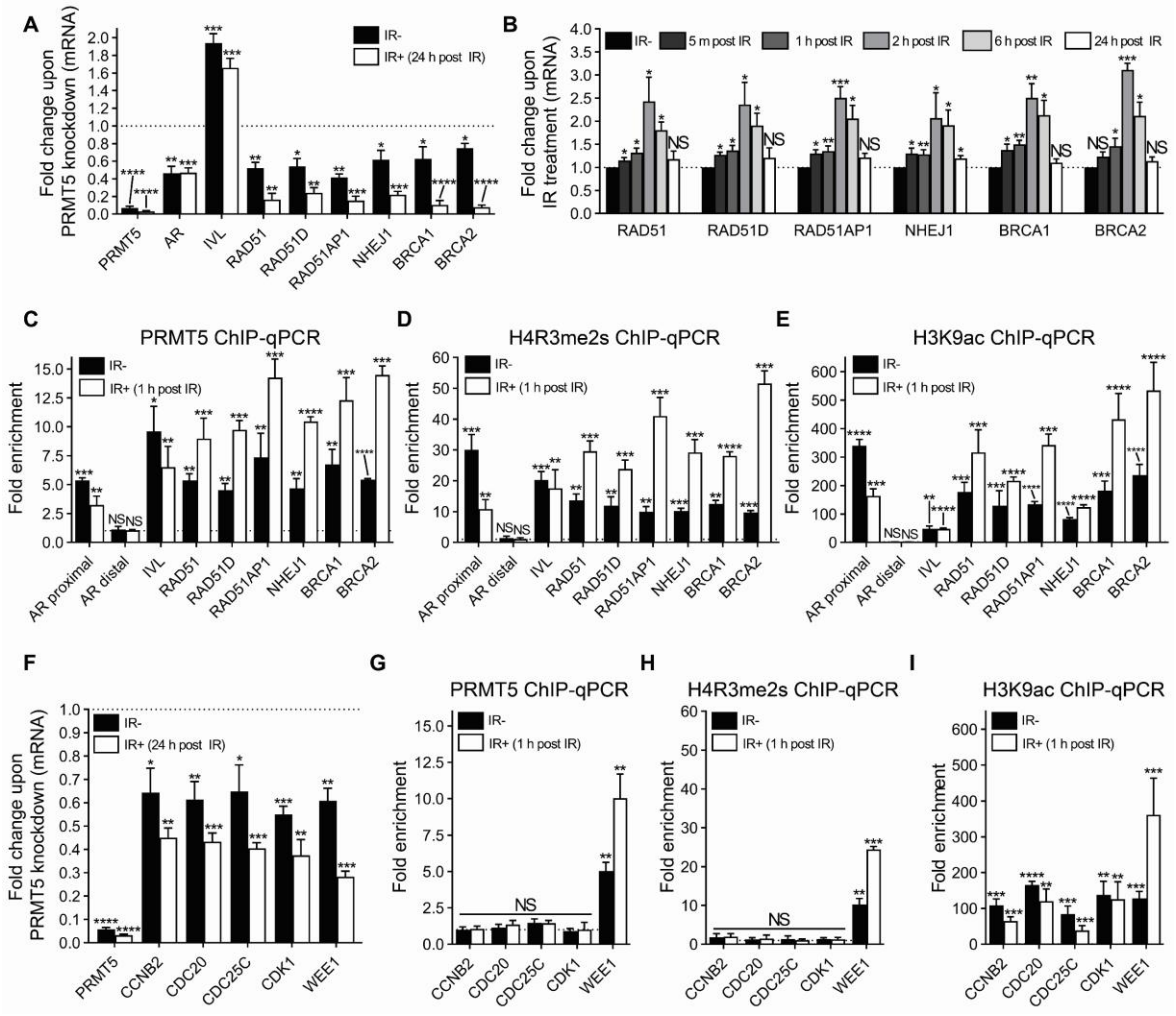


**Figure 2.5: PRMT5 activates transcription of genes that encode proteins involved in the repair of DNA double-strand breaks (DSBs)**

**(A)** and (**F)**, Quantification of mRNA via RT-qPCR 24 h post 2 Gy IR in LNCaP-shPRMT5 cells with (Dox+) and without (Dox-) PRMT5 knockdown. For each biological replicate, the value for Dox+ was normalized to the value for Dox- to calculate the fold change in mRNA expression upon PRMT5 knockdown in both irradiated (IR+) and non-irradiated cells (IR-) (See also **Figure S2.3G**).
**(B)** Quantification of mRNA via RT-qPCR at the indicated time points post IR in irradiated (IR+) and non-irradiated (IR-) LNCaP-shPRMT5 cells without PRMT5 KD. For each biological replicate, the value for IR+ was normalized to the value for IR- to calculate the fold change in mRNA expression upon IR treatment (See also **Figure S2.3A** for experiments with PRMT5 KD).
**(C)-(E)** and (**G)-(I)**, Quantification of enrichment (**C** and **G**: PRMT5, **D** and **H**: H4R3me2s, and **E** and **I**: H3K9ac) at the promoter region of the indicated genes 1 h post 2 Gy IR via ChIP-qPCR in irradiated (IR+) and non-irradiated (IR-) LNCaP-shSC cells via ChIP-qPCR. For each biological replicate, the value for IP was normalized to the value for IgG to calculate the fold enrichment (See also **Figure S2.4**).

All bars are the mean ± s.d. of 3 independent experiments. Statistical analysis for **A**, **B**, and **F** comparing experimental to the control ('Dox-' or 'IR-') was performed using Brown-Forsythe and Welch ANOVA followed by Dunnett's T3 multiple comparisons test while Statistical analysis for **C**-**E** and **G**-**I** comparing experimental to the control ('IgG') was performed using Welch's *t*-test (* $P \leq 0.05$; ** $P \leq 0.01$, *** $P \leq 0.001$, **** $P \leq 0.0001$, NS $P > 0.05$).

Similarly, while this study was ongoing, *Hamard et al.* also reported that PRMT5 regulates DSB repair choice via splicing of Tip60 in hematopoietic cells: PRMT5 is required for appropriate splicing of Tip60, which in turn allows for normal Tip60 acetyltransferase activity, demotes 53BP1 binding to DSBs, and initiates DSB repair via HR[180]. Knockdown of Tip60 did not affect the expression of PRMT5 or the putative PRMT5 target genes we characterized (Figures S2.5E and S2.5F), suggesting that PRMT5-assoicated splicing of Tip60 does not affect the regulation of DDR genes by PRMT5. Given the role of Tip60 in DDR, PRMT5-assoicated splicing of Tip60 likely regulates DSB repair choice but not DSB repair efficiency, or at least does not affect PRMT5-associated transcriptional regulation of genes involved in DDR.

### 2.3.7 *PRMT5 regulates the expression of DNA damage response (DDR) genes and is required to repair IR-induced double-strand breaks (DSBs) in multiple cell types*

To extend our findings and determine if the role of PRMT5 in DSB repair is conserved across multiple cell types, we performed similar experiments in AR-negative prostate cancer cells (DU145), luminal breast cancer cells (MCF7), glioblastoma cells (U87MG), and non-cancerous HEK293T cells. Inhibition of PRMT5 by BLL3.3 hindered repair of IR-induced DSBs in all of these cell types as the cells retained significantly more γH2AX foci 6 h following IR treatment (Figures 2.6A and S2.6A-S2.6E). Although DDR genes were generally upregulated upon IR, targeting PRMT5 also caused a decrease in the expression of PRMT5 target genes involved in DSB repair in both irradiated and non-irradiated cells (Figures 2.6B and S2.6F-S2.6J). These results suggest that PRMT5 may function as a key regulator of DSB repair in multiple cell types.

### 2.3.8 *PRMT5 expression positively correlates with DNA damage response (DDR) genes in human cancer tissues*

To assess potential clinical significance of our findings, we analyzed mRNA expression in 32 clinical cancer data sets achieved from The Cancer Genome Atlas (TCGA) Pan-Cancer analysis[254]. We focused on PRMT5, AR, and DDR genes which were identified as primary target genes of both PRMT5 and AR. The expression of PRMT5 correlated positively with DDR genes in almost all cancers (Figure 2.7A. See also Figure 3.5A). As a control, we assessed if PRMT5 generally correlated with the expression of all genes in the transcriptome. As expected, there was no correlation across the cancer data sets (Figure 2.7A). PRMT5 expression generally did not

correlate with AR and varied significantly for individual cancer types (Figures 2.7A. See also Figure 3.5A). However, the strength of correlations between PRMT5 and several AR target genes involved in DDR seemed independent of the correlation between PRMT5 and AR (See also Figure 3.5A). To assess this further, we sorted the cancer types into three groups based on the correlation coefficient between PRMT5 and AR: positively correlated, negatively correlated, and not correlated. We observed no difference in the correlation between PRMT5 and DDR genes when the cancer types were stratified (Figure 2.7B), indicating that PRMT5 correlates positively with DDR genes independently of any correlation with AR. This leaves the possibility that AR target genes involved in DDR may also be primary target genes of PRMT5. However, similar RT-qPCR and ChIP-qPCR experiments revealed that only DNAPKcs is likely a target gene of PRMT5 at least in prostate cancer cells (Figures S2.4A-S2.4F). DNAPKcs also had the highest correlation with PRMT5 across the 32 clinical cancer data sets (See also Figure 3.5A), further implicating DNAPKcs as a PRMT5 target gene. Collectively, our results suggest that PRMT5 plays a conserved role in activating expression of genes required for the repair of IR-induced DSBs.

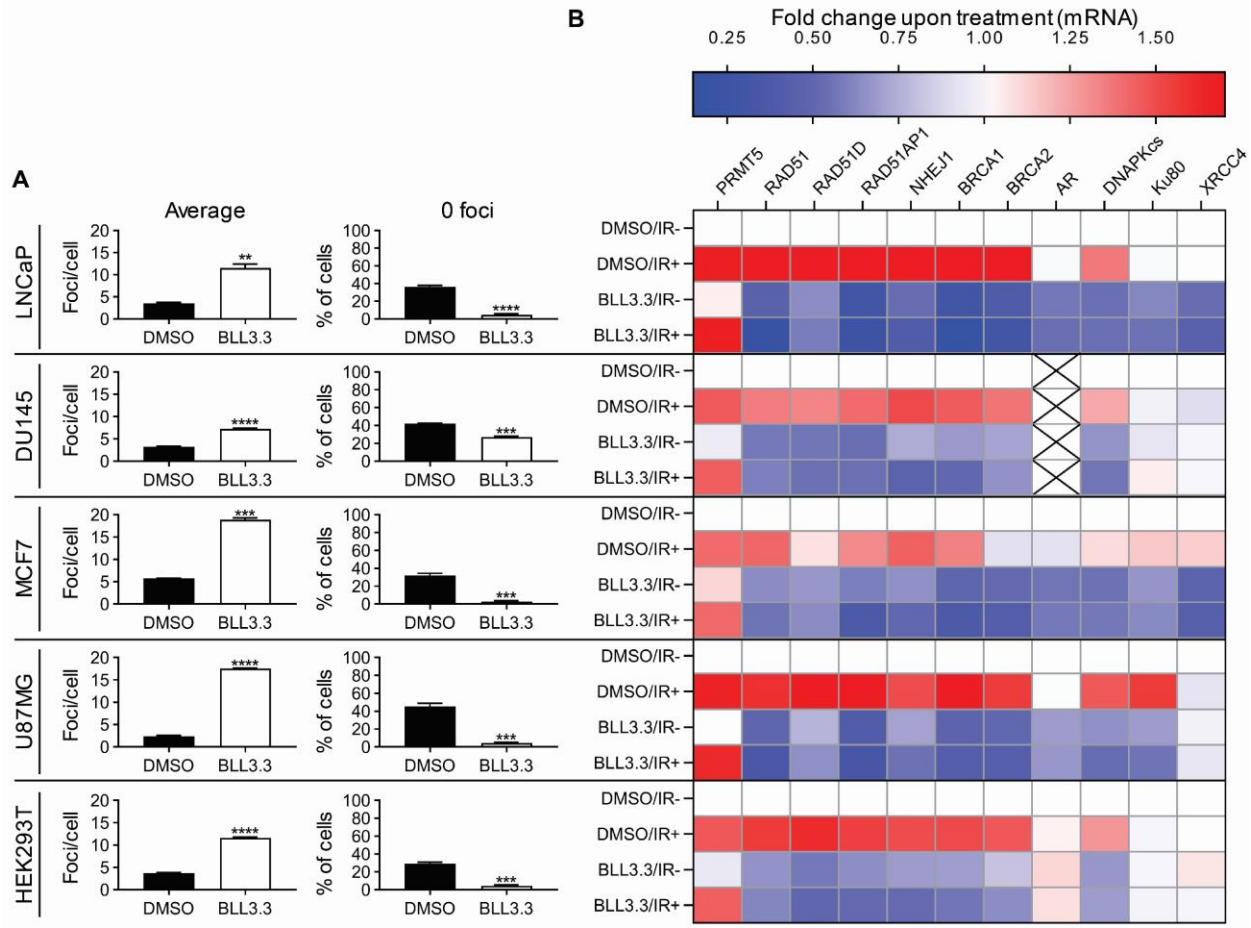


**Figure 2.6: PRMT5 regulates the expression of DNA damage response (DDR) genes and is required to repair IR-induced double-strand breaks (DSBs) in multiple cell types**

**(A)** Quantification of DSBs 6 h post 2 Gy IR in the indicated cell lines with (BLL3.3) and without (DMSO) PRMT5 inhibition as described in **Figure 2B** (See also **Figure S2.6A-S2.6E** for representative images).
**(B)** Quantification of mRNA via RT-qPCR 6 h post 2 Gy IR in the indicated cell lines with (BLL3.3) and without (DMSO) PRMT5 inhibition. For each biological replicate, values were normalized to the value for 'DMSO/IR-' (untreated) to calculate the fold change in mRNA expression upon treatment (See also **Figure S2.6F-S2.6J** for statistical analysis).

Bars in **A** and values used in the heat map in **B** are the mean of 3 independent experiments. Statistical analysis in **A** comparing experimental to the control ('DMSO') was performed using Welch's *t*-test (** $P \leq 0.01$, *** $P \leq 0.001$, **** $P \leq 0.0001$).

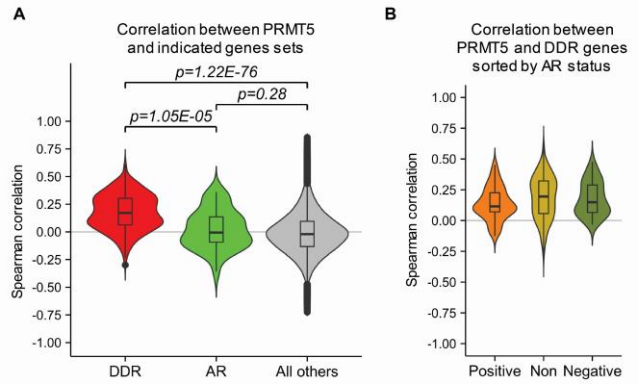


**Figure 2.7: PRMT5 expression positively correlates with DNA damage response (DDR) genes in human cancer tissues**

**(A)** Violin plots representing Spearman correlations comparing the mRNA expression level between PRMT5 and DDR genes (DDR), PRMT5 and AR (AR), or PRMT5 and all other genes (All other) across 32 clinical cancer data sets from TCGA. The gene set for DDR genes was defined as RAD51, RAD51D, RAD51AP1, NHEJ1, BRCA1, BRCA2, WEE1, DNAPKcs, Ku70, Ku80, an XRCC4 (see also **Figure 3.5**).
**(B)** Violin plots representing Spearman correlations comparing the mRNA expression level between DDR genes and PRMT5. Cancer types were stratified by the correlation coefficient (c.c.) between PRMT5 and AR: positively correlated (c.c. > 0 & p < 0.01) (Positive), negatively correlated (c.c. < 0 & p < 0.01) (Negative), or not correlated (p > 0.01) (Non).

Box-and-whiskers plots show the median value (line) and interquartile range between the first and third quartiles (box). The upper whisker extended to the largest value no further than '1.5 x interquartile range' and the lower whisker extended to the smallest value at most '1.5 x interquartile range'. Outliers beyond the whiskers are shown as dots. Statistical analysis was performed using Wilcoxon test and the p-values are displayed.

## 2.4 Discussion

### 2.4.1 *PRMT5 functions as an epigenetic activator to regulate the repair of DSBs*

Upon recognition of DNA DSBs, repair proteins (such as RAD51, BRCA1, and BRCA2) are transiently upregulated to facilitate repair through HR or NHEJ[164–166]. Although this transient upregulation is required for cell survival following genotoxic stresses, there is a long-standing question of how proteins are quickly upregulated to promote repair of DNA damage. Here, we present evidence that PRMT5 functions as a master epigenetic activator of DDR genes to facilitate the repair of DSBs.

In this study, we determined that PRMT5 activated transcription of multiple genes that encode well-characterized repair proteins involved in HR (RAD51, RAD51AP1, RAD51D, BRCA1 and BRCA2) and NHEJ (NHEJ1 and DNAPKcs). DSB repair occurs in three phases: (1) recognition of DSBs via sensor proteins, (2) initiation of repair by repair proteins, and (3) resolution of repair[163]. Our studies suggest that PRMT5 primarily regulates the expression of repair

proteins as opposed to DNA damage sensors or proteins involved in the resolution of repair. Since we also confirmed that PRMT5 regulated the expression of several other genes involved in various phases of DDR by RT-qPCR (Figure S2.3G), it remains to be determined whether these genes are also target genes of PRMT5.

The epigenetic regulation of genes is cell type, temporal, and context dependent. Our data suggests that PRMT5 likely activates transcription of DDR genes in a variety of cell types. However, we cannot rule out the possibility that PRMT5 regulates different DDR genes in different cells. For example, although we determined that PRMT5 activated transcription of RAD51, *Clarke et al.* demonstrated that depletion of PRMT5 impaired HR (reduced IR-induced RAD51 and BRCA1 foci) without affecting the expression of RAD51 or changes in cell cycle[177]. There are a few possible explanations: (1) their experiment was performed in HeLa-shPRMT5 stable cell lines and were not performed in inducible knockdown lines. It is possible that these cells compensated for depleted PRMT5 although all experiments were conducted on low passage cells to minimize effects of chronic PRMT5 depletion. (2) PRMT5 may not regulate RAD51 expression in HeLa cells. (3) HeLa cells may respond differently to depleted PRMT5 as evidenced by a lack of cell cycle changes in HeLa cells that we and others have observed in other cell lines[126,184,215,216]. As an epigenetic regulator, it is possible that PRMT5 may not regulate the same cohort of DDR genes in every tissue but rather regulates the same pathways such as HR, NHEJ, and $G_2$ arrest

During preparation of this manuscript, *Braun et al.* reported that PRMT5 post-transcriptionally regulates the splicing out of detained-introns (DIs) of genes to modulate gene expression[157]. However, our analysis of their data showed that the majority of DEGs we identified either do not contain DIs or DI splicing of our DEGs was not affected by PRMT5 targeting. Additionally, *Tan et al.* reported that PRMT5 is required for appropriate splicing in hematopoietic stem cells and that targeting PRMT5 causes increased intron retention and exon skipping events[158]. In their study, they performed functional enrichment analysis on alternative splicing events upon PRMT5 knockdown and they identified that genes associated with "DNA repair" were enriched. However, there was little overlap between the genes we validated as PRMT5 target genes (RAD51, RAD51AP1, RAD51D, BRCA1, BRCA2, NHEJ1, DNAPKcs, and WEE1) and genes they identified as splicing targets. Interestingly, they functionally validated 5 splicing targets (FANCA, FANCG, MUTYH, RTEL1, and RAD52), and we identified both FANDCA and FANCG as "IR+ only" downregulated DEGs in our RNA-seq analysis. However, we did not pursue further

validation of these genes. Overall, our findings are likely independent of potential splicing changes upon PRMT5 knockdown and the role of PRMT5 in transcriptional regulation of DDR genes likely mediates the transient upregulation of repair proteins upon DNA damage.

### 2.4.2 *PRMT5 is required for efficient repair of DSBs*

We demonstrate that PRMT5 is required for efficient repair of DSBs. Interestingly, knockdown of PRMT5 alone caused an increase in spontaneous DSBs independent of external DNA damage inducers (Figures S2.2A-S2.2F), indicating that PRMT5 is required to repair endogenous DSBs. Two recent studies have also demonstrated that PRMT5 is required for efficient repair of DSBs in additional cell lines[177,180]. We provide evidence that the activation of gene expression by PRMT5 is essential to DSB repair efficiency while the regulation of RuvBL1 and Tip60 by PRMT5 likely only affects DSB repair choice. Specifically, PRMT5-catalyzed methylation of RuvBL1 and PRMT5-associated splicing of Tip60 may promote HR over NHEJ, yet the DSB can be repaired regardless of pathway choice. Therefore, observations that PRMT5 is required for efficient repair of IR-induced DSBs are most likely explained by our finding that PRMT5 activates transcription of DDR genes. Because Tip60 is required for ATM activation[255,256], and ATM phosphorylates H2AX to form γH2AX foci and signal the initiation of DSB repair[257], we did not perform γH2AX foci analysis to assess repair of IR-induced DSBs. Because Tip60 has been shown to be essential for γH2AX foci formation[258,259], we would have observed a decrease in γH2AX regardless if knockdown of Tip60 would affect repair of IR-induced DSBs.

### 2.4.3 *PRMT5 regulates DSB repair independently of AR*

We recently reported that PRMT5 is an epigenetic activator of AR[114]. In prostate cancer cells, AR has been reported to regulate DSB repair via HR and NHEJ[43–46,260,261]. Upon IR, AR is recruited to the promoter of DDR genes to activate their expression[45] (~8-24 h post IR), albeit at a much later time point than the recruitment of PRMT5 to the promoter of DDR genes (~1 h post IR). Knockdown or inhibition of AR signaling has also been shown to directly impair HR[43,260], and recent studies suggest that AR may be essential for HR particularly in castration-resistant prostate cancer (CRPC)[45,260,261]. However, AR's role in regulating NHEJ is more established in that AR transcriptionally activates genes involved in NHEJ[43–46].

As we reported that targeting PRMT5 decreases AR expression[114], the requirement of PRMT5 for efficient repair of DSBs could be mediated through the regulation of AR. Indeed, we demonstrated that targeting PRMT5 caused a decrease in AR expression and concomitant decrease in the expression of AR target genes involved in NHEJ (Ku80, XRCC4, and DNAPKcs). However, several pieces of evidence in our study suggest that PRMT5 also regulates repair of DSBs independently of AR: (1) PRMT5 targeting sensitized both AR-positive and AR-negative prostate cancer cells to IR; (2) exogenous expression of AR only partially rescued the impairment of IR-induced DSB repair by PRMT5 knockdown; (3) targeting PRMT5 hindered the repair of IR-induced DSBs in AR negative DU145 cells and several other cancer cell lines with varying AR expression level; and (4) in clinical cancer data sets, PRMT5 expression was positively correlated with the expression of DDR target genes regardless of its correlation with AR. Collectively, these data strongly suggest that although targeting PRMT5 may mimic targeting AR to sensitize prostate cancer cells to IR, PRMT5 can regulate DSB repair independently of AR expression.

### 2.4.4 *PRMT5 likely regulates the repair of IR-induced DSBs via multiple mechanisms*

In this study, we determined that PRMT5 is required for efficient repair of DSBs via activation of DDR genes. Additionally, there are several reports suggesting that PRMT5 may regulate the repair of DNA damage via multiple mechanisms. As detailed above, recent reports show that PRMT5 regulates the DSB repair choice process and promotes HR through methylation of RuvBL1[177] and altered splicing of Tip60[180]. Indeed, RuvBL1 was identified in our mass-spec analysis (peptide fragment *TISHVIIGLK*) as a potential interacting protein of PRMT5 in LNCaP cells. Therefore, our observation that PRMT5 knockdown decreased HR-associated RAD51 foci may be partially explained by these previous results.

PRMT5 can also regulate protein expression via splicing[157,158]. These two studies identified some PRMT5 splicing targets involved in DDR. For example, PRMT5 is required to maintain appropriate expression of functional RAD52[158], and recent reports demonstrate the importance of RAD52 to HR[181–183]. Future studies may determine if PRMT5-associated splicing directly affects the repair of IR-induced DSBs.

PRMT5 has also been shown to methylate and regulate several proteins associated with DDR: p53[169,184–186], E2F1[187–189], FEN1[190,191], RAD9[192], KLF4[193], and TDP1[194]. As detailed in these studies, DNA damage via etoposide, hydroxyurea, doxorubicin, and UV can induce PRMT5-

catalyzed methylation of these non-histone substrates which alters the cellular response to DNA damage. For example, PRMT5-catlyzed methylation of p53 altered binding to p53 target genes which promoted cell cycle arrest and inhibited apoptosis[169]. However, these studies did not identify a direct role for PRMT5 in the repair of DSBs or in the response to IR. For example, PRMT5-catalyzed methylation of RAD9 was essential to the cellular response to hydroxyurea but did not play a significant role in the cellular response to IR. It is likely that there are unknown PRMT5 substrates involved in DDR and future studies may determine if PRMT5-catalyzed methylation of these proteins directly affects DSB repair efficiency.

In various yeast species, the PRMT5 homologue Hsl7 was shown to interact with and promote degradation of WEE1 homologues to promote $G_2$ progression independently of its methyltransferase activity [230–232]. Although it is unknown if PRMT5 interacts with WEE1 protein in human tissues, the studies in yeast contrast with our study in which PRMT5 activated transcription of WEE1 and promoted DNA damage-induced $G_2$ arrest. The opposing post-translational and transcriptional regulation of WEE1 by PRMT5 may be modulated by PRMT5 methyltransferase activity and/or the absence or presence of DNA damage. In fact, the PRMT5-medaited changes in cell cycle in the Xenopus egg are independent of transcription because Xenopus egg extracts can cycle without *de novo* mRNA transcription [232]. Therefore, PRMT5 likely modulates WEE1-mediated cell cycle changes in multiple ways.

### 2.4.5 *PRMT5 targeting may be explored for cancer treatment*

According to the American Cancer Society, over half of all cancer patients receive RT. RT induces DSBs in DNA which are lethal to cells if not repaired. While potentially curative, tumors can still regrow following RT. For example, ~10-15% of prostate cancer patients with low-risk disease and ~50-60% of patients with high-risk disease treated with RT still experience tumor recurrence[32–35]. Thus, identification of novel therapeutic targets to enhance RT will likely reduce cancer mortality.

PRMT5 is overexpressed in many cancers and its overexpression correlates with poor prognosis[105,110,111]. Our findings suggest that PRMT5 overexpression may increase the efficiency of DSB repair and confer survival advantages particularly following DNA damaging treatments. For example, upregulation of RAD51, a putative PRMT5 target gene, has been shown to promote resistance to DNA damaging agents[262,263] and decreasing RAD51 expression sensitizes cancer cells

to IR[264]. Because targeting DSB repair is a validated therapeutic approach for cancer treatment[265], our findings that PRMT5 expression positively correlates with multiple DDR genes across clinical cancer data sets strongly suggests that PRMT5 targeting may be explored as a monotherapy or in combination with RT or chemotherapy for cancer treatment. PRMT5 may also be a particularly attractive therapeutic target for prostate cancer patients because targeting PRMT5 decreases AR expression[114], and targeting AR signaling via ADT enhances RT for prostate cancer patients[42].

One criticism of PRMT5 targeting is potential systemic adverse effects as epigenetic regulators typically have essential roles in various tissues. Although targeting PRMT5 does not affect the growth of AR-negative DU145 and PC3 cells as well as normal prostate RWPE-1 cells[114], we do find that targeting PRMT5 inhibits repair of IR-induced DSBs in non-cancerous HEK293T cells. It is reasonable to suspect that targeting PRMT5 may also sensitize adjacent normal tissue to RT. Given advances in RT, the amount of adjacent normal tissue that is irradiated is minimalized. Thus, it is likely that the combination of PRMT5 targeting and RT will allow for either a lower dose of drug or IR to limit adverse effects. Alternatively, targeted delivery of PRMT5 inhibitors as radiosensitizers will circumvent systemic toxicity. This can be effectively achieved through prostate specific membrane antigen-based delivery[246]. Nevertheless, our findings here provide convincing evidence that PRMT5 functions as a master epigenetic regulator to activate transcription of DNA damage repair genes and is a potential therapeutic target to enhance RT or chemotherapy for cancer treatment.

## 2.5 Materials and Methods

### 2.5.1 *Cell lines and cell culture*

LNCaP, DU145, PC3, and HEK293T were purchased from ATCC (Manassas, VA, USA) and cultured as described previously[114,121]. MCF7 cells were a gift from the Chun-Ju (Alice) Chang lab, and U87MG cells were a gift from the Emily Dykhuizen lab. Upon arrival, all cell lines were immediately expanded and aliquots were prepared and stored in liquid nitrogen. Cells were maintained for no longer than 30 passages or no longer than 3 months as described previously[49,266]. Cell line authentication for LNCaP cells was performed by IDEXX BioResearch (IMPACT I) and the absence of mycoplasma contamination for all cell lines was verified using LookOut® PCR Mycoplasma Detection Kit (Sigma, St. Louis, MO, USA). Knockdown cell lines were generated using the pLKO-Tet-On system. The pLKO-Tet-On plasmid for shRNA expression was obtained

from Addgene (Cambridge, MA, USA)[267], and shRNA sequences that target PRMT5 #1 (5′-CCCATCCTCTTCCCTATTAAG-3′: referring to #1832)[114], PRMT5 #2 (5'-GCCCAGTTTGAGATGCCTTAT-3′: referring to #1577)[114], and SC (5'-CAACAAGATGAAGAGCACCAA-3') were used for the construction of plasmids for stable cell line generation as described previously[114,266]. Lentiviral stably infected pools with Dox-inducible expression of PRMT5-targeting shRNA (shPRMT5 #2: referring to #1577[114]) (LNCaP-shPRMT5 pool, PC3-shPRMT5 pool, and DU145-shRNA pool) were established and used for clonogenic assays. Stable cell lines with Dox-inducible expression of PRMT5-targeting shRNA (LNCaP-shPRMT5: referring to #1832[114], LNCaP-shPRMT5 #2: referring to #1577[114]) or scramble control-targeting shRNA (shSC) (LNCaP-shSC, PC3-shSC, and DU145-shSC) were established from individual clones and characterized previously[114]. Cell lines are described in Appendix C.

### 2.5.2 *Dox-induced knockdown and inhibitor treatment conditions*

For Dox-inducible cell lines, Dox was applied at the final concentration of 1 μg/mL every 48 h to establish and maintain PRMT5 knockdown (shPRMT5) or express scramble control shRNA (shSC). The number of days of Dox treatment was optimized: shPRMT5 and shSC cells were grown for 4 days and had 4 days of Dox treatment. For parental cell lines, cells were treated with the PRMT5 inhibitor BLL3.3 (10 μM) or an equal volume of DMSO (control) every 48 h beginning 24 h after plating to inhibit PRMT5 activity. For IR experiments, cells were subjected to IR following the knockdown or inhibitor treatment described above.

### 2.5.3 *Ionizing radiation conditions*

For clonogenic assays, cells were irradiated using the GC-220 device (Atomic Energy of Canada, Ottawa, Canada) with a Co-60 radiation source as described previously[48,49]. For all other experiments, cells were irradiated using the X-RAD 320 biological irradiator device (PXi Precision X-Ray, North Branford, CT, USA) with an x-ray tube radiation source at an average dose rate of ~1 Gy/25 sec. All IR treatments were carried out in normal air at room temperature, and cells spent minimal time outside incubators during treatment. Non-irradiated controls were 'mock-irradiated' by being taken out of the incubator for the same time period as irradiated counterparts.

### 2.5.4 *Clonogenic assays*

Clonogenic assays to quantify the surviving fraction following IR was performed similar to previously reported[48,49]. For Dox-inducible cell lines, Dox was applied at the final concentration of 1 μg/mL every 48 h to establish and maintain PRMT5 knockdown (shPRMT5) or express scramble control shRNA (shSC). Additionally, LNCaP cells were treated with the PRMT5 inhibitor BLL3.3 (10 μM) or an equal volume of dimethyl sulfoxide (DMSO) (control) every 48 hours beginning 24 hours after plating to inhibit PRMT5 activity. After 4 days, when cells reached ~80% confluency, cells were subjected to the indicated dose of IR and immediately harvested, collected, counted, and reseeded on fresh 6 well plates for clonogenic assay. After 14 days of growth, the number of colonies were counted to calculate the surviving fraction. The number of cells for reseeding was optimized based upon how much cell death was observed: (LNCaP: 0 Gy-500 cells, 2 Gy-700 cells, 4 Gy-1000 cells, 6 Gy-5000 cells, and 8 Gy-10000 cells), (PC3: 0 Gy-50 cells, 2 Gy-100 cells, 4 Gy-200 cells, 6 Gy-600 cells, and 8 Gy-1000 cells), (DU145: 0 Gy-50 cells, 2 Gy-100 cells, 4 Gy-200 cells, 6 Gy-400 cells, and 8 Gy-800 cells).

### 2.5.5 *Immunocytochemistry for quantification of IR-induced DSBs[167], NHEJ-associated foci[268,269], and HR-associated foci[268,269]*

Cells were seeded on 6 cm dishes containing glass coverslips and treated as described elsewhere. When cells reached ~80% confluency, cells were treated with 2 Gy IR and then fixed with 3.7% formaldehyde in phosphate buffered saline (PBS) at room temperature for 20 minutes at the indicated time points: First, we assessed the formation and repair of DSBs by analyzing γH2AX foci in a time-course following radiation (5 m and 1, 2, 6, and 24 h). Given that the majority of DSBs are repaired within 2-6 h following IR, we assessed the effect of knockdown or inhibitor on the repair of DSBs at the 6 and 24 h time points. To assess potential impact on HR or NHEJ, we assessed RAD51 and Ku70 foci, respectively, at 1 h following IR treatment which is when the majority of repair occurred. After fixation at the indicated time points, cells were permeabilized with 0.2% Triton X-100 in PBS at room temperature for 5 m. Cells were then blocked with 5% milk blocking solution in PBS, stained with the indicated primary antibodies diluted in 5% milk blocking solution in PBS, and stained with 4,6-diamidino-2-phenylindole (DAPI final 10 μg/mL) and indicated secondary antibodies diluted in 5% milk blocking solution in PBS. Cells on coverslips were mounted on glass slides using the ProLong® Antifade Kit (Invitrogen Molecular

Probes, Eugene, OR, USA) and sealed with clear nail polish. Cells were then imaged via the Nikon TE2000 inverted fluorescence microscope under oil immersion (60x objective) (Nikon Instruments Melville, NY, USA). Images were processed via ImageJ[270] and the background was subtracted from the image using the rolling ball method (http://imagej.net/plugins/rolling-ball.html). Gating for minimum and maximum intensity values was set the same for each image. The number of foci was manually recorded for each cell (defined via nuclear DAPI staining). At least 60 cells were counted for each biological replicate. The arrays of foci counts for each biological replicate were subjected to further analysis separately to determine the average number of foci per cell and percentage of cells with zero foci. The primary antibodies used were anti-PRMT5-rabbit (1:1000), -γH2AX-mouse (1:1000), -γH2AX-rabbit (1:200), -AR-mouse (1:1000), -AR-rabbit (1:100), -RAD51-rabbit (1:1000), -Ku70-mouse (1:500), and RuvBL1-rabbit (1:100). Secondary antibodies used were anti-mouse-FITC (1:100) and anti-rabbit-rhodamine red (1:1000). All antibodies are described in Appendix E.

### 2.5.6 *Immunocytochemistry for quantification of protein expression or subcellular localization*

Immunocytochemistry was performed as described above. Images were analyzed via ImageJ[270]. First, the background was subtracted from the image using the rolling ball method (http://imagej.net/plugins/rolling-ball.html). For PRMT5 expression, regions of interest (ROI) were outlined for each individual cell. For AR expression, ROI were outlined for each nucleus (as defined by DAPI staining). The average intensity for each ROI was measured and at least 60 cells were counted for each biological replicate. The arrays of intensity counts for each biological replicate were subjected to further analysis separately and were analyzed via both "D'Agostino & Pearson" and "Shapiro-Wilk" normality tests to evaluate distribution. Because not all samples were normally distributed, the median value was used for each biological replicate.

### 2.5.7 *Comet assay*

To determine if PRMT5 regulates the repair of IR-induced DSBs, we used comet assay to quantify DNA damage directly. LNCaP-shPRMT5 cells were seeded on 6 cm dishes and Dox was applied at the final concentration of 1 µg/mL every 48 h to establish and maintain PRMT5 knockdown. After 4 days, when cells reached ~80% confluency, cells were treated with the

indicated dose of IR and then harvested and counted after either 5 m or 2 h. The 5 m time point indicates how much total DNA damage is induced by radiation. Comparing the 2 h time point to the 5 m time point indicates how much DNA damage is repaired. Twenty thousand cells per group were diluted in 100 µL of 0.5% Low Melting Agarose in PBS at 45°C and 50 µL of diluted cells were immobilized onto pretreated VWR Superfrost Plus slides (previously dipped in 1% Agarose in nanopure water and allowed to dry overnight). Glass coverslips were placed on top of the cell dilution and the slides were placed in 4°C for 10 minutes to solidify the agarose. Slides were moved to room temperature for 5 minutes, the coverslips removed, and immobilized cells were lysed in 4°C neutral lysis buffer (10mM Tris HCl pH 8.0, 100 mM EDTA, 2.5 M NaCl, 1% Sarkosyl, 0.5% Triton X-100) for 60 minutes at 4°C. Slides were removed from lysis buffer and equilibrated in Neutral Comet Electrophoresis Buffer (90 mM Tris HCl pH 8.0, 90 mM Boric Acid, 2 mM EDTA) for 20 minutes. Electrophoresis was performed at 14V, 27mA for 60 minutes. After electrophoresis, slides were equilibrated in 0.4 M Tris-HCl pH 7.4 for 5 minutes at room temperature. The equilibration buffer was replaced with fresh buffer, and the slides were incubated for an additional 5 minutes. This wash was repeated one additional time for a total of three washes. Sixty µL of DAPI (0.5 µg/mL in $H_2O$) was applied dropwise to the agarose pad, and slides were incubated at 4°C for 15 minutes. Comets were then imaged via the Nikon TE2000 inverted fluorescence microscope (20x objective) (Nikon Instruments Melville, NY, USA) and analyzed with ImageJ[270]. To quantify the '% tail DNA' in each cell from the images, we utilized the comet assay plugin created by Robert Bagnell (2011) based on the NIH Image comet assay by Herbert M. Miller (1997). At least 65 cells were analyzed across 3 biological replicates and the '% tail DNA' values were pooled for statistical analysis via Mann-Whitney *U*-test. Although several reports using comet assay have used various data representation and statistical analysis[271–274], because of the high variance within each biological replicate and lack of normal distribution we used the Mann-Whitney *U*-test[275–277].

### 2.5.8 *Etoposide treatment*

To assess if PRMT5 is required for repair of DSBs in general, we used etoposide to induce replication-dependent DSBs. LNCaP-shPRMT5 cells were seeded on 6 cm dishes containing glass coverslips and Dox was applied at the final concentration of 1 µg/mL every 48 h to establish and maintain PRMT5 knockdown. When cells reached ~60% confluency, cells were treated with either

etoposide (10 μM) or an equal volume of DMSO. Forty-eight h after initiation of treatment, coverslips were transferred to a new dish and subjected to γH2AX-foci analysis described above while the remaining cells were harvested and subjected to western blot analysis. Although not shown, experiments with short etoposide treatments (2 h, 6 h) were unsuccessful and the 48 h etoposide treatment time was likely optimal because cells could undergo DNA replication which induced DSBs.

### 2.5.9 *Transient transfection for rescue of AR expression*

To evaluate if the role of PRMT5 in the repair of IR-induced DSBs is independent of AR, LNCaP-shPRMT5 cells were seeded on 6 cm dishes containing glass coverslips and Dox was applied at the final concentration of 1 μg/mL every 48 h to establish and maintain PRMT5 knockdown. Forty-eight h following seeding, cells were transfected with pCMV-Flag2-AR, as described previously[114,266], or pCMV-Empty Vector plasmid using FuGENE HD (Promega, Madison, Wisconsin, USA). pCMV-HA-CFP was used as a transfection control. Upon reaching ~80% confluency (48 h following transfection), cells were treated with 2 Gy IR and subjected to immunocytochemistry analysis. Only transfected cells (CFP+) were subjected to γH2AX foci analysis, while both transfected and non-transfected cells were subjected to protein expression analysis as described above. For the microscope images, we used 3D representation to show the expression of multiple proteins in a single cell at the same time. Each peak is a cell and the height of each peak is the intensity of signal.

### 2.5.10 *RNA-seq for identification of PRMT5 target genes in response to IR*

LNCaP-shPRMT5 cells were seeded on 6 cm dishes and Dox was applied at the final concentration of 1 μg/mL every 48 h to establish and maintain PRMT5 knockdown for 4 days. Cells were harvested 1 h following a 2 Gy IR treatment and total RNA was isolated using Trizol Reagent (Ambion, Carlsbad, CA, USA). PolyA+ RNA libraries were generated according to the Illumina "TruSeq Stranded mRNA Sample Preparation Guide" (15031047E) with the following considerations: (1) an Agilent Bioanalyzer RNA-Nano kit was used to assess RNA concentration and rule out sample degradation. (2) Heat and divalent cation fragmentation of the polyA+ RNA was undertaken for 4 m rather than the default of 8 m. (3) The number of PCR cycles for library

amplification was determined by the yield of cDNA. For both RNA-seq analyses, we ran 8 cycles of PCR instead of the 15 cycles mentioned in the manual. (4) Final cleanup was performed using a 0.8:1 bead:sample ratio with AmPure XP beads instead of the 1:1 mentioned in the manual. IR+ group was run on an Illumina HiSeq 2500 using High Output flowcell to produce paired-end 101 base reads. IR- group was run on an Illumina NovaSeq 6000 S4 flowcell that generated paired-end 151 base reads. Additionally, IR- samples were prepared and run with unique dual indexes to mitigate potential "index-hopping" associated with Illumina instruments using "exclusion amplification" clustering on patterned flowcells.

Raw RNA-seq results were further assessed. RNA library quality was verified by FastQC, and STAR RNA-seq aligner[278] was used to map all high-quality sequences to the human genome (GENCODE GRCh38). Read counts were evaluated using Subread featureCounts[279] to summarize uniquely mapped reads to the gene level according to the GENCODE M25 annotation file. Data was normalized by trimmed mean of M value method to obtain the final profile of gene expression (base-2 log scale). EdgeR[280] was used to perform differential expression analysis by comparing Dox+ (PRMT5 KD) and Dox- (no KD) for IR+ and IR- groups. After removing low-expressed genes (average expression levels lower than 1 for both conditions), we defined genes as differentially expressed genes (DEGs) if their FDR-adjusted p-values were less than 0.01, and the magnitudes of fold-changes (FCs) were larger than log2 (1.25).

Gene Ontology (GO) and pathway analysis were performed on the 'IR+ only' DEGs. GO enrichment analysis was performed using the web-based tool DAVID functional annotation analysis (http://david.abcc.ncifcrf.gov/home.jsp v6.8)[281,282]. Only GO annotations with FDR-adjusted p-values less than 0.05 and the fold enrichment score larger than 1.5 were selected as significantly over-represented GO terms. Pathway analysis on IR+ only DEGs was performed using Ingenuity Pathway Analysis (IPA) (QIAGEN Inc., https://www.qiagenbioinformatics.com/products/ingenuity-pathway-analysis) to identify differentially regulated pathways upon PRMT5 knockdown in irradiated cells.

### 2.5.11 *RNA isolation, reverse transcription, and RT-qPCR*

Cells were seeded on either 6 cm or 10 cm dishes and treated as described elsewhere. Total RNA was isolated using Trizol Reagent (Ambion, Carlsbad, CA, USA). RNA concentration and integrity were verified by agarose gel electrophoresis. cDNA synthesis was done using High

Capacity cDNA Reverse Transcription Kit (Promega, Madison, WI, USA) as described previously[114,121,266]. qPCR was performed using FastStart Universal SYBR Green Master Mix (Thermo Fisher Scientific, Waltham, MA, USA) on the QuantStudio 6 Flex System and QuantStudio™ Real-Time PCR Software (Thermo Fisher, Waltham, MA, USA). Forty cycles were run and samples without $C_T$ values were deemed undetected. Technical duplicates were run for each sample and the $C_T$ values used for further analysis were the average of the technical duplicates. Samples where $C_T$ values for technical duplicates were >0.5 apart were re-run. Non-template controls (NTC)s with autoclaved double-distilled $H_2O$ were also run for each primer set and primer sets where $C_T$ values for NTC were lower than 37 (indicating high background) were re-run. Amplicon size and specificity were verified for each primer set via agarose gel electrophoresis. PRMT5, AR, and GAPDH primers were used previously[114,121]. IVL primers were used previously[253,283]. All primers used are described in Appendix D.

### 2.5.12 *Chromatin immunoprecipitation (ChIP)-qPCR assay*

LNCaP-shPRMT5 or LNCaP-shSC cells were seeded on multiple 10 cm dishes and Dox was applied at the final concentration of 1 µg/mL every 48 h to establish and maintain PRMT5 knockdown (shPRMT5) or express scramble control shRNA (shSC). After 4 days, when cells reached ~80% confluency, cells were treated with 2 Gy IR. One hour following IR (prior to the repair of the majority of DSBs and at the same time as the peak of IR-induced PRMT5 protein expression), cells were fixed/crosslinked and chromatin was prepared for ChIP-qPCR as described previously[114]. Chromatin fragments were verified to be ~500 base pairs by agarose gel electrophoresis. Antibodies used for immunoprecipitation were anti-PRMT5-rabbit, -H4R3me2s-rabbit, -H3K9ac-rabbit, -H3R2me2s-rabbit, -H3R8me2s-rabbit, -H2AR3me2s-rabbit, and IgG-rabbit. All antibodies are described in Appendix E. Primers used for ChIP-qPCR are described in Appendix D.

### 2.5.13 *Flow cytometry cell cycle analysis*

LNCaP-shPRMT5 cells were seeded on 6 cm dishes and Dox was applied at the final concentration of 1 µg/mL every 48 h to establish and maintain PRMT5 knockdown. After 4 days, when cells reached ~80% confluency, IR+ cells were treated with 2 Gy IR. Cells were harvested

24 h following IR, resuspended in PBS, and filtered through a 70 µm nylon cell strainer to remove all cell aggregates. A single cell suspension was prepared and verified via microscopy. Cells were then fixed in 70% ethanol, stained with a Propidium Iodide (PI) containing solution (20 µg/mL PI and RNaseA diluted in PBS) and subjected to flow cytometry analysis via the Guava EasyCyte Flow Cytometer (Guava Technologies, Hayward, CA, USA). At least 20,000 live cells were counted for each biological replicate. Flow cytometry data was analyzed via FlowJo (FlowJo, LLC, Ashland, Oregon, USA). Live cells were gated for analysis to remove any sub-$G_1$ cells and then were subjected to cell cycle analysis via Dean-Jett-Fox modeling[284].

### 2.5.14 *Western blot*

Cells were seeded on either 6 cm or 10 cm dishes and treated as described elsewhere. Cells were harvested in lysis buffer (100 mM Tris-HCl pH 8.0, 15 mM $MgCl_2$, 100 mM KCl, 5 µg/mL of each Chymostatin, Leupeptin, Pepstatin A, and antipan in DMSO, 1% Triton X-100, 1 mM PMSF in ethanol, and 1 mM DTT) or RIPA buffer (10 mM Tris-HCl pH 8.0, 5 mM EDTA, 1% Triton X-100, 0.1% Sodium Deoxycholate, 0.1% SDS, 140 mM NaCl, 5 µg/mL of each Chymostatin, Leupeptin, Pepstatin A, and antipan in DMSO, and 1 mM PMSF in ethanol) and total protein concentration was measured using Bradford method. Approximately 20-30 µg total protein was run on a 10-15% SDS-PAGE and western blotting was performed as described previously[114,121,266]. Band/protein intensity was quantified using Image Lab™ (Bio-rad, Hercules, CA, USA). Antibodies used for western blot were anti-PRMT5-rabbit (1:1000), -AR-rabbit (1:2000), -γH2AX-rabbit (1:1000), -RAD51-rabbit (1:2000), -RAD51D-rabbit (1:2000), -RAD51AP1-rabbit (1:1000), -NHEJ1-rabbit (1:2000), -β-Actin-mouse (1:2000), -RuvBL1-rabbit (1:1000), -Tip60-rabbit (1:500), -rabbit-HRP (horseradish peroxidase) (1:1000), -mouse-HRP (1:1000). All antibodies are described in Appendix E.

### 2.5.15 *Transient knockdown of RuvBL1 and Tip60*

To confirm that the mechanism we describe here is independent of PRMT5-mediated regulation of RuvBL1 and Tip60, we performed similar assays with knockdown of RuvBL1 or Tip60. First, we obtained MISSION® shRNA bacterial glycerol stocks containing shRNA expression plasmids (RuvBL1: TRCN0000018911, TRCN0000018912, TRCN0000018913,

TRCN0000018914, and TRCN0000319216. Tip60: TRCN0000020314, TRCN0000020315, TRCN0000020317, TRCN0000020318, and TRCN0000298504) (Sigma-Aldrich/Millipore Sigma, St. Louis, Missouri, USA). Using maxiprep, we isolated the shRNA expression plasmids and generated viral particles in HEK293T cells as described previously[266] via co-transfection of all 5 shRuvBL1 or all 5 shTip60 expression plasmids along with pCMV-HA-CFP as a control. Although we could have used transient transfection of individual shRNA expression plasmids, we used viral particle transduction with all 5 shRNA expression vectors at once to ensure sufficient knockdown. FuGENE HD (Promega, Madison, Wisconsin, USA) was used as the transfection reagent, pHR'-CMV-8.2ΔVPR was used as the packaging plasmid, and pHR'-CMV-VSV-G was used as the envelope plasmid. Forty-eight hours following transfection, media from the HEK293T cells was collected, passed through a 0.45 μm filter, and applied to the LNCaP cells for viral particle transduction. Viral particles were applied to the LNCaP cells both 24 hours and 72 hours after plating. LNCaP cells were transduced with either shRuvBL1 or shTip60 viral particles once and again after 48 h to establish RuvBL1 or Tip60 knockdown. Cells were then treated with 2 Gy IR and subjected to γH2AX-foci analysis and western blot analysis described above.

### 2.5.16 *Correlation analysis of TCGA clinical cancer data sets*

Gene expression profiles of 32 clinical cancer data sets from TCGA Pan-Cancer analysis[254] were retrieved from cBioPortal[150,151]. Using the mRNA expression of PRMT5, AR, and DDR genes which are primary target genes of both PRMT5 and AR, we calculated the Spearman correlations between gene pairs for each cancer type. The gene set for DDR genes was defined as RAD51, RAD51D, RAD51AP1, NHEJ1, BRCA1, BRCA2, WEE1, DNAPKcs, Ku70, Ku80, an XRCC4. Although we did not perform additional studies on Ku70, Ku70 was included as it is another well-studied, key regulator of NHEJ. In **Figure 7.2B**, a cutoff of $p < 0.01$ was used to determine the significance of correlation between PRMT5 and AR as either positive, negative, or no correlation if $p > 0.01$, in order to stratify the cancers into the different types.

### 2.5.17 *Statistical analysis*

No statistical methods were used to predetermine sample size. For the correlation analysis of TCGA clinical cancer data sets, statistical analysis was performed using Wilcoxon rank sum

test in R 3.5.3. (R Core Team (2013). R: A language and environment for statistical computing. R Foundation for Statistical Computing, Vienna, Austria, https://www.R-project.org/). All other statistical analyses were performed using Graphpad Prism 7.00 and 8.00 for Windows (GraphPad Software, La Jolla California USA, www.graphpad.com). Statistical analysis for comet assay and RNA-seq analysis are described above. For all other experiments, statistical analysis was performed on raw data with assumed normal distribution. For all qPCR experiments, statistical analysis was performed on $\Delta C_T$ values ($C_T$ value of gene normalized to $C_T$ value of GAPDH control). For all ChIP-qPCR experiments, statistical analysis was performed on $\Delta C_T$ values ($C_T$ value of gene normalized to $C_T$ value of IgG control). For all western blot experiments, statistical analysis was performed on normalized raw intensity values (intensity value of protein divided by the intensity value of β-Actin). When comparing two sample groups, unpaired, two-tailed *t*-tests with Welch's correction (Welch's *t*-test) was used because standard deviations were not always equal for all groups. When comparing multiple sample groups, in order to compare the means or medians among all the samples and incorporate the standard deviation of each of the samples, Brown-Forsythe and Welch ANOVA followed by Dunnett's T3 multiple comparisons test was used. For **Figures 2.1A**, **2.1B**, **2.1D**, and **2.1E**, as the variance in the mean among samples were small and the dose-response occurred on a log scale, statistical analysis was performed using Welch's *t*-test of log-transformed data. All relevant statistics are reported in the corresponding legends.

## 2.6 Data Availability and Supplemental Information

RNA-seq datasets generated in this study are available at the Gene Expression Omnibus (GEO) under accession number GSE111620. Supplemental Information can be found online at https://doi.org/10.1016/j.isci.2019.100750.

## 2.7 Supplemental Figures

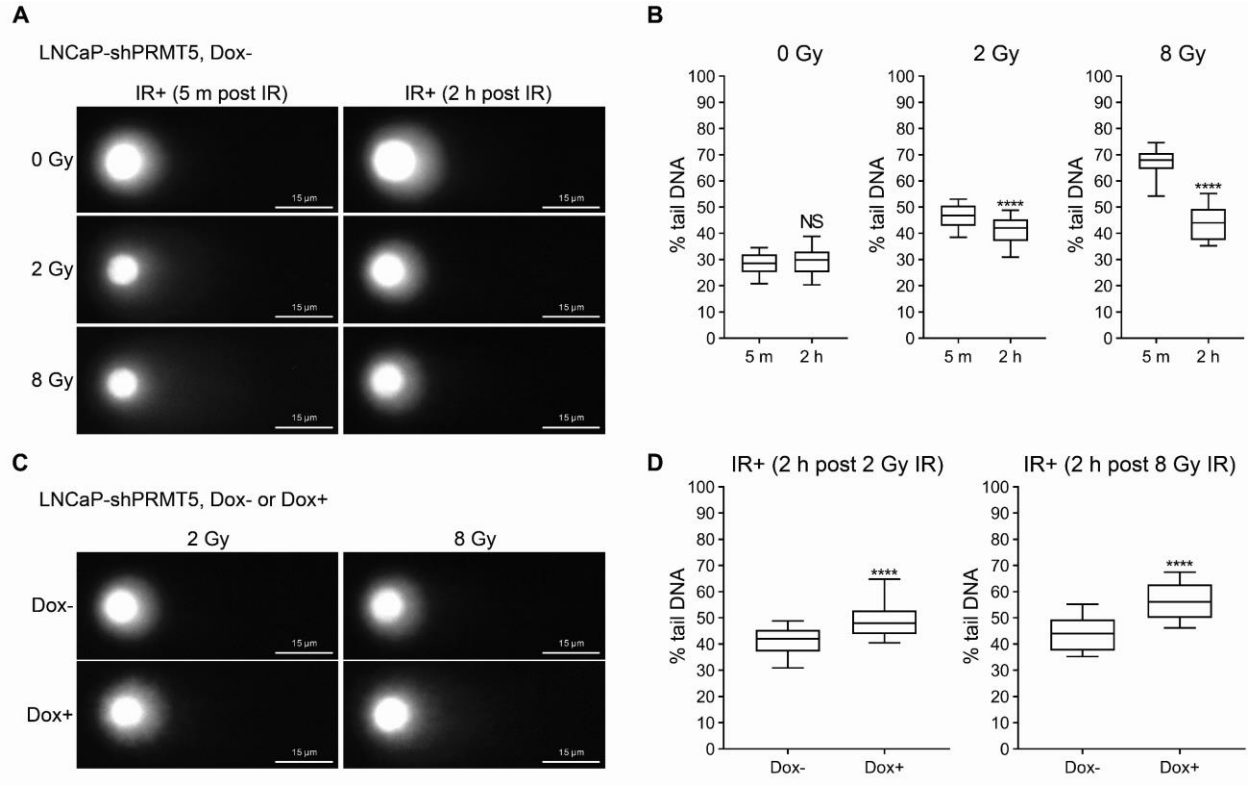


**Figure S2.1: PRMT5 regulates the repair of IR-induced DSBs in prostate cancer cells (Related to Figure 2.2)**

**(A)** Migration of DNA via neutral comet assay at the indicated time points post the indicated dose of IR in LNCaP-shPRMT5 cells without (Dox-) PRMT5 knockdown. The 5 m time point indicates how much DNA damage is induced by the indicated dose of IR. The 2 h time point indicates how much DNA damage is repaired within 2 h post the indicated dose of IR.
**(B)** Quantification of DNA damage in each individual cell via calculating the relative amount of DNA in the tail vs. head of the comet ('% tail DNA') from **A**.
**(C)** Migration of DNA via neutral comet assay 2 h post indicated dose of IR in LNCaP-shPRMT5 cells with (Dox+) and without (Dox-) PRMT5 knockdown.
**(D)** Quantification of DNA damage in each individual cell via calculating the relative amount of DNA in the tail vs. head of the comet ('% tail DNA') from **C**.

Box and whiskers plot in **B** and **D** show the median value (line), interquartile range (box), and 10-90 percentile (whiskers) of pooled '% tail DNA' values from 3 independent experiments. Statistical analysis comparing experimental to the control ('Dox-') was performed using Mann-Whitney *U*-test (**** $P \leq 0.0001$ and NS $P > 0.05$).

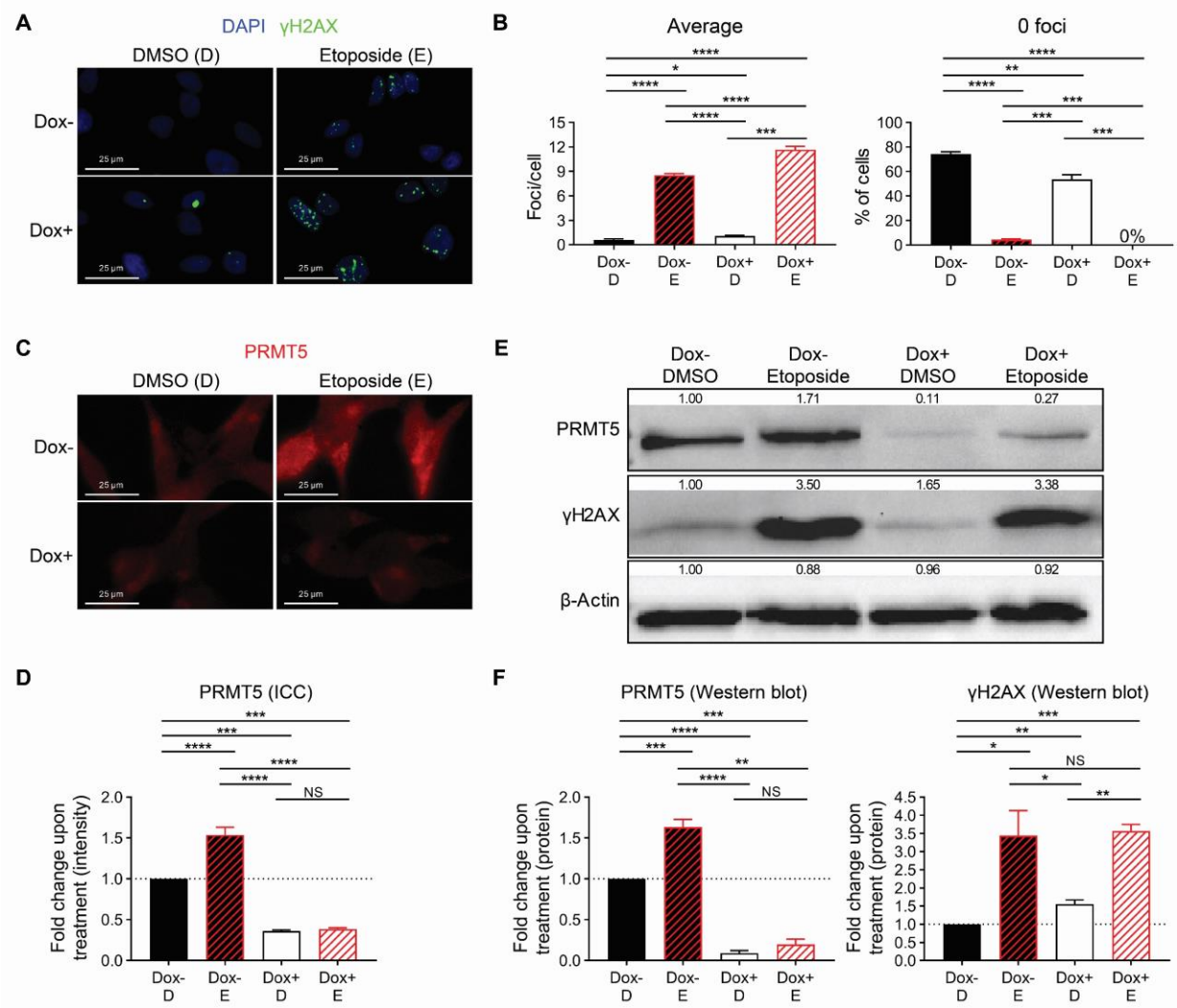


**Figure S2.2: PRMT5 regulates the repair of etoposide-induced DSBs in prostate cancer cells (Related to Figure 2.2)**

**(A)** DSBs after 48 h of etoposide (E) or DMSO (D) treatment in LNCaP-shPRMT5 cells with (Dox+) and without (Dox-) PRMT5 knockdown.
**(B)** Quantification of DSBs in each individual cell from **A** as described in **Figure 2.2B**.
**(C)** PRMT5 expression in cells from **A.**
**(D)** Quantification of PRMT5 expression in images from **C**. For each biological replicate, values were normalized to the value for 'Dox-,DMSO' to calculate the fold change in protein expression upon treatment.
**(E)** Representative western blot showing changes in protein expression in cells from **A.** Values shown indicate the intensity relative to 'Dox-,DMSO' for the biological replicate used as the representative western blot.
**(F)** Quantification of protein expression via western blotting from **E**. For each biological replicate, values were normalized to the value for 'Dox-,DMSO' to calculate the fold change in protein expression upon treatment.

Fluorescence images in **A** and **C** are representative immunocytochemistry images (blue = DAPI, green = γH2AX, and red = PRMT5). Bars in **B** are the mean ± s.d. of 4 independent experiments and Bars in **D** and **F** are the mean ± s.d. of 3 independent experiments. Statistical analysis was performed using Brown-Forsythe and Welch ANOVA followed by Dunnett's T3 multiple comparisons test (* $P \leq 0.05$; ** $P \leq 0.01$, *** $P \leq 0.001$, **** $P \leq 0.0001$, NS $P > 0.05$).

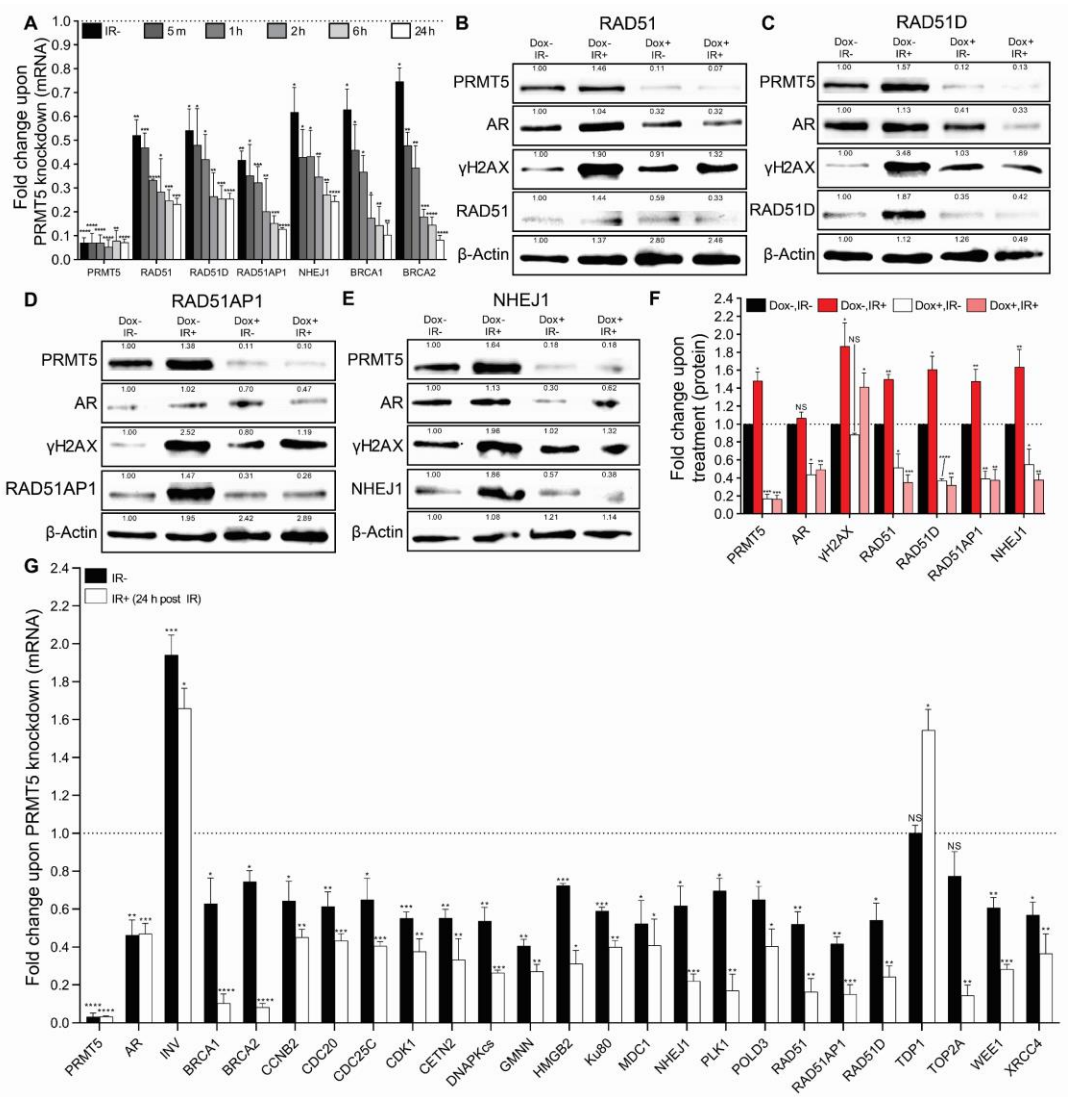


**Figure S2.3: PRMT5 activates transcription of genes that encode proteins involved in the repair of DSBs (Related to Figure 2.5)**

**(A)** Quantification of mRNA via RT-qPCR at the indicated time point post 2 Gy IR in irradiated (IR+) and non-irradiated (IR-) LNCaP-shPRMT5 cells with (Dox+) and without (Dox-) PRMT5 knockdown. For each biological replicate, the value for Dox+ was normalized to the value for Dox- to calculate the fold change in mRNA expression upon PRMT5 knockdown (See also **Figure 2.5B**).
**(B)-(E)** Representative western blots showing protein expression at 6 h post 2 Gy IR in irradiated (IR+) and non-irradiated (IR-) LNCaP-shPRMT5 cells with (Dox+) and without (Dox-) PRMT5 knockdown. Values shown indicate the intensity relative to IR- for the biological replicate used as the representative western blot.
**(F)** Quantification of protein expression via western blotting from **B**-**E**. For each biological replicate, values were normalized to the value for 'Dox-/IR-' to calculate the fold change in protein expression upon treatment.
**(G)** Quantification of mRNA via RT-qPCR 24 h post 2 Gy IR in irradiated (IR+) and non-irradiated (IR-) LNCaP shPRMT5 cells with (Dox+) and without (Dox-). For each biological replicate, the value for Dox+ was normalized to the value for Dox- to calculate the fold change in protein expression upon PRMT5 knockdown (See also **Figure 2.5A** and **2.5F**).

Bars in **A**, **F**, and **G** are the mean ± s.d. of 3 independent experiments. Statistical analysis comparing experimental to the control ('Dox-' or 'Dox- / IR-') was performed using Brown-Forsythe and Welch ANOVA followed by Dunnett's T3 multiple comparisons test (* $P \leq 0.05$; ** $P \leq 0.01$, *** $P \leq 0.001$, **** $P \leq 0.0001$, NS $P > 0.05$).

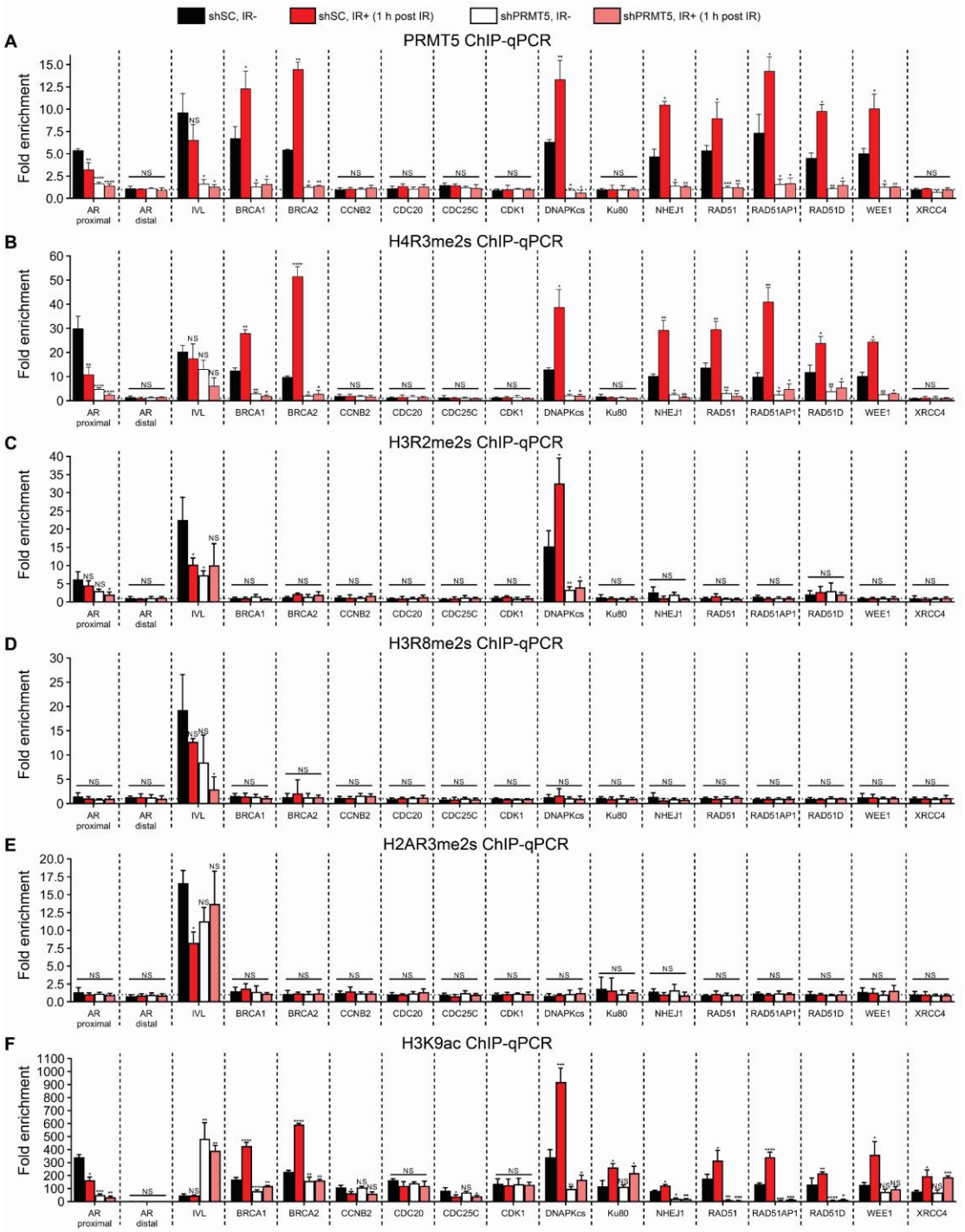


**Figure S2.4: PRMT5 likely functions as an epigenetic activator of genes involved in the repair of DSBs (Related to Figure 2.5)**

**(A)-(F)** Quantification of enrichment (**A**: PRMT5, **B**: H4R3me2s, **C**: H3R2me2s, **D**: H3R8me2s, **E**: H2AR3me2s and **F**: H3K9ac) at the promoter region of the indicated genes 1 h post 2 Gy IR via ChIP-qPCR in irradiated (IR+) and non-irradiated (IR-) LNCaP-shSC or shPRMT5 cells via ChIP-qPCR. For each biological replicate, the value for IP was normalized to the value for IgG to calculate the fold enrichment (See also **Figure 2.5A**).

All bars are the mean ± s.d. of 3 independent experiments. Statistical analysis was performed using Brown-Forsythe and Welch ANOVA followed by Dunnett's T3 multiple comparisons test and the comparison to the control ('shSC, IR-') is shown (* $P \leq 0.05$; ** $P \leq 0.01$, *** $P \leq 0.001$, **** $P \leq 0.0001$, NS $P > 0.05$).

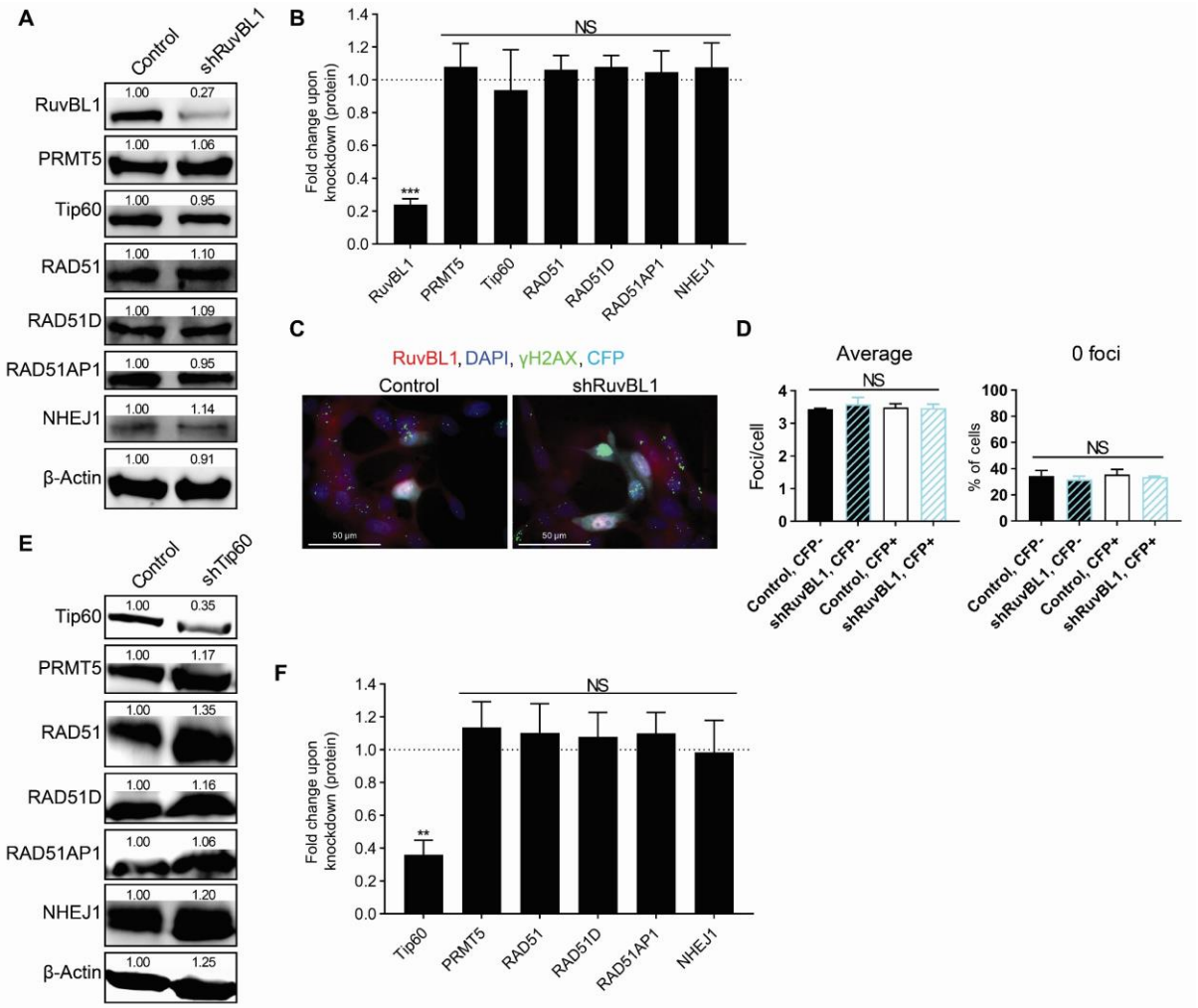


**Figure S2.5: The transcriptional regulation of DSB repair genes by PRMT5 is not dependent on RuvBL1 or Tip60**

**(A)** Representative western blot showing the protein expression in LNCaP cells with (shRuvBL1) and without (control) RuvBL1 knockdown. Values shown indicate the intensity relative to control for the biological replicate used as the representative western blot.
**(B)** Quantification of protein expression via western blotting from **A**. For each biological replicate, values were normalized to the value for 'control' to calculate the fold change in protein expression upon RuvBL1 knockdown.
**(C)** DSBs 6 h post 2 Gy IR in LNCaP cells with (shRuvBL1) and without (control) RuvBL1 knockdown.
**(D)** Quantification of DSBs in each individual cell from **C** as described in **Figure 2.2B**. CFP was used as a transfection control such that RuvBL1 was knocked down solely in CFP+ cells
**(E)** Representative western blot showing the protein expression in LNCaP cells with (shTip60) and without (control) Tip60 knockdown. Values shown indicate the intensity relative to control for the biological replicate used as the representative western blot.
**(F)** Quantification of protein expression via western blotting from **A**. For each biological replicate, values were normalized to the value for 'control' to calculate the fold change in protein expression upon Tip60 knockdown.

Fluorescence images in **C** are representative immunocytochemistry images (blue = DAPI, red = RuvBL1, and cerulean = CFP). Bars in **B**, **D**, and **F** are the mean ± s.d. of 3 independent experiments. Statistical analysis for **B** and **F** comparing experimental to the control ('control') was performed using Welch's *t*-test while statistical analysis for **D** was performed using Brown-Forsythe and Welch ANOVA followed by Dunnett's T3 multiple comparisons test (* $P \leq 0.05$; ** $P \leq 0.01$, *** $P \leq 0.001$, **** $P \leq 0.0001$, NS $P > 0.05$).

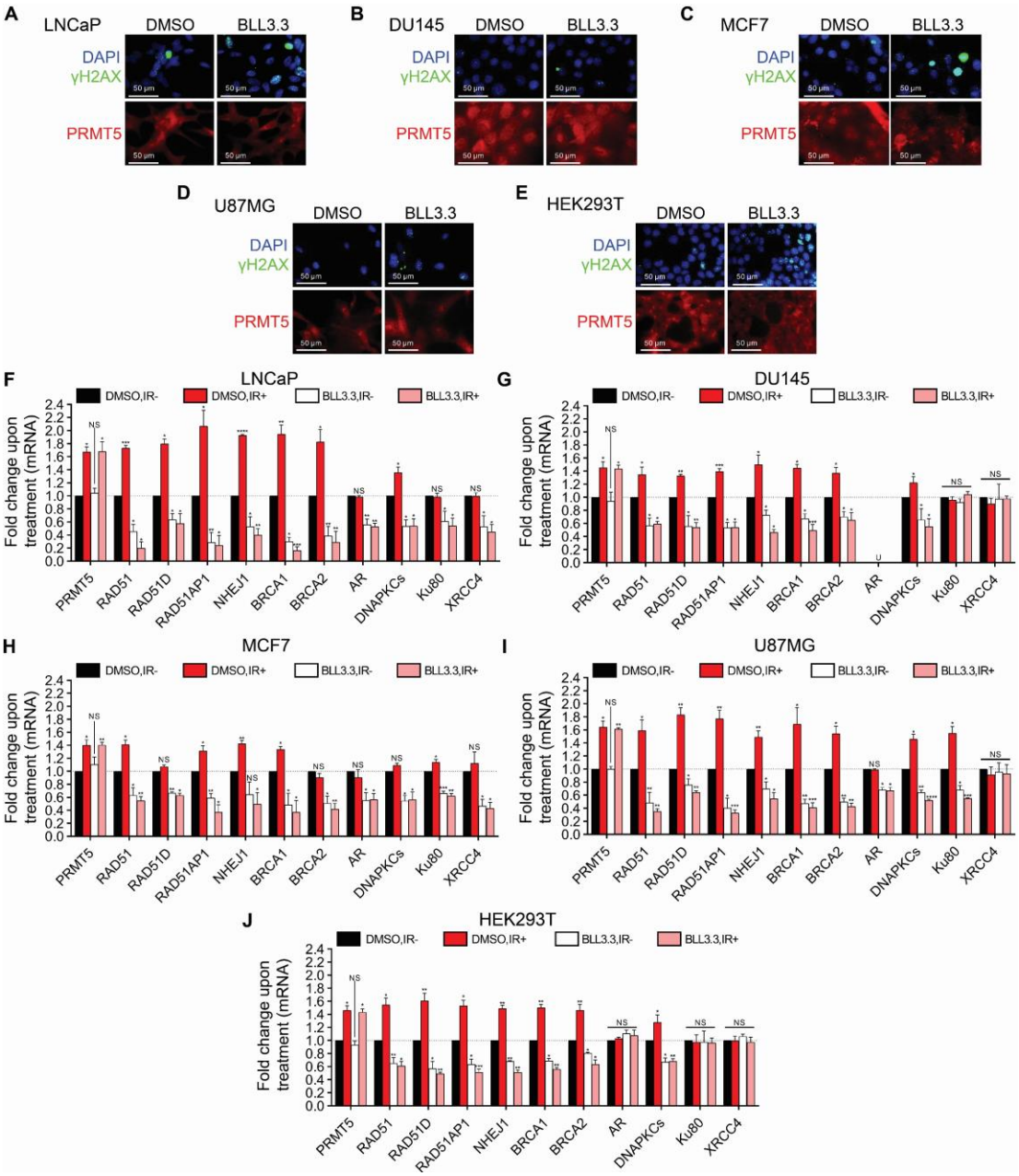


**Figure S2.6: PRMT5 regulates the expression of DNA damage response (DDR) genes and is required to repair IR-induced double-strand breaks (DSBs) in multiple cell types (Related to Figure 2.6)**

**(A)-(E)** DSBs 6 h post 2 Gy IR in the indicated cell lines (**A**: LNCaP, **B**: DU145, **C**: MCF7, **D**: U87MG, **E**: HEK293T) with PRMT5 inhibition (BLL3.3) or without PRMT5 inhibition (DMSO) as described in **Figure 2B**. Fluorescence images in **A-E** are representative immunocytochemistry images (blue = DAPI, green = γH2AX, and red = PRMT5) (see also **Figure 2.6A** for statistical analysis).
**(F)-(J)** Quantification of mRNA via RT-qPCR 6 h post 2 Gy IR in the indicated irradiated (IR+) and non-irradiated (IR-) cell lines (**F**: LNCaP, **G**: DU145, **H**: MCF7, **I**: U87MG, **J**: HEK293T) with PRMT5 inhibition (BLL3.3) or without PRMT5 inhibition (DMSO). For each biological replicate, values were normalized to the value for 'DMSO/IR-' (untreated) to calculate the fold change in mRNA expression upon treatment. (See also **Figure 2.6B**).

Bars are the mean ± s.d. of 3 independent experiments. Statistical analysis comparing experimental to the control ( 'DMSO/IR-') was performed using Forsythe and Welch ANOVA followed by Dunnett's T3 multiple comparisons test (* $P \leq 0.05$; ** $P \leq 0.01$, *** $P \leq 0.001$, **** $P \leq 0.0001$, NS $P > 0.05$).

# CHAPTER 3. SELECTIVE COOPERATION WITH PICLN FACILITATES THE FUNCTION OF PRMT5 AS A MASTER EPIGENETIC ACTIVATOR OF DNA DOUBLE-STRAND BREAK REPAIR GENES

The following chapter was reproduced and modified with permission from[1]:

Owens, J. L. et al. PRMT5 Cooperates with pICln to Function as a Master Epigenetic Activator of DNA Double-Strand Break Repair Genes. iScience 23, 100750 (2020).

## 3.1 Summary

The repair of DNA double-strand breaks (DSBs) is critical for cell survival and genome integrity. To facilitate the repair of DSBs, PRMT5 epigenetically activates transcription of DNA damage response (DDR) genes leading to their transient upregulation. We present evidence that pICln, but not MEP50, likely helps PRMT5 perform this essential role. Under normal conditions, a complex involving PRMT5:pICln maintains basal expression of DDR genes. Ionizing radiation (IR) induces both PRMT5 protein upregulation and pICln nuclear localization which leads to an increase in the PRMT5:pICln interaction in the nucleus. The PRMT5:pICln complex is then recruited to the promoters of DDR genes to activate their expression. Just like targeting PRMT5, targeting pICln also hinders repair of DSBs. pICln expression also positively correlates with DDR genes across 32 clinical cancer data sets. Thus, targeting pICln or the PRMT5:pICln interaction may also be explored in combination with radiation or chemotherapy for cancer treatment.

## 3.2 Introduction

The human genome is constantly exposed to stresses that cause damage to DNA. The DNA damage response (DDR) is an evolutionarily conserved cellular reaction to these genotoxic stresses that allows cells to repair DNA damage and survive. DNA double-strand breaks (DSBs) are the most lethal form of DNA damage[247]. To facilitate the repair of DSBs, Protein arginine methyltransferase 5 (PRMT5) epigenetically activates transcription of DDR genes[1]. However, little is known about how PRMT5 performs this essential epigenetic function to repair DSBs.

PRMT5 is a type II methyltransferase that plays diverse roles in the cell[110,111]. PRMT5 regulates these processes through post-translational methylation of non-histone substrates and

changes in gene expression via symmetrical dimethylation of arginine residues in histones H4R3 (H4R3me2s), H3R2 (H3R2me2s), H3R8 (H3R8me2s), and H2AR3 (H2AR3me2s)[110]. The function of PRMT5 can be regulated based upon the degree of expression and subcellular localization. For example, PRMT5 must be localized to the nucleus to regulate gene expression via histone methylation. PRMT5 activity can also be modulated by several interacting proteins including MEP50, which is believed to be the obligate cofactor of PRMT5 and required for PRMT5 methyltransferase activity[110,111,140,141].

Contrary to our expectation, we observed that MEP50 did not participate in the regulation of PRMT5 target genes involved in DDR. Here, we present evidence that PRMT5 cooperates with pICln, independently of its canonical cofactor MEP50, to function as a master epigenetic activator of DDR genes. Under normal conditions, a complex involving PRMT5:pICln maintains basal expression of DDR genes. Upon DNA damage, PRMT5 protein expression and pICln nuclear localization are increased. This allows PRMT5 and pICln to upregulate target genes that encode proteins involved in homologous recombination (HR) (RAD51, RAD51D, RAD51AP1, BRCA1, and BRCA2), non-homologous end joining (NHEJ) (NHEJ1/XLF and DNAPKcs), and $G_2$ arrest (WEE1). Significantly, both PRMT5 and pICln expression positively correlates with the expression of these target genes across most of the 32 clinical cancer data sets analyzed. Although PRMT5, along with its cofactor MEP50, primarily functions as an epigenetic repressor, our results demonstrate that PRMT5 together with pICln can activate gene expression and further clarify the mechanism for the transient upregulation of repair proteins upon DNA damage.

## 3.3 Results

### 3.3.1 *pICln, but not MEP50, is also required for transcriptional activation of DDR genes and for efficient repair of DSBs*

As MEP50 is believed to be the obligate cofactor of PRMT5 and required for PRMT5 methyltransferase activity[110,285,141,140], we determined if MEP50 plays a role in regulating the expression of DDR genes. Using doxycycline (Dox)-inducible MEP50 knockdown stable cell lines isolated from single-cell-derived clones (LNCaP-shMEP50), we unexpectedly observed that knockdown of MEP50 did not affect the expression of PRMT5 target genes involved in DDR at the mRNA (Figure 3.1A) or protein (Figures S3.1A and S3.1B) level in untreated or irradiated LNCaP-shMEP50 cells. However, consistent with the previous finding that PRMT5 and MEP50

represses IVL expression[253], knockdown of MEP50 caused an increase in IVL expression (Figure 3.1A). Furthermore, MEP50 knockdown did not affect the repair of ionizing radiation (IR)-induced DSBs (Figures 3.1B and 3.1C). These results suggest that PRMT5 may not rely on MEP50 to regulate transcription of genes involved in DDR.

We previously performed mass spectrometry analysis of PRMT5-immunoprecipitated lysate to identify interacting proteins of PRMT5 in LNCaP cells[286]. We predictably identified MEP50 (peptide fragment *ILLWDTR*), but we also identified pICln[154–156,159,287] (peptide fragment *GLGTGTLYIAESR*) as an interacting protein of PRMT5. We then developed Dox-inducible pICln knockdown stable cell lines isolated from single-cell-derived clones (LNCaP-shpICln) and surprisingly observed that knockdown of pICln caused a decrease in PRMT5 target gene expression at the mRNA (Figure 3.1D) and protein (Figures S3.1C and S3.1D) level in untreated and irradiated LNCaP-shpICln cells. Furthermore, knockdown of pICln impaired repair of IR-induced DSBs (Figure 3.1E and 3.1F) to an extent comparable to PRMT5 knockdown. These results demonstrate that knockdown of pICln phenocopies knockdown of PRMT5.

We next assessed the binding of these proteins to the promoters of PRMT5 target genes involved in DDR. Although MEP50 was present at the promoter of the control gene IVL, MEP50 was not present at the promoter of PRMT5 target genes involved in DDR while pICln was present (Figures 3.1G, 3.1H, S3.1E, and S3.1F). Upon IR, binding of pICln to the promoter of DDR genes increased (Figure 3.1H) and knockdown of PRMT5 almost completely abrogated enrichment of pICln (Figure S3.1F), suggesting that PRMT5 recruits pICln to targeted promoter regions. Additionally, other previously identified PRMT5 interacting proteins, RioK1[159] and COPR5[152,153,288], were not found at the promoter of DDR genes in untreated or irradiated LNCaP cells (Figure S3.1G and S3.1H). These results suggest that PRMT5 may cooperate with pICln to regulate transcription of DDR genes.

### 3.3.2 *IR transiently induces PRMT5 protein expression on a timescale similar to the repair of IR-induced double-strand breaks (DSBs)*

Given the importance of PRMT5 in DSB repair and activation of target gene expression upon IR, we hypothesized that IR may induce PRMT5 expression. To test this, we analyzed PRMT5 protein expression via both immunocytochemistry and western blotting at various time points following IR of LNCaP cells. Indeed, IR induced PRMT5 expression as quickly as 5 m, and

the induction lasted for nearly 24 h (Figures 3.2A-3.26D). Importantly, the peak of PRMT5 protein expression (between 5 m and 1 h) coincided with the increased recruitment of PRMT5 to the promoters of DDR genes (1 h). Similarly, changes in PRMT5 expression closely mirrored the time-course of DSB repair. The rapid induction of protein expression likely suggests a post-transcriptional or post-translational regulation. However, RT-qPCR analysis confirmed a small, but significant, sustained induction of PRMT5 expression at the mRNA level (Figure 3.2E). This result suggests that transcriptional activation of PRMT5 also contributes to prolonged elevation of PRMT5 expression. Furthermore, PRMT5 was upregulated at the protein level by etoposide treatment in our previous study[1] (Figures S2.2C-S2.2F), suggesting that DNA damage, in general, can signal the induction of PRMT5. Collectively, these results indicate that PRMT5 is upregulated upon IR to promote repair of IR-induced DSBs, and that the upregulation of DDR genes is likely facilitated by IR-induced upregulation of PRMT5.

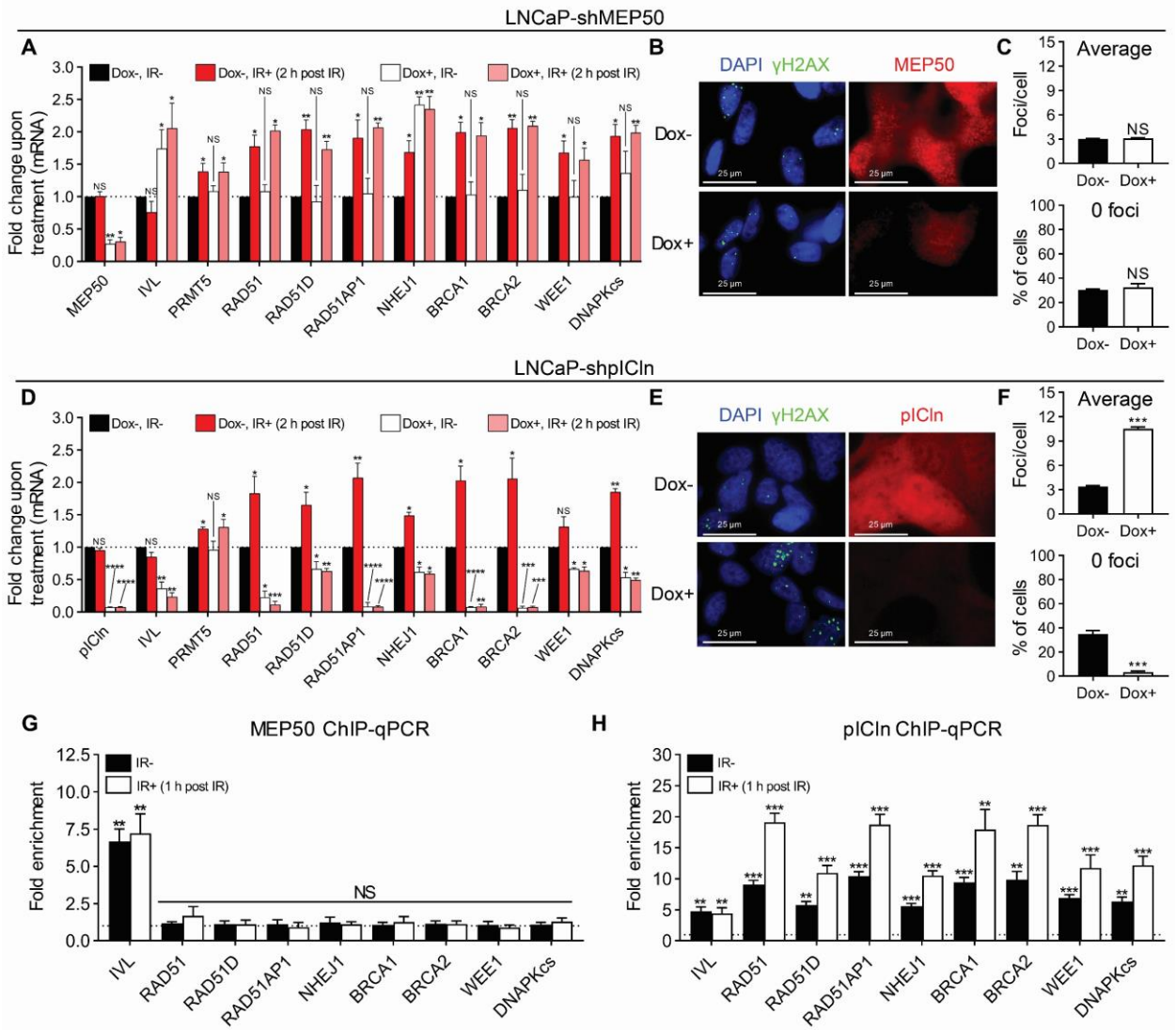


**Figure 3.1: pICln, but not MEP50, is also required for transcriptional activation of DDR genes and for efficient repair of double-strand breaks (DSBs)**

**(A)** Quantification of mRNA via RT-qPCR 2 h post 2 Gy IR in LNCaP-shMEP50 cells with (Dox+) and without (Dox-) MEP50 knockdown. For each biological replicate, values were normalized to the value for 'Dox-,IR-' (untreated) to calculate the fold change in mRNA expression upon treatment.
**(B)** DSBs 6 h post 2 Gy IR in LNCaP-shMEP50 cells with (Dox+) and without (Dox-) MEP50 knockdown.
**(C)** Quantification of DSBs in each individual cell from **B** as described in **Figure 2.2B**.
**(D)** Quantification of mRNA via RT-qPCR 2 h post 2 Gy IR in LNCaP-shpICln cells with (Dox+) and without (Dox-) pICln knockdown. For each biological replicate, values were normalized to the value for 'Dox-,IR-' (untreated) to calculate the fold change in mRNA expression upon treatment.
**(E)** DSBs 6 h post 2 Gy IR in LNCaP-shpICln cells with (Dox+) and without (Dox-) pICln knockdown.
**(F)** Quantification of DSBs in each individual cell from **E** as described in **Figure 2.2B**.
**(G** and **H)** Quantification of enrichment (**G**: MEP50 and **H**: pICln) at the promoter region of the indicated genes 1 h post 2 Gy IR via ChIP-qPCR in irradiated (IR+) and non-irradiated (IR-) LNCaP-shSC cells via ChIP-qPCR. For each biological replicate, the value for IP was normalized to the value for IgG to calculate the fold enrichment (See also **Figure S3.1E** and **S3.1F**).

Fluorescence images in **B** and **E** are representative immunocytochemistry images (blue = DAPI, green = γH2AX, red = MEP50 or pICln). All bars are the mean ± s.d. of 3 independent experiments. Statistical analysis for **A** and **D** comparing experimental to the control ('Dox-,IR-') was performed using Brown-Forsythe and Welch ANOVA followed by Dunnett's T3 multiple comparisons test while statistical analysis for **C**, **F**, **G**, and **H** comparing experimental to the control ('Dox-' or 'IgG') was performed using Welch's *t*-test (* $P \leq 0.05$; ** $P \leq 0.01$, *** $P \leq 0.001$, **** $P \leq 0.0001$, NS $P > 0.05$).

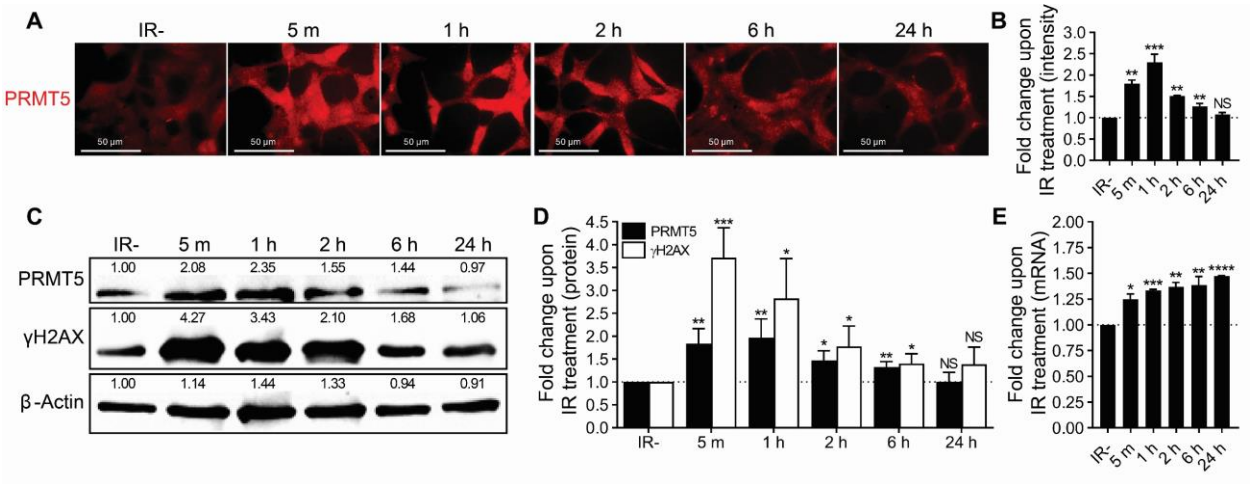


**Figure 3.2: IR transiently induces PRMT5 protein expression on a timescale similar to the repair of IR-induced double-strand breaks (DSBs)**

**(A)** Time-course of PRMT5 expression at the indicated minutes (m) or hours (h) post 2 Gy IR in LNCaP cells.
**(B)** Quantification of PRMT5 expression in images from **A**. For each biological replicate, values were normalized to the value for 'IR-' to calculate the fold change in protein expression upon IR.
**(C)** Representative western blot showing the time-course of protein expression at the indicated minutes (m) or hours (h) post 2 Gy IR in LNCaP cells. Values shown indicate the intensity relative to IR- for the biological replicate used as the representative western blot.
**(D)** Quantification of protein expression via western blotting from **c**. For each biological replicate, values were normalized to the value for 'IR-' to calculate the fold change in protein expression upon IR.
**(E)** Time-course of PRMT5 expression at the mRNA level at the indicated minutes (m) or hours (h) post 2 Gy IR in LNCaP cells via RT-qPCR. For each biological replicate, values were normalized to the value for 'IR-' to calculate the fold change in mRNA expression upon IR.

Fluorescence images in **A** are representative immunocytochemistry images (red = PRMT5). All bars are the mean ± s.d. of 3 independent experiments. Statistical analysis for **B**, **D**, and **E** comparing experimental to the control ('IR-') was performed using Brown-Forsythe and Welch ANOVA followed by Dunnett's T3 multiple comparisons test.

### 3.3.3 *IR induces pICln nuclear localization and MEP50 cytoplasmic localization*

To gain insight on how pICln functions with PRMT5 to regulate the expression of genes involved in DDR, we first determined if IR affects expression of MEP50 or pICln. However, IR did not affect the whole cell protein expression of either MEP50 or pICln (Figures 3.3A-3.3C). We next analyzed the subcellular localization of MEP50 and pICln upon IR. In untreated cells, there is more MEP50 in the nucleus than the cytoplasm (Figure 3.3A). Conversely, there is less pICln in the nucleus than the cytoplasm (Figure 3.3A). Upon IR, the subcellular localization is reversed. This is evident by changes in the nuclear:cytoplasmic (N:C) ratio. Upon IR, the N:C ratio of MEP50 decreased while the N:C ratio of pICln increased (Figures 3.3A-3.3C). This suggests that upon IR there is more pICln and less MEP50 in the nucleus to interact with PRMT5. IR-induced nuclear localization of pICln thus likely contributes to IR-induced pICln binding to the promoters of genes involved in DDR.

### 3.3.4 *IR promotes the PRMT5:pICln interaction, particularly in the nucleus*

To assess the protein-protein interaction (PPI) directly, we utilized bimolecular fluorescence complementation (BiFC) assay [289–292], which is uniquely applicable in assessing the subcellular localization of PPIs in live cells[293]. In untreated cells, PRMT5 interacts with MEP50 about equally in the nucleus and the cytoplasm (Figure 3.4A). However, PRMT5 interacts with pICln more strongly in the cytoplasm than the nucleus (Figure 3.4A). Upon IR, the PRMT5:MEP50 PPI is decreased in both the nucleus and cytoplasm (Figures 3.4A-3.4C) suggesting that DNA damage may inhibit the interaction between PRMT5 and MEP50. Consistent with the change in pICln subcellular localization, BiFC confirmed an IR-induced PPI increase between PRMT5 and pICln particularly in the nucleus (Figures 3.4A-3.4C). Overall, these results suggest that the regulation of genes involved in DDR by PRMT5 is facilitated by the IR-induced PRMT5:pICln interaction in the nucleus.

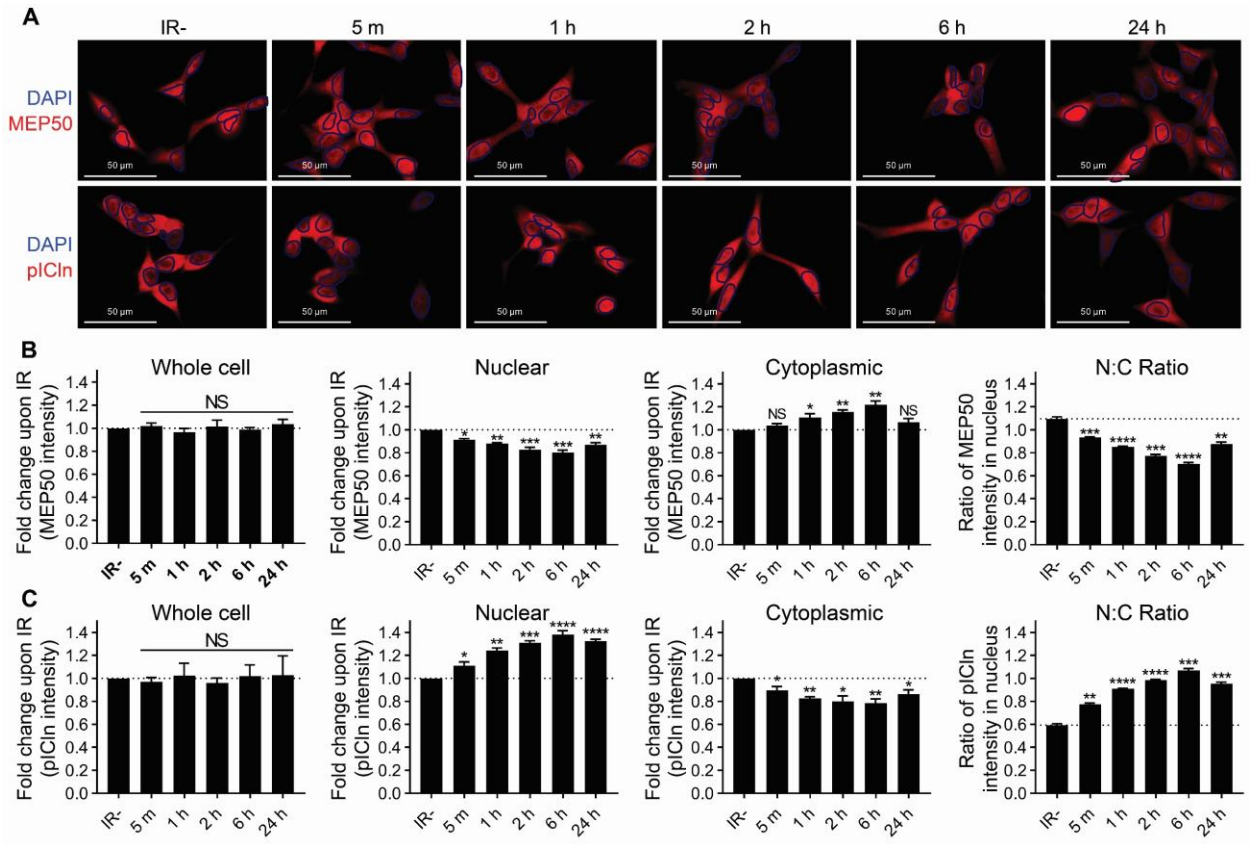


**Figure 3.3: IR induces pICln nuclear localization and MEP50 cytoplasmic localization**

**(A)** Time-course of MEP50/pICln expression/localization at the indicated minutes (m) or hours (h) post 2 Gy IR in LNCaP cells.
**(B)** Quantification of MEP50 expression/localization in images from **A**: 'Whole cell' indicates MEP50 expression in the entire cell, 'Nuclear' indicates MEP50 expression in the nucleus which was defined by DAPI staining, 'Cytoplasmic indicates MEP50 expression in the cytoplasm which was defined as staining outside DAPI, and 'N:C ratio' was calculated by dividing the value for nucleus by the value for cytoplasmic for each cell individually such that an N:C ratio of 1 indicates equal expression in both the nucleus and cytoplasm.
**(C)** Quantification of pICln expression/localization in images from **A** as described above.

Fluorescence images in **A** are representative immunocytochemistry images (blue = DAPI and red = MEP50 or pICln). Blue circles outline DAPI staining to allow for better visibility of expression in the nucleus. All bars are the mean ± s.d. of 3 independent experiments. Statistical analysis for **B** and **C** comparing experimental to the control ('IR-') was performed using Brown-Forsythe and Welch ANOVA followed by Dunnett's T3 multiple comparisons test

### 3.3.5 *The expression of PRMT5 and pICln correlate with the expression of DDR genes in most human cancer tissues*

Previously, to assess potential clinical relevance to our findings that PRMT5 epigenetically activates transcription of DDR genes, we analyzed mRNA expression in 32 clinical cancer data sets achieved from The Cancer Genome Atlas (TCGA) Pan-Cancer analysis[254]. We focused on PRMT5, AR, and DDR genes which were identified as primary target genes of both PRMT5 and

AR. The expression of PRMT5 correlated positively with DDR genes in almost all cancers (Figure 3.5A. See also Figure 2.7A). As our data suggested that pICln, but not MEP50, cooperates with PRMT5 to regulate DDR genes, we also analyzed the correlations between MEP50 or pICln and the same DDR genes. Although MEP50 expression positively correlated with some DDR genes in some cancers (Figures 3.5A and 3.5B), pICln exhibited significantly stronger correlations with these DDR genes than MEP50 in almost all cancers (Figures 3.5A and 3.5B). Furthermore, PRMT5 correlated more significantly with pICln than MEP50 (Figure 3.5B). Collectively, our results suggest that PRMT5 and pICln play a conserved role in activating expression of genes required for the repair of IR-induced DSBs.

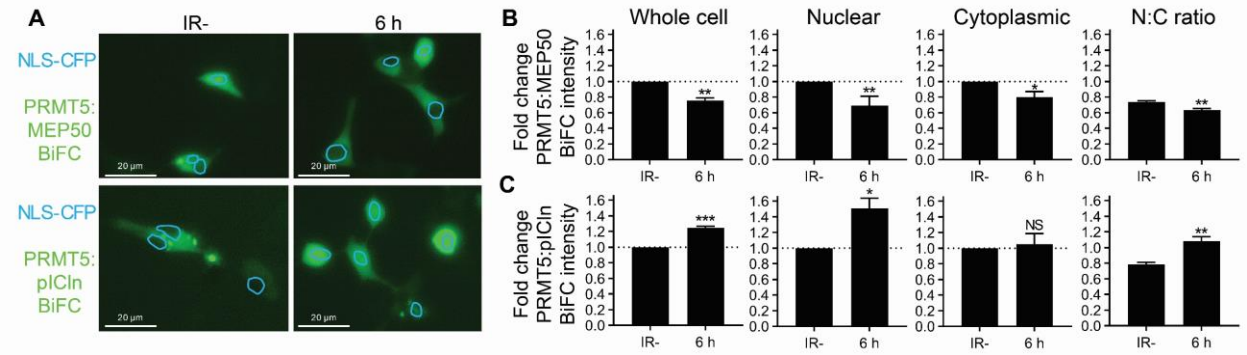


**Figure 3.4: IR promotes the PRMT5:pICln interaction, particularly in the nucleus**

**(A)** PRMT5:MEP50 and PRMT5:pICln interaction 6 h post 2 Gy IR in irradiated (6 h) and non-irradiated (IR-) LNCaP cells via BiFC assay.
**(B)** Quantification of PRMT5:MEP50 BiFC intensity in images from **A**: 'Whole cell' indicates BiFC intensity in the entire cell, 'Nuclear' indicates BiFC intensity in the nucleus which was defined by NLS-CFP signal, 'Cytoplasmic indicates BiFC intensity in the cytoplasm which was defined as staining outside NLS-CFP signal, and 'N:C ratio' was calculated by dividing the value for nucleus by the value for cytoplasmic for each cell individually such that an N:C ratio of 1 indicates equal interaction in both the nucleus and cytoplasm. NLS-CFP was used as a transfection control and a marker of the nucleus.
**(C)** Quantification of PRMT5:pICln BiFC intensity in images from **A** as described above.

Fluorescence images in **A** are representative images from BiFC assay (green = PRMT5:MEP50 and PRMT5:pICln, cerulean = NLS-CFP). Blue circles outline NLS-CFP signal to allow for better visibility of expression in the nucleus. All bars are the mean ± s.d. of 3 independent experiments. Statistical analysis for **B** and **C** comparing experimental to the control ('IR-') was performed using Welch's *t*-test (* $P \leq 0.05$; ** $P \leq 0.01$, *** $P \leq 0.001$, **** $P \leq 0.0001$, NS $P > 0.05$).

### 3.3.6 *PRMT5 cooperates with its cofactor pICln to function as a master epigenetic regulator of double-strand break (DSB) repair*

Combining our findings from chapter 2 and chapter 3, we have developed a model for how PRMT5 regulates the repair of DSBs (Figure 3.6). Under normal conditions, a complex involving PRMT5:pICln maintains basal expression of DDR genes. Targeting PRMT5 or pICln causes a downregulation of DDR genes and coincides with increased spontaneous DSBs independent of external DNA damage inducers. Upon DNA damage, PRMT5 protein is upregulated and pICln nuclear localization increases which leads to an increase in the PRMT5:pICln interaction in the nucleus. The interaction between PRMT5 and MEP50 is also decreased upon DNA damage which may facilitate the increase in binding of pICln to PRMT5. The PRMT5:pICln complex is then recruited to the promoters of genes involved in the DDR where it epigenetically activates expression of target genes via symmetric dimethylation of H4R3 (H4R3me2s). PRMT5:pICln target genes, most notably repair proteins, are then upregulated at the mRNA and protein level. With elevated expression of DDR proteins, the cell is able to repair the DSBs. Once DSBs are repaired, PRMT5 expression as well as the expression of DDR target genes return to basal levels.

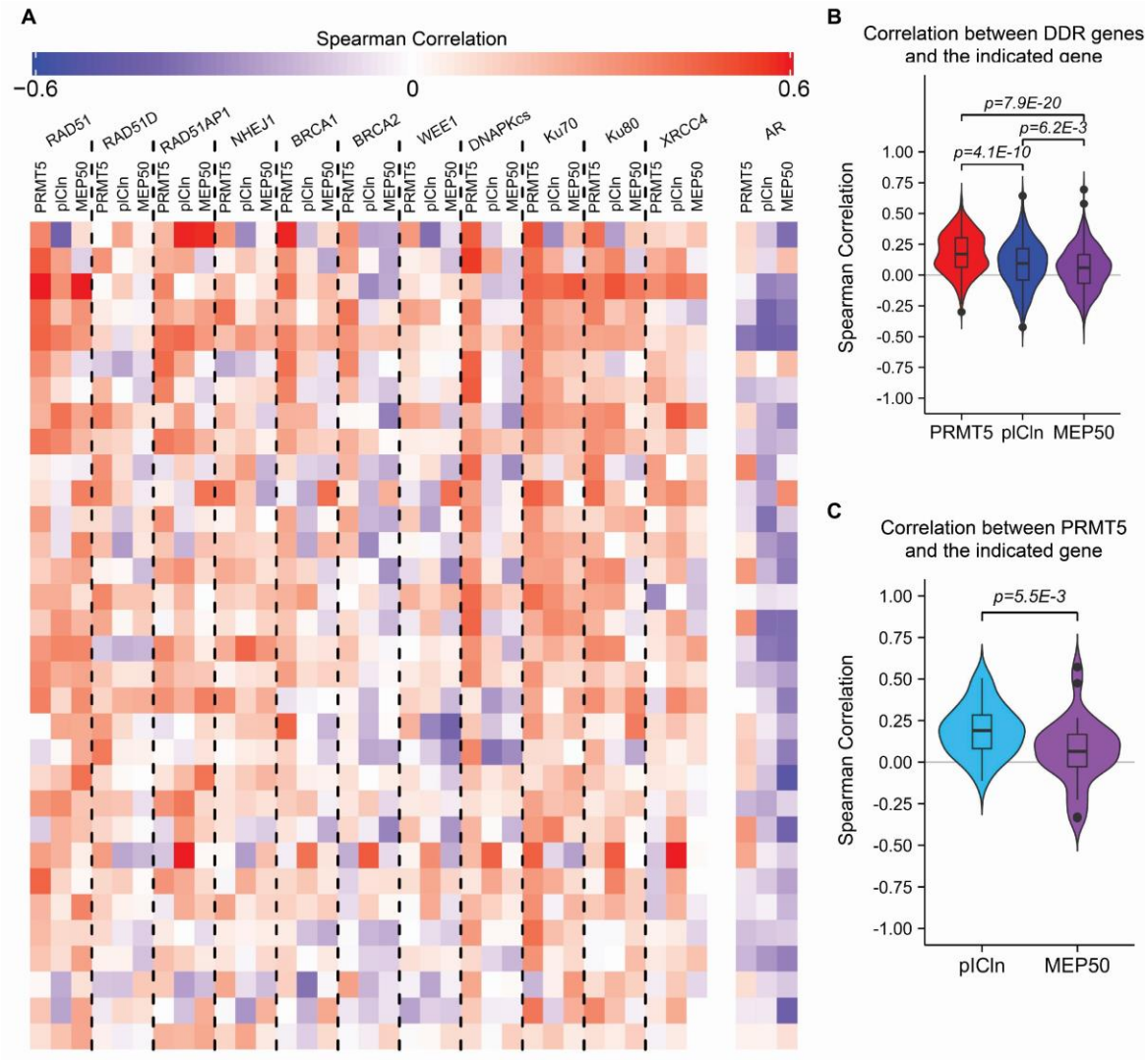


**Figure 3.5: The expression of PRMT5 and pICln correlate with the expression of DDR genes in most human cancer tissues**

**(A)** Heatmap of Spearman correlation values between the indicated DDR genes and either PRMT5, CLNS1A (pICln), or WDR77 (MEP50) at the mRNA level across 32 clinical cancer data sets. The right section shows the correlation values between AR and PRMT5, pICln, or MEP50, respectively. Red indicates a positive correlation while blue indicates a negative correlation. The cancer types (y-axis, not listed) were sorted by the mean value of correlations between PRMT5 and DDR genes. (See also **Figures 2.6C-2.6E**).
**(B)** Violin plot representation of Spearman correlation values between DDR genes and either PRMT5, CLNS1A (pICln), or WDR77 (MEP50).
**(C)** Violin plot representation of Spearman correlation values between CLNS1A (pICln) or WDR77 (MEP50) and PRMT5.

Box-and-whiskers plots in **B** and **C** show the median value (line) and interquartile range between the first and third quartiles (box). The upper whisker extended to the largest value no further than '1.5 x interquartile range' and the lower whisker extended to the smallest value at most '1.5 x interquartile range'. Outliers beyond the whiskers are shown as dots. Statistical analysis in **B** and **C** was performed using Wilcoxon test and the p-values are displayed.

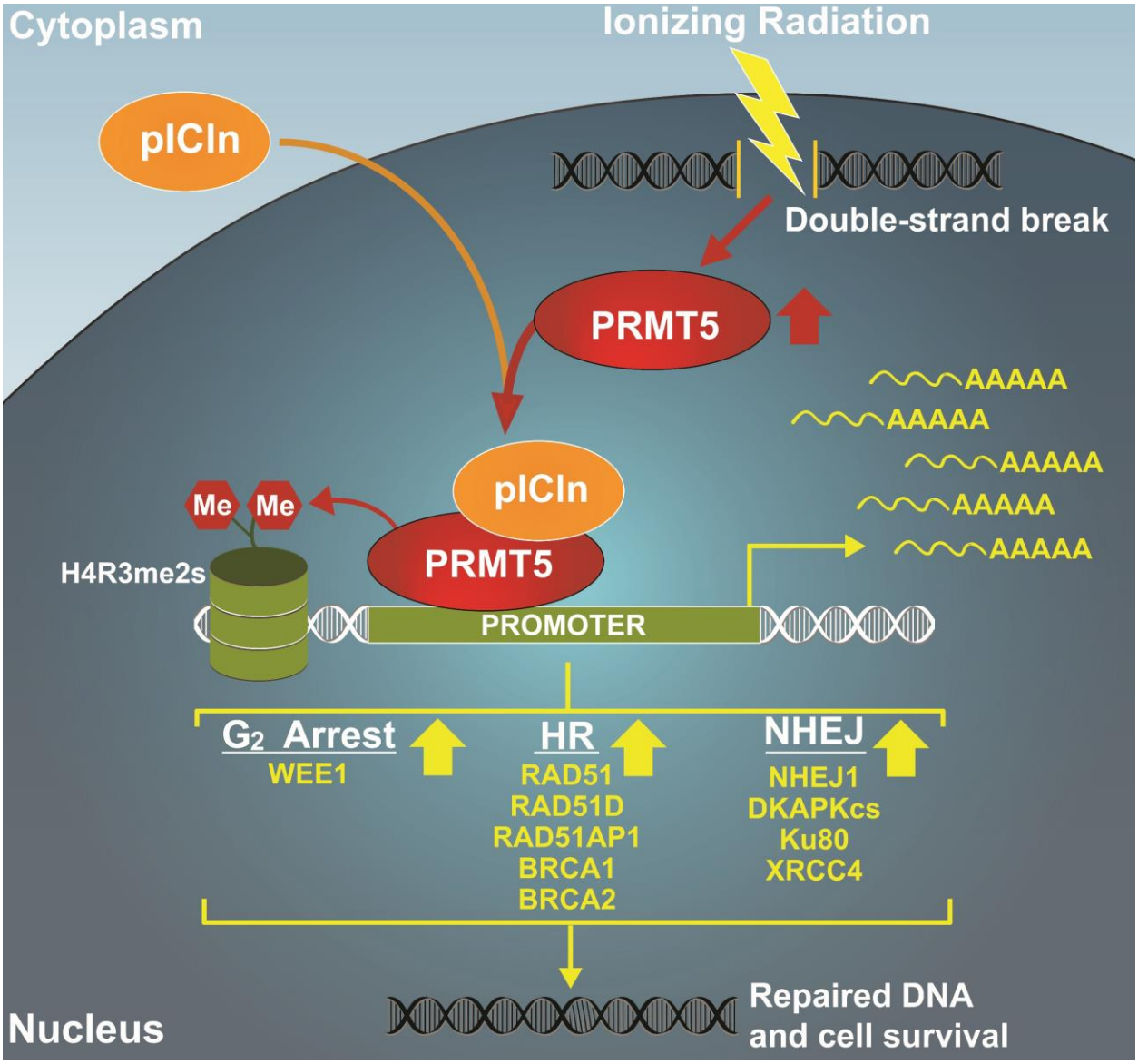


**Figure 3.6: PRMT5 cooperates with its cofactor pICln to function as a master epigenetic regulator of double-strand break (DSB) repair**

Under normal conditions, a complex involving PRMT5:pICln maintains basal expression of DDR genes. IR induces both PRMT5 protein upregulation and pICln nuclear localization which leads to an increase in the PRMT5:pICln interaction in the nucleus. The PRMT5:pICln complex is then recruited to the promoters of genes involved in the DDR where it epigenetically activates expression of target genes via symmetric dimethylation of H4R3 (H4R3me2s). PRMT5:pICln target genes, most notably repair proteins, are then upregulated at the mRNA and protein level to facilitate the repair of IR-induced DSBs via HR, NHEJ, and G2 arrest. Genes in green are validated epigenetic targets of PRMT5 while genes in blue are potential secondary targets of PRMT5.

## 3.4 Discussion

### 3.4.1 *PRMT5 is upregulated in response to DNA damage*

PRMT5 plays an essential role in the repair of DSBs through epigenetic activation of DDR genes. Upon IR, PRMT5 is upregulated at both the protein and mRNA level. Several reports show that PRMT5 protein is upregulated in response several DSB inducers such as IR[1,193], etoposide[1], and Methyl methanesulfonate (MMS)[234]. Collectively, these reports suggest that DSBs, in general, can signal for the upregulation of PRMT5 expression.

PRMT5 protein is quickly upregulated (within 5 min) in response to 2 Gy IR treatment (Figures 3.2A-D), suggesting a post-transcriptional or post-translational regulation. The peak of elevated PRMT5 protein expression is somewhere between 5 min and 1 hour which coincides with increased binding to target genes to facilitate its role as an epigenetic activator of DDR gene transcription. Another study demonstrated that the protein levels of PRMT5, along with a methylation target KLF4, are also increased in response to a higher dose of IR (5 Gy in U2OS cells)[193]. The changes in PRMT5 protein expression were similar to our report (in response to 2 Gy in LNCaP cells) except that it was prolonged (remained elevated through the 12 hour time point[193]), likely as a response to a higher dose of IR. Consistent with this, the protein expression of the PRMT5 homologue SKB1 in plants was dose-dependently induced by MMS[234]. This also suggests that the upregulation of PRMT5 protein in response to DSBs is evolutionarily conserved. SKB1 was not upregulated in response to NaCl treatment[234]. Therefore, upregulation of PRMT5 likely occurs more selectively in response to DSBs compared to other environmental stresses. Future studies may determine if PRMT5 protein is upregulated in response to other DNA damages.

### 3.4.2 *DNA damage-induced upregulation of PRMT5 may be due to transcriptional activation*

DNA damage might promote upregulation of PRMT5 at the protein level through transcriptional activation of PRMT5. Upon IR, PRMT5 is also slightly upregulated at the mRNA level (Figure 3.2E). However, this upregulation is much less than the protein upregulation and is sustained for a longer duration. Aflatoxin B1, a DNA intercalating mutagen that can promote DNA damage, can also induce PRMT5 mRNA expression and global symmetric dimethylation

of arginine in a variety of normal and cancer cell types[294]. Therefore, transcriptional activation of PRMT5 may be a common response to DNA damage.

Although it is unknown how PRMT5 is upregulated at the transcript level upon DNA damage, there are several reports describing transcriptional regulation of PRMT5. The PRMT5 promoter contains multiple motifs for transcription factors including NFYA, E2F1, CREB, GATA, and SP1[121,295]. Although we determined that GATA and SP1 likely do not regulate PRMT5 expression in LNCaP cells[121], other reports demonstrate that SP1 may regulate PRMT5 expression different cells types[296,297]. Thus, the transcriptional regulation of PRMT5 may differ based upon cell type and is likely context dependent, such as upon DNA damage.

We previously reported that NFYA activates PRMT5 expression[121] which was confirmed in a recent study[295]. NFYA protein expression is induced upon MMS or UV treatment and activates transcription of DDR genes such as GADD45[298] and OGG1[70]. Interestingly, upon DNA damage, the long form (46 kDa) of NFYA but not the short form (42 kDa) appear to be upregulated while NFYB and NFYC expression were unaffected or may even be downregulated[70,298]. It is possible that upregulation of NFYA may contribute to the increased mRNA levels of PRMT5 upon DNA damage.

Interestingly, E2F1 was also found to bind to the PRMT5 promoter[295]. Cadmium, which leads to oxidative stress-induced DNA damage[299], promotes upregulation of PRMT5[295]. Knockdown of both NYFA and E2F1 causes a decrease in PRMT5 protein expression in both untreated and cadmium-treated MCF7 cells[295], suggesting that NFYA and E2F1 may be at least partially responsible for the upregulation of PRMT5 mRNA upon DNA damage.

PRMT5 also methylates E2F1. PRMT5-catalyzed arginine methylation of E2F1 reduces both E2F1 stability and DNA-binding activity to inhibit transcriptional activation of at least a subset of E2F1 target genes[187]. However, methylation of E2F1 is actually reduced upon DNA damage[187]. Thus, it is possible that upon DNA damage there is a positive feedback loop where reduced methylation of E2F1 promotes transcription of PRMT5. This may also explain why the upregulation of PRMT5 at the mRNA level lags behind the upregulation at the protein level.

### 3.4.3 *DNA damage-induced upregulation of PRMT5 may be due to translational activation*

DNA damage might promote upregulation of PRMT5 at the protein level through increased translation of PRMT5 mRNA into protein. mRNA translation can be affected by

several factors including (1) mRNA stability, (2) initiation of translation, (3) translation elongation rate, and (4) translation termination rate. Because PRMT5 protein is quickly upregulated (within 5 min) in response IR (Figures 3.2A-D), it is possible that the pre-existing pool of mRNA is quickly translated into protein to induce PRMT5 protein expression.

mRNA stability is regulated by microRNAs (miRNAs). PRMT5 is targeted by several miRNAs and a downregulation of PRMT5-targeting miRNAs upon DNA damage could allow for PRMT5 translation and account for increased PRMT5 protein. In response to DNA damage, the levels of miRNAs in cells drastically change[300]. For example, miR-106b is downregulated in response to IR to induce p21-mediated $G_2$ arrest[301]. The miR-106b-25 cluster is predicted to regulate PRMT5, and the time-course of IR-induced upregulation of PRMT5 mRNA we observed closely mimics the time-course of IR-induced downregulation of miR-106b[301]. Interestingly, miR-96, which targets PRMT5[302], also downregulates RAD51 expression[303]. Therefore, a reduction in mi-96 may allow for increased expression of PRMT5 and concomitant increase in RAD51. Another PRMT5-targeting miRNA, miR-15b[304], is actually upregulated quickly upon IR and decreases expression starting 2 hours following IR[305], which may further explain the lag in PRMT5 upregulation at the mRNA level. Overall, changes in expression of several miRNAs upon DNA damage, each with different time-courses and degrees of changes, may regulate PRMT5 protein level.

### 3.4.4 *DNA damage-induced upregulation of PRMT5 may be due to changes in protein stability and proteasomal degradation*

DNA damage might promote upregulation of PRMT5 at the protein level through changes in protein stability or proteasomal degradation. For example, PRMT5 may be post-translationally modified to increase its stability leading to elevation in protein expression. However, it is unknown if PRMT5 is post-translationally modified in response to DNA damage. Post-translational modifications play a particularly important role in DSB repair. Under normal conditions, the MRN complex is distributed evenly in the nucleus. Upon recognition of a DSB, MRN forms foci around the site of damage and recruits ATM[306]. Accumulated MRN/ATM phosphorylate histone H2AX on serine S139 to form γ-H2AX foci within seconds of DNA damage. Activated ATM subsequently phosphorylates several downstream targets[306]. Future

studies may assess if DNA damage-induced ATM signaling promotes changes in PRMT5 protein expression.

Upon IR, the PRMT5:MEP50 PPI is decreased in both the nucleus and cytoplasm while the PRMT5:pICln PPI is increased particularly in the nucleus (Figures 3.4A-3.4C). It is possible that changes in which proteins PRMT5 interacts with can alter PRMT5 stability. For example, SHARPIN is shown to directly interact with PRMT5 and SHARPIN knockdown dramatically decreased PRMT5 protein expression[307]. SHARPIN plays a role in the DDR through the regulation of p53[308]. Therefore, it is possible SHARPIN stabilizes PRMT5 protein upon DNA damage. Future studies may assess the PRMT5 interaction in the presence and absence of IR to see if this may explain how PRMT5 is upregulated upon DNA damage.

DNA damage may also inhibit degradation of PRMT5. We previously reported that PRMT5 protein expression is regulated by the E3 ubiquitin ligase CHIP which mediates ubiquitination and proteasomal degradation[286]. A recent study also implicated CHIP in the DDR via ubiquitination and degradation of p21[309], which is consistent with a previous report where CHIP regulates $G_1$ checkpoint[310]. Although the protein level of CHIP does not appear to be affected by IR-induced DNA damage[309], it is possible that DNA damage demotes the interaction between PRMT5 and CHIP. Therefore, inhibition of proteasomal degradation may contribute to the induction of PRMT5 protein expression.

### 3.4.5 *pICln may function as a cofactor of PRMT5 to epigenetically regulate gene expression independently of MEP50*

There is a long-standing view in the field that the cofactor MEP50 is required for PRMT5 methyltransferase activity and epigenetic function[110,111,140,141]. In solution, PRMT5 can exist as a homodimer or homotetramer. With MEP50, PRMT5 forms a hetero-octameric complex ($PRMT5_4$:$MEP50_4$)[142]. Consistent with these structural studies, biochemical studies have provided evidence that purified PRMT5:MEP50 complex can catalyze dimethylation of various histone substrates including H4R3[140,143]. However, our data suggests that PRMT5 works with pICln for the transcriptional activation of DDR genes via H4R3me2s. This is inconsistent with a previous report where *Pesiridis et al.* showed that titration of pICln decreased H3 and H4 methylation by PRMT5 in an *in vitro* methylation assay[145]. However, as PRMT5 functions in a larger complex, the *in vitro* assay using proteins from a bacterial expression system might not recapitulate the

biochemical and cellular conditions required for H4R3me2s *in vivo*. In our study, knockdown of MEP50 did not affect the expression of PRMT5 target genes involved DDR, and MEP50 was not present at any of the target gene promoters characterized. Instead, pICln was present at the promoter regions of PRMT5 target genes along with H4R3me2s and knockdown of pICln caused a decrease in PRMT5 target gene expression and impaired IR-induced DSB repair. Thus, it is likely that pICln may function as a cofactor of PRMT5 to activate transcription of DDR genes. As the epigenetic regulation of gene expression likely involves formation of a larger protein complex in a gene-specific manner, future characterization of PRMT5 and its cofactors or interacting proteins *in vivo* will provide mechanistic insight into the regulation of expression of PRMT5 target genes.

Although PRMT5-catalyzed histone methylation is predominantly repressive[110], recent studies show PRMT5 can function as an activator of gene expression[114,141,144]. Activation or repression is not likely dependent solely on PRMT5-catalyzed histone methylation as H4R3me2s has been shown to be both a repressive[141] and active chromatin mark[114]. Therefore, additional factors are required to mediate the positive or negative epigenetic regulation by PRMT5. As PRMT5 does not contain a DNA binding domain, additional proteins that recruit PRMT5 to sites on the genome may play a role in mediating the epigenetic function of PRMT5. Future studies will elucidate the full structure and interactome of PRMT5 on DNA and will determine differences between its active and repressive complexes. This will also provide an answer for how the same PRMT5-catalyzed histone modifications can mediate gene repression and activation. As we reported that PRMT5 functions as an epigenetic activator of AR expression[114], future work will determine if this is dependent on pICln. It is possible that pICln promotes activation by PRMT5 while other cofactors, such as MEP50, may promote repression by PRMT5.

### 3.4.6 *Limitations of this study*

We present evidence that PRMT5 cooperates with pICln to function as a master epigenetic activator of DDR genes in various cell types. Although this potentially explains the long-standing question of how repair proteins are quickly upregulated to promote the repair of DNA damage, the precise molecular mechanisms how PRMT5 and pICln function together to activate gene expression remain to be determined. Our findings also suggest that the regulatory role of PRMT5 in the activation of DDR genes is independent of its canonical cofactor MEP50: MEP50 was not present at the promoter of DDR genes and knockdown of MEP50 did not affect expression of DDR

genes nor did it affect repair of IR-induced DSBs. Although we provide several lines of evidence suggesting that pICln, but not MEP50, may participate in transcriptional regulation of DDR genes by PRMT5, it is possible that our knockdown of MEP50 was not sufficient to prevent the regulation of DDR gene expression. Thus, future studies with CRISPR-based knockout or PRMT5:MEP50 protein-protein interaction inhibitors may be needed to further evaluate a potential role for MEP50 in the regulation of PRMT5 target genes involved in DDR. Given that previous biochemical assays demonstrate that PRMT5 requires MEP50 for methyltransferase activity, further biochemical assays of PRMT5 with its cofactors in the presence of nucleosomes may provide mechanistic insight into the modulation of PRMT5 catalytic activity by its cofactors in the context of transcriptional regulation. These studies combined with both structural analysis of the PRMT5 complex at the promoter of target genes involved in DDR and genome-wide analyses such as ChIP-seq and ATAC-seq will likely provide mechanistic evidence for how PRMT5 functions with pICln and/or other cofactors to regulate transcription of DDR target genes.

## 3.5 Materials and Methods

### 3.5.1 *Cell lines and cell culture*

LNCaP cells were purchased from ATCC (Manassas, VA, USA) and cultured as described previously[114,121]. Upon arrival, the cell line was immediately expanded and aliquots were prepared and stored in liquid nitrogen. Cells were maintained for no longer than 30 passages or no longer than 3 months as described previously[49,266]. Cell line authentication was performed by IDEXX BioResearch (IMPACT I) and the absence of mycoplasma contamination was verified using LookOut® PCR Mycoplasma Detection Kit (Sigma, St. Louis, MO, USA). Knockdown cell lines were generated using the pLKO-Tet-On system. The pLKO-Tet-On plasmid for shRNA expression was obtained from Addgene (Cambridge, MA, USA)[267], and shRNA sequences that target PRMT5 #1 (5′-CCCATCCTCTTCCCTATTAAG-3′: referring to #1832)[114], SC (5'-CAACAAGATGAAGAGCACCAA-3'), MEP50 (5'- CCTCACAAGGACTCTGTGTTT-3'), and pICln (5'-CCAACAGTTGCTGGACAGTTT-3') were used for the construction of plasmids for stable cell line generation as described previously[114,266]. Stable cell lines with Dox-inducible expression of PRMT5-targeting shRNA (LNCaP-shPRMT5: referring to #1832[114]) or scramble control-targeting shRNA (shSC) (LNCaP-shSC) were established from individual clones and

characterized previously[114]. Stable cell lines with Dox-inducible expression of MEP50-targeting shRNA or pICln-targeting shRNA (LNCaP-shMEP50 and LNCaP-shpICln) were established from individual clones and characterized in this study[1]. Cell lines are described in Appendix C.

### 3.5.2 *Dox-induced knockdown and inhibitor treatment conditions*

For Dox-inducible cell lines, Dox was applied at the final concentration of 1 µg/mL every 48 h to establish and maintain PRMT5 knockdown (shPRMT5), MEP50 knockdown (shMEP50), pICln knockdown (shpICln), or express scramble control shRNA (shSC). The number of days of Dox treatment was optimized: shPRMT5 and shSC cells were grown for 4 days and had 4 days of Dox treatment, shMEP50 were grown for 4 days and had 2 days of growth followed by 2 days of Dox treatment, and shpICln cells were grown for 5 days and had 5 days of Dox treatment. For IR experiments, cells were subjected to IR following the knockdown described above.

### 3.5.3 *Ionizing radiation conditions*

Cells were irradiated using the X-RAD 320 biological irradiator device (PXi Precision X-Ray, North Branford, CT, USA) with an x-ray tube radiation source at an average dose rate of ~1 Gy/25 sec. All IR treatments were carried out in normal air at room temperature, and cells spent minimal time outside incubators during treatment. Non-irradiated controls were 'mock-irradiated' by being taken out of the incubator for the same time period as irradiated counterparts.

### 3.5.4 *Immunocytochemistry for quantification of IR-induced DSBs*[167]

Cells were seeded on 6 cm dishes containing glass coverslips and treated as described elsewhere. When cells reached ~80% confluency, cells were treated with 2 Gy IR and then fixed with 3.7% formaldehyde in phosphate buffered saline (PBS) at room temperature for 20 minutes at the indicated time points: First, we assessed the formation and repair of DSBs by analyzing γH2AX foci in a time-course following radiation (5 m and 1, 2, 6, and 24 h). Given that the majority of DSBs are repaired within 2-6 h following IR, we assessed the effect of knockdown on the repair of DSBs at the 6 h time point. After fixation at the indicated time point, cells were permeabilized with 0.2% Triton X-100 in PBS at room temperature for 5 m. Cells were then blocked with 5% milk blocking solution in PBS, stained with the indicated primary antibodies diluted in 5% milk

blocking solution in PBS, and stained with 4,6-diamidino-2-phenylindole (DAPI final 10 µg/mL) and indicated secondary antibodies diluted in 5% milk blocking solution in PBS. Cells on coverslips were mounted on glass slides using the ProLong® Antifade Kit (Invitrogen Molecular Probes, Eugene, OR, USA) and sealed with clear nail polish. Cells were then imaged via the Nikon TE2000 inverted fluorescence microscope under oil immersion (60x objective) (Nikon Instruments Melville, NY, USA). Images were processed via ImageJ[270] and the background was subtracted from the image using the rolling ball method (http://imagej.net/plugins/rolling-ball.html). Gating for minimum and maximum intensity values was set the same for each image. The number of foci was manually recorded for each cell (defined via nuclear DAPI staining). At least 60 cells were counted for each biological replicate. The arrays of foci counts for each biological replicate were subjected to further analysis separately to determine the average number of foci per cell and percentage of cells with zero foci. The primary antibodies used were anti-MEP50-rabbit (1:100), -pICln-rabbit (1:1000), and -γH2AX-mouse. Secondary antibodies used were anti-mouse-FITC (1:100) and anti-rabbit-rhodamine red (1:1000). All antibodies are described in All antibodies are described in Appendix E.

### 3.5.5 *Immunocytochemistry for quantification of protein expression or subcellular localization*

Immunocytochemistry was performed as described above. Images were analyzed via ImageJ[270]. First, the background was subtracted from the image using the rolling ball method (http://imagej.net/plugins/rolling-ball.html). For PRMT5 expression, regions of interest (ROI) were outlined for each individual cell. For MEP50 and pICln expression and subcellular localization, ROI were outlined for each individual cell (whole cell), nucleus only (as defined by DAPI staining), and cytoplasm only (as defined by signal outside of DAPI staining). The average intensity for each ROI was measured and at least 60 cells were counted for each biological replicate. The arrays of intensity counts for each biological replicate were subjected to further analysis separately and were analyzed via both “D’Agostino & Pearson” and “Shapiro-Wilk” normality tests to evaluate distribution. Because not all samples were normally distributed, the median value was used for each biological replicate. To determine the nuclear:cytoplasmic ratio (N:C), the value for nucleus was divided by the value for cytoplasmic for each cell individually such that an N:C ratio of 1 indicates equal expression in both the nucleus and cytoplasm.

### 3.5.6 *RNA isolation, reverse transcription, and RT-qPCR*

Cells were seeded on either 6 cm or 10 cm dishes and treated as described elsewhere. Total RNA was isolated using Trizol Reagent (Ambion, Carlsbad, CA, USA). RNA concentration and integrity were verified by agarose gel electrophoresis. cDNA synthesis was done using High Capacity cDNA Reverse Transcription Kit (Promega, Madison, WI, USA) as described previously[114,121,266]. qPCR was performed using FastStart Universal SYBR Green Master Mix (Thermo Fisher Scientific, Waltham, MA, USA) on the QuantStudio 6 Flex System and QuantStudio™ Real-Time PCR Software (Thermo Fisher, Waltham, MA, USA). Forty cycles were run and samples without $C_T$ values were deemed undetected. Technical duplicates were run for each sample and the $C_T$ values used for further analysis were the average of the technical duplicates. Samples where $C_T$ values for technical duplicates were >0.5 apart were re-run. Non-template controls (NTC)s with autoclaved double-distilled $H_2O$ were also run for each primer set and primer sets where $C_T$ values for NTC were lower than 37 (indicating high background) were re-run. Amplicon size and specificity were verified for each primer set via agarose gel electrophoresis. PRMT5 and GAPDH primers were used previously[114,121]. IVL primers were used previously[253,283]. All primers used are described in Appendix D.

### 3.5.7 *Chromatin immunoprecipitation (ChIP)-qPCR assay*

LNCaP, LNCaP-shPRMT5, or LNCaP-shSC cells were seeded on multiple 10 cm dishes and Dox was applied at the final concentration of 1 µg/mL every 48 h to establish and maintain PRMT5 knockdown (shPRMT5) or express scramble control shRNA (shSC). After 4 days, when cells reached ~80% confluency, cells were treated with 2 Gy IR. One hour following IR (prior to the repair of the majority of DSBs and at the same time as the peak of IR-induced PRMT5 protein expression), cells were fixed/crosslinked and chromatin was prepared for ChIP-qPCR as described previously[114]. Chromatin fragments were verified to be ~500 base pairs by agarose gel electrophoresis. Antibodies used for immunoprecipitation were anti-MEP50-rabbit, anti-pICln-rabbit, -RioK1-rabbit, -COPR5-rabbit, and IgG-rabbit. All antibodies are described in Appendix E. Primers used for ChIP-qPCR are described in Appendix D.

### 3.5.8 *Western blot*

Cells were seeded on either 6 cm or 10 cm dishes and treated as described elsewhere. Cells were harvested in lysis buffer (100 mM Tris-HCl pH 8.0, 15 mM $MgCl_2$, 100 mM KCl, 5 μg/mL of each Chymostatin, Leupeptin, Pepstatin A, and antipan in DMSO, 1% Triton X-100, 1 mM PMSF in ethanol, and 1 mM DTT) or RIPA buffer (10 mM Tris-HCl pH 8.0, 5 mM EDTA, 1% Triton X-100, 0.1% Sodium Deoxycholate, 0.1% SDS, 140 mM NaCl, 5 μg/mL of each Chymostatin, Leupeptin, Pepstatin A, and antipan in DMSO, and 1 mM PMSF in ethanol) and total protein concentration was measured using Bradford method. Approximately 20-30 μg total protein was run on a 10-15% SDS-PAGE and western blotting was performed as described previously[114,121,266]. Band/protein intensity was quantified using Image Lab™ (Bio-rad, Hercules, CA, USA). Antibodies used for western blot were anti-MEP50-rabbit (1:500), -pICln-rabbit (1:2000), -γH2AX-rabbit (1:1000), -PRMT5-rabbit (1:1000), -RAD51-rabbit (1:2000), -RAD51D-rabbit (1:2000), -RAD51AP1-rabbit (1:1000), -NHEJ1-rabbit (1:2000), -β-Actin-mouse (1:2000), -rabbit-HRP (horseradish peroxidase) (1:1000), -mouse-HRP (1:1000). All antibodies are described in Appendix E.

### 3.5.9 *Bimolecular Fluorescence Complementation (BiFC) assay*

LNCaP cells were grown to ~60% confluency and transfected with plasmids to visualize the PRMT5:MEP50 interaction (pMYC-VN155-PRMT5, pHA-VC-MEP50, and pFlag-NLS-CFP) and PRMT5:pICln interaction (pMYC-VN155-PRMT5, pHA-VC-pICln, and pFlag-NLS-CFP). Forty-eight hours following transfection, cells were treated with 2 Gy IR. Immediately prior to IR and 6 h following IR (the time point with the largest changes in MEP50 and pICln subcellular localization), cells were imaged via the Nikon TE2000 inverted fluorescence microscope (20x objective) (Nikon Instruments Melville, NY, USA). Images were then analyzed with ImageJ[270]. First, the background was subtracted from the image using the rolling ball method (http://imagej.net/plugins/rolling-ball.html). ROI were outlined for each individual cell, nucleus only (as defined by NLS-CFP staining), and cytoplasm only (as defined by staining outside NLS-CFP signal). The average intensity for each ROI was measured and at least 50 cells were counted for each biological replicate. The arrays of intensity counts for each biological replicate were subjected to further analysis separately and were analyzed via both “D’Agostino & Pearson” and

"Shapiro-Wilk" normality tests to evaluate distribution. Because not all samples were normally distributed, the median value was used for each biological replicate. To determine the nuclear:cytoplasmic ratio (N:C) the value for nucleus was divided by the value for cytoplasmic for each cell individually such that an N:C ratio of 1 indicates equal protein-protein interaction in both the nucleus and cytoplasm.

### 3.5.10 *Correlation analysis of TCGA clinical cancer data sets*

Gene expression profiles of 32 clinical cancer data sets from TCGA Pan-Cancer analysis[254] were retrieved from cBioPortal[150,151]. Using the mRNA expression of PRMT5, pICln, MEP50, AR, and DDR genes which are primary target genes of both PRMT5 and AR, we calculated the Spearman correlations between gene pairs for each cancer type. The gene set for DDR genes was defined as RAD51, RAD51D, RAD51AP1, NHEJ1, BRCA1, BRCA2, WEE1, DNAPKcs, Ku70, Ku80, an XRCC4. Although we did not perform additional studies on Ku70, Ku70 was included as it is another well-studied, key regulator of NHEJ.

### 3.5.11 *Statistical analysis*

No statistical methods were used to predetermine sample size. For the correlation analysis of TCGA clinical cancer data sets, statistical analysis was performed using Wilcoxon rank sum test in R 3.5.3. (R Core Team (2013). R: A language and environment for statistical computing. R Foundation for Statistical Computing, Vienna, Austria, https://www.R-project.org/). All other statistical analyses were performed using Graphpad Prism 7.00 and 8.00 for Windows (GraphPad Software, La Jolla California USA, www.graphpad.com). Statistical analysis was performed on raw data with assumed normal distribution. For all qPCR experiments, statistical analysis was performed on $\Delta C_T$ values ($C_T$ value of gene normalized to $C_T$ value of GAPDH control). For all ChIP-qPCR experiments, statistical analysis was performed on $\Delta C_T$ values ($C_T$ value of gene normalized to $C_T$ value of IgG control). For all western blot experiments, statistical analysis was performed on normalized raw intensity values (intensity value of protein divided by the intensity value of β-Actin). When comparing two sample groups, unpaired, two-tailed *t*-tests with Welch's correction (Welch's *t*-test) was used because standard deviations were not always equal for all groups. When comparing multiple sample groups, in order to compare the means or medians

among all the samples and incorporate the standard deviation of each of the samples, Brown-Forsythe and Welch ANOVA followed by Dunnett's T3 multiple comparisons test was used. All relevant statistics are reported in the corresponding legends.

### 3.6 Supplemental Information

Supplemental Information can be found online at https://doi.org/10.1016/j.isci.2019.100750.

## 3.7 Supplemental Figure

**Figure S3.1: pICln is also required for transcriptional activation of DDR genes and for efficient repair of double-strand breaks (DSBs)**

**(A)** Representative western blots showing protein expression at 2 h post 2 Gy IR in irradiated (IR+) and non-irradiated (IR-) LNCaP-shMEP50 cells with (Dox+) and without (Dox-) MEP50 knockdown. Values shown indicate the intensity relative to 'Dox-,IR-' for the biological replicate used as the representative western blot.
**(B)** Quantification of protein expression via western blotting from **A**. For each biological replicate, values were normalized to the value for 'Dox-/IR-' to calculate the fold change in protein expression upon treatment.
**(C)** Representative western blots showing protein expression at 2 h post 2 Gy IR in irradiated (IR+) and non-irradiated (IR-) LNCaP-shpICln cells with (Dox+) and without (Dox-) pICln knockdown. Values shown indicate the intensity relative to 'Dox-,IR-' for the biological replicate used as the representative western blot.
**(D)** Quantification of protein expression via western blotting from **C**. For each biological replicate, values were normalized to the value for 'Dox-/IR-' to calculate the fold change in protein expression upon treatment.
**(E)-(F)** Quantification of enrichment (**E**: MEP50 and **F**: pICln) at the promoter region of the indicated genes 1 h post 2 Gy IR via ChIP-qPCR in irradiated (IR+) and non-irradiated (IR-) LNCaP-shSC or shPRMT5 cells via ChIP-qPCR. Dox was applied establish and maintain PRMT5 knockdown (shPRMT5) or express scramble control shRNA (shSC). For each biological replicate, the value for IP was normalized to the value for IgG to calculate the fold enrichment (See also **Figures 3.1G** and **3.1H**).
**(G)**- **(H)** Quantification of enrichment (**G**: RioK1 and **H**: COPR5) at the promoter region of the indicated genes 1 h post 2 Gy IR via ChIP-qPCR in irradiated (IR+) and non-irradiated (IR-) LNCaP cells via ChIP-qPCR. For each biological replicate, the value for IP was normalized to the value for IgG to calculate the fold enrichment.

Bars in **B** and **E-H** are the mean ± s.d. of 3 independent experiments. Bars in **D** are the mean ± s.d. of 6 independent experiments. Statistical analysis for **B**, **D**, **E**, and **F** was performed using Brown-Forsythe and Welch ANOVA followed by Dunnett's T3 multiple comparisons test and the comparison to the control ('shSC, IR-') is shown while for **G** and **H**, statistical analysis comparing experimental to the control ('IR-') was performed using Welch's *t*-test (* $P \leq 0.05$; ** $P \leq 0.01$, *** $P \leq 0.001$, **** $P \leq 0.0001$, NS $P > 0.05$).

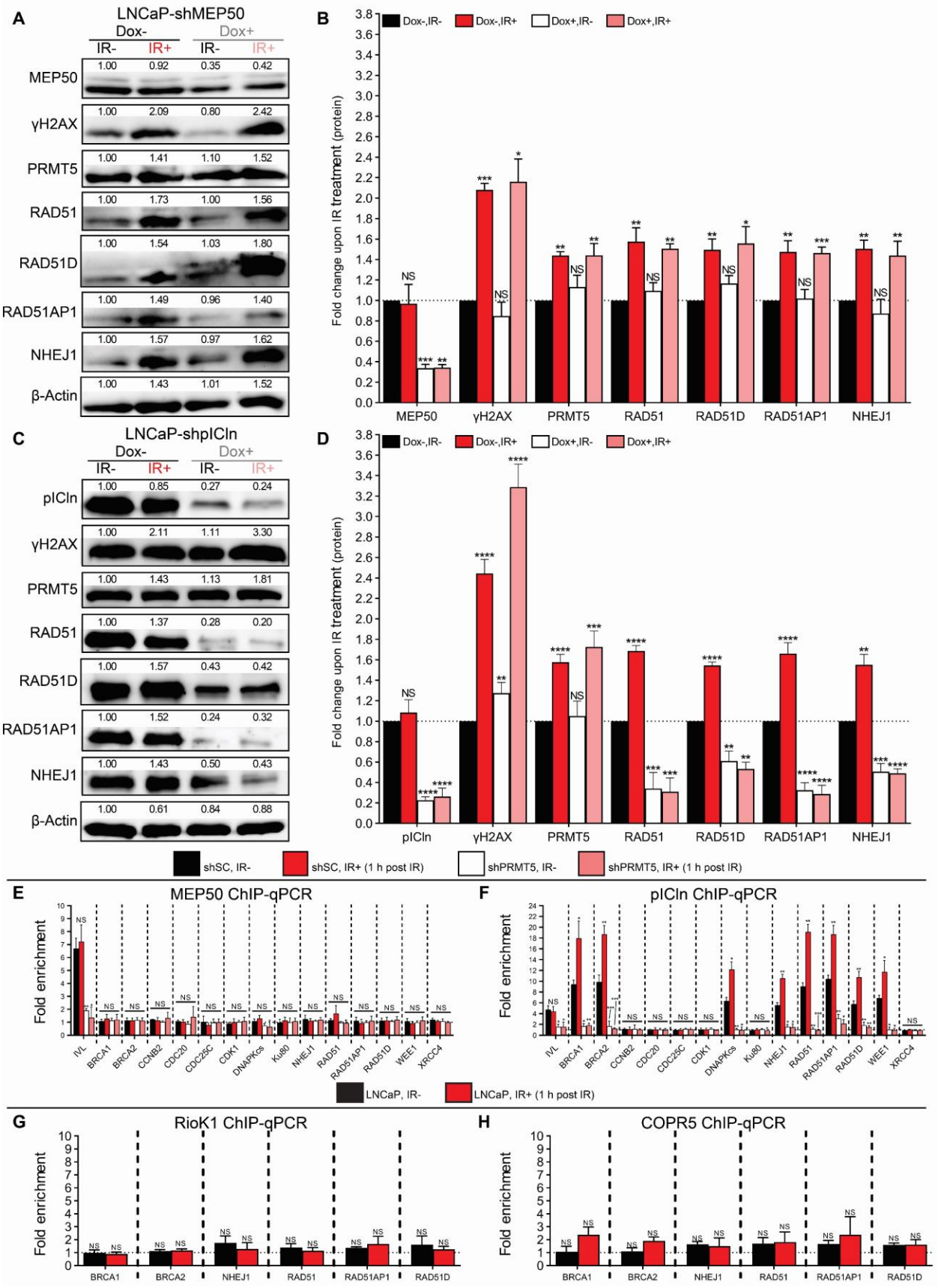
A
LNCaP-shMEP50
Dox-
Dox+
IR-
IR+
IR-
IR+
MEP50
1.00 0.92 0.35 0.42
γH2AX
1.00 2.09 0.80 2.42
PRMT5
1.00 1.41 1.10 1.52
RAD51
1.00 1.73 1.00 1.56
RAD51D
1.00 1.54 1.03 1.80
RAD51AP1
1.00 1.49 0.96 1.40
NHEJ1
1.00 1.57 0.97 1.62
β-Actin
1.00 1.43 1.01 1.52
B
Dox-,IR-
Dox-,IR+
Dox+,IR-
Dox+,IR+
Fold change upon IR treatment (protein)
MEP50
γH2AX
PRMT5
RAD51
RAD51D
RAD51AP1
NHEJ1
C
LNCaP-shpICln
Dox-
Dox+
IR-
IR+
IR-
IR+
pICln
1.00 0.85 0.27 0.24
γH2AX
1.00 2.11 1.11 3.30
PRMT5
1.00 1.43 1.13 1.81
RAD51
1.00 1.37 0.28 0.20
RAD51D
1.00 1.57 0.43 0.42
RAD51AP1
1.00 1.52 0.24 0.32
NHEJ1
1.00 1.43 0.50 0.43
β-Actin
1.00 0.61 0.84 0.88
D
Dox-,IR-
Dox-,IR+
Dox+,IR-
Dox+,IR+
Fold change upon IR treatment (protein)
pICln
γH2AX
PRMT5
RAD51
RAD51D
RAD51AP1
NHEJ1
shSC, IR-
shSC, IR+ (1 h post IR)
shPRMT5, IR-
shPRMT5, IR+ (1 h post IR)
E
MEP50 ChIP-qPCR
Fold enrichment
IVL
BRCA1
BRCA2
CCNB2
CDC20
CDC25C
CDK1
DNAPKcs
Ku80
NHEJ1
RAD51
RAD51AP1
RAD51D
WEE1
XRCC4
F
pICln ChIP-qPCR
Fold enrichment
LNCaP, IR-
LNCaP, IR+ (1 h post IR)
G
RioK1 ChIP-qPCR
Fold enrichment
BRCA1
BRCA2
NHEJ1
RAD51
RAD51AP1
RAD51D
H
COPR5 ChIP-qPCR
Fold enrichment
BRCA1
BRCA2
NHEJ1
RAD51
RAD51AP1
RAD51D

# CHAPTER 4. PRMT5 IS A KEY REGULATOR OF FIR-INDUCED NEUROENDOCRINE DIFFERENTIATION AND IS A PUTATIVE THERAPEUTIC TARGET TO ENHANCE RADIATION THERAPY FOR CANCER TREATMENT

The following chapter was not published at the time of dissertation deposit

## 4.1 Summary

Prostate cancer remains the second leading cause of cancer death among men in the United States. Although radiation therapy (RT) is a potentially curative treatment for localized disease, failure to manage localized disease contributes to the majority of prostate cancer deaths. Neuroendocrine differentiation (NED) is an emerging mechanism of resistance to several cancer treatments including RT. We present evidence that protein arginine methyltransferase 5 (PRMT5), along with cofactors pICln and MEP50, are essential for initiation and maintenance of NED in response to fractionated ionizing radiation (FIR). Additionally, the combination of targeting PRMT5, pICln, or MEP50 during any phase of FIR-induced NED killed almost all prostate cancer cells. Lastly, targeting PRMT5 sensitized prostate cancer xenograft tumors in mice to RT, significantly reduced and delayed tumor recurrence, and prolonged overall survival. Incredibly, while 100% of control mice died, targeting PRMT5 effectively cured ~85% of mice from their xenograft tumor. Our results strongly demonstrate that PRMT5 is essential for NED upon FIR treatment and that targeting PRMT5 would likely enhance RT for the treatment of prostate cancer.

## 4.2 Introduction

Prostate cancer remains the second leading cause of cancer death and the most common non-cutaneous cancer among men in the United States[2]. Surgery and radiation therapy (RT) are the only curative treatments for prostate cancer patients. Given that ~78% of current patients have localized disease[2] and ~96-97% of patients present with localized disease upon diagnosis[8], RT remains a viable treatment option for the majority of current and newly diagnosed prostate cancer patients.

Failure to manage localized prostate cancer eventually leads to disease progression and contributes to the majority of prostate cancer deaths. Although RT is potentially curative, ~10-15% of patients with low-risk disease and ~50-60% of patients with high-risk disease experience recurrence within 5 years of completing RT[32–35]. Additionally, ~20-30% of patients with high-risk prostate cancer die within 10 years[33,36–38]. Mechanistic studies that identify how prostate cancer cells become resistant will help improve RT and reduce cancer mortality.

Neuroendocrine differentiation (NED) is an emerging mechanism of resistance to several cancer treatments[50,60,77,81,83,88–91]. Our lab reported that prostate cancer cells undergo NED in response to fractionated ionizing radiation (FIR), as performed in RT[48,49]. Although neuroendocrine (NE) cells constitute <1% of epithelial cells in the prostate gland[57], the proportion of NE-like cells is elevated in nearly all prostate cancer tumors[50,57,73–75]. Prostate cancer cells can transdifferentiate into NE-like cells via NED[81–83,193]. NE-like cells express specific NE-associated proteins (e.g. neuron specific enolase and chromogranin A) and display NE-like morphology (presence of long, neurite projections)[50,53–56]. These NE-like cells are resistant to apoptosis and secrete signaling molecules to communicate with surrounding cells to promote survival of the tumor. Clinical evidence suggests that NED correlates with poor prognosis and treatment-resistance[53,56,75,92]. NED likely contributes significantly to the incidence of tumor recurrence following RT.

Currently, the only clinical approach to improve RT is androgen deprivation therapy (ADT), which targets androgen receptor (AR) signaling to decrease the efficiency of DNA double strand break (DSB) repair[39–46]. ADT is limited mainly to patients with high-risk disease due to associated adverse effects[12–14]. Thus, identification of novel therapeutic targets that confer resistance to RT will likely improve outcome or extend survival of prostate cancer patients. Additional to NED[50], a recent review detailed 4 targetable processes that may enhance RT: (1) androgen signaling (detailed above as the only clinical radiosensitization approach), (2) tumor hypoxia, (3) abnormal cell signaling pathways (including PTEN/PI3K/AKT/mTOR, EGFR, and immune checkpoint), and (4) the DNA damage response (DDR), particularly DSB repair[47]. Our recent finding that protein arginine methyltransferase 5 (PRMT5) functions as a master epigenetic regulator of DSB repair genes raised the possibility that targeting PRMT5 may sensitize prostate cancer cells to FIR.

FIR in combination with targeting PRMT5 was able to kill almost all prostate cancer cells. Remarkably, targeting PRMT5 also blocked NED and reversed NE-like morphology that had

already occurred in response to FIR. Here, we present evidence that PRMT5 is a key regulator of FIR-induced NED and is a putative therapeutic target to enhance RT for cancer treatment. PRMT5, as well as cofactors pICln and MEP50, are upregulated upon FIR treatment and significantly upregulated in FIR-induced NE-like cells. Additionally, pICln and MEP50 are similarly required for FIR-induced NED and cell survival upon FIR. Lastly, we assessed if targeting PRMT5 can enhance RT for the treatment of prostate cancer xenograft tumors in mice. Targeting PRMT5 sensitized prostate cancer xenografts to FIR, significantly reduced and delayed tumor recurrence, and prolonged survival. Incredibly, while 100% of control mice died, targeting PRMT5 effectively cured ~85% of mice from their xenograft tumor. Our results strongly demonstrate that PRMT5 is essential for NED upon FIR treatment and that targeting PRMT5 would likely enhance RT for the treatment of prostate cancer.

## 4.3 Results

### 4.3.1 *PRMT5 is essential for initiation of NED, maintenance of NED, and survival upon fractionated ionizing radiation (FIR)*

Targeting the DDR, particularly DSB repair, is a promising approach to enhance RT[47]. Because we recently identified PRMT5 as key regulator of DSB repair[1], we tested whether targeting PRMT5 sensitizes prostate cancer cells to FIR. To this end, we used our previously characterized mimic of clinical RT[49,50]. Briefly, prostate cancer cells were treated with FIR (2 Gy per fraction, 5 fractions per week) for a total of 4 weeks to deliver a cumulative dose of 40 Gy. In our model, prostate cancer cells also undergo NED in two phases: (1) *radiation resistance acquisition (RA)* and (2) *neuroendocrine differentiation (NED)*. The RA phase occurs during the first 2 weeks or 0-20 Gy. During this phase, the majority of cells die and the surviving cells begin to display NE-like cell morphology. Most notably, neurite projections begin to grow out from the cell body. The NED phase occurs during the final 2 weeks or 20-40 Gy. During this phase, cells express specific NE-associated proteins and fully display NE-like morphology. The morphological changes of FIR-induced NED are shown in Figure 4.1A (LNCaP) and are reported previously[48,49].

Using a previously characterized single-cell-derived doxycycline (Dox)-inducible PRMT5 knockdown stable cell line (LNCaP-shPRMT5)[1,114], we assessed how targeting PRMT5 affects the different phases of FIR-induced NED. Specifically, PRMT5 was knocked-down during the RA phase (0-20 Gy),

NED phase (20-40 Gy), or both phases (0-40 Gy). LNCaP cells and LNCaP-shPRMT5 cells without Dox treatment were used as controls to demonstrate NED as a mechanism of resistance to FIR treatment.

Consistent with our previous findings that targeting PRMT5 inhibits DSB repair[1], knockdown of PRMT5 during the RA phase (0-20 Gy) killed almost all of the prostate cancer cells (Figures 4.1A, 4.1B, and S4.1). Additionally, when PRMT5 was knocked-down during the RA phase only (0-20 Gy), cells were unable to regrow during the NED phase (20-40 Gy). Importantly, PRMT5 knockdown during the NED phase only (20-40 Gy) was able to kill cells that had already undergone NED (Figures 4.1A, 4.1B, and S4.1). At the end of FIR treatment (cumulative dose of 40 Gy), ~15% of control cells survived (LNCaP or control). However, if PRMT5 was knocked-down during any phase, <0.05% of cells survived. Consequently, we were unable to observe a statistically significant benefit for targeting PRMT5 during the entire FIR protocol (both) over the RA or NED phase only. Collectively, these results strongly suggest that targeting PRMT5 during any point of treatment could enhance RT by sensitizing prostate cancer cells to FIR.

We also assessed the effect of PRMT5 knockdown on FIR-induced NED by quantifying NE-like cells. NE-like cells were defined as cells where the longest neurite projection was at least two times longer than the cell body diameter. Although the percentage of NE-like cells increased dose-dependently during FIR treatment for control cells (LNCaP or control), knockdown of PRMT5 during the RA phase (0-20 Gy) was able to prevent NED (Figures 4.1A, 4.1C, and S4.2). PRMT5 knockdown on cells that had already undergone NED quickly reversed NE-like morphology (Figures 4.1A, 4.1C, and S4.2) prior to their death. This suggests that PRMT5 is also required to maintain NE-like morphology. Additionally, the few cells that survived PRMT5 knockdown during 0-20 Gy (RA) were unable to undergo NED during 20-40 Gy (Figures 4.1A, 4.1C, and S4.2). Thus, targeting PRMT5 early likely prevents future FIR-induced NED. More specifically, knockdown of PRMT5 during the RA phase only (0-20 Gy) blocked FIR-induced elongation of neurites while knockdown of PRMT5 during the NED phase only (20-40 Gy) caused shrinkage of pre-existing neurites (Figure S4.4) indicating that PRMT5 is critical maintain neurite projections. Note that LNCaP-shPRMT5 cells that did not receive Dox treatment (control) behaved nearly the same as parental LNCaP and LNCaP-shSC cells (Figures 4.1A-4.1C, and S4.2-S4.26), indicating that selection of the stable clone did not affect the response to FIR.

Inhibition of PRMT5 by our inhibitor BLL3.3[114,249] conferred similar results as PRMT5 knockdown: BLL3.3 sensitized LNCaP cells to FIR (Figures 4.1D, 4.1E, and S4.1), blocked initiation of FIR-induced NED (Figures 4.1D, 4.1F, and S4.2), and reversed FIR-induced NED (Figures 4.1D, 4.1F, and S4.2). During this experiment, we also assessed the effect of long-term treatment with BLL3.3 or DMSO alone. BLL3.3 significantly stunted LNCaP cell growth over the first 6 days of treatment (Figures S4.5A and S4.5B), which was nearly identical to our previous study where we assessed the effect of 2, 4, and 6

days of BLL3.3 treatment on LNCaP cell growth using MTT assay[114]. DMSO treated cells grew to 100% confluency and begun to pile in large clumps by 10 days. After 10 days, the cells begun to die. However, cell death was likely due to over-confluence and not due to DMSO treatment. Conversely, cells treated with BLL3.3 never grew to 100% confluency and begun to die around 6 days of treatment (Figures S4.5A and S4.5B). Following 32 days of BLL3.3 treatment, only ~15% of cells survived (Figures S4.5A and S4.5B). Interestingly, some of the cells treated with BLL3.3 underwent NED (Figures S4.5A and S4.5C) which is converse to the duel treatment of BLL3.3 and FIR. However, further treatment of BLL3.3 begun to kill some of the NE-like cells. Although not tested, it is possible that longer-term BLL3.3 treatment would reverse NED and/or kill these NE-like cells. Collectively, although targeting PRMT5 as a monotherapy may kill prostate cancer cells, combination with FIR offers a better approach to prevent NED and kill prostate cancer cells.

To confirm that targeting PRMT5 inhibits FIR-induced NED, we assessed the effect of PRMT5 knockdown on FIR-induced neuron-specific enolase (NSE) protein expression. We previously reported that NSE protein expression is elevated by FIR treatment[48] and NSE is a biomarker of NE-like cells[54]. Specifically, we analyzed protein expression following a cumulative dose of 10 Gy FIR. Although 10 Gy is considered in the RA phase, because the majority of cells were dead by a cumulative dose of 20 Gy FIR, western blot during the NED phase was not feasible. However, during FIR-induced NED, upregulation of NSE can be seen as early as a cumulative dose of 10 Gy FIR. Therefore, blocking upregulation of NSE protein would suggest inhibition of FIR-induced NED. Additionally, we assessed cells 24 h following the last dose of IR to allow cells to return to their basal state and to negate acute changes due to a single dose of IR. As expected, we observed that knockdown of PRMT5 results in a concomitant decrease in NSE protein expression (Figures 4.1G and 4.2H). This finding was corroborated using a second previously characterized single-cell-derived Dox-inducible knockdown stable cell line (LNCaP-shPRMT5 #2)[1,114] (Figures 4.1I and 4.1J).

### 4.3.2 *Fractionated ionizing radiation (FIR)-induced gene expression profile confirms NED and suggests NE-like cells preferentially repair DSBs via NHEJ over HR*

We next sought to characterize FIR-induced NE-like cells in more detail by performing RNA-seq analysis on prostate cells treated with a cumulative dose of 40 Gy FIR. Comparing non-irradiated (FIR-) and irradiated (FIR+) LNCaP cells, we identified 2,493 differentially expressed genes (DEGs) upon FIR-induced NED including 1,346 upregulated and 1,147 downregulated genes (Figure 4.2A). Using Gene Ontology (GO) analysis, pathways related to NED, cell-cell signaling, and ion channels were upregulated in FIR-induced NE-like cells (Figure 4.2B) while

pathways related to cell cycle progression, cell division and proliferation, homologous recombination (HR), and response to IR were downregulated in FIR-induced NE-like cells (Figure 4.2C). This is consistent with previous reports: (1) FIR induces NED[49,50], (2) NE-like cells secrete signaling molecules to support tumor growth and cell survival[61–63], (3) NE-like cells express high levels of ion channels to facilitate intracellular and extracellular signaling pathways[64–68], (4) NE-like cells are resistant to apoptosis and do not divide[72], (5) non-cycling cells mostly rely on NHEJ as opposed to HR[311], and NE-like cells are able to survive FIR treatment[49,50].

**Figure 4.1: PRMT5 is essential for initiation of NED, maintenance of NED, and survival upon fractionated ionizing radiation (FIR)**

**(A)** and **(D)** Time-course of FIR-induced NED in the indicated cells (**A**: LNCaP-shPRMT5 cells and **D**: LNCaP cells). Cells were treated with FIR (2 Gy per fraction, 5 fractions per week) and were assessed 24 h after the indicated cumulative dose of FIR. Cells in **A** were treated with Dox (1 μg/mL) during the indicated phases to assess the effect of PRMT5 knockdown on FIR-induced NED. Cells in **D** were treated with BLL3.3 (10 μM) or DMSO during the indicated phases to assess the effect of PRMT5 inhibition on FIR-induced NED. For '1) control', PRMT5 was not targeted during any phase. For '2) RA', PRMT5 was targeted during 0-20 Gy, also known as the resistance acquisition phase. For '3) NED', PRMT5 was targeted during 20-40 Gy, also known as the neuroendocrine differentiation phase. For '4) Both', PRMT5 was targeted during 0-40 Gy.
**(B)** and **(E)** Quantification of live cells from **A** or **D** using trypan blue staining. The value for FIR+ was normalized to the value for IR- to calculate the surviving fraction (% Survival) for each data point.
**(C)** and **(F)** Quantification of NE-like cells from **A** and **D**. The neurite length and cell body length were quantified for each individual cell. NE-like cells were defined as cells where the longest neurite projection was at least two times longer than the cell body diameter. The number of NE-like cells was normalized to the total number of live cells to calculate the percentage of cells that are NE-like.
**(G)** and **(I)** Representative western blots showing the effect of PRMT5 knockdown on FIR-induced upregulation of NSE in the indicated cells (**G**: LNCaP-shPRMT5 and **I**: LNCaP-shPRMT5 #2). Cells were treated with FIR (2 Gy per fraction, 5 fractions per week) and were assessed 24 h after a cumulative dose of 10 Gy FIR. Values shown indicate the intensity relative to Dox- for the biological replicate used as the representative western blot.
**(H)** and **(J)** Quantification of protein expression via western blotting from **G** and **I**. For each biological replicate, values for 'Dox+' were normalized to the value for 'Dox-' to calculate the fold change in protein expression upon PRMT5 knockdown.

Images in **A** and **D** are representative bright field images. For **A**-**F**, LNCaP cells are shown as a control. The same experiment was also performed on LNCaP-shSC cells as a control (See also **Figures S4.2**-**S4.6**)**.** Data points in **B**, **C**, **E,** and **F** are the mean ± s.d. of 3 independent experiments. Bars in **H** are the mean ± s.d. of 2 independent experiments while bars in **J** are the mean ± s.d. of 3 independent experiments. Statistical analysis for **B** and **E** is shown in **Figure S4.2** while statistical analysis for **C** and **F** is shown in **Figure S4.3**. Statistical analysis for **H** and **J** comparing 'Dox+' to the control ('Dox-') was performed using Welch's *t*-test (* $P \leq 0.05$; ** $P \leq 0.01$, *** $P \leq 0.001$, **** $P \leq 0.0001$, NS $P > 0.05$).

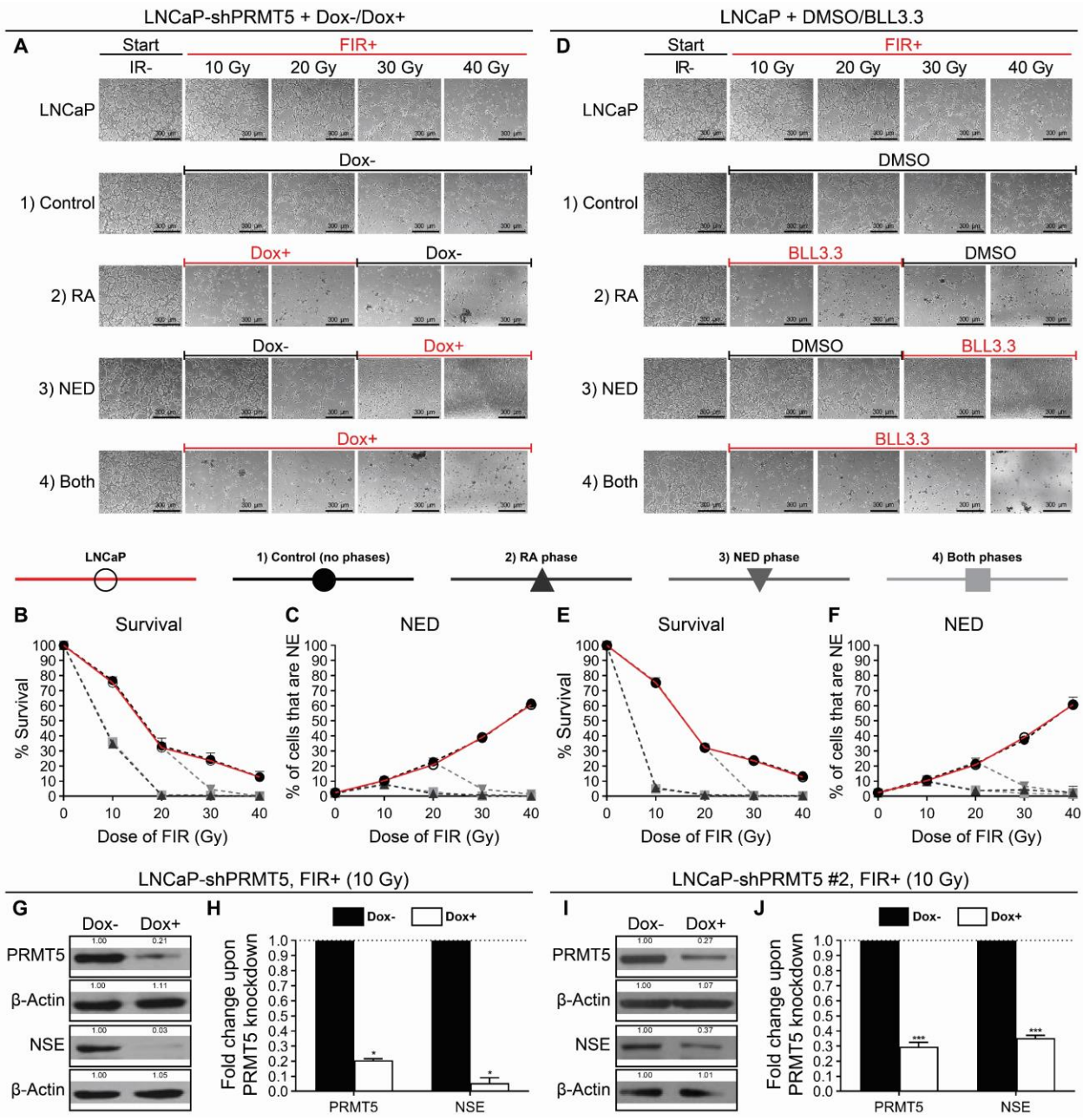
LNCaP-shPRMT5 + Dox-/Dox+
LNCaP + DMSO/BLL3.3
A
D
Start
FIR+
IR-
10 Gy
20 Gy
30 Gy
40 Gy
LNCaP
1) Control
2) RA
3) NED
4) Both
Dox-
Dox+
DMSO
BLL3.3
LNCaP
1) Control (no phases)
2) RA phase
3) NED phase
4) Both phases
B
C
E
F
Survival
NED
% Survival
% of cells that are NE
Dose of FIR (Gy)
LNCaP-shPRMT5, FIR+ (10 Gy)
LNCaP-shPRMT5 #2, FIR+ (10 Gy)
G
H
I
J
PRMT5
β-Actin
NSE
Fold change upon PRMT5 knockdown

Ingenuity pathway analysis (IPA) of the DEGs conferred similar outcomes as GO analysis and further revealed that senescence and cAMP-mediated signaling pathways are associated with FIR-induced NED (Figure 4.2D). This is consistent with previous reports: (1) cAMP or cAMP-inducing agents can induce NED in LNCaP cells[61], (2) cAMP response element-binding protein (CREB), which is activated by cAMP signaling, activates chromogranin A (CgA) transcription[84], (3) CREB is a critical regulator of FIR-induced NED[85], and (4) at least a subpopulation of prostate cancer cells treated with FIR undergo senescence[312]. Senescent cells are typically larger than proliferating cells[313]. In support of elevated senescence upon FIR, when calculating the percentage of NE-like cells, we also observed that the median cell body length increased dose-dependently during FIR-induced NED (Figure S4.6).

We then used reverse transcriptase quantitative real-time PCR (RT-qPCR) to individually verify expression changes in several genes critical to these pathways. All the genes associated with NED that we tested were significantly upregulated upon a cumulative dose of 40 Gy FIR (Figure 4.2E). The majority of genes that encode HR proteins were downregulated including RAD51 (Figure 4.2E), which is similar to a previous report where RAD51 is undetectable in non-proliferating cells[311]. Conversely, genes that encode NHEJ proteins were mostly unchanged (Figure 4.2E), which is consistent with reports that non-cycling cells mostly rely on NHEJ[311]. As expected, NHEJ genes were not identified as DEGs and NHEJ was not identified as an overrepresented pathway by GO or IPA. Collectively, these results support the idea that FIR-induced NE-like cells are similar to other NE-like cells, depend more on NHEJ instead of HR, and exhibit senescent-like properties.

**Figure 4.2: Fractionated ionizing radiation (FIR)-induced gene expression profile confirms NED and suggests NE-like cells preferentially repair DSBs via NHEJ over HR**

**(A)** RNA-seq analysis to identify DEGs upon FIR-induced NED in LNCaP cells. Gene expression in LNCaP cells treated with a cumulative dose of 40 Gy FIR (FIR+) was compared to untreated cells (FIR-). The volcano plot shows genes based on statistical significance (false discovery rate, FDR-corrected *p*-values) vs fold change (fold change in logarithm scale with base 2) between FIR+ and FIR-. Upregulated DEGs (red) and downregulated DEGs (blue) are indicated in color, respectively.
**(B)**-**(C)** Gene ontology (GO) enrichment analysis of DEGs that were upregulated (**B**) or downregulated (**C**) in FIR-induced NED cells. Groups of GO terms related to NED, cell-cell signaling, and ion channels were identified to be significantly over-represented in the upregulated DEG set. Groups of GO terms related to cell cycle progression, cell division and proliferation, homologous recombination, and response to IR were identified to be significantly over-represented in the downregulated DEG set. The height of each bar represents the enrichment score for corresponding GO term, while the q-value (FDR-corrected *p*-value) in red indicates the significance of enrichment. The number in the bar indicates the number of DEGs associated with the corresponding GO annotation.
**(D)** Ingenuity Pathway Analysis (IPA) of DEGs to identify upregulated and downregulated pathways associated with FIR-induced NED. The pathways with the highest significance are shown and the bars represent the degree of significance in terms of -log (*p*-value). Pathways shown in blue (negative z-score) are inhibited in FIR-induced NED cells while pathways in orange (positive z-score) are activated in FIR-induced NED cells
**(E)** Quantification of mRNA via RT-qPCR of LNCaP cells treated with a cumulative dose of 40 Gy FIR. For each biological replicate, the value for FIR+ (40 Gy) was normalized to the value for FIR- to calculate the fold change in mRNA expression upon FIR-induced NED.

Bars in **E** are the mean ± s.d. of 3 independent experiments. Statistical analysis for **E** comparing experimental to the control ('FIR-') was performed using Welch's *t*-test (* $P \leq 0.05$; ** $P \leq 0.01$, *** $P \leq 0.001$, **** $P \leq 0.0001$, NS $P > 0.05$, U = undetected).

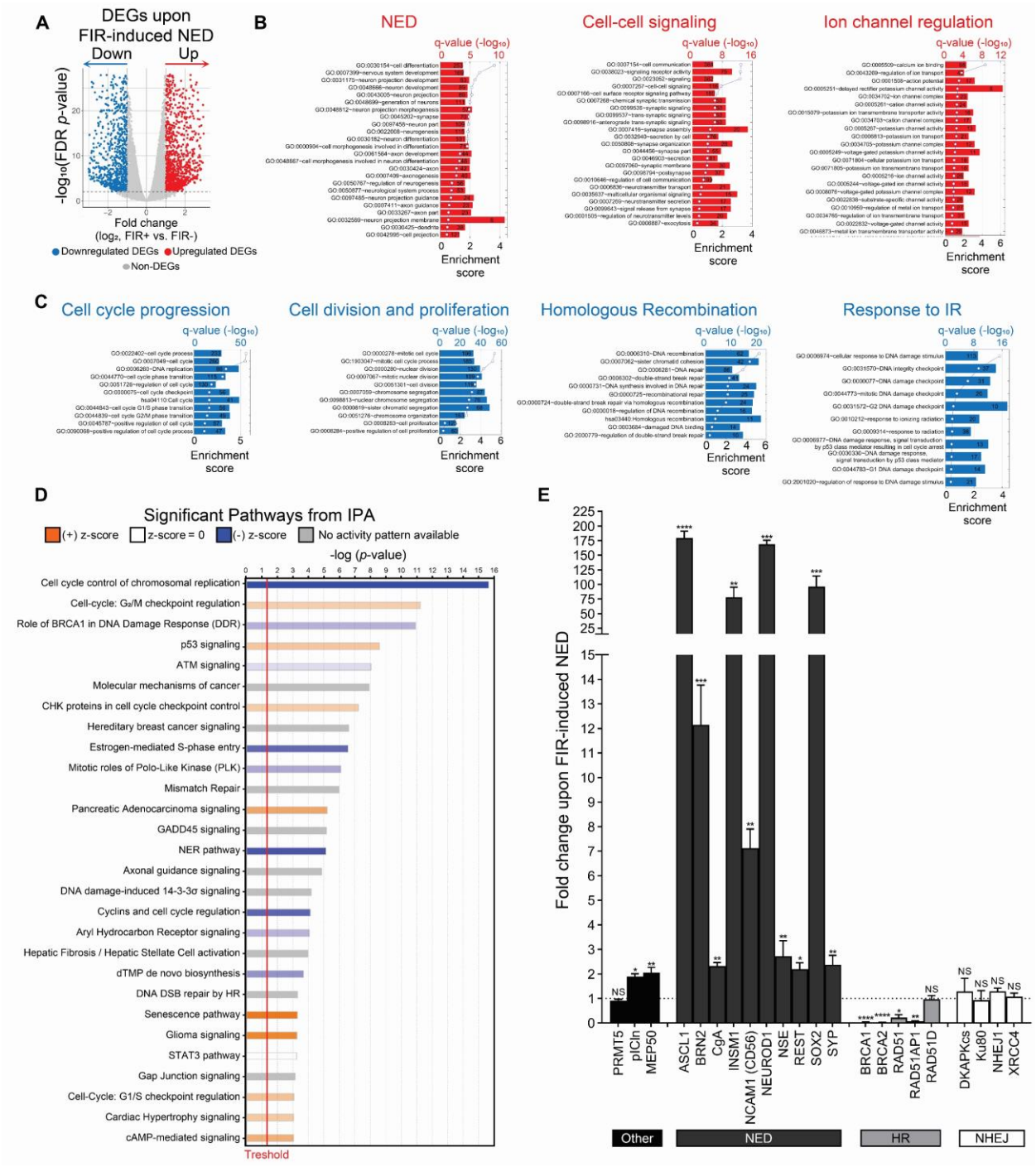
A
DEGs upon FIR-induced NED
Down
Up
-log10(FDR p-value)
Fold change (log2, FIR+ vs. FIR-)
Downregulated DEGs
Upregulated DEGs
Non-DEGs
B
NED
Cell-cell signaling
Ion channel regulation
q-value (-log10)
Enrichment score
C
Cell cycle progression
Cell division and proliferation
Homologous Recombination
Response to IR
D
Significant Pathways from IPA
(+) z-score
z-score = 0
(-) z-score
No activity pattern available
-log (p-value)
Cell cycle control of chromosomal replication
Cell-cycle: G2/M checkpoint regulation
Role of BRCA1 in DNA Damage Response (DDR)
p53 signaling
ATM signaling
Molecular mechanisms of cancer
CHK proteins in cell cycle checkpoint control
Hereditary breast cancer signaling
Estrogen-mediated S-phase entry
Mitotic roles of Polo-Like Kinase (PLK)
Mismatch Repair
Pancreatic Adenocarcinoma signaling
GADD45 signaling
NER pathway
Axonal guidance signaling
DNA damage-induced 14-3-3σ signaling
Cyclins and cell cycle regulation
Aryl Hydrocarbon Receptor signaling
Hepatic Fibrosis / Hepatic Stellate Cell activation
dTMP de novo biosynthesis
DNA DSB repair by HR
Senescence pathway
Glioma signaling
STAT3 pathway
Gap Junction signaling
Cell-Cycle: G1/S checkpoint regulation
Cardiac Hypertrophy signaling
cAMP-mediated signaling
Treshold
E
Fold change upon FIR-induced NED
PRMT5
pICln
MEP50
ASCL1
BRN2
CgA
INSM1
NCAM1 (CD56)
NEUROD1
NSE
REST
SOX2
SYP
BRCA1
BRCA2
RAD51
RAD51AP1
RAD51D
DKAPKcs
Ku80
NHEJ1
XRCC4
Other
NED
HR
NHEJ

### 4.3.3 *PRMT5 protein is dose-dependently upregulated in response to fractionated ionizing radiation (FIR) in prostate cancer cells*

We previously reported that a single dose of IR transiently induces PRMT5 protein expression on a timescale similar to the repair of IR-induced DSBs[293]. Given that PRMT5 is required for FIR-induced NED, we hypothesized that PRMT5 may be upregulated in FIR-induced NE-like cells. Previously, we isolated IR-resistant (IRR) NE-like LNCaP cell lines[48]: Briefly, LNCaP cells were treated with a cumulative dose of 40 Gy FIR. Following FIR, the majority of cells died and the surviving cells underwent NED. These NE-like cells did not reproliferate for at least 2 months and 3 months following FIR, we established IRR cell lines from individual clones. As expected, PRMT5 protein expression was elevated in the IRR LNCaP cell lines which coincided with elevated global symmetrical dimethylation of arginine residues in histone H4R3 (H4R3me2s), a marker of PRMT5 activity (Figures 4.3A and 4.3B). These results suggest that PRMT5 protein is upregulated and highly active in prostate cancer cells that underwent FIR-induced NED.

To further confirm that FIR induces PRMT5 protein expression, we analyzed protein levels in LNCaP cells via western blotting 24 h following a cumulative dose of 10, 20, 30, and 40 Gy FIR. There was an obvious dose-dependent induction of PRMT5 protein expression upon FIR treatment (Figures 4.3C and 4.3D). Interestingly, the induction of H4R3me2s was not obviously dose-dependent (Figures 4.3C and 4.3D). Specifically, H4R3me2s was significantly upregulated following a cumulative dose of either 10 Gy or 40 Gy FIR but an obvious upregulation following 20 and 30 Gy FIR was not observed (Figures 4.3C and 4.3D). However, we only assessed H4R3me2s levels following 20 and 30 Gy FIR once and it is likely that additional biological replicates will reveal a dose-dependent increase in H4R3me2s similar to the induction of PRMT5. Interestingly, PRMT5 was not upregulated at the mRNA level in LNCaP cells following a cumulative dose of 40 Gy FIR (Figure 4.2E). Collectively, these results indicate that PRMT5 protein is upregulated upon FIR to promote FIR-induced NED.

### 4.3.4 *Fractionated ionizing radiation (FIR) induces upregulation of PRMT5, pICln, and MEP50 protein expression in both the nucleus and cytoplasm during FIR-induced NED*

Because FIR promotes upregulation of PRMT5 protein, we sought to determine if FIR may also alter its subcellular localization. To this end, we used immunocytochemistry (ICC) to assess

the expression and localization of PRMT5 24 h following a cumulative dose of 10, 20, 30, 40, and 70 Gy FIR. We included the 70 Gy time point because many prostate cancer patients receive a cumulative dose of ~70 Gy clinically[27,35]. 70 Gy FIR kills almost all LNCaP cells, and assays that rely on larger cell numbers such as western blotting are not feasible. However, ICC is a single-cell analysis and requires less cells. Therefore, we were able to use ICC to assess the 70 Gy time point.

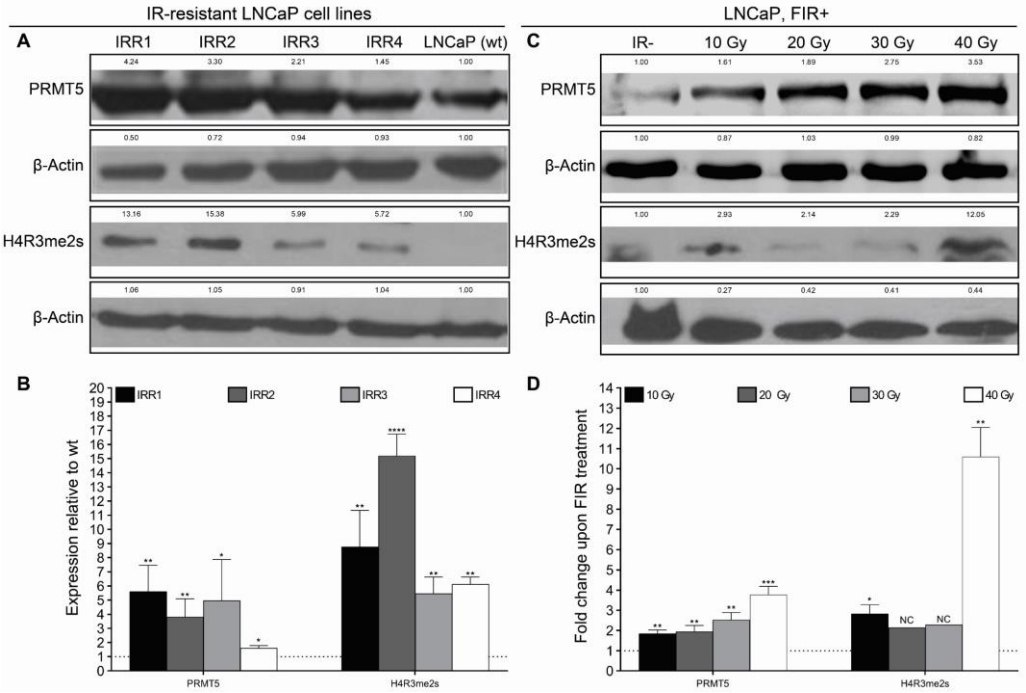


**Figure 4.3: PRMT5 protein is dose-dependently upregulated in response to fractionated ionizing radiation (FIR) in prostate cancer cells**

**(A)** and **(C)** Representative western blots showing the expression of PRMT5 during different phases of FIR-induced NED (**A**: isolated IR-resistant LNCaP cells and **C**: LNCaP cells treated with FIR). Cells in **A** are previously reported: Briefly, LNCaP cells were treated with a cumulative dose of 40 Gy FIR and individual cells were isolated to develop IR-resistant (IRR) cell lines. Untreated wild-type (wt) LNCaP cells were used as a control. Cells in **C** were treated with FIR (2 Gy per fraction, 5 fractions per week) and were assessed 24 h after the indicated cumulative dose of FIR. Values shown indicate the intensity relative to IR- for the biological replicate used as the representative western blot.
**(B)** and **(D)** Quantification of protein expression via western blotting from **A** and **C**. For each biological replicate in **B**, values for 'IRR' were normalized to the value for 'wt' to calculate the expression relative to wt. For each biological replicate in **D**, values for 'FIR+' were normalized to the value for 'IR-' to calculate the fold change in protein expression upon FIR treatment.

Bars for IRR1, IRR2, and IRR3 in **B** are the mean ± s.d. of 5 independent experiments while bars for IRR6 in **B** are the mean ± s.d. of 3 independent experiments. Bars for PRMT5 in **D** are the mean ± s.d. of 4 independent experiments, bars for H4R3me2s 10 Gy and 40 Gy in **D** are the mean ± s.d. of 3 independent experiments, and bars for H4R3me2s 20 Gy and 30 Gy in **D** are the value from 1 independent experiment. Statistical analysis for **B** and **D** comparing experimental to the control ('wt' or 'IR-') was performed using Welch's *t*-test (* $P \leq 0.05$; ** $P \leq 0.01$, *** $P \leq 0.001$, **** $P \leq 0.0001$, NS $P > 0.05$, NC not calculated).

As the first control, we confirmed that the LNCaP cells underwent FIR-induced NED. The first way we quantified NE-like cells was the presence of neurites (as described in Figure 4.1). As expected, the percentage of NE-like cells increased during the time-course of FIR-induced NED (Figures 4.4A and 4.4B), almost the same as in Figure 4.1. The second way we assessed NE-like cells was the presence of chromogranin A (CgA) staining. We previously reported that CgA protein expression is elevated by FIR treatment[48], and CgA is a biomarker of NE-like cells[53,55,56]. Given the subcellular distribution of CgA, we would expect CgA-positive cells to have foci surrounding the nucleus in the rough endoplasmic reticulum where CgA is synthesized, in the cytoplasm inside free secretory vesicles, or within the Golgi apparatus. Using CgA staining, we also observed an increase in the percentage of NE-like cells upon FIR treatment (Figures 4.4A and 4.4C). Interestingly, the increase in CgA-positive cells occurred prior to neurite extension: for each time point, there were more cells defined as NE-like by the presence of CgA compared to the presence of neurites (Figures 4.4A-4.4C). This indicates that the upregulation of CgA may precede some NED-associated morphological changes. Importantly, virtually all the cells that survived a cumulative dose of 70 Gy FIR were NE-like, further supporting FIR-induced NED as a clinical mechanism of radiation resistance.

As a second control, we also stained for γH2AX as a marker of IR-induced DSBs. LNCaP cells are able to repair almost all IR-induced DSBs within 24 h following a single dose of IR treatment. However, cells average about twice the basal level of DSBs and about 10% fewer cells have no DSBs (Figures 2.2A and 2.2B and reported previously[1]). Therefore, it is reasonable to suspect that multiple doses of FIR would cause accumulation of DSBs. Indeed, cells treated with FIR had elevated numbers of DSBs and very few cells had no DSBs (Figures 4.4A and 4.4D). However, it is interesting to note that the presence of DSBs decreased upon larger cumulative doses of FIR (Figures 4.4A and 4.4D). This suggests that the cells that survive FIR-induced NED either repair IR-induced DSBs more efficiently or do not display γH2AX foci as a marker of DSBs in the same way. Further, it is possible that elevated PRMT5 protein expression may facilitate enhanced DSB repair.

As a third control, we assessed the time-course of phosphorylated CREB (pCREB) levels and subcellular localization during FIR-induced NED. We previously reported that FIR induces phosphorylation of CREB at S133 leading to its activation[48]. Additionally, we further determined that CREB may be a therapeutic target to enhance prostate cancer cells to FIR and prevent FIR-

induced NED[85]. A cumulative dose of 10 Gy FIR causes a dramatic induction of nuclear pCREB and might slightly increase whole cell and cytoplasmic expression[48]. Indeed, we did not see a statistically significant increase in whole cell or cytoplasmic pCREB, but we observed a large induction of nuclear pCREB (Figures 4.4A and 4.4E). With larger cumulative doses of FIR, we observed increases in whole cell and cytoplasmic pCREB and an even larger induction of nuclear pCREB (Figures 4.4A and 4.4E). This further supports our finding that cAMP-mediated signaling is upregulated upon FIR-induced NED (Figure 4.2D) and corroborates previous findings that activated nuclear pCREB plays an important role in FIR-induced NED.

We previously reported that although a single dose of IR induces PRMT5 protein expression, it does not alter the subcellular localization[1] (Figures 3.2 and 3.3). However, we sought to determine if FIR may alter the subcellular localization of PRMT5. Consistent with the obvious dose-dependent induction of PRMT5 protein expression upon FIR treatment we observed from western blotting (Figures 4.3C and 4.3D), ICC analysis conferred similar results (Figures 4.4A and 4.4F). There was a dramatic increase in both nuclear and cytoplasmic PRMT5 during FIR-induced NED (Figures 4.4A and 4.4F). Interestingly, we also observed a slight increase in the nuclear:cytoplasmic (N:C) ratio at higher cumulative doses of FIR (where almost all surviving cells are NE-like) (Figures 4.4A and 4.4F). This suggests that nuclear PRMT5 may be particularly important in NE-like cells.

PRMT5 activity can be modulated by several interacting proteins including MEP50, which is believed to be the obligate cofactor of PRMT5 and required for PRMT5 methyltransferase activity[110,111,140,141]. However, we previously reported PRMT5 cooperates with pICln, independently of its canonical cofactor MEP50, to function as a master epigenetic activator of DDR genes[1]. In that study, we also reported that a single dose of IR alters the subcellular localization of the PRMT5 cofactors pICln and MEP50, as shown in Figure 3.3[1]. Specifically, a single dose of IR induces pICln nuclear localization and MEP50 cytoplasmic localization. However, the overall expression of pICln and MEP50 was not affected by a single dose of IR. We sought to determine if the expression and subcellular localization of PRMT5 cofactors pICln and MEP50 change during the time-course of FIR-induced NED. Both pICln and MEP50 were upregulated by FIR treatment (Figures 4.4A, 4.4G, and 4.4H). Similarly, both pICln and MEP50 were upregulated at the mRNA level in FIR-induced NE-like cells (Figure 4.2E) suggesting that increased transcription may contribute to the increased pICln and MEP50 protein observed upon

FIR. Interestingly, there was little change in pICln expression in the cytoplasm suggesting that the increase in whole cell expression is due to increased nuclear expression (Figures 4.4A and 4.4G). Congruently, while the basal distribution of pICln was predominantly cytoplasmic, pICln became predominantly nuclear upon FIR treatment (Figures 4.4A and 4.4G). The increase in MEP50 expression was less drastic than pICln, however the subcellular distribution in cells treated with FIR (predominantly nuclear) was similar to pICln (Figures 4.4A, 4.4G, and 4.4H). Unexpectedly, we observed that MEP50 (but not PRMT5 or pICln) formed foci in the cytoplasm of ~25% of cells treated with a cumulative dose of 40 or 70 Gy FIR (arrows in MEP50 of Figure 4.4A). This suggests that MEP50 plays an additional role in NE-like cells independent of PRMT5 or pICln. Overall, these results suggest that the maintenance of cytoplasmic levels and the increase in nuclear levels of the PRMT5 cofactors pICln and MEP50 are important to FIR-induced NED.

**Figure 4.4: Fractionated ionizing radiation (FIR) induces upregulation of PRMT5, pICln, and MEP50 protein expression in both the nucleus and cytoplasm during FIR-induced NED**

**(A)** Time-course of protein expression/localization during FIR-induced NED in LNCaP cells. Cells were treated with FIR (2 Gy per fraction, 5 fractions per week) and were assessed 24 h after the indicated cumulative dose of FIR.
**(B)** Quantification of NE-like cells in live images from **A** as described in **Figure 4.1C**.
**(C)** Quantification of NE-like cells in CgA images from **A**. CgA signal was assessed for each individual cell. CgA-positive cells have foci surrounding the nucleus in the rough endoplasmic reticulum, in the cytoplasm inside free secretory vesicles, or within the Golgi apparatus.
**(D)** Quantification of DSBs in each individual cell in γH2AX images from **A**: 'average' indicates the average number of DSBs in each cell and '0 foci' indicates the percentage of cells that do not contain any DSBs.
**(E)-(H)** Quantification of pCREB **E**, PRMT5 **F**, pICln **G**, and MEP50 **H** expression/localization in images from **A**: 'Whole cell' indicates expression in the entire cell, 'Nuclear' indicates expression in the nucleus which was defined by DAPI staining, 'Cytoplasmic' indicates expression in the cytoplasm which was defined as staining outside DAPI, and 'N:C ratio' was calculated by dividing the value for nucleus by the value for cytoplasmic for each cell individually such that an N:C ratio of 1 indicates equal expression in both the nucleus and cytoplasm.

Fluorescence images in **A** are representative immunocytochemistry images. Blue circles outline DAPI staining to allow for better visibility of expression in the nucleus. White arrows show foci. All bars are the mean ± s.d. of 3 independent experiments. Statistical analysis for **B**-**H** comparing experimental to the control ('0 Gy') was performed using Brown-Forsythe and Welch ANOVA followed by Dunnett's T3 multiple comparisons test (* $P \leq 0.05$; ** $P \leq 0.01$, *** $P \leq 0.001$, **** $P \leq 0.0001$, NS $P > 0.05$).

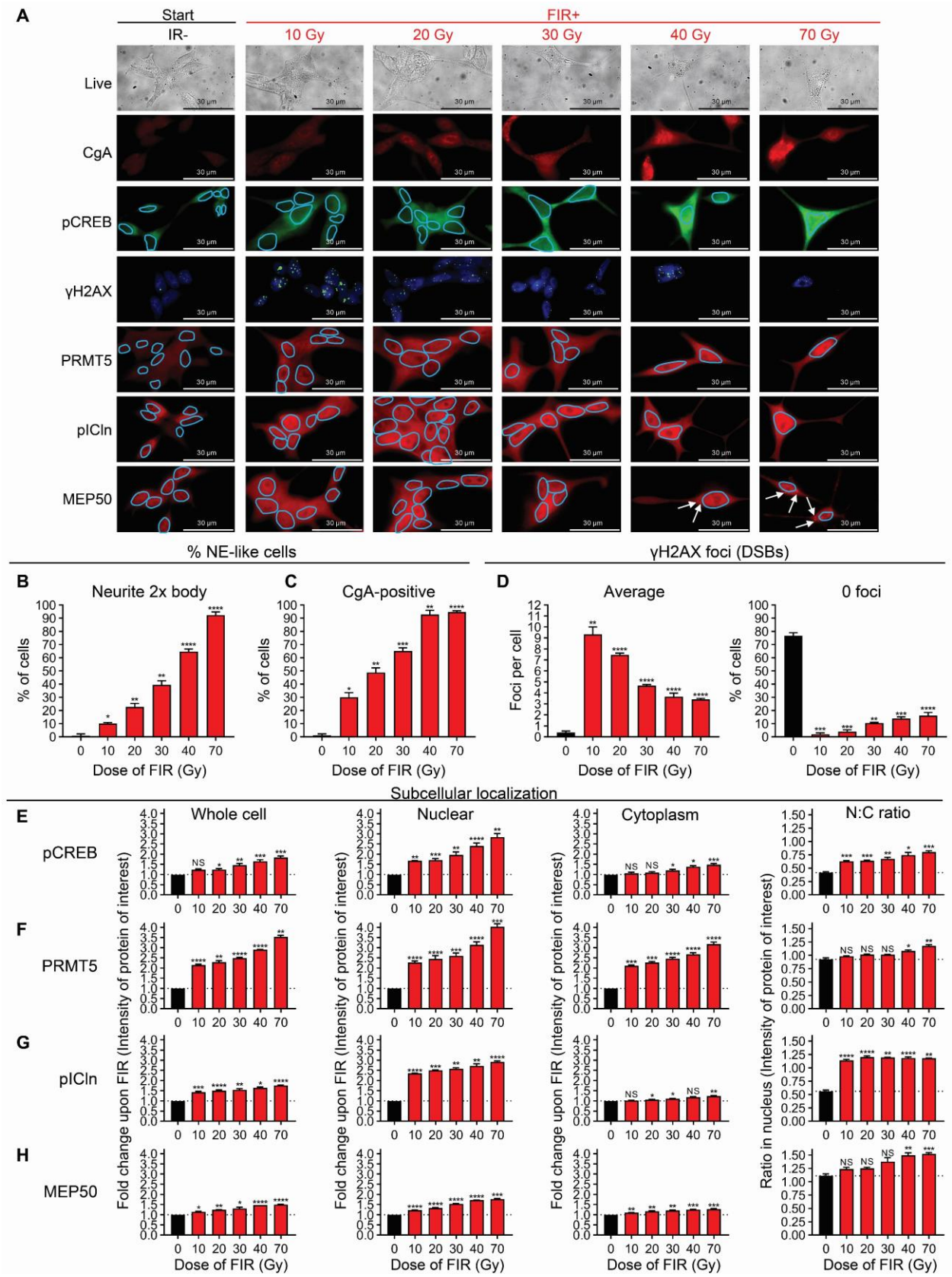
A
Start
IR-
FIR+
10 Gy
20 Gy
30 Gy
40 Gy
70 Gy
Live
CgA
pCREB
γH2AX
PRMT5
pICln
MEP50
% NE-like cells
γH2AX foci (DSBs)
B
Neurite 2x body
% of cells
Dose of FIR (Gy)
C
CgA-positive
% of cells
Dose of FIR (Gy)
D
Average
Foci per cell
Dose of FIR (Gy)
0 foci
% of cells
Dose of FIR (Gy)
Subcellular localization
E
pCREB
F
PRMT5
G
pICln
H
MEP50
Whole cell
Nuclear
Cytoplasm
N:C ratio
Fold change upon FIR (Intensity of protein of interest)
Ratio in nucleus (Intensity of protein of interest)
Dose of FIR (Gy)

### 4.3.5 *Both pICln and MEP50 are also essential for initiation of NED, maintenance of NED, and survival upon fractionated ionizing radiation (FIR)*

Because PRMT5 activity is modulated by cofactors, and both pICln and MEP50 are upregulated by FIR treatment, we tested whether targeting pICln or MEP50 sensitizes prostate cancer cells to FIR. To this end, we used our previously characterized mimic of clinical RT[49,50] and targeted pICln or MEP50 using previously characterized single-cell-derived Dox-inducible knockdown stable cell lines (LNCaP-shpICln and LNCaP-shMEP50)[1]. Specifically, we assessed how targeting pICln or MEP50 affects the different phases of FIR-induced NED. pICln or MEP50 was knocked-down during the RA phase (0-20 Gy), NED phase (20-40 Gy), or both phases (0-40 Gy). LNCaP cells and LNCaP-shpICln/LNCaP-shMEP50 cells without Dox treatment were used as controls to demonstrate NED as a mechanism of resistance to FIR treatment. This experiment followed the same protocol as in Figure 4.1.

Consistent with our previous findings that targeting pICln inhibits DSB repair[1], knockdown of pICln during any phase sensitized LNCaP cells to FIR (Figures 4.5A, 4.5B, and S4.1). However, compared to knockdown of PRMT5, knockdown of pICln was more effective during the RA phase and less effective during the NED phase (Figure S4.1). Additionally, when pICln was knocked-down during the RA phase only (0-20 Gy), cells were unable to regrow during the NED phase (20-40 Gy) (Figures 4.5A, 4.5C, and S4.2). Compared to knockdown of PRMT5, knockdown of pICln was more effective at preventing FIR-induced NED (Figure S4.2). Contrastingly, knockdown of pICln was less effective than knockdown of PRMT5 at reversing NE-like morphology of cells that had already undergone NED (Figures 4.5A, 4.5C, and S4.2). These results suggest that pICln plays a bigger role in survival and a lesser role in NED upon FIR treatment.

Although we previously reported that targeting MEP50 did not inhibit DSB repair[1], knockdown of MEP50 during any phase sensitized LNCaP cells to FIR (Figures 4.5D, 4.5E, and S4.1). However, compared to knockdown of PRMT5, knockdown of MEP50 was more effective during the RA phase and had about the same effectiveness during the NED phase (Figure S4.1). Knockdown of MEP50 during the RA phase (0-20 Gy) killed almost all the prostate cancer cells so further timepoints were not quantified (Figures 4.5D, 4.5E, and S4.1). Knockdown of MEP50 during the RA phase (0-20 Gy) prevented NED and MEP50 knockdown on cells that had already undergone NED quickly reversed NE-like morphology (Figures 4.5D, 4.5F, and S4.2). Interestingly, MEP50 knockdown caused regression of neurites and sensitized cells that had already undergone NED within a few days (observation was not quantified because it happened prior to the 30 Gy time point), which was quicker than PRMT5 knockdown (Figures 4.5D, 4.5F, S4.2, and S4.4). Because MEP50 does not play a significant role in repair of FIR-induced DSBs, it is likely that MEP50 plays an essential role in other survival pathways as well as NED. Collectively, it is likely that PRMT5:pICln is more essential for repair of IR-induced DSBs and PRMT5:MEP50 is more

essential for NED. However, it is likely that PRMT5's role in FIR-induced NED is dependent several factors additional to interaction with cofactors and we cannot rule out roles for pICln and MEP50 independent of PRMT5.

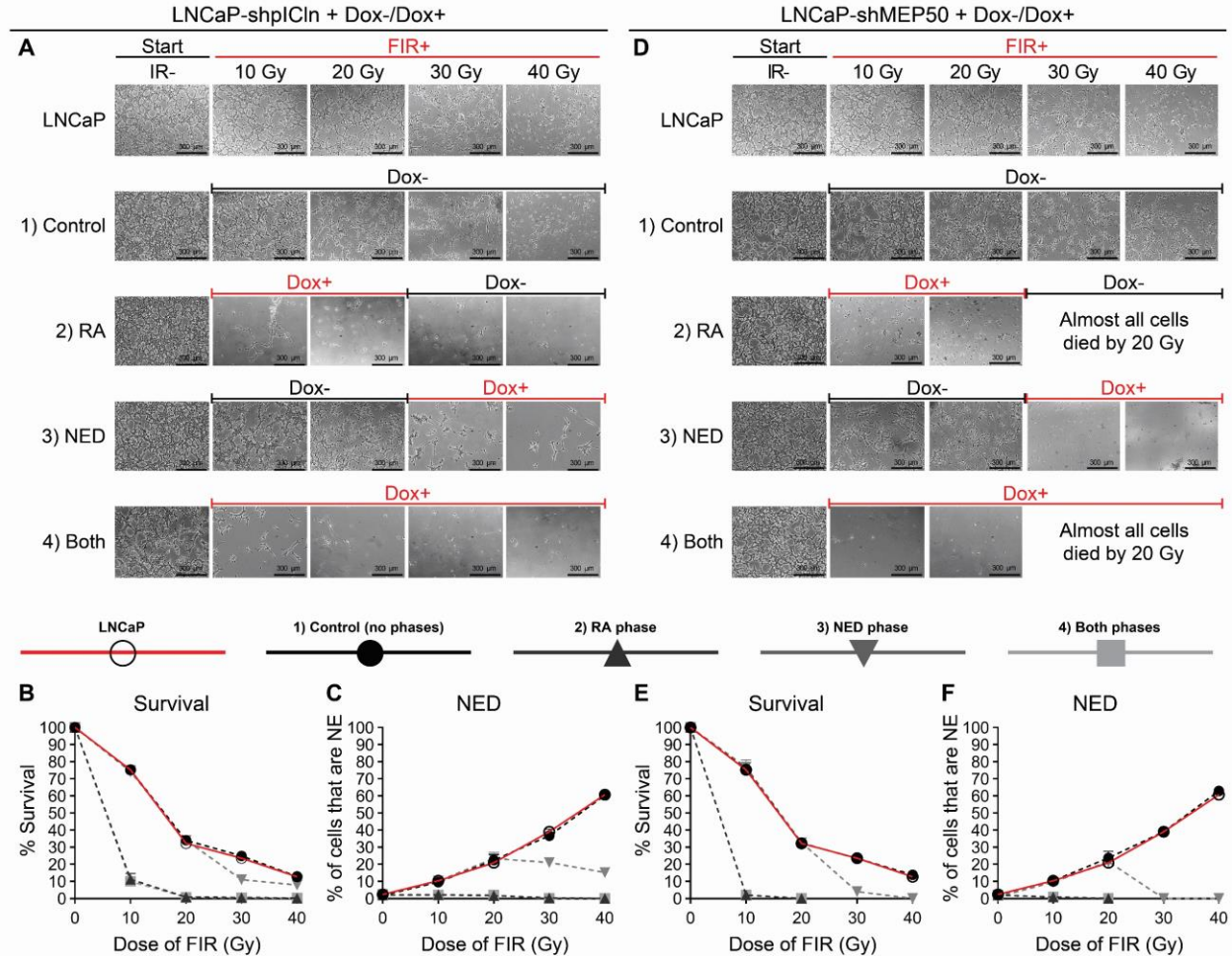


**Figure 4.5: Both pICln and MEP50 are also essential for initiation of NED, maintenance of NED, and survival upon fractionated ionizing radiation (FIR)**

**(A)** and **(D)** Time-course of FIR-induced NED in the indicated cells (**A**: LNCaP-shpICln cells and **D**: LNCaP-shMEP50 cells). Cells were treated with FIR (2 Gy per fraction, 5 fractions per week) and were assessed 24 h after the indicated cumulative dose of FIR. Cells were treated with Dox (1 μg/mL) during the indicated phases to assess the effect of pICln or MEP50 knockdown on FIR-induced NED. For '1) control', pICln/MEP50 was not targeted during any phase. For '2) RA', pICln/MEP50 was targeted during 0-20 Gy, also known as the resistance acquisition phase. For '3) NED', pICln/MEP50 was targeted during 20-40 Gy, also known as the neuroendocrine differentiation phase. For '4) Both', pICln/MEP50 was targeted during 0-40 Gy.
**(B)** and **(E)** Quantification of live cells from **A** or **D** as described in **in Figure 4.1B**.
**(C)** and **(F)** Quantification of NE-like cells from **A** and **D** as described **in Figure 4.1C**.

Images in **A** and **D** are representative bright field images. For **A-F**, LNCaP cells are shown as a control. The same experiment was also performed on LNCaP-shSC cells as a control (See also **Figures S4.2-S4.6**). Data points in **B**, **C**, **E,** and **F** are the mean ± s.d. of 3 independent experiments. Statistical analysis for **B** and **E** is shown in **Figure S4.2** while statistical analysis for **C** and **F** is shown in **Figures S4.3**.

### 4.3.6 *Targeting PRMT5 sensitizes prostate cancer xenograft tumors in mice to FIR, prevents tumor recurrence, and increases survival*

To extend our findings, we assessed if targeting PRMT5 can sensitize prostate cancer tumors to RT in a preclinical mouse study. The protocol for this study is outlined in Figure 4.6A and is similar to our previous study[49]. Twenty adult male NRG mice were injected with LNCaP-shSC cells while 20 adult male NRG mice were injected with LNCaP-shPRMT5 cells. Cells (6 X $10^6$) were suspended in 100 μL media + 100 μL matrigel for injection into the flank. Once xenograft tumors grew to ~200-300 $mm^3$ (generally between 4-6 weeks after injection), mice were given Dox-containing drinking water (1 mg/mL) to establish and maintain PRMT5 knockdown (shPRMT5), or express scramble control shRNA (shSC) in the xenograft tumors. Three days following the switch to Dox-containing water (enough time for efficient PRMT5 knockdown), tumors were subjected to their first IR treatment. Tumors were treated with FIR (5 Gy dose, 2 days a week) until a cumulative dose of 40 Gy FIR was reached. Dox treatment was stopped after the last dose of IR treatment so PRMT5 could return to basal levels. The tumor size was monitored twice weekly and mice with tumors larger than 1,500 $mm^3$ were sacrificed due to tumor burden. The experiment was terminated several weeks following the tumor recurrence of the last control (shSC) mice.

Control shSC tumors continued to grow during RT treatment to an average of ~135% their original volume (Figure 4.6B), and 65% of these shSC tumors were actually larger following 40 Gy FIR. However, only 1 of these shSC tumors was larger than 400 $mm^3$ (our cutoff for tumor recurrence) (Figure 4.6C). This indicates that during RT treatment the growth of shSC tumors was small and most tumors were static. Conversely, 100% of the shPRMT5 tumors shrunk following the RT treatment, and on average shrunk to ~25% of the original tumor volume (Figure 4.6B). This indicates that targeting PRMT5 sensitized the prostate cancer tumors to FIR treatment.

shSC tumors begun to regrow almost immediately following the completion of RT treatment and continued to grow until termination of the study. Therefore, our preclinical mouse study models clinical resistance to RT. Strikingly, the tumor volume for 17/20 mice in the shPRMT5 group was negligible (<100 $mm^3$) following RT treatment and remained negligible until termination of the experiment. Tumor volumes for the shSC and shPRMT5 groups started to be statistically significant 10 days following the first IR treatment and remained statistically significant throughout (Figure 4.6B). As only tumor volumes from live mice were used to calculate

the average tumor volume, the average tumor volume of the shSC group began to fluctuate when mice with large tumors begun to die (arrow on Figure 4.6B). Despite a stringent model where the prostate cancer tumors are inherently resistant to FIR treatment, our results suggest that targeting PRMT5 in combination with RT may be able to kill virtually all prostate cancer cells.

Half of the shSC tumors recurred within 35 days following the end of FIR treatment (63 days following the beginning of FIR treatment) and 95% of the shSC tumors recurred within 85 days following end of FIR treatment (Figure 4.6C). Only 15% (3/20) of shPRMT5 tumors recurred and the recurrence was significantly delayed (Figure 4.6C). It took between 141-155 days following the end of FIR treatment (169-183 days following the beginning of FIR treatment) for these 3 shPRMT5 tumors to recur, all of which recurred at least 56 days after 95% of the shSC tumors (Figure 4.6C). Overall, it took about 6 months longer for shPRMT5 tumors to begin to recur. Considering that a typical NRG mouse lives between 1.5-2 years, an extra 6 months of cancer-free life would be nearly 20-30 years for a human. Overall, this suggests that targeting PRMT5 in combination with RT likely, at the very least, significantly delays tumor recurrence.

The first death in the shSC group occurred 85 days following the end of FIR treatment (113 days following beginning of FIR treatment) and 50% of mice with shSC tumors died before 113 days following the end of FIR treatment (141 days following beginning of FIR treatment) (Figure 4.6D). Although 85% of the mice with shPRMT5 tumors survived the entire duration of the experiment, for the 3/20 mice with shPRMT5 tumors that did succumb to their disease, they died much later than their shSC counterparts (Figure 4.6D). These 3 mice died between 162-178 days following the end of FIR treatment (190-206 days following beginning of FIR treatment) (Figure 4.6D). Further, these 3 mice survived on average about 3 months longer than mice with shSC tumors. Considering that a typical NRG mouse lives between 1.5-2 years, an extra 3 months of life would be nearly 10-15 years for a human prostate cancer patient. Collectively, these results provide compelling preclinical evidence that targeting PRMT5 in combination with RT may better cure a prostate cancer patient and at the very least delay tumor recurrence and prolong life.

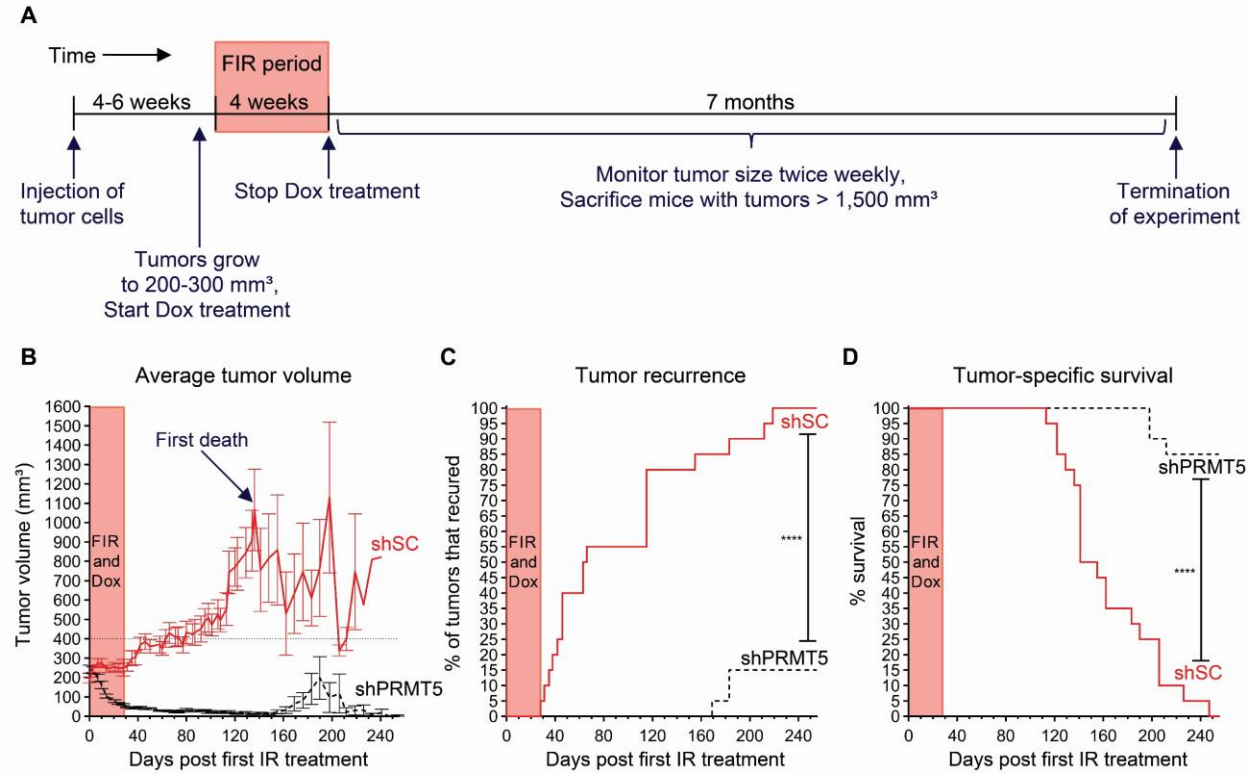


**Figure 4.6: Targeting PRMT5 sensitizes prostate cancer xenograft tumors in mice to FIR, prevents tumor recurrence, and increases survival**

**(A)** Protocol for xenograft tumor study. Twenty mice were injected with LNCaP-shSC cells while 20 mice were injected with LNCaP-shPRMT5 cells. Once tumors grew to ~200-300 $mm^3$, mice were given Dox-containing drinking water (1 mg/mL) to establish and maintain PRMT5 knockdown (shPRMT5), or express scramble control shRNA (shSC) in the xenograft tumors. 3 days following the switch to Dox-containing water, mice tumors were subjected to their first IR treatment. Tumors were treated with FIR (2 Gy per fraction, 5 fractions per week) until a cumulative dose of 40 Gy FIR was reached. Dox treatment was stopped after the last dose of IR treatment. The tumor size was monitored twice weekly and mice with tumors larger than 1,500 $mm^3$ were sacrificed due to tumor burden.
**(B)** Average tumor volume following FIR treatment. Tumor volume was calculated by multiple the length, width, and height of the tumor. Only tumor volumes from live mice were used to calculate the average
**(C)** Tumor recurrence following FIR treatment. First tumor recurrence was defined as the time point when a tumor reached a size larger than 400 $mm^3$. For each time point, the number of tumors that had experienced tumor recurrence was normalized to the total number of tumors to calculate the percentage of tumors that recurred.
**(D)** Tumor-specific survival following FIR treatment. The number of living mice (with or without tumors) was normalized to the total number of mice to calculate the percent survival.

Statistical analysis for **B** comparing 'shPRMT5' to the control ('shSC') was performed using 2way ANOVA. Although not shown, statistical analysis was performed for every time point and was statistically significant with a $p$-value $\leq 0.01$ for every time post 10 days following the last IR treatment.
Statistical analysis for **C** comparing 'shPRMT5' to the control ('shSC') was performed using Fisher's exact test (one-tail). Statistical analysis for **D** comparing 'shPRMT5' to the control ('shSC') was performed using Kaplan-Meier survival analysis followed by both Log-rank (Mantel-Cox) and Gehan-Breslow-Wilcoxon tests ( **** $P \leq 0.0001$).

## 4.4 Discussion

### 4.4.1 *FIR-induced NE-like cells have similar and different characteristics to other NE-like cells*

NED of prostate cancer cells is an emerging mechanism of resistance to several cancer treatments including FIR/RT[48–50,60,77,81,83,88–91]. Here, we identified DEGs associated with FIR-induced NED. To our knowledge, we are the first to perform RNA-seq analysis on FIR-induced NE-like prostate cancer cells. Subsequently, we performed GO and IPA analysis on the DEGs to identify enriched pathways. Cumulatively, the identified pathways are supported by several other studies. However, FIR-induced NE-like cells may have some different characteristics compared to other NE-like cells.

There are several kinds of NE-like prostate cells including normal prostate NE cells, *de novo* NE-like prostate cancer cells, and treatment-induced NE-like prostate cancer cells. Additionally, several cancer treatments including ADT, certain chemotherapies, and RT can promote NED. The biological role of normal prostate NE cells remains largely unknown[60]. Similarly, although some studies suggest that *de novo* NE-like prostate cancer cells are different in both morphology and behavior, they are understudied largely due to limited clinical distinction between *de novo* and treatment-induced NE-like prostate cancer cells[77,78]. Treatment-induced NE-like prostate cancer cells are more comprehensively characterized. However, ADT-induced NED is better characterized than FIR-induced NED.

Our analysis of FIR-induced NE-like cells suggests they are similar to other NE-like cells. As expected, pathways associated with NED, cell-cell signaling, ion channels, cAMP signaling, and senescence were upregulated in FIR-induced NE-like cells. NE-like cells typically display certain morphology such as the presence of long, neurite projections. We determined that GO terms associated with neuron development, axon development, and neurite projections were upregulated in FIR-induced NE-like cells which we confirmed by analysis of microscope images. NE-like cells secrete signaling molecules to support tumor growth and cell survival[61–63], as well as express high levels of ion channels to facilitate intracellular and extracellular signaling pathways[64–68]. We determined that GO terms associated with cell-cell communication and ion channels including more specific pathways associated with neurotransmitter secretion, synaptic signaling, calcium signaling, and potassium signaling were upregulated in FIR-induced NE-like cells. Future studies may confirm enhanced cell-cell signaling and the presence of ion channels as

well as assess differences in the abundance, type, and role of cell-cell signaling and ion channels compared to other NE-like cells. NE-like cells utilize cAMP signaling[61,84,85], and we determined that IPA pathways associated cAMP-mediated signaling were upregulated in FIR-induced NE-like cells. Additionally, we confirmed increased cAMP-mediated signaling by analysis of ICC images. NE-like cells may display senescence-like features and at least a subpopulation of prostate cancer cells treated with FIR undergo senescence[312]. We determined that IPA pathways associated senesce were upregulated in FIR-induced NE-like cells. Senescent cells are typically larger than proliferating cells[313], and we observed that the median cell body diameter was larger in FIR-induced NE-like cells. NE-like cells are Ki67-negative[71] and the general consensus is that they do not proliferate. As expected, pathways associated with cell cycle progression, cell division, and proliferation were downregulated in FIR-induced NE-like cells. Similarly, by visualizing the same field of cells under the microscope over the time-course of FIR-induced NED, it was obvious that the NE-like cells were no longer dividing. This was also supported by our quantification of live cells during the time-course of FIR-induced NED. Overall, this suggests that FIR-induced NE-like cells share many common characteristics with other NE-like cells

Our analysis of FIR-induced NE-like cells suggests they may also have different characteristics than other NE-like cells. For example, cellular response to IR was downregulated in FIR-induced NE-like cells including cellular response to DNA damage stimulus, response to IR, and DNA integrity/damage checkpoint. Note that this is separate from DNA damage repair. This suggests that FIR-induced NE-like cells utilize different DNA damage sensing and signaling pathways in response to DNA damage. For example, non-proliferating cells typically sustain p53 signaling in response to DNA damage[311]. Conversely, the GO terms associated with DNA damage-induced p53 signaling were downregulated in FIR-induced NE-like cells. Because FIR-induced NE-like cells underwent NED due to DNA damaging stimulus, it is possible that other NE-like cells will not share this feature. Future studies may determine if these pathways are also downregulated and if other NE-like cells have altered responses to IR and DNA damage.

Another potential difference concerns the expression and activity of AR. NE-like prostate cancer cells do not stain for AR or PSA protein[71] and the general consensus is that they do not utilize AR signaling. However, our FIR-induced NE-like cells continued to express AR and PSA at least at the mRNA level: In our RNA-seq analysis, AR (Fold change ~1.15) and PSA (Fold change ~0.77) were not identified as DEGs. Additionally, we assessed their expression via qRT-

PCR and neither AR (Fold change ~1.28) nor PSA (Fold change ~1.22) were differentially expressed (data not shown). We previously reported that AR protein is nearly undetectable in LNCaP cells following a cumulative dose of 40 Gy FIR (Figure 5A from[48]). This would indicate that AR protein is downregulated by a non-transcriptional mechanism. IRR NE-like LNCaP cell lines are cross-resistant to other prostate cancer treatments including ADT[48,49]. This further supports that although AR mRNA may still be expressed (which is different than other NE-like cells), AR signaling may not be required for FIR-induced NE-like cells (which is similar to other NE-like cells). Interestingly, AR expression is maintained in some FIR-treated IRR LNCaP cell lines[48]. Because the IRR lines were generated from individual clones, it is possible that AR protein is still expressed in a small subset of LNCaP cells treated with FIR. This may be assessed by ICC analysis of AR-stained FIR-induced NE-like cells. Analysis using the cBioPortal database[150,151] shows that ~80% of NE prostate cancer tumors have almost undetectable levels of AR mRNA. For the 20% of NE prostate cancer tumors where AR mRNA is detectable, the expression level is generally lower than in CRPC tumors. Although our FIR-induced NED model shows no change in AR mRNA levels, the clinical data suggests that downregulation of AR at the mRNA level is the most prominent mechanism leading to undetectable AR protein in NE prostate cancer tumors.

Several recent reviews have outlined genes associated with NED. It is worth discussing one review that developed a 12-gene signature of NE prostate cancer[96]. This gene list was created by analysis of both literature and the Beltran NE prostate cancer dataset[89] which assessed castration-resistant prostate cancer. Therefore these 12 genes are likely representative of ADT-induced NE-like prostate cancer cells. Although the role of the proteins encoded by these genes in NED has been well-studied, how they may be upregulated at the mRNA level is unknown. For example, EZH2 protein is activated by pCREB to promote NED[314], but how EZH2 mRNA is upregulated in NE-like cells is unknown. Nine of the signature genes were upregulated in NE prostate cancer (ASCL1, CgA, EZH2, FOXA2, INSM1, NCAM1, SOX2, SRRM4, and SYP). Consistent with this, we confirmed ASCL1, CgA, INSM1, NCAM1, SOX2, and SYP are upregulated at the mRNA level using qRT-PCR. We did not perform qRT-PCR of EZH2, FOXA2, SRMM4. However, EZH2 was identified as a downregulated DEG (Fold change 0.21) while FOXA2 and SRMM4 were not identified as DEGs. Future studies may confirm the regulation of these genes and identify potential mechanisms that explain the difference in expression in FIR-induced NE-like cells compared to in ADT-induced NE-like cells. Three of the signature genes

were downregulated in NE prostate cancer (AR, REST, SPDEF). Consistent with this, SPDEF was downregulated (fold change ~0.67) in our FIR-induced NE-like cells, although was not identified as a DEG. As described above, our studies revealed that AR mRNA expression was maintained in FIR-induced NE-like cells. Interestingly, REST was not identified as a DEG (Fold change ~1.16). REST and AR share similar roles in suppressing genes associated with NED and androgens inhibit REST protein turnover[315]. Therefore, ADT can promote degradation of REST protein to facilitate the expression of NED-associated genes[79]. Downregulation of REST at the mRNA level, as observed in clinical ADT-induced NE prostate cancer[96], may confer a similar phenotype. It is possible ADT may promote downregulation of REST at the mRNA level in at least a subset of prostate cancer patients. However, this may not be the case under the selection pressure of RT as we show that FIR-induced NE-like cells continue to express REST at the mRNA level. However, future studies may determine if REST protein is still expressed and biologically active in FIR-induced NE-like cells.

One key difference between our model and clinical NE-like prostate cancer cells is that our FIR-induced NE-like cells originate from a presumed isogenic prostate adenocarcinoma cell line. Clinical prostate cancer is heterogenic and prostate cancer tumors commonly have small areas of NE-like cells, typically defined as prostate adenocarcinoma with focal NED[57,79,80]. Selection pressure, by ADT for example, can also drive focal NED[81]. Clinically, there are several confounding factors that contribute to the initiation and maintenance of NED that cannot be replicated in our *in vitro* studies.

In the clinical setting, it is likely that there are several kinds of NE-like prostate cancer cells. The differences in their characteristics may be due to different cell or origin or different selection pressures. For example, it is reasonable to suspect that some prostate cancer tumors survive RT by undergoing FIR-induced NED. This recurrent tumor would be treated by ADT and ultimately progress to castration resistant prostate cancer. Therefore, this clinical NE-like prostate cancer cells may have blended characteristics with both FIR-induced NE-like cells and ADT-induced NE-like cells. Overall, our FIR-induced NE-like prostate cancer cells share several characteristics with other NE-like cells. Nevertheless, there are also some observed differences that likely arise due to the particular stimulus that promotes NED.

### 4.4.2 *FIR-induced NE-like cells likely rely on NHEJ instead of HR for repair of DSBs*

Although repair of DSBs has not previously been studied in NE-like cells, we provide initial evidence that NE-like cells may preferentially repair DSBs via NHEJ over HR. We did not assess HR or NHEJ repair directly. However, HR genes were downregulated in FIR-induced NE-like cells and qRT-PCR analysis confirmed that several were almost undetectable. qRT-PCR analysis of NHEJ genes revealed that they are expressed at similar levels in FIR-induced NE-like cells. Similarly, NHEJ genes were not identified as DEGs and NHEJ was not identified as an upregulated or downregulated pathway by GO or IPA. The mRNA expression profile of FIR-induced NE-like cells therefore suggests they are primed to repair DSBs via NHEJ and not HR.

DSB repair pathway choice is dependent on the cell cycle. NHEJ can occur at any point during the cell cycle but is mainly employed during $G_1$. Following DNA replication in S phase, chromosomes have been duplicated which allows for homology-based repair. HR utilizes this identical sequence as a template for repair and thus is the major DSB repair mechanism in late S phase and $G_2$ phase. Cell cycle analysis studies demonstrate that the majority of NE-like cells are in $G_1$ phase with very few in S or $G_2$ phase[316]. Likewise, LNCaP cells treated with ADT undergo NED as well as accumulate in $G_0/G_1$ phases[317,318]. Therefore, these NE-like cells that no longer proliferate are likely arrested in $G_0/G_1$ phases, have not undergone DNA replication, and cannot use HR for DSB repair. This is consistent with a previous report where non-proliferating cells mostly rely on NHEJ as opposed to HR[311]. Furthermore, the key HR protein RAD51 is undetectable in these non-proliferating cells[311]. Therefore, NE-like cells may stop transcription of HR genes and utilize cellular resources elsewhere. Although our studies were performed on FIR-induced NE-like cells, because other NE-like cells no longer proliferate and are arrested in $G_0/G_1$ phases, favoring NHEJ over HR is likely a common characteristic of NE-like cells.

### 4.4.3 *PRMT5 likely functions as an epigenetic regulator of FIR-induced NED*

Epigenetic regulation of gene expression mediates the development, progression, and therapeutic response of cancer[98,99]. DNA methylation was the first epigenetic mechanism to be linked to cancer while histone modification was the most recent[100]. Most studies have focused on histone lysine methylation; however, histone arginine methylation has emerged as an important regulatory event in cancer. Histone arginine methylation plays a key role in the regulation of gene

expression[101,102]. For example, PRMT5-mediated H4R3me2s represents one of the most repressive methylations in CD4+ T cells among the 20 histone methylations examined[113]. Therefore, new studies have established PRMT5 as an emerging epigenetic regulator of gene expression in cancer[105,110,112,120].

Several reports demonstrate that PRMT5 regulates gene expression on a global genomic scale. Given that mRNA expression changes significantly during FIR-induced NED, it is likely that PRMT5 mediates at least some of these gene expression changes. Ideally, ChIP-seq studies to characterize PRMT5 binding and identify putative target genes would be helpful to characterize an epigenetic function of PRMT5 in FIR-induced NED. However, ChIP-seq on FIR-induced NE-like cells is beyond our current capabilities. The main challenge is that ChIP-seq requires too many cells. Advances in ChIP-like technologies that require less cells or easier ways to incubate, irradiate, and prepare cells for ChIP might make these studies more feasible.

We previously reported that PRMT5 functions as a master epigenetic regulator to activate transcription of DSB repair genes[1]. In this study, we also provide initial evidence that NE-like cells may preferentially repair DSBs via NHEJ over HR. We assessed the mRNA expression of PRMT5 target genes involved in DSB repair. Expression of PRMT5 target genes associated with NHEJ (NHEJ1 and DNAPKcs) was maintained in FIR-induced NE-like cells which suggests PRMT5 still maintains their basal expression. Although PRMT5 activates HR genes in normal prostate cancer cells[1], all the PRMT5 target genes associated with HR (RAD51, RAD51AP1, RAD51D, BRCA1 and BRCA2) were downregulated following FIR-induced NED. This indicates that PRMT5 no longer activates their expression in FIR-induced NE-like cells. Given that FIR-induced NE-like cells are arrested in $G_0/G_1$ phase, it is possible that PRMT5's regulation of DDR genes is dependent on the cell cycle. For example, BRCA1 is significantly upregulated in $G_2$/M phase compared to $G_1$ phase[174]. NED signaling is likely responsible for the downregulation of HR genes in NE-like cells, and this mechanism may be the same or similar to the cell cycle-dependent regulation of HR genes. Future studies such as ChIP-seq comparing PRMT5 occupancy in $G_1$ vs. $G_2$ arrested cells may provide an answer to this.

There are several possible explanations for the observed downregulation of HR genes in FIR-induced NE-like cells. It is possible PRMT5 no longer binds to activate the transcription of HR genes, or PRMT5 may function in a different complex to repress their transcription. One additional explanation is changes in the interaction between PRMT5 and cofactors. Upon a single

dose of IR, there is more pICln and less MEP50 in the nucleus to interact with PRMT5. IR-induced nuclear localization of pICln thus likely contributes to IR-induced pICln binding to the promoters of genes involved in DDR to facilitate their activation. However, the nuclear levels of both pICln and MEP50 increase during FIR-induced NED. Therefore, increased nuclear MEP50 may prevent the PRMT5:pICln interaction to prevent activation of HR genes. This, however, does not explain the selectivity between NHEJ and HR genes. As discussed previously, future studies will provide mechanistic evidence for how PRMT5 can function as either an epigenetic activator or repressor (3.4.5 and 3.4.6), particularly to regulate genes involved in DSB repair and NED.

### 4.4.4 *PRMT5 may be required for FIR-induced activation of CREB*

Phosphorylation and activation of CREB is a common mechanism during NED[48,50,61,62,84,85,319]. Our RNA-seq analysis confirmed that cAMP-mediated signaling pathways are upregulated in FIR-induced NE-like cells. We previously reported that a cumulative dose of 10 Gy FIR induces phosphorylation of CREB at S133 leading to its activation[48]. Here, we also confirmed that pCREB is upregulated, particularly in the nucleus, following a cumulative dose of 10 Gy FIR. pCREB levels dose-dependently increased during the time-course of FIR and elevated pCREB is maintained in FIR-induced NE-like cells all the way up to a cumulative dose of 70 Gy FIR, further confirming the importance of pCREB to NE-like cells.

A previous report demonstrated that targeting PRMT5 decreases the phosphorylation of CREB under basal conditions as well as when stimulated with glucagon[320]. There are several arginine residues within RGG/RG motifs on CREB that may be methylated by PRMT5. Future studies may determine if PRMT5 methylates CREB and/or mediates FIR-induced phosphorylation and activation of CREB. CREB activation can also be regulated by interaction with p300/CBP. CARM1/PRMT4, a type I arginine methyltransferase that asymmetrically dimethylates proteins, methylates the KIX domain of p300/CBP to inhibit the phosphorylation and activation of CREB[321]. PRMT5 also methylates the p300/CBP ortholog CBP-1 in *C. elegans* [228]. The GRG motif of CEP-1 that is methylated by PRMT5 in *C. elegans* is conserved in the N-terminal domain of mammalian p300/CBP. Although not previously studied, it is possible that human PRMT5 may also methylate and regulate p300/CBP. Future studies may determine if PRMT5 methylates p300/CBP as another potential mechanism to mediate FIR-induced phosphorylation and activation of CREB.

### 4.4.5 *PRMT5 is upregulated in during FIR-induced NED*

PRMT5 is essential for initiation of NED, maintenance of NED, and survival upon FIR. The upregulation of PRMT5 protein in response to FIR likely facilitates NED. We have previously discussed several mechanisms by which PRMT5 may be upregulated at the protein level by a single dose of IR including transcriptional (3.4.2), translational (3.4.3), and post-translational (3.4.4). Most of these mechanisms could possibly explain FIR-induced upregulation of PRMT5 protein. However, because PRMT5 was not upregulated at the mRNA level in LNCaP cells following a cumulative dose of 40 Gy FIR, transcriptional changes are unlikely to promote the upregulation of PRMT5 in FIR-induced NE-like prostate cancer cells. Future studies may determine how PRMT5 is upregulated by FIR treatment.

PRMT5 is overexpressed in many cancers and its overexpression correlates with poor prognosis[105,110,111]. It will be interesting to see if PRMT5 is also upregulated in normal prostate NE-like cells, *de novo* NE-like prostate cancer cells, ADT-induced NE-like prostate cancer cells, FIR-induced NE-like prostate cancer cells, or NE-like cells of other cancers. We previously analyzed clinical expression of PRMT5 at the mRNA level[1]. Analysis of the "Neuroendocrine Prostate Cancer" data set[89] revealed that PRMT5 mRNA expression was mostly unchanged even in cases when the PRMT5 gene was amplified. This is consistent with our findings that PRMT5 mRNA is unchanged despite FIR-induced upregulation at the protein level. Because the "Neuroendocrine Prostate Cancer" data set[89] represents castration-resistant ADT-induced NE-like prostate cancer cells, this finding supports our suggestion that NE-like cells share common characteristics (4.4.1) PRMT5 protein expression in prostate cancer following RT has not been studied, and unfortunately tumor biopsies following long-term RT treatment are uncommon. There is an urgent need for these tumor biopsies and their analysis of could confirm if PRMT5 protein is upregulated by RT treatment clinically and further characterize clinical FIR-induced NE-like cells.

### 4.4.6 *PRMT5 along with cofactors pICln and MEP50 contribute to FIR-induced NED*

PRMT5 plays diverse roles in the cell by regulating processes such as gene expression, splicing, translation, and protein-protein interactions[110,111]. PRMT5 regulates these processes through methylation of either histone or non-histone substrates. The function of PRMT5 can be regulated based upon the degree of expression and subcellular localization. PRMT5 activity is also

modulated by several interacting proteins. There is a long-standing view in the field that the cofactor MEP50 is required for PRMT5 methyltransferase activity and specifically for epigenetic function[110,111,140,141]. However, we previously reported that PRMT5 cooperates with pICln, but not MEP50, for the transcriptional activation of genes involved in the DDR[1], and discussed the potential for pICln as a novel epigenetic cofactor of PRMT5 (3.4.5). Thus, the role of PRMT5 cofactors appears to be complex and warrants future studies.

Here, we present evidence that PRMT5, pICln, and MEP50 are essential for the initiation of NED, maintenance of NED, and survival upon FIR. However, the degree in which these proteins are involved in the different phases of NED differs. For example, pICln likely plays a bigger role in surviving FIR treatment and less of a role in facilitating NED. This is consistent with our previous report where targeting pICln inhibited DSB repair[1]. Conversely, targeting MEP50 did not inhibit DSB repair[1]. However, MEP50 was required for surviving FIR treatment. Thus, it is likely that MEP50 plays an essential role in other survival pathways. Additionally, targeting MEP50 caused regression of neurites and sensitized cells that had already undergone NED rather quickly, especially compared to targeting PRMT5 or pICln. Collectively, it is likely that PRMT5:pICln is more essential for repair of IR-induced DSBs and PRMT5:MEP50 is more essential for NED.

Although PRMT5, pICln, and MEP50 play some role in FIR-induced NED, we did not assess what specific biological processes they may regulate nor if they regulate them in a cooperative function. We cannot rule out the possibility that PRMT5 plays roles in NED independently of pICln or MEP50. Likewise, we cannot rule out the possibility that pICln or MEP50 plays roles in NED independently of PRMT5. However, it is likely that PRMT5's role in FIR-induced NED is dependent on several factors additional to interaction with cofactors.

There are several challenges that make it difficult to determine the role of PRMT5, pICln, and MEP50 in FIR-induced NED. As discussed earlier, there are technical challenges that make ChIP-seq of FIR-induced NE-like cells not feasible (4.4.3). Thus, it is difficult to assess a potential epigenetic role in FIR-induced NED. Furthermore, combination of knockdown and FIR treatment kill almost all of the cells, and common experiments that assess the role of a particular protein by knockdown or drug targeting are not feasible. Utilization of other techniques or advances in technology may allow for further mechanistic studies for the role of PRMT5, pICln, and MEP50 in FIR-induced NED.

### 4.4.7 *PRMT5 along with cofactors pICln and MEP50 may contribute to ADT-induced NED*

We have already discussed the importance of PRMT5, pICln, and MEP50 in FIR-induced NED (4.4.6). However, NED is a common mechanism of treatment-resistance[50,60,77,81,83,88–91], and NE-like cells share common characteristics (4.4.1). Furthermore, we recently identified PRMT5 as a novel epigenetic regulator of AR[114], the target of clinical ADT. Because FIR-induced NE-like cells are similar to ADT-induced NE-like cells, further studies on role of PRMT5, pICln, and MEP50 in ADT-induced NED are warranted.

### 4.4.8 *Targeting PRMT5 may be explored to enhance RT for prostate cancer treatment*

After our finding that PRMT5 is an essential regulator of DSB repair[1], we proposed PRMT5 may be an effective therapeutic target to enhance RT for cancer treatment (2.4.5). This suggestion was based on analysis of the DDR following a single dose of IR. Here, we assessed PRMT5 targeting in combination with FIR treatment both *in vitro* and *in vivo*. Using our previously characterized *in vitro* mimic of clinical RT[49,50], if PRMT5 was knocked-down during any phase, <0.05% of cells survived. To corroborate these *in vitro* findings, we assessed if targeting PRMT5 can sensitize prostate cancer tumors to RT in a preclinical mouse study. Our mice study provided compelling preclinical evidence that targeting PRMT5 in combination with RT may better cure a prostate cancer patient and at the very least delay tumor recurrence and prolong life.

Both our *in vitro* and *in vivo* studies assessed a cumulative dose of 40 Gy FIR. Clinically, prostate cancer patients commonly receive cumulative doses even past 70 Gy FIR[27,35]. This would suggest that targeting PRMT5 is effective in enhancing RT and may allow for lower cumulative doses of FIR when appropriate. When comparing these studies to clinical RT, we have to consider the biologically effective dose (BED) which facilitates a better comparison of RT protocols with different doses per fraction, cumulative doses, or overall treatment time. Calculation of BED utilizes an α/β ratio to describe the equation of the cell survival curve. The α/β ratio is specific for each tissue and each cancer. It is classically assumed that prostate cancer has an α/β ratio of ~1.5[22], however recent reviews suggest it may be higher at ~2.7-4.9[23–26]. The appropriate α/β ratio for FIR of prostate cancer cells *in vitro* has not been determined. Using the radiation BED calculator tool created by Dr. John F. Fowler (https://www.mdcalc.com/radiation-biologically-effective-dose-bed-calculator) with an α/β ratio of between 1.5-5, our *in vitro* studies of 40 Gy (2 Gy per fraction,

5 fractions per week) used a BED of 56-93.33 Gy, while our *in vivo* studies of 40 Gy (5 Gy per fraction, 2 fractions per week) used a BED of 80-173.33 Gy. Considering most RT protocols use a BED between 98-200 Gy[27], our experiments are applicable to lower cumulative doses of clinical RT. This supports the potential for PRMT5 as a potential therapeutic target to enhance RT clinically.

NED is an emerging mechanism of resistance to RT[50]. Our *in vitro* clinical mimic of RT also models clinical resistance to FIR via NED: Briefly, prostate cancer cells undergo NED in two phases: (1) *radiation resistance acquisition (RA)* and (2) *neuroendocrine differentiation (NED)*[49,50] (4.3.1). Here, we provide evidence that targeting PRMT5 prevents FIR-induced NED as well as kills pre-existing FIR-induced NE-like cells. Clinical evidence suggests that NED correlates with poor prognosis and treatment-resistance[53,56,75,92]. NED likely contributes significantly to the incidence of tumor recurrence following RT. Therefore, our findings that targeting PRMT5 inhibits FIR-induced NED *in vitro* and significantly prevented tumor recurrence *in vivo* raise the exciting possibility for PRMT5 as a therapeutic target to enhance RT. Future studies may confirm if targeting PRMT5 prevented FIR-induced NED in our LNCaP xenograft tumors to further support the combination treatment of targeting PRMT5 during RT.

PRMT5 is likely a versatile therapeutic target for treating prostate cancer. Additional to enhancing RT, we have previously demonstrated that targeting PRMT5 decreases AR expression to suppress prostate cancer cell growth[114]. Here, we also determined that long-term treatment with a PRMT5 inhibitor can kill prostate cancer cells. Therefore, PRMT5 inhibitors alone may be effective in the treatment of prostate cancer. Given that several cancer treatments can induce NED, it is possible PRMT5 inhibitors may enhance these therapies and prevent treatment-resistance via NED. For example, it will be interesting to assess if a combination treatment of PRMT5 targeting along with ADT is more effective than ADT alone by targeting AR signaling at multiple levels. ADT is also used as a radiosensitization approach to enhance RT for localized prostate cancer patients[42]. Therefore, a triple treatment combination of a PRMT5 inhibitor, ADT, and RT may be effective clinically or may allow lower drug concentrations or lower radiation doses to limit adverse effects. However, because targeting PRMT5 can mimic ADT by decreasing expression of AR[114], it is possible co-targeting of PRMT5 with RT may be just as effective the triple treatment.

There are some potential criticisms of PRMT5 targeting for cancer treatment. In this study, we assessed the effect of long-term BLL3.3 treatment alone on prostate cancer cells. Interestingly, some of the cells treated with BLL3.3 underwent NED. Further BLL3.3 treatment caused death of

some of the NE-like cells. Although we terminated the experiment following 32 days of drug treatment, it would be interesting to see if even further BLL3.3 could fully reverse NED and/or kill the NE-like cells. Additionally, it remains unknown how normal cells respond to long-term treatment with PRMT5 inhibitors and we have previously discussed the criticism of potential systemic adverse effects[1] (2.4.5). Importantly, targeting PRMT5 does not affect the growth of AR-negative DU145 and PC3 prostate cancer cells as well as normal prostate RWPE-1 cells[114].

Nonetheless, if future clinical trials determine there are significant adverse effects associated with PRMT5 inhibitors, there are several options to make PRMT5 inhibitors more tolerable. Targeted delivery could be applied to either PRMT5 inhibitors or radioactive microparticles to limit the off-target effects. This can be effectively achieved through prostate specific membrane antigen-based delivery[246] or other delivery systems developed in the future. Furthermore, advances in RT may facilitate a lower, more tolerable concentration of PRMT5 inhibitors. Meta-analysis of several RT clinical trials demonstrated that increases in BED significantly correlate with better outcomes but do not associate with adverse effects to a significant extent[27]. Instead, other factors are better predictors of adverse effects than BED and increases in BED are typically well-tolerated[28]. Advances in RT technology such better image guiding technology, robot assistance, hydrogel spacers that separate the prostate from other organs, and proton therapy can further increase the tolerability of RT[29–31].Taking this into account, this leaves the possibility of maintaining a high BED while using a lower concentration of a PRMT5-targeting drug to mitigate potential adverse effects. Lastly, a novel approach would be to target protein-protein interactions between PRMT5 and its cofactors which may increase specificity/selectivity towards specific contexts such as DDR or NED. For example, given that it is likely that pICln, and not MEP50, is involved in the epigenetic activation of DDR genes by PRMT5, a PRMT5:pICln PPI inhibitor may be more selective to inhibit this specific function. Overall, our findings here provide compelling evidence that PRMT5 is a critical mediator of FIR-induced NED and is likely a clinically relevant therapeutic target to enhance RT for cancer treatment.

## 4.5 Materials and methods

### 4.5.1 *Cell lines and cell culture*

LNCaP cells were purchased from ATCC (Manassas, VA, USA) and cultured as described previously[1,114,121]. Upon arrival, the cell line was immediately expanded and aliquots were prepared and stored in liquid nitrogen. Cells were maintained for no longer than 30 passages or no longer than 3 months as described previously[1,49,266]. Cell line authentication was performed by IDEXX BioResearch (IMPACT I) and the absence of mycoplasma contamination was verified using LookOut® PCR Mycoplasma Detection Kit (Sigma, St. Louis, MO, USA). Knockdown cell lines were generated using the pLKO-Tet-On system as described previously[1]. The pLKO-Tet-On plasmid for shRNA expression was obtained from Addgene (Cambridge, MA, USA)[267], and shRNA sequences that target PRMT5 #1 (5′-CCCATCCTCTTCCCTATTAAG-3′: referring to #1832)[114], PRMT5 #2 (5'-GCCCAGTTTGAGATGCCTTAT-3′: referring to #1577)[114], SC (5'-CAACAAGATGAAGAGCACCAA-3'), MEP50 (5'- CCTCACAAGGACTCTGTGTTT-3'), and pICln (5'-CCAACAGTTGCTGGACAGTTT-3') were used for the construction of plasmids for stable cell line generation as described previously[1,114,266]. Stable cell lines with Dox-inducible expression of PRMT5-targeting shRNA (LNCaP-shPRMT5: referring to #1832[114], LNCaP-shPRMT5 #2: referring to #1577[114]) or scramble control-targeting shRNA (shSC) (LNCaP-shSC, PC3-shSC, and DU145-shSC) were established from individual clones and characterized previously[114]. Stable cell lines with Dox-inducible expression of MEP50-targeting shRNA or pICln-targeting shRNA (LNCaP-shMEP50 and LNCaP-shpICln, respectively) were established from individual clones and characterized previously[1]. Cell lines are described in Appendix C.

### 4.5.2 *Dox-induced knockdown and inhibitor treatment conditions*

For Dox-inducible cell lines, Dox was applied at the final concentration of 1 µg/mL every 48 h to establish and maintain PRMT5 knockdown (shPRMT5), pICln knockdown (shpICln), MEP50 knockdown (shMEP50), or express scramble control shRNA (shSC). The number of days of Dox treatment was optimized: shPRMT5 and shSC cells were grown for 4 days and had 4 days of Dox treatment, shMEP50 were grown for 4 days and had 2 days of growth followed by 2 days of Dox treatment, and shpICln cells were grown for 5 days and had 5 days of Dox treatment. For FIR experiments, cells were subjected to IR following the knockdown described above. During

FIR periods, Dox was applied 3 times a week. Specifically, each week cells were subjected to IR on days 1-5 and Dox was applied on days 1, 3, and 5 as described below:

| Day 1 | Day 2 | Day 3 | Day 4 | Day 5 | Day 6 | Day 7 |
|---|---|---|---|---|---|---|
| 2 Gy<br>Dox | 2 Gy | 2 Gy<br>Dox | 2 Gy | 2 Gy<br>Dox | | |

For experiments to assess the percentage of cells that survived a particular cumulative dose of FIR combined with PRMT5, pICln, or MEP50 knockdown, cells were treated as described above with the following considerations: The parental cell line (LNCaP) was used as a control. For '1) control', Dox was not applied during any phase. The purpose of '1) control' is to account for leaky expression of the shRNA and is expected to perform the same as the parental cell line (LNCaP). For '2) RA', Dox was applied during weeks 1-2 or 0-20 Gy. For '3) NED', Dox was applied 3 days before and during weeks 3-4 or 20-40 Gy. For '4) Both', Dox was applied during all 4 weeks or 0-40 Gy. Dox treatment is as described below:

| Group | Week 1<br>(0-10 Gy)<br>FIR days 1-5 | Week 2<br>(10-20 Gy)<br>FIR days 1-5 | Week 3<br>(20-30 Gy)<br>FIR days 1-5 | Week 4<br>(30-40 Gy)<br>FIR days 1-5 |
|---|---|---|---|---|
| LNCaP | | | | |
| 1) Control | | | | |
| 2) RA | Days 1,3,5 | Days 1,3,5 | | |
| 3) NED | | Day 5 | Days 1,3,5 | Days 1,3,5 |
| 4) Both | Days 1,3,5 | Days 1,3,5 | Days 1,3,5 | Days 1,3,5 |

For parental cell lines, cells were treated with the PRMT5 inhibitor BLL3.3 (10 μM) or an equal volume of DMSO (control) every 48 h beginning 24 h after plating to inhibit PRMT5 activity. The number of days of drug treatment was optimized: LNCaP cells were grown for 5 days and had 1 day of growth followed by 4 days of drug treatment. For FIR experiments, cells were subjected to IR following the drug treatment described above. During FIR periods, drug was applied 3 days a week. Specifically, each week cells were subjected to IR on days 1-5 and drug was applied on days 1, 3, and 5 as described below:

| Day 1 | Day 2 | Day 3 | Day 4 | Day 5 | Day 6 | Day 7 |
|---|---|---|---|---|---|---|
| 2 Gy<br>Drug | 2 Gy | 2 Gy<br>Drug | 2 Gy | 2 Gy<br>Drug | | |

Experiments to assess the effect of long-term PRMT5 inhibitor treatment alone were performed in parallel. LNCaP cells were treated the same as described above but without FIR treatment

### 4.5.3 *Ionizing radiation conditions*

Previously isolated IR-resistant (IRR) NE-like LNCaP cell lines[48] were irradiated using the GC-220 device (Atomic Energy of Canada, Ottawa, Canada) with a Co-60 radiation source as described previously[48,49]. For all other experiments, cells/mice were irradiated using the X-RAD 320 biological irradiator device (PXi Precision X-Ray, North Branford, CT, USA) with an x-ray tube radiation source at an average dose rate of ~1 Gy/25 sec. All IR treatments were carried out in normal air at room temperature, and cells spent minimal time outside incubators during treatment. Non-irradiated controls were 'mock-irradiated' by being taken out of the incubator for the same time period as irradiated counterparts.

### 4.5.4 *Trypan blue staining for quantification of cell survival following fractionated ionizing radiation (FIR) treatment and quantification of viable cells following PRMT5 inhibition*

Trypan blue staining was used to assess the percentage of cells that survived FIR treatment combined with PRMT5, pICln, or MEP50 knockdown or PRMT5 inhibition. For each end point, cells were seeded on 2, 15 cm dishes and treated as described elsewhere. When cells reached ~80-90% confluency, cells for the IR- sample were collected, while cells for the FIR+ sample were treated with their first dose of 2 Gy IR. Cells for the FIR+ sample were collected 24 h following the last IR treatment. Immediately prior to cell collection, microscope images were taken as described below. For cell collection, cells were washed with PBS and then trypsinized. Once cells begun to detach, cells were resuspended in media. Cells from the same sample that were grown on different 15 cm dishes were combined. Cells were pelleted using centrifugation (350 x g @ 4°C for 5 m), the supernatant was removed, and the cells were resuspended in PBS. Four separate 1:1 aliquots of cells:trypan blue solution (Corning, Corning, NY, USA) were prepared. Viable cells for the 4 aliquots were totaled using Countess™ II FL reusable slides and the Countess™ II automated cell counter (Thermo Fisher, Waltham, MA, USA). The average value of the 4 aliquots

was used as the number of viable cells. To calculate the surviving fraction (% survival), the value for FIR+ was normalized to the value for IR-.

Trypan blue staining was also used to assess the number of viable cells following treatment with the PRMT5 inhibitor BLL3.3[114,249] alone. For each end point, cells were seeded on 2, 15 cm dishes and treated as described elsewhere. DMSO or BLL3.3 treatment begun immediately and continued through the duration of the experiment. Cell collection and trypan blue staining was performed as described above. To calculate fold change in number of cells, the value for the particular time point was normalized to initial number of cells.

### 4.5.5 *Quantification of NE-like cells by assessing presence of neurites*

The percentage of NE-like cells was determined as described previously[48]. Briefly, microscope images of cells were analyzed for cell morphology changes associated with NED. Cells were treated as described above from the trypan blue staining experiment. Prior to cell collection and trypan blue staining, cells were imaged via the Nikon TE2000 inverted fluorescence microscope (10x and 20x objective) (Nikon Instruments Melville, NY, USA). 10x images were used for further analysis. The length of the cell body and the length of the longest neurite projection was manually recorded for each cell. At least 100 cells were counted for each biological replicate. The arrays of length counts for each biological replicate were first analyzed via both "D'Agostino & Pearson" and "Shapiro-Wilk" normality tests to evaluate distribution. Because not all samples were normally distributed, median values were used instead of mean values for each biological replicate. For each individual cell, to calculate the neurite:body (N:B) ratio, the length of the longest neurite projection was divided by the length of the body. NE-like cells were defined as cells where the longest neurite projection was at least two times longer than the cell body diameter (giving a N:B ratio of $\geq 2$). To calculate the % of NE-like cells, the number of NE-like cells was divided by the total number of cells. The arrays of neurite projection and cell body length counts for each biological replicate were also subjected to further analysis separately to determine the median fold change in neurite length and body length compared to untreated.

### 4.5.6 *Western blot*

Western blot was used to assess changes in protein expression associated with FIR-induced NED. When assessing FIR+ cells, we wanted to analyze only stable changes and not changes due to IR-induced activation of the DDR. Therefore, we performed western blot 24 h following the last dose of IR to allow cells to return to their basal state and to negate acute changes due to a single dose of IR. Cells were seeded on either 10 cm (IRR cell line experiment) or 15 cm dishes (all other experiments) and treated as described elsewhere. Cells were harvested in lysis buffer (100 mM Tris-HCl pH 8.0, 15 mM $MgCl_2$, 100 mM KCl, 5 µg/mL of each Chymostatin, Leupeptin, Pepstatin A, and antipan in DMSO, 1% Triton X-100, 1 mM PMSF in ethanol, and 1 mM DTT) for IRR cell line experiment or RIPA buffer (10 mM Tris-HCl pH 8.0, 5 mM EDTA, 1% Triton X-100, 0.1% Sodium Deoxycholate, 0.1% SDS, 140 mM NaCl, 5 µg/mL of each Chymostatin, Leupeptin, Pepstatin A, and antipan in DMSO, and 1 mM PMSF in ethanol) for all other experiments. Total protein concentration was measured using Bradford method. Approximately 20-30 µg total protein was run on a 10-15% SDS-PAGE and western blotting was performed as described previously[114,121,266]. Band/protein intensity was quantified using ImageJ[270]. Antibodies used for western blot were anti-PRMT5-rabbit (1:1000), -β-Actin-mouse (1:2000), -NSE-rabbit (1:1000), -H4R3me2s-rabbit (1:1000), -rabbit-HRP (horseradish peroxidase) (1:1000), -mouse-HRP (1:1000). All antibodies are described in Appendix E.

### 4.5.7 *RNA-seq for identification of genes associated with FIR-induced NED*

LNCaP cells were seeded on 15 cm dishes. When cells reached ~80-90% confluency, cells for the FIR- sample were harvested, while cells for the FIR+ sample were treated with their first dose of 2 Gy IR. Cells for the FIR+ sample were treated with a cumulative dose of 40 Gy FIR (2 Gy per fraction, 5 fractions per week) and harvested 24 h following the last IR treatment. When assessing FIR+ cells, we wanted to analyze only stable changes and not changes due to IR-induced activation of the DDR. Therefore, we isolated RNA 24 h following the last dose of IR to allow cells to return to their basal state and to negate acute changes due to a single dose of IR. Total RNA was isolated using Trizol Reagent (Ambion, Carlsbad, CA, USA) sent to Novogene Corporation Inc. USA (Sacramento, CA, USA) for RNA library preparation and sequencing.

RNA samples were first subjected to quality control assessment. Preliminary quality control was performed by agarose gel electrophoresis and Nanodrop. RNA integrity was confirmed using Agilent 2100 and purity was confirmed by Nanodrop. RNA quality was evaluated by RNA integrity number (RIN) (intact RNA is 10 while totally degraded RNA is 1)[322]. The RIN value for each sample was between 8.4-9.5 indicating high quality isolated RNA.

To prepare the RNA library, samples were run on an Illumina NovaSeq 6000 S4 flowcell which generated paired-end 151 base reads. Briefly, mRNA was enriched using oligo(dT) beads and randomly fragmented using fragmentation buffer. Fragmented mRNA was converted to cDNA by reverse transcription. cDNA fragments were converted into the library by ligation to sequencing adapters containing specific sequences that interact with the surface of the flow-cell. Library underwent clonal amplification by cluster generation and final sequences were generated via paired end sequencing. RNA library was then subject to quality control assessment. Qubit 2.0 was used to test the library concentration, Agilent 2100 was used to test the insert size, and qPCR was used to verify the effective concentration of the library precisely. Library preparation generated between 21,300,374-27,928,372 raw reads per sample and between 21,013,658- 27,413,187 clean reads per sample. Across all the samples, between 97.83%-98.65% of the reads were clean reads. Illumina Q-scores for each base were calculated to assess the probability of an error in base calling. On average across all the samples, Q-scores were between 35-37, indicating an error rate of 1/3000-1/5000. Illumina suggests that 75% of bases should have a Q-score of $\geq 30$ while Novogene suggests that 80% of bases should have a Q-score of $\geq 30$. Across all the samples, between 93.19-95.04% of bases had a Q-score of $\geq 30$ indicating that the RNA library was of significantly high-quality.

Raw RNA-seq results were further assessed. RNA library quality was verified by FastQC, and STAR RNA-seq aligner[278] was used to map all high-quality sequences to the human genome (GENCODE GRCh38) with the parameter "--outSAMmapqUnique 60". Read counts were evaluated using featureCounts (v1.6.2)[279] with the following parameters: "-s 0 –p –Q 10 -O" to summarize uniquely mapped reads to the gene level according to the GENCODE 31 annotation file. Genes with low expression levels were filtered out if they had a raw read count of less than 10 in half or more of the samples. The rest of the genes were normalized by trimmed mean of M value (TMM) method to obtain the final profile of gene expression (base-2 log scale). EdgeR (v3.28.1) [280,323] was used to perform differential expression analysis by comparing FIR+ (40 Gy)

vs FIR- (untreated) groups. We defined genes as differentially expressed genes (DEGs) if their FDR-adjusted *p*-values were less than 0.01, and the magnitudes of fold-changes (FCs) in logarithmic scale (base 2) were larger than one.

Gene Ontology (GO) and pathway analysis were performed on the DEGs. GO enrichment analysis was performed using the web-based tool DAVID functional annotation analysis (http://david.abcc.ncifcrf.gov/home.jsp v6.8)[281,282]. Upregulated and downregulated DEG lists were analyzed separately and GO annotations with FDR-adjusted *p*-values less than 0.05 were recognized to be significantly over-represented. Pathway analysis was performed using Ingenuity Pathway Analysis (IPA) (QIAGEN Inc., https://www.qiagenbioinformatics.com/products/ingenuity-pathway-analysis) to identify differentially regulated pathways upon FIR-induced NED. Using IPA, pathways were predicted to be either activated or inhibited in FIR-induced NE-like cells.

### 4.5.8 *RNA isolation, reverse transcription, and RT-qPCR*

LNCaP cells were seeded on 15 cm dishes. When cells reached ~80-90% confluency, cells for the FIR- sample were harvested, while cells for the FIR+ sample were treated with their first dose of 2 Gy IR. Cells for the FIR+ sample were treated with a cumulative dose 40 Gy FIR (2 Gy per fraction, 5 fractions per week) and harvested 24 h following the last IR treatment. When assessing FIR+ cells, we wanted to analyze only stable changes and not changes due to IR-induced activation of the DDR. Therefore, we isolated RNA 24 h following the last dose of IR to allow cells to return to their basal state and to negate acute changes due to a single dose of IR. Total RNA was isolated using Trizol Reagent (Ambion, Carlsbad, CA, USA).

RNA concentration and integrity were verified by agarose gel electrophoresis. cDNA synthesis was done using High Capacity cDNA Reverse Transcription Kit (Promega, Madison, WI, USA) as described previously[1,114,121,266]. qPCR was performed using FastStart Universal SYBR Green Master Mix (Thermo Fisher Scientific, Waltham, MA, USA) on the QuantStudio 6 Flex System and QuantStudio™ Real-Time PCR Software (Thermo Fisher, Waltham, MA, USA). Forty cycles were run and samples without $C_T$ values were deemed undetected. Technical duplicates were run for each sample and the $C_T$ values used for further analysis were the average of the technical duplicates. Samples where $C_T$ values for technical duplicates were >0.5 apart were re-run. Non-template controls (NTC)s with autoclaved double-distilled $H_2O$ were also run for each

primer set and primer sets where $C_T$ values for NTC were lower than 37 (indicating high background) were re-run. Amplicon size and specificity were verified for each primer set via agarose gel electrophoresis. PRMT5, AR, and GAPDH primers were used previously[1,114,121]. IVL primers were used previously[1,253,283]. pICln, MEP50, BRCA1, BRCA2, RAD51, RAD51AP1, RAD51D, DNAPKcs, Ku80, NHEJ1, and XRCC4 were used previously[1]. CgA primers were used previously[324,325]. NSE primers were used previously[325]. Lastly, BRN primers were used previously[326]. All primers used are described in Appendix D.

#### 4.5.9 *Immunocytochemistry for quantification of NE-like cells, FIR-induced DSBs[167], protein expression, and protein subcellular localization*

LNCaP cells were seeded on 15 cm dishes containing glass coverslips and treated as described elsewhere. When cells reached ~80-90% confluency, cells for the IR- sample were fixed, while cells for the FIR+ sample were treated with their first dose of 2 Gy IR. Cells for the FIR+ sample were fixed 24 h following the last IR treatment. When assessing FIR+ cells, we wanted to analyze only stable changes and not changes due to IR-induced activation of the DDR. Therefore, we fixed cells 24 h following the last dose of IR to allow cells to return to their basal state and to negate acute changes due to a single dose of IR

Cells were fixed with 3.7% formaldehyde in phosphate buffered saline (PBS) at room temperature for 20 minutes at the indicated time points. After fixation, cells were permeabilized with 0.2% Triton X-100 in PBS at room temperature for 5 m. Cells were then blocked with 5% milk blocking solution in PBS, stained with the indicated primary antibodies diluted in 5% milk blocking solution in PBS, and stained with 4,6-diamidino-2-phenylindole (DAPI final 10 µg/mL) and indicated secondary antibodies diluted in 5% milk blocking solution in PBS. Cells on coverslips were mounted on glass slides using the ProLong® Antifade Kit (Invitrogen Molecular Probes, Eugene, OR, USA) and sealed with clear nail polish. Cells were then imaged via the Nikon TE2000 inverted fluorescence microscope under oil immersion (60x objective) (Nikon Instruments Melville, NY, USA). The primary antibodies used were anti-CgA-rabbit (1:500), -pCREB-rabbit (1:800), -γH2AX-mouse (1:1000), -PRMT5-rabbit (1:1000), -pICln-rabbit (1:1000), and -MEP50-rabbit (1:100). Secondary antibodies used were anti-mouse-FITC (1:100) and anti-rabbit-rhodamine red (1:1000). All antibodies are described in Appendix E.

For quantification of NE-like cells, immunocytochemistry was performed as described above. Bright field microscope images of cells (live) were analyzed for cell morphology changes associated with NED and the percentage of NE-like cells was assessed by the presence of neurites as described above. At least 40 cells were counted for each biological replicate. CgA microscope images were analyzed and the percentage of NE-like cells was assessed by the presence of CgA-positive cells. CgA-positive cells have foci surrounding the nucleus in the rough endoplasmic reticulum where CgA is synthesized, in the cytoplasm inside free secretory vesicles, or within the Golgi apparatus. Images were processed via ImageJ[270] and the background was subtracted from the image using the rolling ball method (http://imagej.net/plugins/rolling-ball.html). Gating for minimum and maximum intensity values was set the same for each image. The presence or absence of CgA foci was manually recorded for each cell. At least 40 cells were counted for each biological replicate.

For quantification of FIR-induced DSBs, immunocytochemistry was performed as described above. Images were processed via ImageJ[270] and the background was subtracted from the image using the rolling ball method (http://imagej.net/plugins/rolling-ball.html). Gating for minimum and maximum intensity values was set the same for each image. The number of γH2AX foci was manually recorded for each cell (defined via nuclear DAPI staining). At least 50 cells were counted for each biological replicate. The arrays of foci counts for each biological replicate were subjected to further analysis separately to determine the average number of foci per cell and percentage of cells with zero foci.

For quantification or protein expression and subcellular localization, immunocytochemistry was performed as described above. Images were analyzed via ImageJ[270]. First, the background was subtracted from the image using the rolling ball method (http://imagej.net/plugins/rolling-ball.html). Gating for minimum and maximum intensity values was set the same for each image. For pCREB, PRMT5, pICln, and MEP50 expression and subcellular localization, regions of interest (ROI) were outlined for each individual cell (whole cell), nucleus only (as defined by DAPI staining), and cytoplasm only (as defined by signal outside of DAPI staining).The average intensity for each ROI was measured and at least 40 cells were counted for each biological replicate. The arrays of intensity counts for each biological replicate were subjected to further analysis separately and were analyzed via both “D’Agostino & Pearson” and “Shapiro-Wilk” normality tests to evaluate distribution. Because not all samples were

normally distributed, the median value was used for each biological replicate. To determine the nuclear:cytoplasmic ratio (N:C), the value for nucleus was divided by the value for cytoplasmic for each cell individually such that an N:C ratio of 1 indicates equal expression in both the nucleus and cytoplasm.

### 4.5.10 *Preclinical mouse study to assess if targeting PRMT5 can sensitize prostate cancer xenograft tumors to RT*

The protocol for the development, treatment, and analysis of xenograft tumors is similar to described previously[49]. Briefly, cells (6 X $10^6$) were suspended in 100 μL media + 100 μL matrigel for injection into the flank. Twenty adult male NRG mice (The Jackson Laboratory, Bar Harbor, ME, USA) were injected with LNCaP-shSC cells while 20 adult male NRG mice were injected with LNCaP-shPRMT5 cells. Once xenograft tumors grew to ~200-300 $mm^3$ (generally between 4-6 weeks after injection), mice were fed Dox-containing drinking water (1 mg/mL) to establish and maintain PRMT5 knockdown (shPRMT5), or express scramble control shRNA (shSC) in the xenograft tumors. Three days following the switch to Dox-containing water (enough time for efficient PRMT5 knockdown), tumors were subjected to their first IR treatment. Tumors were treated with FIR (5 Gy per fraction, 2 fractions per week) until a cumulative dose of 40 Gy FIR was reached. During each radiation treatment, mice were given airflow containing isoflurane as a general inhalation anesthetic. Radiation was focused directly on the tumor while the rest of the body was protected from radiation by lead plates. The 5 Gy dose was delivered within roughly 4-5 minutes and mice were returned to normal air conditions directly after radiation. Dox treatment was stopped after the last dose of IR treatment so PRMT5 could return to basal levels.

The tumor volume was recorded twice weekly and mice with tumors larger than 1,500 $mm^3$ were sacrificed due to tumor burden. Only tumor volumes from live mice were used to calculate the average, thus tumor volumes began to fluctuate when mice with large tumors begun to die. The array of tumor volumes was subjected to further analysis to determine tumor recurrence following FIR treatment. First tumor recurrence was defined as the time point when a tumor reached a size larger than 400 $mm^3$. For each time point, the number of tumors that had experienced tumor recurrence was normalized to the total number of tumors to calculate the percentage of tumors that recurred. Tumor-specific survival following FIR treatment was also determined. The number of living mice (with or without tumors) was normalized to the total number of mice to calculate the

percent survival. The experiment was terminated several weeks following the tumor recurrence of the last control (shSC) mouse.

This mouse experiment was performed in the Biological Evaluation Facility of the Purdue University Center for Cancer Research and was approved by Purdue Animal Care and Use Committee (PACUC) (Coeus # 1112000342, formerly PACUC 08-127). All animal use followed the 'Assurance of Compliance with Public Health Services Policy on Human Care and Use of Laboratory Animals' (Welfare Assurance # A3231-01)

### 4.5.11 *Statistical analysis*

No statistical methods were used to predetermine sample size. All statistical analyses were performed using Graphpad Prism 8.00 for Windows (GraphPad Software, La Jolla California USA, www.graphpad.com). Statistical analysis was performed on raw data with assumed normal distribution. For all qPCR experiments, statistical analysis was performed on $\Delta C_T$ values ($C_T$ value of gene normalized to $C_T$ value of GAPDH control). For all western blot experiments, statistical analysis was performed on normalized raw intensity values (intensity value of protein divided by the intensity value of β-Actin). When comparing two sample groups, unpaired, two-tailed *t*-tests with Welch's correction (Welch's *t*-test) was used because standard deviations were not always equal for all groups. When comparing multiple sample groups, in order to compare the means or medians among all the samples and incorporate the standard deviation of each of the samples, Brown-Forsythe and Welch ANOVA followed by Dunnett's T3 multiple comparisons test was used. For experiments where % NE-like cells was calculated (as defined by the neurite length being 2x the length of body), in cases where no NE-like cells were recorded in all of the 3 biological replicates, one of the zero values was replaced with '1 x e-99' (virtually zero) in order for the statistical analysis to be valid. Statistical analysis for 4.6B (comparing average tumor volume) was performed for every time point using two-way ANOVA. Statistical analysis for 4.6C (comparing tumor recurrence) was performed for final time point using Fisher's exact test (one-tail). Statistical analysis for 4.6D (comparing tumor-specific survival) was performed using Kaplan-Meier survival analysis followed by both Log-rank (Mantel-Cox) and Gehan-Breslow-Wilcoxon tests. All relevant statistics are reported in the corresponding legends.

## 4.6 Supplemental figures

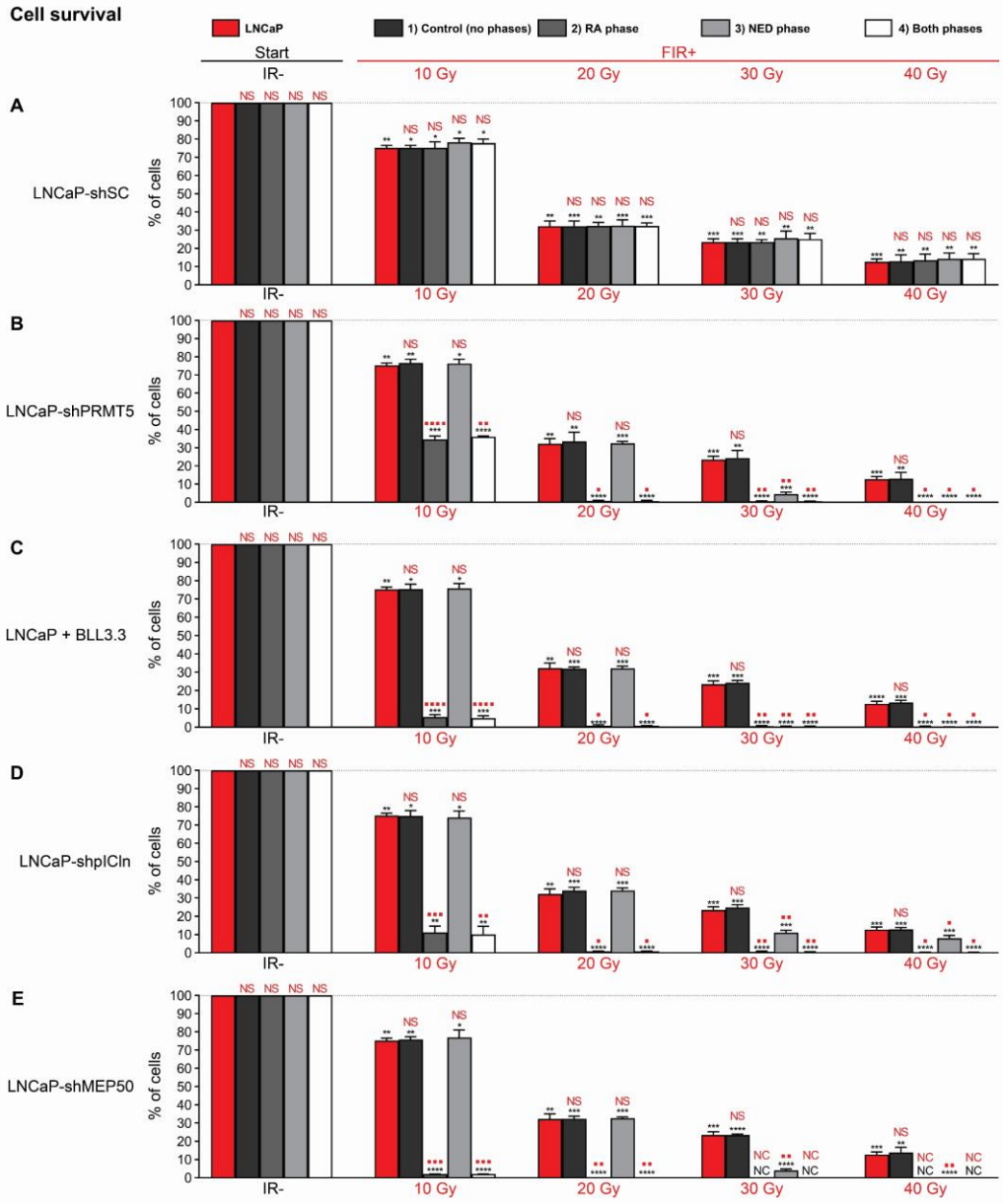


**Figure S4.1: PRMT5, pICln, and MEP50 are essential for survival upon fractionated ionizing radiation (FIR) (Related to figures 4.1 and 4.5)**

**(A)-(E)** Quantification of live cells from **Figure 4.1A**, **Figure 4.1D**, **Figure 4.5A**, and **Figure 4.5D** as described in **Figure 4.1B** (**A**: LNCaP-shSC, **B**: LNCaP-shPRMT5, **C**: LNCaP + BLL3.3, **D**: LNCaP-shpICln, and **F**: LNCaP-shMEP50).

All bars are the mean ± s.d. of 3 independent experiments. Statistical analysis comparing different doses for the same treatment group to the control ('IR-) was performed using Brown-Forsythe and Welch ANOVA followed by Dunnett's T3 multiple comparisons test and shown in black. Statistical analysis comparing different treatment groups for the same dose to the control ('LNCaP) was performed using Brown-Forsythe and Welch ANOVA followed by Dunnett's T3 multiple comparisons test and shown in red (* $P \leq 0.05$; ** $P \leq 0.01$, *** $P \leq 0.001$, **** $P \leq 0.0001$, NS $P > 0.05$).

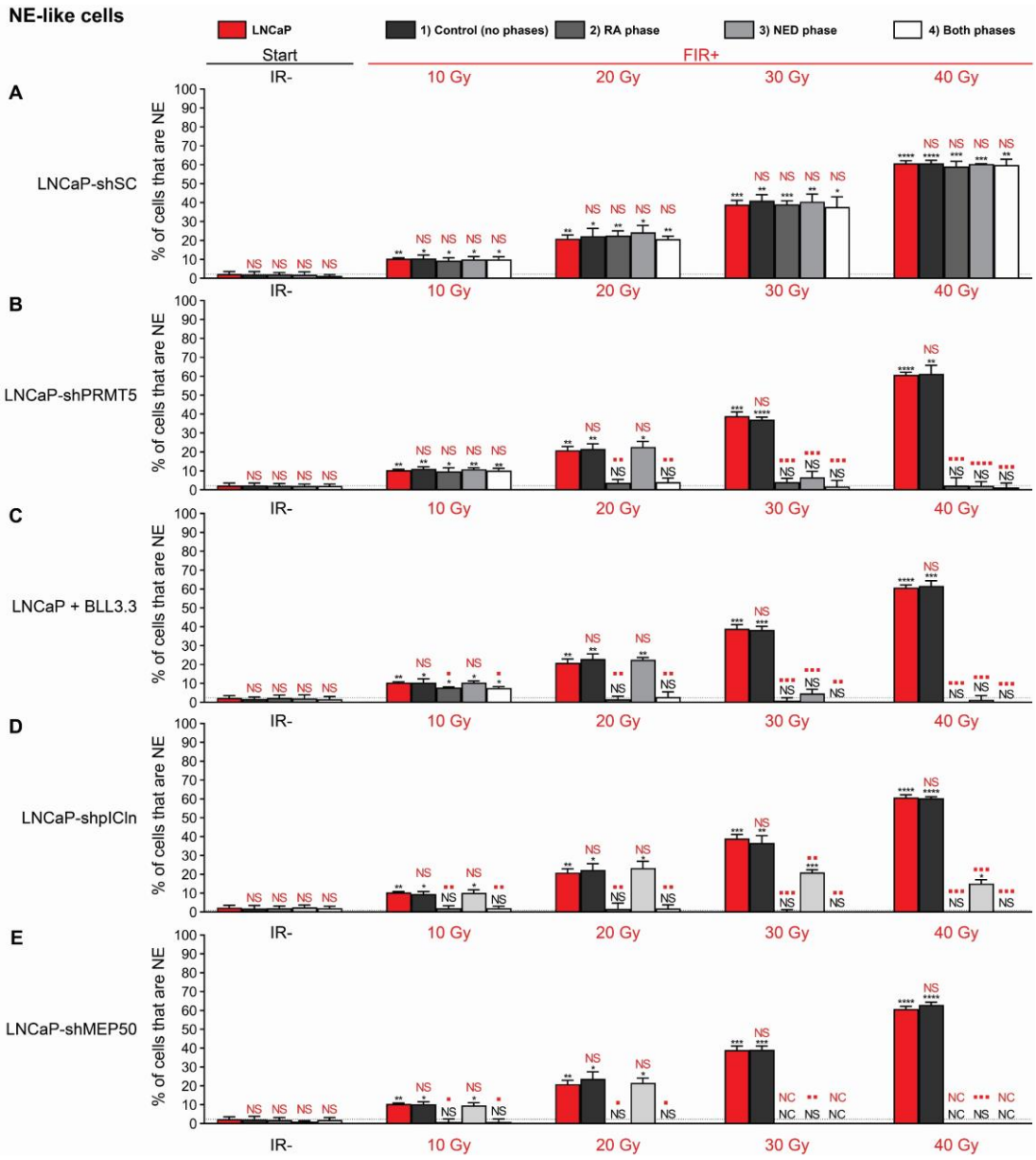


**Figure S4.2: PRMT5, pICln, and MEP50 are essential for initiation and maintenance of NED upon fractionated ionizing radiation (FIR) (Related to figures 4.1 and 4.5)**

**(A)-(E)** Quantification of NE-like cells from **Figure 4.1A**, **Figure 4.1D**, **Figure 4.5A**, and **Figure 4.5D** as described in **Figure 4.1C** (**A**: LNCaP-shSC, **B**: LNCaP-shPRMT5, **C**: LNCaP + BLL3.3, **D**: LNCaP-shpICln, and **F**: LNCaP-shMEP50). NE-like cells were defined as cells where the longest neurite projection was at least two times longer than the cell body diameter.

All bars are the mean ± s.d. of 3 independent experiments. Statistical analysis comparing different doses for the same treatment group to the control ('IR-) was performed using Brown-Forsythe and Welch ANOVA followed by Dunnett's T3 multiple comparisons test and shown in black. Statistical analysis comparing different treatment groups for the same dose to the control ('LNCaP) was performed using Brown-Forsythe and Welch ANOVA followed by Dunnett's T3 multiple comparisons test and shown in red (* $P \leq 0.05$; ** $P \leq 0.01$, *** $P \leq 0.001$, **** $P \leq 0.0001$, NS $P > 0.05$).

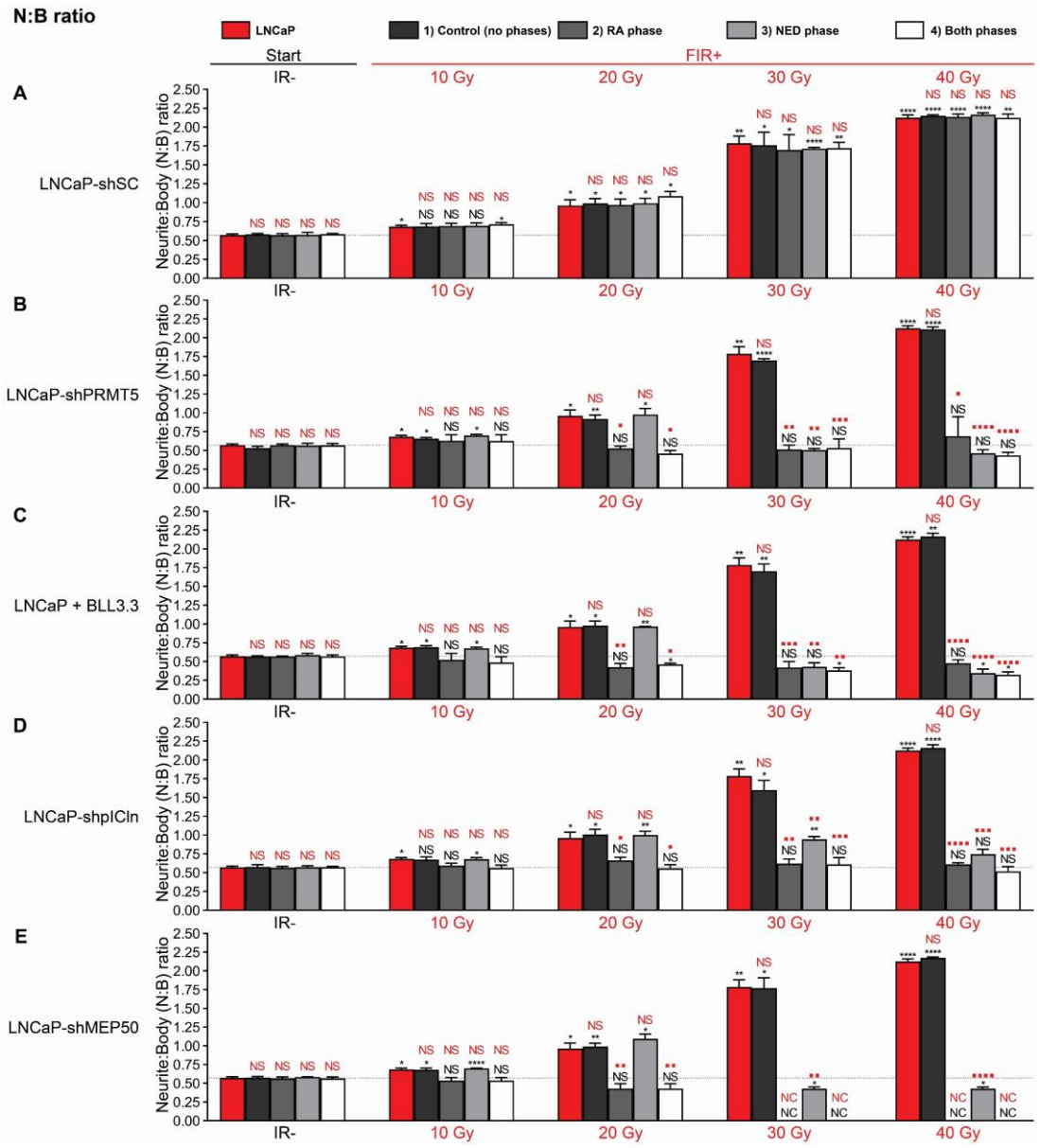


**Figure S4.3: PRMT5, pICln, and MEP50 are essential for initiation and maintenance of NED upon fractionated ionizing radiation (FIR) (Related to figures 4.1 and 4.5)**

**(A)-(E)** Quantification of the neurite:body (N:B) ratio in cells from **Figure 4.1A**, **Figure 4.1D**, **Figure 4.5A**, and **Figure 4.5D** (**A**: LNCaP-shSC, **B**: LNCaP-shPRMT5, **C**: LNCaP + BLL3.3, **D**: LNCaP-shpICln, and **F**: LNCaP-shMEP50). The longest neurite projection length and the cell body diameter length were quantified for each individual cell. The neurite length was divided by the body length to calculate the N:B ratio.

All bars are the mean ± s.d. of 3 independent experiments. Statistical analysis comparing different doses for the same treatment group to the control ('IR-) was performed using Brown-Forsythe and Welch ANOVA followed by Dunnett's T3 multiple comparisons test and shown in black. Statistical analysis comparing different treatment groups for the same dose to the control ('LNCaP) was performed using Brown-Forsythe and Welch ANOVA followed by Dunnett's T3 multiple comparisons test and shown in red (* $P \leq 0.05$; ** $P \leq 0.01$, *** $P \leq 0.001$, **** $P \leq 0.0001$, NS $P > 0.05$).

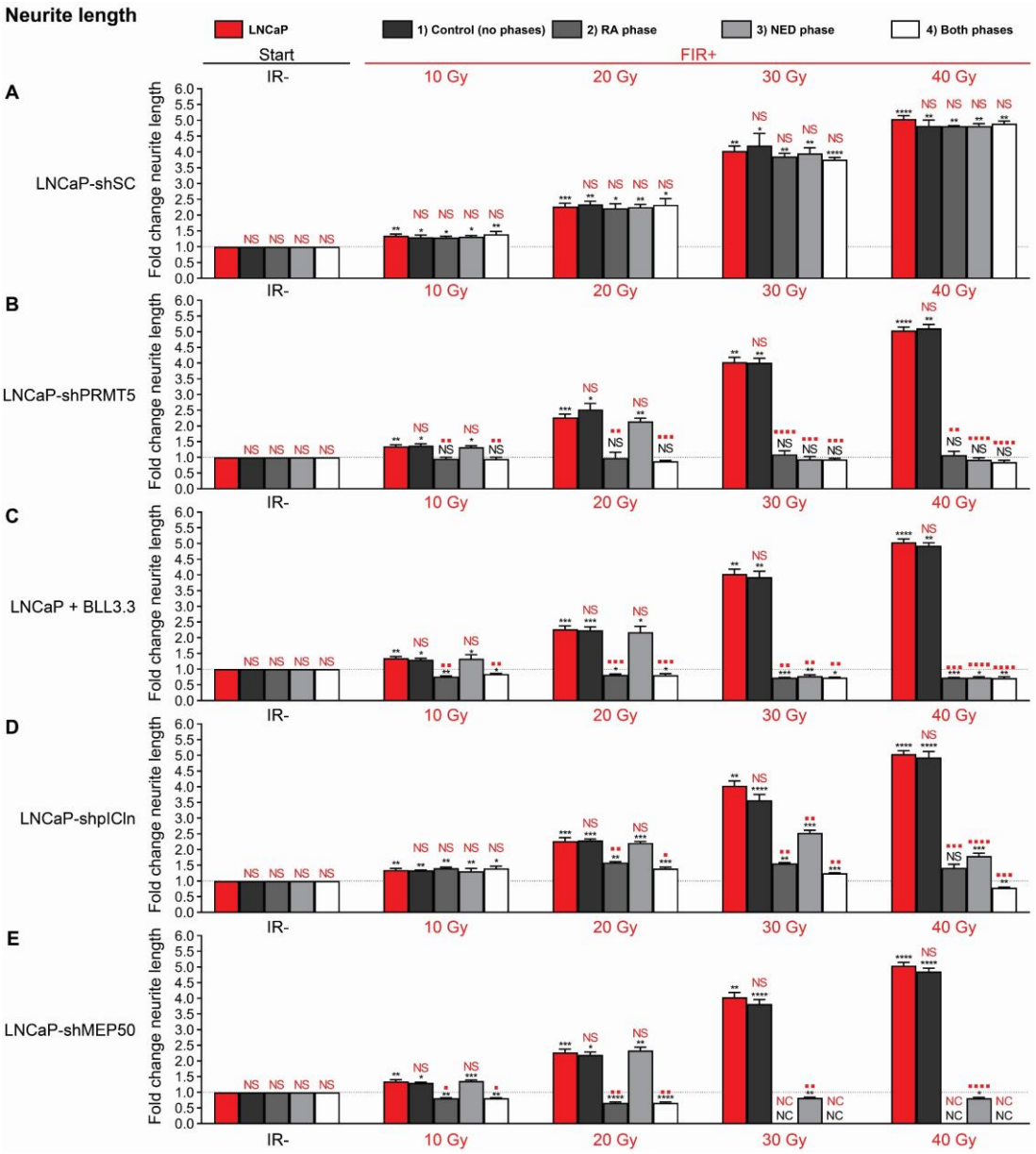


**Figure S4.4: PRMT5, pICln, and MEP50 are essential for neurite projection upon fractionated ionizing radiation (FIR) (Related to figures 4.1 and 4.5)**

**(A)-(E)** Quantification of neurite lengths in cells from **Figure 4.1A**, **Figure 4.1D**, **Figure 4.5A**, and **Figure 4.5D** (**A**: LNCaP-shSC, **B**: LNCaP-shPRMT5, **C**: LNCaP + BLL3.3, **D**: LNCaP-shpICln, and **F**: LNCaP-shMEP50). The longest neurite projection length was quantified for each individual cell.

All bars are the mean ± s.d. of 3 independent experiments. Statistical analysis comparing different doses for the same treatment group to the control ('IR-) was performed using Brown-Forsythe and Welch ANOVA followed by Dunnett's T3 multiple comparisons test and shown in black. Statistical analysis comparing different treatment groups for the same dose to the control ('LNCaP) was performed using Brown-Forsythe and Welch ANOVA followed by Dunnett's T3 multiple comparisons test and shown in red (* $P \leq 0.05$; ** $P \leq 0.01$, *** $P \leq 0.001$, **** $P \leq 0.0001$, NS $P > 0.05$).

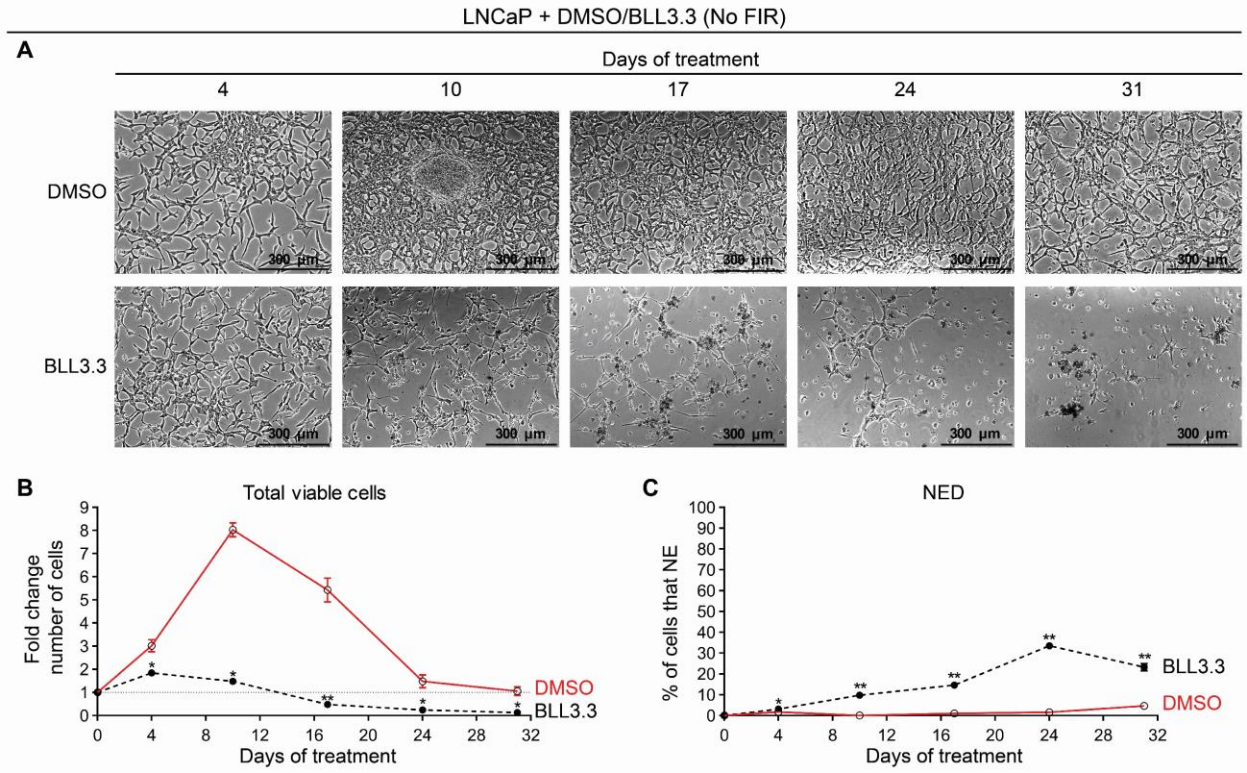


**Figure S4.5: Long-term targeting of PRMT5 alone can cause prostate cancer cell death (Related to figure 4.1)**

**(A)** Time-course of PRMT5-targeting treatment in LNCaP cells. Cells were treated with either BLL3.3 (10 µM) or DMSO as a control for the indicated number of days.
**(B)** Quantification of live cells from **A** as described in **Figure 4.1B**.
**(C)** Quantification of NE-like cells from **A** as described in **Figure 4.1C**.

Images in **A** are representative bright field images. Data points in **B** and **C** are the mean ± s.d. of 3 independent experiments. Statistical analysis for **B** and **C** comparing 'BLL3.3' to the control ('DMSO') was performed using Brown-Forsythe and Welch ANOVA followed by Dunnett's T3 multiple comparisons test (* $P \leq 0.05$; ** $P \leq 0.01$, *** $P \leq 0.001$, **** $P \leq 0.0001$, NS $P > 0.05$).

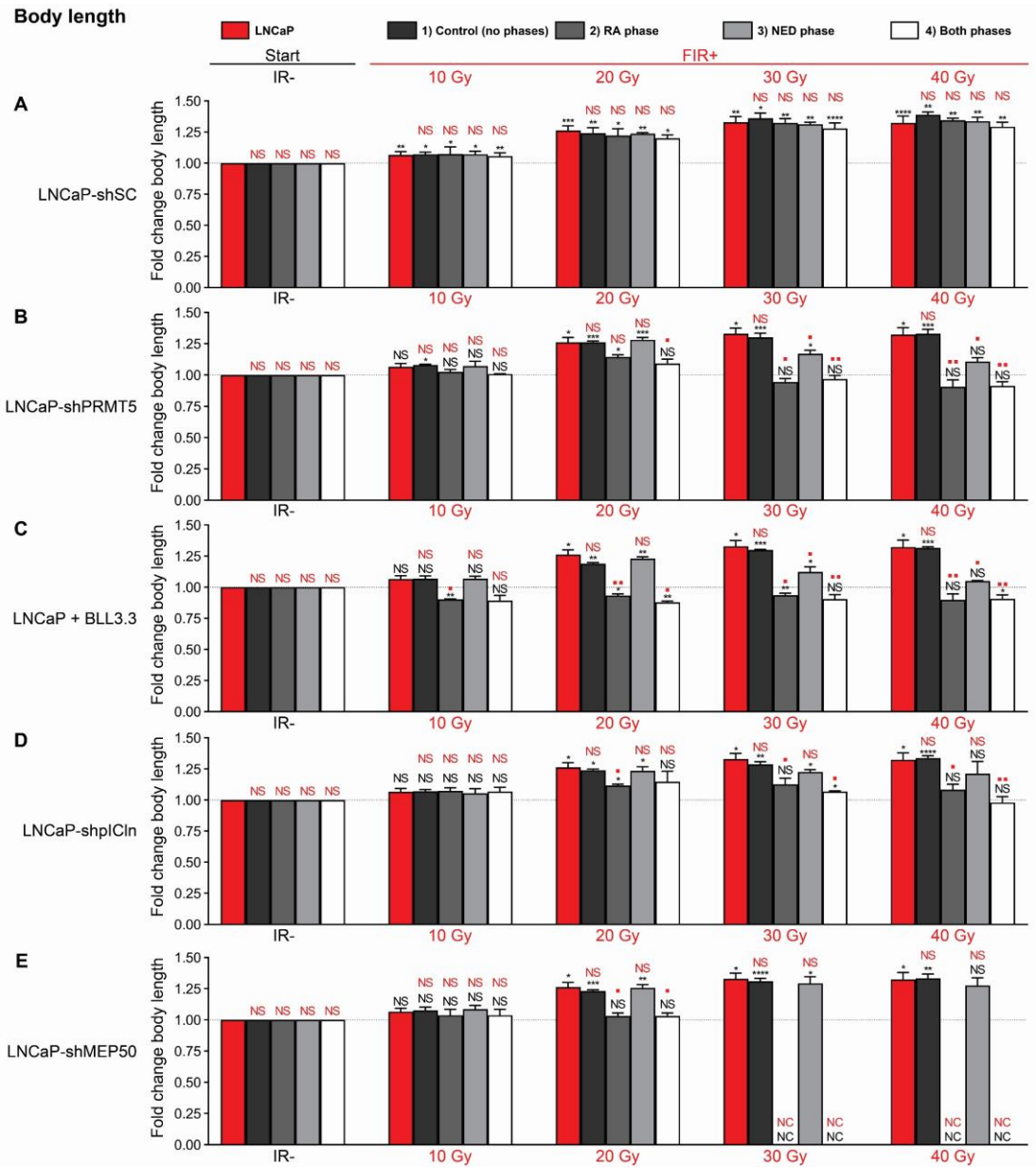


**Figure S4.6: PRMT5, pICln, and MEP50 are essential for increased cell body size upon fractionated ionizing radiation (FIR) (Related to figures 4.1 and 4.5)**

**(A)-(E)** Quantification of cell body length in cells from **Figure 4.1A**, **Figure 4.1D**, **Figure 4.5A**, and **Figure 4.5D** (**A**: LNCaP-shSC, **B**: LNCaP-shPRMT5, **C**: LNCaP + BLL3.3, **D**: LNCaP-shpICln, and **F**: LNCaP-shMEP50). The cell body diameter length was quantified for each individual cell.

All bars are the mean ± s.d. of 3 independent experiments. Statistical analysis comparing different doses for the same treatment group to the control ('IR-) was performed using Brown-Forsythe and Welch ANOVA followed by Dunnett's T3 multiple comparisons test and shown in black. Statistical analysis comparing different treatment groups for the same dose to the control ('LNCaP) was performed using Brown-Forsythe and Welch ANOVA followed by Dunnett's T3 multiple comparisons test and shown in red (* $P \leq 0.05$; ** $P \leq 0.01$, *** $P \leq 0.001$, **** $P \leq 0.0001$, NS $P > 0.05$).

# CHAPTER 5. FUTURE DIRECTIONS

## 5.1 Determine how protein arginine methyltransferase 5 (PRMT5) protein expression is upregulated upon ionizing radiation (IR)

In both chapter 3 and chapter 4, we determined that Protein arginine methyltransferase 5 (PRMT5) is upregulated at the protein level by ionizing radiation (IR) treatment. In response to a single dose of IR, PRMT5 is transiently upregulated on a timescale similar to the repair of IR-induced DNA double strand breaks (DSBs). In response to fractionated ionizing radiation (FIR), PRMT5 is dose-dependently upregulated and the elevated expression is maintained. However, it remains unknown how PRMT5 protein is upregulated by a single dose of IR or cumulative FIR. Protein expression is regulated at multiple levels including transcription, translation, and degradation. Because it appears that transcriptional activation plays a minor role, our future studies will focus on the translation and degradation of PRMT5 in response to IR and FIR.

### 5.1.1 *Does ionizing radiation (IR) or fractionated ionizing radiation (FIR) promote post-translational modification of protein arginine methyltransferase (PRMT5)?*

IR might promote upregulation of PRMT5 at the protein level through changes in protein stability or proteasomal degradation. PRMT5 may be post-translationally modified to increase its stability leading to elevation in protein expression. However, it is unknown if PRMT5 is post-translationally modified in response to IR or FIR.

Post-translational modifications (PTMs) play a particularly important role in the cellular response to DNA damage. Under normal conditions, the MRN complex is distributed evenly in the nucleus. Upon recognition of a DSB, MRN forms foci around the sites of damage and recruits ATM[306]. Accumulated MRN/ATM phosphorylate histone H2AX on serine S139 to form γ-H2AX foci within seconds of DNA damage. Activated ATM subsequently phosphorylates several downstream targets[306] which leads to various PTMs throughout the proteasome. It is possible DNA damage promotes upregulation of PRMT5 protein expression through PTMs.

For example, PRMT5 was recently shown to be phosphorylated by LKB1[327], a protein involved in the DDR in response to IR[328]. Phosphorylation of PRMT5 by LKB1 promotes the dissociation of PRMT5 with cofactors (at least MEP50, pICln, and RioK1) and inhibits PRMT5 methyltransferase activity[327]. Knockdown of LKB1 inhibits repair of IR-induced DSBs[328]

potentially due to inhibition of homologous recombination (HR). It is possible that PRMT5 is de-phosphorylated upon IR leading to association with cofactors and subsequent activation. IR induces ATM-mediated phosphorylation of LKB1[328], thus LKB1 may have different phosphorylation targets upon DNA damage and may no longer phosphorylate PRMT5.

PTMs are commonly assessed via immunoprecipitation followed by mass-spectrometry (IP-MS)[329,330]. Briefly, a specific protein is isolated using immunoprecipitation (IP), fragmented, and subjected to mass-spectrometry (MS) analysis to identify amino acid residues that are likely modified under the specified condition. Putative PTMs can be further characterized by the generation and use of PTM-specific antibodies. We may utilize these techniques to assess if PRMT5 is modulated by PTMs upon a single dose of IR or cumulative FIR.

### 5.1.2 *Does ionizing radiation (IR) or fractionated ionizing radiation (FIR) inhibit the interaction between protein arginine methyltransferase (PRMT5) and the E3 ubiquitin ligase CHIP to inhibit protein degradation?*

IR might promote upregulation of PRMT5 protein by inhibiting proteasomal degradation. We previously reported that PRMT5 protein expression is regulated by the E3 ubiquitin ligase CHIP which mediates ubiquitination and proteasomal degradation[286]. A recent study also implicated CHIP in the DDR via ubiquitination and degradation of p21[309], which is consistent with a previous report where CHIP regulates $G_1$ checkpoint[310]. It is possible that DNA damage blocks the interaction between PRMT5 and CHIP. Co-immunoprecipitation (CoIP) may be used to assess changes the interaction between PRMT5 and CHIP upon IR and FIR. Changes in the PRMT5:CHIP interaction would likely also result in changes in PRMT5 ubiquitination levels. Downregulation of CHIP during FIR-induced NED may also facilitate PRMT5 protein upregulation and changes in CHIP mRNA and protein can be assessed via qPCR and western blotting. Overall, inhibition of proteasomal degradation may contribute to the induction of PRMT5 protein expression.

### 5.1.3 *Does ionizing radiation (IR) promote translation of protein arginine methyltransferase (PRMT5) to induce protein expression?*

Because PRMT5 protein is quickly upregulated (within 5 min) in response to a single dose of IR, it is likely that the pre-existing pool of mRNA is quickly translated into protein to induce

PRMT5 protein expression. Upon DNA damage, global translation is repressed while translation of mRNAs encoding DDR proteins is selectively activated[331,332]. IR inhibits proteasomal degradation of 4E-BP1 which sequesters eIF4E, thus inhibiting global translation[333]. One study suggested that IR preferentially activates the eIF2α/ATF4 translation pathway[334]. However, how translation of select genes is activated by IR remains largely unknown.

Translational activation of genes can be assessed by analyzing protein expression when the translation inhibitor cycloheximide[286,335,336] is applied so that new mRNA is not produced. The proteasome inhibitor MG132[286] is commonly co-applied to negate potential effects of protein degradation. For example, we may assess PRMT5 protein expression at various time points post-IR while cycloheximide and MG132 are applied. If PRMT5 protein upregulation is dependent on translation, we would expect to see a decrease upon cycloheximide treatment. Because cycloheximide treatment induces cell death, it would be difficult to assess translation directly during FIR.

The rate of translation can be affected by miroRNAs (miRNAs) and the levels of miRNAs change upon DNA damage[300]. PRMT5 is targeted by several miRNAs and a downregulation of PRMT5-targeting miRNAs could allow for PRMT5 translation. For example, miR-106b, a potential PRMT5-targeting miRNA[301], is downregulated in response to IR[301]. Genome-wide miRNA expression analysis upon a single dose of IR or cumulative FIR may provide an answer to whether PRMT5-targeting miRNAs are downregulated upon radiation to facilitate elevated PRMT5 protein levels.

### 5.2 Determine how protein arginine methyltransferase 5 (PRMT5) activity is regulated by cofactors, particularly pICln and MEP50

In chapter 2 and chapter 3, we determined that PRMT5 cooperates with pICln, independently of its canonical cofactor MEP50, to function as a master epigenetic activator of DDR genes. Our report was the first to demonstrate that PRMT5 can epigenetically regulate gene expression without MEP50. There is a long-standing view in the field that the cofactor MEP50 is required for PRMT5 methyltransferase activity and epigenetic function[110,111,140,141]. Biochemical studies using *in vitro* methylation assays have also provided evidence that purified PRMT5:MEP50 complex can catalyze dimethylation of various histone substrates including H4R3[140,143], while titration of pICln decreased H3 and H4 methylation by PRMT5[145]. However, our work demonstrates that

PRMT5 utilizes pICln and not MEP50 for the transcriptional activation of DDR genes via H4R3me2s[1]. Our future studies will focus on analyzing the PRMT5:pICln complex to explain how pICln can enhance PRMT5 activity.

### 5.2.1 *Characterize the structure of the PRMT5:pICln and PRMT5:MEP50:pICln complexes*

PRMT5 can exist as a homodimer or homotetramer in solution. With MEP50, PRMT5 forms a hetero-octameric complex ($PRMT5_4$:$MEP50_4$). The crystal structure of this PRMT5:MEP50 complex was solved in 2012[142]. The structure of the PRMT5:pICln complex has yet to be solved. Although previous reports suggest a complex involving PRMT5, MEP50, and pICln might exist, it will be interesting to see if a structure can be solved for a PRMT5:MEP50:pICln complex. Solving the structure of these complexes may suggest how PRMT5 epigenetic activity is modulated by selective interaction with MEP50 and/or pICln. Additionally, comparing the interaction surfaces may suggest biochemical mechanisms for how IR promotes the PRMT5:pICln interaction and demotes the PRMT5:MEP50 interaction.

### 5.2.2 *Assess the methyltransferase activity of the PRMT5:pICln and PRMT5:MEP50:pICln complexes, particularly towards histone targets*

Several studies have assessed the methyltransferase activity of PRMT5 along with cofactors using *in vitro* methylation assays. Results from these experiments have provided the basis for the assumption that PRMT5 requires MEP50 for methyltransferase activity. Our studies suggest that PRMT5 can activate transcription without MEP50 present. Previous studies that performed *in vitro* assays using proteins from a bacterial expression system might not recapitulate the biochemical and cellular conditions required for histone methylation *in vivo*. To assess the methyltransferase activity of various PRMT5 complexes, it may be more appropriate to utilize recombinant proteins from sf9 insect cells to allow for similar protein processing as mammalian cells or in-tact nucleosomes to recreate the biological context as much as possible. The epigenetic regulation of genes is complex and requires large multi-subunit complexes and *in vitro* methylation assays might not represent the mechanism *in vivo*. Therefore, experiments that knock-out MEP50 in live cells will confirm if PRMT5 has some activities independently of MEP50.

## 5.3 Further clarify the mechanisms for how protein arginine methyltransferase 5 (PRMT5) functions as an epigenetic activator of DNA double-strand break (DSB) repair genes

In chapter 2, we determined that protein arginine methyltransferase 5 (PRMT5) functions as a master epigenetic activator of DNA double-strand break (DSB) repair genes and in chapter 3, we determined that this is dependent on selective cooperation with pICln. In 3.3.6 we detail a model for this mechanism: Under normal conditions, a complex involving PRMT5:pICln maintains basal expression of DDR genes. Upon DNA damage, PRMT5 protein is upregulated and pICln nuclear localization increases which leads to an increase in the PRMT5:pICln interaction in the nucleus. The interaction between PRMT5 and MEP50 is also decreased upon DNA damage which may facilitate the increase in binding of pICln to PRMT5. The PRMT5:pICln complex is then recruited to the promoters of genes involved in the DDR where it epigenetically activates expression of target genes via symmetric dimethylation of H4R3 (H4R3me2s). PRMT5:pICln target genes are then upregulated at the mRNA and protein level. With elevated expression of DDR proteins, the cell is able to repair the DSBs. Once DSBs are repaired, PRMT5 expression as well as the expression of DDR target genes return to basal levels.

Although we demonstrate that PRMT5 binding and subsequent H4R3me2s likely contributes to activation of DDR genes, previous reports demonstrate that PRMT5-catalyzed histone methylation can be involved in both epigenetic activation or repression[110]. Therefore, PRMT5-catalyzed methylation of histones is not sufficient to confer activation or repression. We previously demonstrated that PRMT5 recruits BRG1, an activator of gene expression, to the AR promoter to facilitate epigenetic activation[114]. Thus, PRMT5 may modulate expression of genes by recruitment of chromatin remodelers to increase or decrease chromatin accessibility.

Many questions still remain that if answered could help explain the mechanism for how PRMT5 functions as an epigenetic activator of DDR genes:

- Without a DNA binding domain, how is PRMT5 specifically targeted to the promotors of DDR genes to regulate basal expression under normal conditions?
- What promotes increased binding upon DNA damage?
- What facilitates the interaction between PRMT5 and specific epigenetic cofactors?
- How does PRMT5 function as either an activator or repressor of gene expression?
- What other proteins are involved in the different PRMT5-assoicated epigenetic complexes?

Structural studies that identify members of the PRMT5 complex at the promoter of target genes involved in DDR may help explain how PRMT5:pICln cooperates to epigenetically activate transcription of DDR genes. Using the novel technique engineered DNA-binding molecule-mediated chromatin immunoprecipitation (enChIP)[337,338], we can isolate and characterize proteins that are at specific sites on the genome such as PRMT5 target genes. The enChIP system utilizes the Cas9/gRNA complex, which is extremely specific in DNA binding, to immunoprecipitate certain regions of DNA. A catalytically inactive form of Cas9 (dCas9) is co-expressed with a guide RNA (gRNA) which targets the dCas9 to a particular DNA sequence. Chromatin is extracted from fixed cells and incubated with antibody to pull-down the dCas9 (same method as normal ChIP). Because fixation crosslinks proteins to DNA, the proteins are pulled-down as well. Pull-down samples are reverse crosslinked and can be used for subsequent analysis. enChIP has already been coupled with mass spectrometry (MS) to identify proteins at a particular genomic site. It is possible enChIP can be coupled with use cryo-electron microscopy (cryo-EM) to solve the structure of complexes on DNA. These studies may identify which proteins are present in PRMT5-associated epigenetic complexes as well as identify transcription factors that recruit PRMT5 to specific genomic sites. Additionally, comparison of activation and repressive complexes may suggest mechanisms for how PRMT5 modulates transcription in either direction.

Genome-wide analyses of changes in chromatin occupancy as well as chromatin structure upon IR may also help explain how PRMT5:pICln cooperates to epigenetically activate transcription of DDR genes. Assay for Transposase-Accessible Chromatin (ATAC)-seq is a powerful tool to assess changes in chromatin accessibility. Thus, performing ATAC-seq under various conditions in combination with the analysis of genome wide binding of PRMT5, pICln, MEP50, and H4R3me2s using ChIP-seq may provide evidence for how PRMT5 and its cofactors epigenetically activate DDR genes selectively. Subsequent transcription factor motif analysis of the ChIP-seq data may elucidate putative transcription factors that facilitate the selective recruitment of the PRMT5 epigenetic activation complex to the cohort of DDR genes. Path-LZerD[339] analysis may be used to predict the assembly order of different PRMT5-associated epigenetic complexes. Altogether, these studies should help identify and characterize members of the different PRMT5-associated epigenetic complexes and determine how PRMT5 selectively activates transcription of DDR genes upon IR treatment.

## 5.4 Determine how protein arginine methyltransferase 5 (PRMT5) regulates fractionated ionizing radiation (FIR)-induced neuroendocrine differentiation (NED)

In chapter 4, we determined that PRMT5 is essential to both initiate and maintain FIR-induced NED. Targeting PRMT5 prevented neurite outgrowth and caused shrinkage of pre-existing neurites indicating that PRMT5 is critical for neurite formation/axonogensis and maintenance of neurite projections. However, it remains unknown how PRMT5 mediates these changes in neurites or if PRMT5 regulates other pathways essential for FIR-induced NED.

### 5.4.1 *Determine if protein arginine methyltransferase 5 (PRMT5) modulates CREB to promote FIR-induced NED*

cAMP signaling and activation of CREB is essential for NED in general[61,84,85] which we confirmed is also essential for FIR-induced NED. FIR promotes nuclear localization of activated CREB where it can function as a transcriptional regulator to promote differentiation[85]. Because both CREB phosphorylation/activation and PRMT5 protein expression gradually increases throughout FIR-induced NED, it is possible that PRMT5 may promote FIR-induced NED through regulating the activity of CREB. Indeed, it has been reported that PRMT5 can promote CREB phosphorylation in response to metabolic stress[320]. Therefore, we may assess if PRMT5 regulates FIR-induced phosphorylation and activation of CREB to regulate NED. For example. PRMT5 may interact with and/or methylate CREB to promote phosphorylation and activation. Alternatively, PRMT5 may participate in the CREB-associated transcription factor complex to promote expression of NE-associated genes. Future studies that assess the potential interplay between PRMT5 and CREB may provide a mechanism for how PRMT5 regulates FIR-induced NED.

### 5.4.2 *Determine if protein arginine methyltransferase 5 (PRMT5) epigenetically regulates genes to promote FIR-induced NED*

PRMT5 is an epigenetic regulator that modulates gene expression on a global genomic scale. Given that mRNA expression changes significantly during FIR-induced NED, it is likely that PRMT5 mediates at least some of these gene expression changes. Future studies may identify and characterize putative PRMT5 target genes involved in NED. For example, PRMT5 may activate some of the genes in the 12-gene signature of NE prostate cancer[96].

Although ChIP-seq is commonly used to assess genome occupancy and identify putative target genes, because ChIP-seq requires a large number of cells and FIR kills the majority of cells (~13% of cells survive a cumulative dose of 40 Gy FIR) it may be more appropriate to utilize other assays that require less cells. For example, we may utilize the novel technique Cleavage Under Targets and Release Using Nuclease (Cut&Run) [340]. While ChIP uses DNA fragmentation followed by IP pull-down of the protein of interest cross-linked to DNA to isolate the chromatin binding locations, Cut&Run uses targeted cleavage of DNA surrounding the protein of interest to isolate the chromatin binding locations. This allows Cut&Run to be significantly more robust and thus requires less cells (only 100,000 cells). Thus, Cut&Run may help identify putative PRMT5 target genes involved in initiation or maintenance of NED.

## 5.5 Further validate protein arginine methyltransferase 5 (PRMT5) as a therapeutic target to enhance radiation therapy (RT) for prostate cancer treatment

Throughout this dissertation, we have provided strong evidence for PRMT5 as a therapeutic target for cancer treatment. PRMT5 plays an essential role in the cellular response to both a single dose of IR and cumulative FIR. Further, targeting PRMT5 sensitized prostate cancer xenograft tumors in mice to RT, significantly reduced and delayed tumor recurrence, and prolonged overall survival. Incredibly, while 100% of control mice died, targeting PRMT5 effectively cured ~85% of mice from their xenograft tumor. Although we provide strong evidence, future research will further validate PRMT5 as a therapeutic target to enhance RT for prostate cancer treatment.

### 5.5.1 *Determine if protein arginine methyltransferase 5 (PRMT5) prevents FIR-induced NED in prostate xenograft tumors in mice*

In figure 4.6, we determined that targeting PRMT5 sensitizes prostate cancer xenograft tumors in mice to FIR, prevents tumor recurrence, and increases survival. To extend our findings we plan to assess if targeting PRMT5 also prevents FIR-induced NED. We have previously assessed FIR-induced NED in LNCaP xenograft tumors in nude mice[49] and will use similar techniques on samples from our experiment in figure 4.6. As part of this mice experiment, we collected several blood samples as well as obtained slides of fixed tumors. We plan to analyze serum CgA levels as a biomarker of NED and expect to see that the shPRMT5 group has lower

CgA levels than the shSC group (control). We also plan to perform immunohistochemistry (IHC) analysis of tumors to assess NE morphology, expression of NE-associated proteins, and expression of PRMT5 and PRMT5 cofactors. Results to these studies can verify if targeting PRMT5 prevents FIR-induced NED of prostate cancer xenograft tumors in mice.

### 5.5.2 *Determine if orally bioavailable protein arginine methyltransferase 5 (PRMT5) inhibitors sensitize prostate cancer xenograft tumors to radiation therapy (RT) in mice*

In figure 4.6, described above, we used PRMT5 knockdown xenograft tumors to assess the effect of targeting PRMT5 knockdown during RT. To further validate PRMT5 as a therapeutic target, we plan to assess an orally bioavailable inhibitor such as GSK3235025[341] or JNJ-64619178 which is in human clinical trials. First, we would perform similar experiments as in figure 4.1 to confirm that the inhibitor works *in vitro*. Then we can perform the same mice experiment as in figure 4.6. and include analysis of FIR-induced NED as described above in 5.5.1. Results to these studies can verify if a clinically applicable, orally bioavailable PRMT5 inhibitor sensitizes prostate cancer xenograft tumors in mice and prevents FIR-induced NED. This would provide very convincing evidence that targeting PRMT5 during RT should be assessed clinically.

### 5.5.3 *Validate protein arginine methyltransferase 5 (PRMT5) as a therapeutic target to enhance radiation therapy (RT) in other prostate cancer models*

We also plan to repeat similar experiments in additional prostate cancer models. We have previously determined that DU145 and PC3 (AR-negative prostate cancer) cell lines undergo FIR-induced NED[49]. Therefore, we may perform similar experiments as described in figure 4.1, figure 4.6, and 5.5.1 in other prostate cancer models including DU145 and PC3. We have already developed stable cell lines with Dox-inducible expression of PRMT5-targeting shRNA for DU145 and PC3 cells. Results from this study could suggest that targeting PRMT5 during RT may be effective to treat a broad range of prostate cancer tumors clinically.

### 5.5.4 *Characterize clinical recurrent prostate cancer following radiation therapy (RT) including protein arginine methyltransferase 5 (PRMT5)-associated pathways*

Clinical evidence demonstrating that PRMT5 plays a role in FIR-induced NED in prostate cancer tumors may further validate PRMT5 as a therapeutic target to enhance RT. To support our

findings, we may study prostate tumor biopsies and blood samples pre- and post-RT. As FIR can induce NED, we would expect tumors to recur at the same location indicating that *de novo* tumors from other areas of the prostate likely do not explain tumor recurrence. As NE prostate cancer is highly aggressive, we would also expect the recurrent tumor to be more aggressive than the pre-RT tumor. IHC analysis of these prostate tumor biopsies may be used to assess differences in protein expression. Given that we demonstrate that PRMT5 protein is upregulated in NE-like prostate cancer cells, we also expect PRMT5 protein to be higher in post-RT recurrent tumors as opposed to pre-RT tumors. Additionally, the level of PRMT5 protein expression likely correlates positively with other identifiers of NED. For example, as CgA levels in the blood are elevated in prostate cancer patients treated with RT[49,97], it is likely PRMT5 protein expression positively correlates with blood CgA levels. These studies would further suggest PRMT5 plays a role in resistance to clinical RT and promote clinical trials to assess PRMT5 inhibitors as a cotreatment with RT for the treatment of prostate cancer.

# APPENDIX A. GENE ONTOLOGY (GO) TERMS AND ASSOCIATED DIFFERENTIALLY EXPRESSED GENES (DEGS) FROM FUNCTIONAL ENRICHMENT ANALYSIS ON ALTERNATIVE SPLICING EVENTS UPON PRMT5 KNOCKDOWN

Two studies aimed to identify PRMT5 splicing targets and performed functional enrichment analysis on alternative splicing events upon PRMT5 knockdown[157,158]. Below is a list of gene ontology (GO) terms and associated differentially expressed genes (DEGs) demonstrating pathways that PRMT regulates by the splicing of genes.

| GO term | DEGs |
|---|---|
| Base excision repair (BER) | MPG[158], MUTYH[158], NEIL1[158], NEIL3[158], PARP2[157], POLD1[157], POLD2[157], PNKP[158], RAD1[158], RAD9A[157,158], RECQL5[157,158], STUB1[158] |
| DNA damage sensing and signaling | ATM[157,158], CHEK1[158], CHEK2[158], HSF1[158], RAD50[157], SMG1[158] |
| Helicase, nuclease, and polymerase function | APEX[158], ATRX[158], CHD1L[158], DCLRE1C[158], DDX11[158], EME1[158], EME2[158], HELQ[158], POLI[158], POLD3[158], POLD4[158], RECQL[158], RECQL4[158], REV1[158], RFC3[158], RTEL1[158], SLX1B[158], UPF1[158] |
| Homologous Recombination (HR) | AP5Z1[158], ATRX[158], MMS22L[158], MUS81[158], PARP2[157], PDS5B[158], RAD9A[157,158], RAD21[157], RAD52[157,158], RAD54L[158], SLX1B[158], TONSL[158], XAB2[158], XRCC3[157], ZFYVE26[158] |
| Interstrand cross-link repair | FANCA[157,158], FANCG[158], FANCI[157], RECQL5[157,158] |
| Mismatch repair | PMS2[158], POLD1[157], POLD2[157], RAD9A[157,158] |
| Non-homologous end joining (NHEJ) | DCLRE1C[158], PNKP[158] |
| Nucleotide excision repair (NER) | ERCC3[158], ERCC4[158], ERCC5[157], POLD1[157], POLD2[157], UVSSA[158], XPA[158], XPC[157] |

# APPENDIX B. CLINICAL TRIALS ASSESSING PRMT5 INHIBITORS AS OF JUNE 2020

Below is a list of clinical trials assessing PRMT5 inhibitors for cancer treatment as of June 2020. Links to the NCI thesaurus page are provided which includes information such as drug target, mechanism of action, or alternative names. Links to the ClinicalTirals.gov page are provided which gives information about the specific clinical trials.

| Drug | Clinical trial | Stage | Cancers tested |
|---|---|---|---|
| GSK3326595 | NCT02783300<br>NCT03614728 | Phase 1<br>Phase 1 | Solid tumors and Non-Hodgkin's Lymphoma (NHL)<br>Myelodysplastic Syndrome (MDS) and Acute Myeloid Leukemia (AML) |
| JNJ-64619178 | NCT03573310 | Phase 1 | Advanced solid tumors, NHL, and lower risk MDS |
| PF-06939999 | NCT03854227 | Phase 1 | Advanced or Metastatic solid tumors |
| PRT543 | NCT03886831 | Phase 1 | Advanced solid tumors and Hematologic Malignancies |
| PRT811 | NCT04089449 | Phase 1 | Advanced solid tumors and Gliomas |

# APPENDIX C. CELL LINES

| Cell line | Description |
|---|---|
| DU145 | Androgen-insensitive human prostate cancer (unsure of cell type) |
| DU145-shRNA pool | Lentiviral stably infected pools with Dox-inducible expression of PRMT5-targeting shRNA (referring to #1577[114]) |
| DU145-shSC | Stable cell lines with Dox-inducible expression of scramble control-targeting shRNA (shSC) |
| HEK293T | Human embryonic kidney cells that express a mutant version of the SV40 large T antigen |
| LNCaP | AR-positive and androgen-sensitive human prostate adenocarcinoma |
| LNCaP-shMEP50 | Stable cell lines with Dox-inducible expression of MEP50-targeting shRNA or (shpICln) |
| LNCaP-shpICln | Stable cell lines with Dox-inducible expression of pICln-targeting shRNA (shpICln) |
| LNCaP-shPRMT5 | Stable cell lines with Dox-inducible expression of PRMT5-targeting shRNA (referring to #1832[114]) |
| LNCaP-shPRMT5 #2 | Stable cell lines with Dox-inducible expression of PRMT5-targeting shRNA (shPRMT5 #2, referring to #1577[114]) |
| LNCaP-shPRMT5 pool | Lentiviral stably infected pool with Dox-inducible expression of PRMT5-targeting shRNA (referring to #1577[114]) |
| LNCaP-shSC | Stable cell lines with Dox-inducible expression of scramble control-targeting shRNA (shSC) |
| MCF7 | Luminal breast adenocarcinoma |
| PC3 | Androgen-insensitive human prostate cancer (could be adenocarcinoma or small cell neuroendocrine carcinoma) |
| PC3-shPRMT5 pool | Lentiviral stably infected pools with Dox-inducible expression of PRMT5-targeting shRNA (referring to #1577[114]) |
| PC3-shSC | Stable cell lines with Dox-inducible expression of scramble control-targeting shRNA (shSC) |
| U87MG | Glioblastoma astrocytoma |

# APPENDIX D. LIST OF PRIMERS

## qRT-PCR primers

| Gene | Forward primer | Reverse primer | Amplicon size (bp) |
|---|---|---|---|
| AR | 5'-GTGGAAGCTGCAAGGTCTTC-3' | 5'-CGAAGACGACAAGATGGACA-3' | 124 |
| ASCL1 | 5'-CAGGAGCTTCTCGACTTCACC-3' | 5'-CCTCCCAACGCCACTGACA-3' | 133 |
| BRCA1 | 5'-GTTGTTATGAAAACAGATGCTGAGTTTGTG-3' | 5'-CTGGGTCACCCAGAAATAGCTAAC-3' | 105 |
| BRCA2 | 5'-CCAAAGTTTGTGAAGGGTCGTCAG-3' | 5'-GCTTCTTCATTTCTGACTATGAGCACAG-3' | 146 |
| BRN2 | 5'-ACACTGACGATCTCCACGCAGTA-3' | 5'-GAGGGTGTGGGACCCTAAATATGAC-3' | 85 |
| CCNB2 | 5'-CAAGGAAAATGGAACTTAAAGCAGCAG-3' | 5'-GCATACTTATTCTTGATGGCGATGAATTTAG-3' | 143 |
| CDC20 | 5'-CTGAGGTGCAGCTATGGGATG-3' | 5'-CAGAACGTGAACCACTGGACAG-3' | 120 |
| CDC25C | 5'-CCTAAGCATTTTGTCTGGAGGAACC-3' | 5'-GAAGAATCCAGGTGACCAGTTTCATC-3' | 129 |
| CDK1 | 5'-CGTCATCCAAATATAGTCAGTCTTCAGG-3' | 5'-GGTATAAATAACTCTTAACAAGTGAAGAATCCATG-3' | 157 |
| CETN2 | 5'-CATAGATGTTAAAGAACTGAAGGTGGCAATG-3' | 5'-GTATCTTTCTCAGACATTTTCTGGGTCATC-3' | 165 |
| CgA | 5'-GCGGTGGAAGAGCCATCAT-3' | 5'-TCTGTGGCTTCACCACTTTTCTC-3' | 83 |
| DNAPKcs | 5'-GAACCTTTCATCAAACGAAGCAATATCC-3' | 5'-CTGAGGACGTGACTGTCAGAAG-3' | 116 |
| GAPDH | 5'-CTGACTTCAACAGCGACACC-3' | 5'-CCCTGTTGCTGTAGCCAAAT-3' | 120 |
| GMNN | 5'-CAAAGAGAATATAAAGAATAGTTCTGTCCCAAGAAG-3' | 5'-CCTGCGGACAGCTCATTTTCTC-3' | 105 |
| INSM1 | 5'-ATTATGGCTTGTGAACTGCT-3' | 5'-GCATCTTCGGAACACTCCC-3' | 158 |
| IVL | 5'-CCTCAGCCTTACTGTGAG-3' | 5'-GGGAGGCAGTGGAGTTGG-3' | 167 |
| Ku80 | 5'- CCAAGACAACCATGAAGATGGACC-3' | 5'- CACACTTCCAACAGAGGTGACAC-3' | 115 |
| MDC1 | 5'-GAGGCATCAGAAAGGCCTC-3' | 5'-CTGATCGCCCCTGGAAAC-3' | 94 |
| MEP50 | 5'-GCCTCTCCTCACAAGGACTC-3' | 5'-CCAGCGAGGTAGGAAGGTAG-3' | 133 |
| NCAM1 | 5'-CCATCTATAACGCCAACATCGAC-3' | 5'-CGCATTCTTGAACATGAGCTT-3' | 125 |
| NEUROD1 | 5'-TGCGAGATCCCCATAGACA-3' | 5'-TTTGCAGCAGTAGTACCCAA-3' | 195 |
| NHEJ1 | 5'-CAAGGCGCTGGAGATCCTC-3' | 5'-CTGAAGTACCCGTGGACTCTTTC-3' | 139 |
| NSE | 5'-AGCTGCCCCTGCCTTAC-3' | 5'-GAGACAAACAGCGTTACTTAG-3' | 218 |
| pICln | 5'-TCAGCGTTGGAGGCAATGTT-3' | 5'-CCCTGTCCTTGTTCATGTGCTTC-3' | 128 |
| PLK1 | 5'-GTCCATTGGGTGTATCATGTATACCTTG-3' | 5'-GGTTGATGTGCTTGGGAATACTGTATTC-3' | 122 |
| POLD3 | 5'-CAGGCCAAACAGATGCTGTATG-3' | 5'-CAACCTTGTGGCAGGAATGTC-3' | 127 |
| PRMT5 | 5'-CAGAGAAGGAGTTCTGCTCCTAC-3' | 5'-ATGGCCTGCTGGTACTGAGAGT-3′ | 205 |
| RAD51 | 5'-GTTGGGACTACAGGTGGAATTGAG-3' | 5'-CAATGGGAAGCTGGCAGGTG-3' | 115 |
| RAD51AP1 | 5'-CTCTCAAGATAAAAGCATTGAAAAACATGG-3' | 5'-CACAGTAATCTTATCCAAATCTAAATAATCACTG-3' | 121 |
| RAD51D | 5'-GTGGCCCAGCAGGTGAC-3' | 5'-CAAGGCCAAGCCTTCCCTC-3' | 114 |
| REST | 5'-GACCAAACCCTTTCGCTGT-3' | 5'-TTGCCTGCTTCTCTGCACT-3' | 125 |
| SOX2 | 5'-TAAGCGGCTGCGAGCG-3' | 5'-CCCGCTCGCCATGCTATT-3' | 145 |
| SYP | 5'-CTAGTTAGCTCATCGGCAT-3' | 5'-TCTCCTTAAACACGAACCAC-3' | 217 |
| TDP1 | 5'-CACACCACACGAAAATGATGCTG-3' | 5'-CTCAACCATATTCCTTGAGTTTTCTGGTG-3' | 115 |
| TOP2A | 5'-GTGGAATTAGTGACCCAGCAAATGTG-3' | 5'-GTCCGCAGCATTAACTAGAATCTCATC-3' | 123 |
| WEE1 | 5'-GTTATGTTTAAAATAGGTGATCTTGGGCATG-3' | 5'-GGTAGATGGGTATAATTCTCCTGTAAAACTTC-3' | 119 |
| XRCC4 | 5'-CAAACAAGAAGGGGAAACTGCAATC-3' | 5'-CTTACAGCAGCTGAAGCCAAC-3' | 129 |

## ChIP-qPCR primers

| Gene | Forward primer | Reverse primer | Amplicon size (bp) |
|---|---|---|---|
| AR distal | 5'-CTGTAGTTCCCATAATCCCCAC-3' | 5'-GCAAAGGCACGTCTTACAAG-3' | 193 |
| AR proximal | 5'-TATCTGCTGGCTTGGTCATGGCTTG-3' | 5'-CTGCTTCCTGAATAGCTCCTGCTT-3' | 268 |
| BRCA1 | 5'-GATGCAATAAGCCGCAACTGG-3' | 5'-CCTCTTCCGTCTCTTTCCTTTTACG-3' | 99 |
| BRCA2 | 5'-GAGAAGAGAACACACACTCCAGC-3' | 5'-GGTATTTCTCAGTGTGGCGAAAG-3' | 100 |
| CCNB2 | 5'-CCAGGCCAACACAACTTAAACC-3' | 5'-CCTCATCTACGAATTTCTCTCGACG-3' | 102 |
| CDC20 | 5'-CCTTCTTCCTGCTCCCAAGC-3' | 5'-CAAGGCGCTTGAGCCGTTC-3' | 95 |
| CDC25C | 5'-CTCCTAGTATTACCCTAGTGAATGGAC-3' | 5'-CCACACCCTTTCTGTTTTCCTCG-3' | 103 |
| CDK1 | 5'-CCTAAGTATTAGAAGTGAAAGTAATGGAATC-3' | 5'-CTCCCAGCATTGGCACAGTTC-3' | 108 |
| DNAPKcs | 5'-CAAACTTGGAACTCTTGACCTAGG-3' | 5'-CTGACCTGCGGAGGTAGTTTG-3' | 109 |
| IVL | 5'-TCAGCTGTATCCACTGCCCTCTTT-3' | 5'-TCACACCGGTCTTATGGGTTAGCA-3' | 164 |
| Ku80 | 5'-CGACTACGGCGGAATGGAG-3' | 5'-CGAGCATGCGCAGATTCTC-3' | 101 |
| NHEJ1 | 5'-GATGATGGAGAAATGAAGCAGGAGAG-3' | 5'-GTCCTCCACCAGCACTAGAG-3' | 103 |
| RAD51 | 5'- CGAGCTTCCTCAGCTCCTC-3' | 5'- GTCAGCTTTTGGCACTTCTGGTC-3' | 100 |
| RAD51AP1 | 5'-GGATCCGCGAACGTAGATTCG-3' | 5'-GTTGGGACATAGGGGCACTTG-3' | 89 |
| RAD51D | 5'-GCTTTGCTGCTTCTTGACACC-3' | 5'-CCAGGGAGCTTACTGTGAGC-3' | 102 |
| WEE1 | 5'-CCAGGCTCGCTCATAGG-3' | 5'-GGAAGGACCAGCTACGCG-3' | 110 |
| XRCC4 | 5'-GCAGCCACATCACCCTTCC-3' | 5'-GTAGGCGGTGCCGTGAC-3' | 107 |

# APPENDIX E. LIST OF ANTIBODIES

| Antibody Target | Catalog name | Additional name | Company | Secondary/ species | Clonality | Target site | Western dilution | ICC dilution | IP |
|---|---|---|---|---|---|---|---|---|---|
| α-AR | sc-7305 | 441 | Santa Cruz | Mouse | monoclonal | 299 -315 | | 1:1000 | |
| α-AR | N-20 | sc-816 | Santa Cruz | Rabbit | polyclonal | 1-20 | 1:2000 | 1:100 | |
| α-βActin | A1978 | | Sigma-Aldrich/ Millipore Sigma | Mouse | monoclonal | N-term | 1:2000 | | |
| α-CgA | ab15160 | | Abcam | Rabbit | polyclonal | C-term | | 1:500 | |
| α-H2AR3me2s | ab22397 | | Abcam | Rabbit | polyclonal | 1-100 | | | Yes |
| α-H3K9Ac | NB21-1074 | | Novus Biologicals | Rabbit | polyclonal | | | | Yes |
| α-H3R2me2s | ABE460 | | Sigma-Aldrich/ Millipore Sigma | Rabbit | polyclonal | | | | Yes |
| α-H3R8me2s | ab130740 | | Abcam | Rabbit | polyclonal | 1-100 | | | Yes |
| α-H4R3me2s | ab5823 | | Abcam | Rabbit | polyclonal | 1-100 | | | Yes |
| IgG | sc-2027 | | Santa Cruz | Rabbit | | | | | Yes |
| α-Ku70 | ab3114 | N3H10 | Abcam | Mouse | monoclonal | | | 1:500 | |
| α-NSE | ab227301 | | Abcam | Rabbit | polyclonal | | 1:1000 | | |
| α-MEP50 | 2823S | | New England Biolabs (NEB) | Rabbit | polyclonal | surrounding S225 | 1:500 | 1:100 | Yes |
| α-Mouse | NA931V | NA931-1ML | Sigma-Aldrich/ Millipore Sigma | HRP | | | 1:1000 | | |
| α-Mouse | 115-095-003 | | Jackson ImmunoResearch | FITC | polyclonal | | | 1:100 | |
| α-NHEJ1 | ab33499 | | Abcam | Rabbit | polyclonal | 250- C-term | 1:2000 | | |
| α-pCREB | CST 9191 | | Cell Signaling | Rabbit | polyclonal | Surrounding S133 | | 1:800 | |
| α-pICln (CLNS1A) | ab192907 | | Abcam | Rabbit | polyclonal | 187-237 | 1:2000 | 1:1000 | Yes |
| α-PRMT5 | 07-405 | | Sigma-Aldrich/ Millipore Sigma | Rabbit | polyclonal | 60-79 | 1:1000 | 1:1000 | Yes |
| α-Rabbit | NA934V | NA934-1ML | Sigma-Aldrich/ Millipore Sigma | HRP | | | 1:1000 | | |
| α-Rabbit | 111-295-144 | | Jackson ImmunoResearch | Rhodamine red | polyclonal | | | 1:1000 | |
| α-RAD51AP1 | ab101321 | | Abcam | Rabbit | polyclonal | 1-100 | 1:1000 | | |
| α-RAD51D | ab202063 | EPR16205 | Abcam | Rabbit | monoclonal | 1-100 | 1:2000 | | |
| α-RAD51 | ab63801 | | Abcam | Rabbit | polyclonal | full length | 1:2000 | 1:1000 | |
| α-RuvBL1 | SAB4200194 | clone 5G3-11 | Sigma-Aldrich/ Millipore Sigma | Mouse | monoclonal | | 1:1000 | 1:100 | |
| α-Tip60 | GTX112197 | | GeneTex | Rabbit | polyclonal | Center region | 1:500 | | |
| α-γH2AX | 05-636 | JBW301 | Sigma-Aldrich/ Millipore Sigma | Mouse | monoclonal | | | 1:1000 | |
| α-γH2AX | 9718S | 20E3 | Cell Signaling | Rabbit | monoclonal | | 1:1000 | 1:200 | |

# REFERENCES


1. Owens, J. L. *et al.* PRMT5 Cooperates with pICln to Function as a Master Epigenetic Activator of DNA Double-Strand Break Repair Genes. *iScience* **23**, 100750 (2020).
2. Siegel, R. L., Miller, K. D. & Jemal, A. Cancer statistics, 2020. *CA. Cancer J. Clin.* **70**, 7–30 (2020).
3. Bancroft, E. K. *et al.* Targeted Prostate Cancer Screening in BRCA1 and BRCA2 Mutation Carriers: Results from the Initial Screening Round of the IMPACT Study. *Eur. Urol.* **66**, 489–499 (2014).
4. Oh, M. *et al.* The association of *BRCA1* and *BRCA2* mutations with prostate cancer risk, frequency, and mortality: A meta-analysis. *The Prostate* **79**, 880–895 (2019).
5. Vickers, A. J. & Brewster, S. F. PSA velocity and doubling time in diagnosis and prognosis of prostate cancer. *Br. J. Med. Surg. Urol.* **5**, 162–168 (2012).
6. Ingham, M. D., Lee, R. J., MacDermed, D. & Olumi, A. F. Prostate cancer in transgender women. *Urol. Oncol. Semin. Orig. Investig.* **36**, 518–525 (2018).
7. Deebel, N. A. *et al.* Prostate Cancer in Transgender Women: Incidence, Etiopathogenesis, and Management Challenges. *Urology* **110**, 166–171 (2017).
8. Ryan, C. J., Elkin, E. P., Cowan, J. & Carroll, P. R. Initial treatment patterns and outcome of contemporary prostate cancer patients with bone metastases at initial presentation: Data from CaPSURE. *Cancer* **110**, 81–86 (2007).
9. Litwin, M. S. & Tan, H.-J. The Diagnosis and Treatment of Prostate Cancer: A Review. *JAMA* **317**, 2532 (2017).
10. Ahdoot, M., Lebastchi, A. H., Turkbey, B., Wood, B. & Pinto, P. A. Contemporary treatments in prostate cancer focal therapy: *Curr. Opin. Oncol.* **31**, 200–206 (2019).

11. Huggins, C. Studies on Prostatic Cancer: The Effect of Castration, of Estrogen and of Androgen Injection on Serum Phosphatases in Metastatic Carcinoma of the Prostate. *Cancer Res.* **1**, 293–297 (1941).
12. Higano, C. S. Side effects of androgen deprivation therapy: monitoring and minimizing toxicity. *Urology* **61**, 32–38 (2003).
13. Elliott, S. *et al.* Androgen Deprivation Therapy for Prostate Cancer: Recommendations to Improve Patient and Partner Quality of Life. *J. Sex. Med.* **7**, 2996–3010 (2010).
14. Walker, L. M., Tran, S., Wassersug, R. J., Thomas, B. & Robinson, J. W. Patients and partners lack knowledge of androgen deprivation therapy side effects. *Urol. Oncol. Semin. Orig. Investig.* **31**, 1098–1105 (2013).
15. Saad, F. & Fizazi, K. Androgen Deprivation Therapy and Secondary Hormone Therapy in the Management of Hormone-sensitive and Castration-resistant Prostate Cancer. *Urology* **86**, 852–861 (2015).
16. Cooperberg, M. R., Broering, J. M. & Carroll, P. R. Time Trends and Local Variation in Primary Treatment of Localized Prostate Cancer. *J. Clin. Oncol.* **28**, 1117–1123 (2010).
17. Gay, H. A. & Michalski, J. M. Radiation Therapy for Prostate Cancer. *Mo. Med.* **115**, 146–150 (2018).
18. Hamdy, F. C. *et al.* 10-Year Outcomes after Monitoring, Surgery, or Radiotherapy for Localized Prostate Cancer. *N. Engl. J. Med.* **375**, 1415–1424 (2016).
19. Donovan, J. L. *et al.* Patient-Reported Outcomes after Monitoring, Surgery, or Radiotherapy for Prostate Cancer. *N. Engl. J. Med.* **375**, 1425–1437 (2016).

20. J.F. Ward. DNA damage produced by ionizing radiation in mammalian cells identities, mechanisms of formation, and reparability. *Prog. Nucleic Acid Res. Mol. Biol.* **35**, 95–125 (1988).

21. Whitaker, S. J. DNA damage by drugs and radiation: What is important and how is it measured? *Eur. J. Cancer* **28**, 273–276 (1992).

22. Brenner, D. J. & Hall, E. J. Fractionation and protraction for radiotherapy of prostate carcinoma. *Int. J. Radiat. Oncol.* **43**, 1095–1101 (1999).

23. Ivan R Vogelius & Søren M Bentzen. Dose Response and Fractionation Sensitivity of Prostate Cancer After External Beam Radiation Therapy: A Meta-analysis of Randomized Trials. *Int. J. Radiat. Oncol. Biol. Phys.* **100**, 858–865 (2018).

24. Niloy R. Datta, Emanuel Stutz, Susanne Rogers & Stephan Bodis. Clinical Estimation of αβ Values for Prostate Cancer From Isoeffective Phase III Randomized Trials With Moderately Hypofractionated Radiotherapy. *Acta Oncol.* **57**, 883–894 (2018).

25. van Leeuwen, C. M. *et al.* The alfa and beta of tumours: a review of parameters of the linear-quadratic model, derived from clinical radiotherapy studies. *Radiat. Oncol.* **13**, (2018).

26. Cosset, J.-M., Chargari, C. & Créhange, G. Which Alpha/Beta Ratio for Prostate Cancer in 2019? *Cancer/Radiothérapie* **23**, 342–345 (2019).

27. Zaorsky, N. G. *et al.* What is the ideal radiotherapy dose to treat prostate cancer? A meta-analysis of biologically equivalent dose escalation. *Radiother. Oncol.* **115**, 295–300 (2015).

28. Cahlon, O. *et al.* Ultra-High Dose (86.4 Gy) IMRT for Localized Prostate Cancer: Toxicity and Biochemical Outcomes. *Int. J. Radiat. Oncol.* **71**, 330–337 (2008).

29. Afkhami Ardekani, M. & Ghaffari, H. Optimization of prostate brachytherapy techniques with polyethylene glycol–based hydrogel spacers: A systematic review. *Brachytherapy* **19**, 13–23 (2020).

30. Karsh, L. I. *et al.* Absorbable Hydrogel Spacer Use in Prostate Radiotherapy: A Comprehensive Review of Phase 3 Clinical Trial Published Data. *Urology* **115**, 39–44 (2018).

31. Podder, T. K., Fredman, E. T. & Ellis, R. J. Advances in Radiotherapy for Prostate Cancer Treatment. in *Molecular & Diagnostic Imaging in Prostate Cancer* (ed. Schatten, H.) vol. 1126 31–47 (Springer International Publishing, 2018).

32. Boorjian, S. A. *et al.* Long-term survival after radical prostatectomy versus external-beam radiotherapy for patients with high-risk prostate cancer. *Cancer* **117**, 2883–2891 (2011).

33. D'Amico, A. V., Chen, M.-H., Renshaw, A. A., Loffredo, B. & Kantoff, P. W. Risk of Prostate Cancer Recurrence in Men Treated With Radiation Alone or in Conjunction With Combined or Less Than Combined Androgen Suppression Therapy. *J. Clin. Oncol.* **26**, 2979–2983 (2008).

34. Gregory W. Allen, Andrew R. Howard, David F. Jarrard & Mark A. Ritter. Management of prostate cancer recurrences after radiation therapy-brachytherapy as a salvage option. *Am. Cancer Soc.* **110**, 1405–1416 (2007).

35. Ganswindt, U. *et al.* 70 Gy or more: which dose for which prostate cancer? *J. Cancer Res. Clin. Oncol.* **131**, 407–419 (2005).

36. Kuban, D. A. *et al.* Long-term multi-institutional analysis of stage T1–T2 prostate cancer treated with radiotherapy in the PSA era. *Int. J. Radiat. Oncol.* **57**, 915–928 (2003).

37. Anthony L. Zietman *et al.* Comparison of conventional-dose vs high-dose conformal radiation therapy in clinically localized adenocarcinoma of the prostate. A randomized controlled trial. *JAMA* **284**, 1233–1239 (2005).

38. Agarwal, P. K. *et al.* Treatment failure after primary and salvage therapy for prostate cancer: Likelihood, patterns of care, and outcomes. *Cancer* **112**, 307–314 (2008).

39. D'Angelillo, R. M. *et al.* Combination of androgen deprivation therapy and radiotherapy for localized prostate cancer in the contemporary era. *Crit. Rev. Oncol. Hematol.* **93**, 136–148 (2015).

40. Jones, C. U. *et al.* Radiotherapy and short-term androgen deprivation for localized prostate cancer. *N. Engl. J. Med.* **365**, 107–118 (2011).

41. Zelefsky, M. J., Reuter, V. E., Fuks, Z., Scardino, P. & Shippy, A. Influence of Local Tumor Control on Distant Metastases and Cancer Related Mortality After External Beam Radiotherapy for Prostate Cancer. *J. Urol.* **179**, 1368–1373 (2008).

42. Golabek, T. *et al.* Evidence-based recommendations on androgen deprivation therapy for localized and advanced prostate cancer. *Cent. Eur. J. Urol.* **69**, 131–138 (2016).

43. Polkinghorn, W. R. *et al.* Androgen Receptor Signaling Regulates DNA Repair in Prostate Cancers. *Cancer Discov.* **3**, 1245–1253 (2013).

44. Spratt, D. E. *et al.* Androgen Receptor Upregulation Mediates Radioresistance after Ionizing Radiation. *Cancer Res.* **75**, 4688–4696 (2015).

45. Goodwin, J. F. *et al.* A Hormone-DNA Repair Circuit Governs the Response to Genotoxic Insult. *Cancer Discov.* **3**, 1254–1271 (2013).

46. Tarish, F. L. *et al.* Castration radiosensitizes prostate cancer tissue by impairing DNA double-strand break repair. *Sci. Transl. Med.* **7**, 312re11–312re11 (2015).

47. Dal Pra, A., Locke, J. A., Borst, G., Supiot, S. & Bristow, R. G. Mechanistic Insights into Molecular Targeting and Combined Modality Therapy for Aggressive, Localized Prostate Cancer. *Front. Oncol.* **6**, (2016).

48. Deng, X. *et al.* Ionizing Radiation Induces Prostate Cancer Neuroendocrine Differentiation through Interplay of CREB and ATF2: Implications for Disease Progression. *Cancer Res.* **68**, 9663–9670 (2008).

49. Deng, X. *et al.* Ionizing radiation induces neuroendocrine differentiation of prostate cancer cells in vitro, in vivo and in prostate cancer patients. *Am J Cancer Res* **1**, 834–844 (2011).

50. Hu, C.-D., Choo, R. & Huang, J. Neuroendocrine Differentiation in Prostate Cancer: A Mechanism of Radioresistance and Treatment Failure. *Front. Oncol.* **5**, (2015).

51. Metz, S. A. & Levine, R. J. Neuroendocrine tumours that secrete biologically active peptides and amines. *Clin. Endocrinol. Metab.* **6**, 719–744 (1977).

52. Scalettar, B. A. *et al.* Hindered submicron mobility and long-term storage of presynaptic dense-core granules revealed by single-particle tracking. *Dev. Neurobiol.* **72**, 1181–1195 (2012).

53. Krauss, D. J. *et al.* Chromogranin a staining as a prognostic variable in newly diagnosed Gleason score 7-10 prostate cancer treated with definitive radiotherapy: Gleason Score 7-10 Prostate Cancer. *The Prostate* **74**, 520–527 (2014).

54. Mjønes, P., Sagatun, L., Nordrum, I. S. & Waldum, H. L. Neuron-Specific Enolase as an Immunohistochemical Marker Is Better Than Its Reputation. *J. Histochem. Cytochem.* **65**, 687–703 (2017).

55. Sarkar, D. *et al.* Plasma chromogranin A: Clinical implications in patients with castrate resistant prostate cancer receiving docetaxel chemotherapy. *Cancer Biomark.* **8**, 81–87 (2011).

56. Khan, M. O. & Ather, M. H. Chromogranin A – serum marker for prostate cancer. *J Pak Med Assoc* **61**, 4 (2011).

57. Vashchenko, N. & Abrahamsson, P.-A. Neuroendocrine Differentiation in Prostate Cancer: Implications for New Treatment Modalities. *Eur. Urol.* **47**, 147–155 (2005).

58. Santamaría, L., Martín, R., Martín, J. J. & Alonso, L. Stereologic Estimation of the Number of Neuroendocrine Cells in Normal Human Prostate Detected by Immunohistochemistry: *Appl. Immunohistochem. Mol. Morphol.* **10**, 275–281 (2002).

59. Per-Anders Abrahamsson & P Anthony di Sant'Agnese. Neuroendocrine Cells in the Human Prostate Gland. *J. Androl.* **14**, 307–309 (1993).

60. Huang, Y.-H., Zhang, Y.-Q. & Huang, J.-T. Neuroendocrine cells of prostate cancer: biologic functions and molecular mechanisms. *Asian J. Androl.* **21**, 291 (2019).

61. Cox, M. E., Deeble, P. D., Lakhani, S. & Parsons, S. J. Acquisition of Neuroendocrine Characteristics by Prostate Tumor Cells Is Reversible: Implications for Prostate Cancer Progression. *Cancer Res.* **59**, 3821–3830 (1999).

62. Deeble, P. D., Murphy, D. J., Parsons, S. J. & Cox, M. E. Interleukin-6- and Cyclic AMP-Mediated Signaling Potentiates Neuroendocrine Differentiation of LNCaP Prostate Tumor Cells. *Mol. Cell. Biol.* **21**, 8471–8482 (2001).

63. Amorino, G. P., Deeble, P. D. & Parsons, S. J. Neurotensin stimulates mitogenesis of prostate cancer cells through a novel c-Src/Stat5b pathway. *Oncogene* **26**, 745–756 (2007).

64. Zaninetti, R. *et al.* Activation of TRPV4 channels reduces migration of immortalized neuroendocrine cells: TRPV4 and migration. *J. Neurochem.* **116**, 606–615 (2011).

65. Kim, J. H. *et al.* Voltage-dependent ion channel currents in putative neuroendocrine cells dissociated from the ventral prostate of rat. *Pflüg. Arch. - Eur. J. Physiol.* **446**, 88–99 (2003).

66. Hall, M. *et al.* Androgen receptor signaling regulates T-type Ca2+ channel expression and neuroendocrine differentiation in prostate cancer cells. 16.

67. Gackière, F. *et al.* CaV3.2 T-type Calcium Channels Are Involved in Calcium-dependent Secretion of Neuroendocrine Prostate Cancer Cells. *J. Biol. Chem.* **283**, 10162–10173 (2008).

68. Fukami, K. *et al.* Hydrogen Sulfide and T-Type $Ca^{2+}$ Channels in Pain Processing, Neuronal Differentiation and Neuroendocrine Secretion. *Pharmacology* **99**, 196–203 (2017).

69. Masumori, N. *et al.* An Allograft Model of Androgen Independent Prostatic Neuroendocrine Carcinoma Derived From a Large Probasin Promoter-T Antigen Transgenic Mouse Line. *J. Urol.* **171**, 439–442 (2004).

70. Lee, M.-R. *et al.* Transcription Factors NF-YA Regulate the Induction of Human OGG1 Following DNA-alkylating Agent Methylmethane Sulfonate (MMS) Treatment. *J. Biol. Chem.* **279**, 9857–9866 (2004).

71. Huang, J. *et al.* Immunohistochemical characterization of neuroendocrine cells in prostate cancer. *The Prostate* **66**, 1399–1406 (2006).

72. Nianzeng Xing, Junqi Qian, David Bostwick, Erik Bergstralh & Charles Y.F. Young. Neuroendocrine cells in human prostate over-express the anti-apoptosis protein survivin. *The Prostate* **48**, 7–15 (2001).

73. di Sant'Agnese, P. A. Neuroendocrine differentiation in prostatic carcinoma: An update on recent developments. *Ann. Oncol.* **12**, S135–S140 (2001).

74. Bonkhoff, H. Neuroendocrine differentiation in human prostate cancer. Morphogenesis, proliferation and androgen receptor status. *Ann. Oncol.* **12**, S141–S144 (2001).

75. Nelson, E. C. *et al.* Clinical implications of neuroendocrine differentiation in prostate cancer. *Prostate Cancer Prostatic Dis.* **10**, 6–14 (2007).

76. Volante, M., Rindi, G. & Papotti, M. The grey zone between pure (neuro)endocrine and non-(neuro)endocrine tumours: a comment on concepts and classification of mixed exocrine–endocrine neoplasms. *Virchows Arch.* **449**, 499–506 (2006).

77. Priemer, D. S. *et al.* Neuroendocrine Tumors of the Prostate: Emerging Insights from Molecular Data and Updates to the 2016 World Health Organization Classification. *Endocr. Pathol.* **27**, 123–135 (2016).

78. Monn, M. F. & Cheng, L. Emerging trends in the evaluation and management of small cell prostate cancer: a clinical and molecular perspective. *Expert Rev. Anticancer Ther.* **16**, 1029–1037 (2016).

79. Komiya, A. *et al.* Neuroendocrine differentiation in the progression of prostate cancer: Neuroendocrine differentiation in prostate cancer. *Int. J. Urol.* **16**, 37–44 (2009).

80. Li, Q., Zhang, C. S. & Zhang, Y. Molecular aspects of prostate cancer with neuroendocrine differentiation. *Chin J Cancer Res* **28**, 8 (2016).

81. Patel, Chugh & Tripathi. Neuroendocrine Differentiation of Prostate Cancer—An Intriguing Example of Tumor Evolution at Play. *Cancers* **11**, 1405 (2019).

82. Santoni, M. *et al.* Neuroendocrine differentiation in prostate cancer: Novel morphological insights and future therapeutic perspectives. *Biochim. Biophys. Acta BBA - Rev. Cancer* **1846**, 630–637 (2014).

83. Kardoust Parizi, M. *et al.* Focal Neuroendocrine Differentiation of Conventional Prostate Adenocarcinoma as a Prognostic Factor after Radical Prostatectomy: A Systematic Review and Meta-Analysis. *Int. J. Mol. Sci.* **20**, 1374 (2019).

84. Luo, Y. *et al.* Epithelial-mesenchymal transition and migration of prostate cancer stem cells is driven by cancer-associated fibroblasts in an HIF-1α/β-catenin-dependent pathway. *Mol. Cells* **36**, 138–144 (2013).

85. Suarez, C. D., Deng, X. & Hu, C.-D. Targeting CREB inhibits radiation-induced neuroendocrine differentiation and increases radiation-induced cell death in prostate cancer cells. *Am J Cancer Res* **4**, 850–61 (2014).

86. Yuan, T.-C. *et al.* Androgen deprivation induces human prostate epithelial neuroendocrine differentiation of androgen-sensitive LNCaP cells. *Endocr. Relat. Cancer* 151–167 (2006) doi:10.1677/erc.1.01043.

87. Jiborn, T., Bjartell, A. & Abrahamsson, P.-A. Neuroendocrine Differentiation in Prostatic Carcinoma During Hormonal Treatment. *Urology* **51**, 585–589 (1998).

88. Oronsky, B., Ma, P. C., Morgensztern, D. & Carter, C. A. Nothing But NET: A Review of Neuroendocrine Tumors and Carcinomas. *Neoplasia* **19**, 991–1002 (2017).

89. Beltran, H. *et al.* Divergent clonal evolution of castration-resistant neuroendocrine prostate cancer. *Nat. Med.* **22**, 298–305 (2016).

90. Niu, Y. *et al.* ADT with antiandrogens in prostate cancer induces adverse effect of increasing resistance, neuroendocrine differentiation and tumor metastasis. *Cancer Lett.* **439**, 47–55 (2018).

91. Davies, A. H., Beltran, H. & Zoubeidi, A. Cellular plasticity and the neuroendocrine phenotype in prostate cancer. *Nat. Rev. Urol.* **15**, 271–286 (2018).

92. Cindolo, L., Cantile, M., Vacherot, F., Terry, S. & de la Taille, A. Neuroendocrine Differentiation in Prostate Cancer: From Lab to Bedside. *Urol. Int.* **79**, 287–296 (2007).

93. Aggarwal, R. *et al.* Clinical and Genomic Characterization of Treatment-Emergent Small-Cell Neuroendocrine Prostate Cancer: A Multi-institutional Prospective Study. *J. Clin. Oncol.* **36**, 2492–2503 (2018).

94. Small, E. J. *et al.* Clinical and genomic characterization of metastatic small cell/neuroendocrine prostate cancer (SCNC) and intermediate atypical prostate cancer (IAC): Results from the SU2C/PCF/AACRWest Coast Prostate Cancer Dream Team (WCDT). *J. Clin. Oncol.* **34**, 5019–5019 (2016).

95. Nadal, R., Schweizer, M., Kryvenko, O. N., Epstein, J. I. & Eisenberger, M. A. Small cell carcinoma of the prostate. *Nat. Rev. Urol.* **11**, 213–219 (2014).

96. Cheng, S. & Yu, X. Bioinformatics analyses of publicly available NEPCa datasets. **7**, 327–340 (2019).

97. Lilleby, W., Paus, E., Skovlund, E. & Foss, S. D. Prognostic value of neuroendocrine serum markers and PSA in irradiated patients with pN0 localized prostate cancer. *The Prostate* **46**, 126–133 (2001).

98. Flavahan, W. A., Gaskell, E. & Bernstein, B. E. Epigenetic plasticity and the hallmarks of cancer. *Science* **357**, eaal2380 (2017).

99. Jones, P. A. & Baylin, S. B. The fundamental role of epigenetic events in cancer. *Nat. Rev. Genet.* **3**, 415–428 (2002).

100. Feinberg, A. P. & Tycko, B. The history of cancer epigenetics. *Nat. Rev. Cancer* **4**, 143–153 (2004).

101. Lorton, B. M. & Shechter, D. Cellular consequences of arginine methylation. *Cell. Mol. Life Sci.* (2019) doi:10.1007/s00018-019-03140-2.

102. Di Lorenzo, A. & Bedford, M. T. Histone arginine methylation. *FEBS Lett.* **585**, 2024–2031 (2011).

103. Evich, M., Stroeva, E., Zheng, Y. G. & Germann, M. W. Effect of methylation on the side-chain p $K_a$ value of arginine: Effect of Methylation on Arginine p $K_a$ Values. *Protein Sci.* **25**, 479–486 (2016).

104. Blanc, R. S. & Richard, S. Arginine Methylation: The Coming of Age. *Mol. Cell* **65**, 8–24 (2017).

105. Yang, Y. & Bedford, M. T. Protein arginine methyltransferases and cancer. *Nat. Rev. Cancer* **13**, 37–50 (2013).

106. Feng, Y. *et al.* Mammalian Protein Arginine Methyltransferase 7 (PRMT7) Specifically Targets R *X* R Sites in Lysine- and Arginine-rich Regions. *J. Biol. Chem.* **288**, 37010–37025 (2013).

107. Auclair, Y. & Richard, S. The role of arginine methylation in the DNA damage response. *DNA Repair* **12**, 459–465 (2013).

108. Raposo, A. E. & Piller, S. C. Protein arginine methylation: an emerging regulator of the cell cycle. *Cell Div.* **13**, (2018).

109. Pollack, B. P. *et al.* The Human Homologue of the Yeast Proteins Skb1 and Hsl7p Interacts with Jak Kinases and Contains Protein Methyltransferase Activity. *J. Biol. Chem.* **274**, 31531–31542 (1999).

110. Stopa, N., Krebs, J. E. & Shechter, D. The PRMT5 arginine methyltransferase: many roles in development, cancer and beyond. *Cell. Mol. Life Sci.* **72**, 2041–2059 (2015).

111. Karkhanis, V., Hu, Y.-J., Baiocchi, R. A., Imbalzano, A. N. & Sif, S. Versatility of PRMT5-induced methylation in growth control and development. *Trends Biochem. Sci.* **36**, 633–641 (2011).

112. Shailesh, H., Zakaria, Z. Z., Baiocchi, R. & Sif, S. Protein arginine methyltransferase 5 (PRMT5) dysregulation in cancer. *Oncotarget* **9**, (2018).

113. Xu, X., Hoang, S., Mayo, M. W. & Bekiranov, S. Application of machine learning methods to histone methylation ChIP-Seq data reveals H4R3me2 globally represses gene expression. *BMC Bioinformatics* **11**, (2010).

114. Deng, X. *et al.* Protein arginine methyltransferase 5 functions as an epigenetic activator of the androgen receptor to promote prostate cancer cell growth. *Oncogene* **36**, 1223–1231 (2017).

115. Liu, F. *et al.* PRMT5-mediated histone arginine methylation antagonizes transcriptional repression by polycomb complex PRC2. *Nucleic Acids Res.* **48**, 2956–2968 (2020).

116. Daniel P. Harris, Unnikrishnan M. Chandrasekharan, Smarajit Bandyopadhyay, Belinda Willard & Paul E. DiCorleto. PRMT5-Mediated Methylation of NF-κB p65 at Arg174 Is Required for Endothelial CXCL11 Gene Induction in Response to TNF-α and IFN-γ Costimulation. *PLoS ONE* **11**, (2016).

117. Bandyopadhyay, S. *et al.* HOXA9 Methylation by PRMT5 Is Essential for Endothelial Cell Expression of Leukocyte Adhesion Molecules. *Mol. Cell. Biol.* **32**, 1202–1213 (2012).

118. Hsu, J.-M. *et al.* Crosstalk between Arg 1175 methylation and Tyr 1173 phosphorylation negatively modulates EGFR-mediated ERK activation. *Nat. Cell Biol.* **13**, 174–181 (2011).

119. Richters, A. Targeting protein arginine methyltransferase 5 in disease. *Future Med. Chem.* **9**, 2081–2098 (2017).

120. Xiao, W. *et al.* Role of protein arginine methyltransferase 5 in human cancers. *Biomed. Pharmacother.* **114**, 108790 (2019).

121. Zhang, H.-T., Zhang, D., Zha, Z.-G. & Hu, C.-D. Transcriptional activation of PRMT5 by NF-Y is required for cell growth and negatively regulated by the PKC/c-Fos signaling in prostate cancer cells. *Biochim. Biophys. Acta BBA - Gene Regul. Mech.* **1839**, 1330–1340 (2014).

122. Bao, X. *et al.* Overexpression of PRMT5 Promotes Tumor Cell Growth and Is Associated with Poor Disease Prognosis in Epithelial Ovarian Cancer. *J. Biol. Chem.* **61**, 206–217 (2013).

123. Jiang, H. *et al.* PRMT5 promotes cell proliferation by inhibiting BTG2 expression via the ERK signaling pathway in hepatocellular carcinoma. *Cancer Med.* **7**, 869–882 (2018).

124. Gu, Z. *et al.* Protein arginine methyltransferase 5 is essential for growth of lung cancer cells. *Biochem. J.* **446**, 235–241 (2012).

125. Zhang, B. *et al.* Targeting protein arginine methyltransferase 5 inhibits colorectal cancer growth by decreasing arginine methylation of eIF4E and FGFR3. *Oncotarget* **6**, (2015).

126. Wei, T.-Y. W. *et al.* Protein arginine methyltransferase 5 is a potential oncoprotein that upregulates G1 cyclins/cyclin-dependent kinases and the phosphoinositide 3-kinase/AKT signaling cascade. *Cancer Sci.* **103**, 1640–1650 (2012).

127. Gu, Z. *et al.* Protein Arginine Methyltransferase 5 Functions in Opposite Ways in the Cytoplasm and Nucleus of Prostate Cancer Cells. *PLoS ONE* **7**, e44033 (2012).

128. Yan, F. *et al.* Genetic Validation of the Protein Arginine Methyltransferase PRMT5 as a Candidate Therapeutic Target in Glioblastoma. *Cancer Res.* **74**, 1752–1765 (2014).

129. Han, X. *et al.* Expression of PRMT5 correlates with malignant grade in gliomas and plays a pivotal role in tumor growth in vitro. *J. Neurooncol.* **118**, 61–72 (2014).

130. Dai, C., Heemers, H. & Sharifi, N. Androgen Signaling in Prostate Cancer. *Cold Spring Harb. Perspect. Med.* **7**, a030452 (2017).

131. Culig, Z. & Santer, F. R. Androgen receptor signaling in prostate cancer. *Cancer Metastasis Rev.* **33**, 413–427 (2014).

132. Nevedomskaya, E., Baumgart, S. & Haendler, B. Recent Advances in Prostate Cancer Treatment and Drug Discovery. *Int. J. Mol. Sci.* **19**, 1359 (2018).

133. Elshan, N. G. R. D., Rettig, M. B. & Jung, M. E. Molecules targeting the androgen receptor (AR) signaling axis beyond the AR-Ligand binding domain. *Med. Res. Rev.* **39**, 910–960 (2019).

134. Snow, O. *et al.* Androgen receptor plasticity and its implications for prostate cancer therapy. *Cancer Treat. Rev.* **81**, 101871 (2019).

135. Nakayama, T. *et al.* Epigenetic regulation of androgen receptor gene expression in human prostate cancers. *Lab. Invest.* **80**, 1789–1796 (2000).

136. Cucchiara, V. *et al.* Epigenomic Regulation of Androgen Receptor Signaling: Potential Role in Prostate Cancer Therapy. *Cancers* **9**, 9 (2017).

137. Gao, L. & Alumkal, J. Epigenetic regulation of androgen receptor signaling in prostate cancer. *Epigenetics* **5**, 100–104 (2010).

138. Peter W. Faber, H C van Rooij, H J Schipper, A O Brinkmann & J Trapman. Two Different, Overlapping Pathwayosf Transcription InitiationAre Active on the TATA-lesHs uman Androgen Receptor Promoter. *J. Biol. Chem.* **268**, 9296–9301 (1993).

139. Wu, Q. *et al.* The BRG1 ATPase of human SWI/SNF chromatin remodeling enzymes as a driver of cancer. *Epigenomics* **9**, 919–931 (2017).

140. Burgos, E. S. *et al.* Histone H2A and H4 N-terminal Tails Are Positioned by the MEP50 WD Repeat Protein for Efficient Methylation by the PRMT5 Arginine Methyltransferase. *J. Biol. Chem.* **290**, 9674–9689 (2015).

141. Hongshan Chen, Benjamin Lorton, Varun Gupta & David Shechter. Chen 2017 - A TGFβ-PRMT5-MEP50 axis regulates cancer cell invasion through histone H3 and H4 arginine methylation coupled transcriptional activation and repression. *Oncogene* **36**, 373–386 (2017).

142. Antonysamy, S. *et al.* Crystal structure of the human PRMT5:MEP50 complex. *Proc. Natl. Acad. Sci.* **109**, 17960–17965 (2012).

143. Wang, M., Fuhrmann, J. & Thompson, P. R. Protein Arginine Methyltransferase 5 Catalyzes Substrate Dimethylation in a Distributive Fashion. *Biochemistry* **53**, 7884–7892 (2014).

144. Tarighat, S. S. *et al.* The dual epigenetic role of PRMT5 in acute myeloid leukemia: gene activation and repression via histone arginine methylation. *Leukemia* **30**, 789–799 (2016).

145. Pesiridis, G. S., Diamond, E. & Van Duyne, G. D. Role of pICLn in Methylation of Sm Proteins by PRMT5. *J. Biol. Chem.* **284**, 21347–21359 (2009).

146. Gurung, B. & Hua, X. Menin/PRMT5/hedgehog signaling: a potential target for the treatment of multiple endocrine neoplasia type 1 tumors. *Epigenomics* **5**, 469–471 (2013).

147. Gurung, B. *et al.* Menin Epigenetically Represses Hedgehog Signaling in MEN1 Tumor Syndrome. *Cancer Res.* **73**, 2650–2658 (2013).

148. Gurung, B., Feng, Z. & Hua, X. Menin Directly Represses Gli1 Expression Independent of Canonical Hedgehog Signaling. *Mol. Cancer Res.* **11**, 1215–1222 (2013).

149. Matkar, S., Thiel, A. & Hua, X. Menin: a scaffold protein that controls gene expression and cell signaling. *Trends Biochem. Sci.* **38**, 394–402 (2013).

150. Gao, J. *et al.* Integrative Analysis of Complex Cancer Genomics and Clinical Profiles Using the cBioPortal. *Sci. Signal.* **6**, 1–34 (2013).

151. Cerami, E. *et al.* The cBio Cancer Genomics Portal: An Open Platform for Exploring Multidimensional Cancer Genomics Data. *Cancer Discov.* **2**, 401–404 (2012).

152. Matthieu Lacroix *et al.* The histone-binding protein COPR5 is required for nuclear functions of the protein arginine methyltransferase PRMT5. **9**, 452–458 (2008).

153. Paul, C., Sardet, C. & Fabbrizio, E. The histone- and PRMT5-associated protein COPR5 is required for myogenic differentiation. *Cell Death Differ.* **19**, 900–908 (2012).

154. Friesen, W. J. *et al.* The Methylosome, a 20S Complex Containing JBP1 and pICln, Produces Dimethylarginine-Modified Sm Proteins. *Mol. Cell. Biol.* **21**, 8289–8300 (2001).

155. Friesen, W. J. *et al.* A Novel WD Repeat Protein Component of the Methylosome Binds Sm Proteins. *J. Biol. Chem.* **277**, 8243–8247 (2002).

156. Meister, G. *et al.* Methylation of Sm proteins by a complex containing PRMT5 and the putative U snRNP assembly factor pICln. *Curr. Biol.* **11**, 1990–1994 (2001).

157. Braun, C. J. *et al.* Coordinated Splicing of Regulatory Detained Introns within Oncogenic Transcripts Creates an Exploitable Vulnerability in Malignant Glioma. *Cancer Cell* **32**, 411-426.e11 (2017).

158. Tan, D. Q. *et al.* PRMT5 Modulates Splicing for Genome Integrity and Preserves Proteostasis of Hematopoietic Stem Cells. *Cell Rep.* **26**, 2316-2328.e6 (2019).

159. Guderian, G. *et al.* RioK1, a New Interactor of Protein Arginine Methyltransferase 5 (PRMT5), Competes with pICln for Binding and Modulates PRMT5 Complex Composition and Substrate Specificity. *J. Biol. Chem.* **286**, 1976–1986 (2011).

160. Marjon, K. *et al.* MTAP Deletions in Cancer Create Vulnerability to Targeting of the MAT2A/PRMT5/RIOK1 Axis. *Cell Rep.* **15**, 574–587 (2016).

161. Kryukov, G. V. *et al.* MTAP deletion confers enhanced dependency on the PRMT5 arginine methyltransferase in cancer cells. *Science* **351**, 1214–1218 (2016).

162. Mavrakis, K. J. *et al.* Disordered methionine metabolism in MTAP/CDKN2A-deleted cancers leads to dependence on PRMT5. *Science* **351**, 1208–1213 (2016).

163. Thompson, L. H. Recognition, signaling, and repair of DNA double-strand breaks produced by ionizing radiation in mammalian cells: The molecular choreography. *Mutat. Res. Mutat. Res.* **751**, 158–246 (2012).

164. Rieger, K. E. Portrait of transcriptional responses to ultraviolet and ionizing radiation in human cells. *Nucleic Acids Res.* **32**, 4786–4803 (2004).

165. Russell, J. S. *et al.* Gleevec-mediated inhibition of Rad51 expression and enhancement of tumor cell radiosensitivity. *Cancer Res.* **63**, 7377–7383 (2003).

166. Khalil, H., Tummala, H. & Zhelev, N. ATM in focus: A damage sensor and cancer target. *BioDiscovery* **5**, 1–60 (2012).

167. Kuo, L. J. & Yang, L.-X. γ-H2AX-a novel biomarker for DNA double-strand breaks. *In Vivo* **22**, 305–309 (2008).

168. Olive, P. L., Wlodek, D. & Banáth, J. P. DNA Double-Strand Breaks Measured in Individual Cells Subjected to Gel Electrophoresis. *Cancer Res.* **51**, 4671–4676 (1991).

169. Jansson, M. *et al.* Arginine methylation regulates the p53 response. *Nat. Cell Biol.* **10**, 1431–1439 (2008).

170. Ceccaldi, R., Rondinelli, B. & D'Andrea, A. D. Repair Pathway Choices and Consequences at the Double-Strand Break. *Trends Cell Biol.* **26**, 52–64 (2016).

171. Scully, R., Panday, A., Elango, R. & Willis, N. A. DNA double-strand break repair-pathway choice in somatic mammalian cells. *Nat. Rev. Mol. Cell Biol.* **20**, 698–714 (2019).

172. Chapman, J. R., Taylor, M. R. G. & Boulton, S. J. Playing the End Game: DNA Double-Strand Break Repair Pathway Choice. *Mol. Cell* **47**, 497–510 (2012).

173. Symington, L. S. & Gautier, J. Double-Strand Break End Resection and Repair Pathway Choice. *Annu. Rev. Genet.* **45**, 247–271 (2011).

174. Ruffner, H. & Verma, I. M. BRCA1 is a cell cycle-regulated nuclear phosphoprotein. *Proc. Natl. Acad. Sci.* **94**, 7138–7143 (1997).

175. Sun, Y. *et al.* Histone H3 methylation links DNA damage detection to activation of the tumour suppressor Tip60. *Nat. Cell Biol.* **11**, 1376–1382 (2009).

176. Tang, J. *et al.* Acetylation limits 53BP1 association with damaged chromatin to promote homologous recombination. *Nat. Struct. Mol. Biol.* **20**, 317–325 (2013).

177. Clarke, T. L. *et al.* PRMT5-Dependent Methylation of the TIP60 Coactivator RUVBL1 Is a Key Regulator of Homologous Recombination. *Mol. Cell* **65**, 900-916.e7 (2017).

178. Grigoletto, A., Lestienne, P. & Rosenbaum, J. The multifaceted proteins Reptin and Pontin as major players in cancer. *Biochim. Biophys. Acta BBA - Rev. Cancer* **1815**, 147–157 (2011).

179. Gospodinov, A., Tsaneva, I. & Anachkova, B. RAD51 foci formation in response to DNA damage is modulated by TIP49. *Int. J. Biochem. Cell Biol.* **41**, 925–933 (2009).

180. Hamard, P.-J. *et al.* PRMT5 Regulates DNA Repair by Controlling the Alternative Splicing of Histone-Modifying Enzymes. *Cell Rep.* **24**, 2643–2657 (2018).

181. Manthey, G. M., Clear, A. D., Liddell, L. C., Negritto, M. C. & Bailis, A. M. Homologous recombination in budding yeast expressing the human RAD52 gene reveals a Rad51-independent mechanism of conservative double-strand break repair. *Nucleic Acids Res.* **45**, 1879–1888 (2017).

182. Mahajan, S., Raina, K., Verma, S. & Rao, B. J. Human RAD52 protein regulates homologous recombination and checkpoint function in BRCA2 deficient cells. *Int. J. Biochem. Cell Biol.* **107**, 128–139 (2019).

183. Hanamshet, K., Mazina, O. & Mazin, A. Reappearance from Obscurity: Mammalian Rad52 in Homologous Recombination. *Genes* **7**, 63 (2016).

184. Scoumanne, A., Zhang, J. & Chen, X. PRMT5 is required for cell-cycle progression and p53 tumor suppressor function. *Nucleic Acids Res.* **37**, 4965–4976 (2009).

185. Durant, S. T., Cho, E. C. & La Thangue, N. B. p53 methylation—the Arg-ument is clear. *Cell Cycle* **8**, 801–802 (2009).

186. Du, W., Amarachintha, S., Erden, O., Wilson, A. & Pang, Q. The Fanconi anemia pathway controls oncogenic response in hematopoietic stem and progenitor cells by regulating PRMT5-mediated p53 arginine methylation. *Oncotarget* **7**, 60005–60020 (2016).

187. Cho, E.-C. *et al.* Arginine methylation controls growth regulation by E2F-1. *EMBO J.* **31**, 1785–1797 (2012).

188. Zheng, S. *et al.* Arginine Methylation-Dependent Reader-Writer Interplay Governs Growth Control by E2F-1. *Mol. Cell* **52**, 37–51 (2013).

189. Wu, L., Yang, X., Duan, X., Cui, L. & Li, G. Exogenous expression of marine lectins DlFBL and SpRBL induces cancer cell apoptosis possibly through PRMT5-E2F-1 pathway. *Sci. Rep.* **4**, 4505 (2015).

190. Guo, Z. *et al.* Methylation of FEN1 suppresses nearby phosphorylation and facilitates PCNA binding. *Nat. Chem. Biol.* **6**, 766–773 (2010).

191. Guo, Z. *et al.* Sequential Posttranslational Modifications Program FEN1 Degradation during Cell-Cycle Progression. *Mol. Cell* **47**, 444–456 (2012).

192. He, W. *et al.* A role for the arginine methylation of Rad9 in checkpoint control and cellular sensitivity to DNA damage. *Nucleic Acids Res.* **39**, 4719–4727 (2011).

193. Hu, D. *et al.* Interplay between arginine methylation and ubiquitylation regulates KLF4-mediated genome stability and carcinogenesis. *Nat. Commun.* **6**, (2015).

194. Rehman, I. *et al.* PRMT5-mediated arginine methylation of TDP1 for the repair of topoisomerase I covalent complexes. *Nucleic Acids Res.* **46**, 5601–5617 (2018).

195. Zheng, L., Dai, H., Qiu, J., Huang, Q. & Shen, B. Disruption of the FEN-1/PCNA Interaction Results in DNA Replication Defects, Pulmonary Hypoplasia, Pancytopenia, and Newborn Lethality in Mice. *Mol. Cell. Biol.* **27**, 3176–3186 (2007).

196. Soza, S. *et al.* DNA Ligase I Deficiency Leads to Replication-Dependent DNA Damage and Impacts Cell Morphology without Blocking Cell Cycle Progression. *Mol. Cell. Biol.* **29**, 2032–2041 (2009).

197. Asagoshi, K. *et al.* FEN1 Functions in Long Patch Base Excision Repair Under Conditions of Oxidative Stress in Vertebrate Cells. *Mol. Cancer Res.* **8**, 204–215 (2010).

198. Chen, M.-J., Lin, Y.-T., Lieberman, H. B., Chen, G. & Lee, E. Y.-H. P. ATM-dependent Phosphorylation of Human Rad9 Is Required for Ionizing Radiation-induced Checkpoint Activation. *J. Biol. Chem.* **276**, 16580–16586 (2001).

199. St.Onge, R. P., Besley, B. D. A., Pelley, J. L. & Davey, S. A Role for the Phosphorylation of hRad9 in Checkpoint Signaling. *J. Biol. Chem.* **278**, 26620–26628 (2003).

200. Roos-Mattjus, P. *et al.* Phosphorylation of Human Rad9 Is Required for Genotoxin-activated Checkpoint Signaling. *J. Biol. Chem.* **278**, 24428–24437 (2003).

201. Pandita, R. K. *et al.* Mammalian Rad9 Plays a Role in Telomere Stability, S- and G2-Phase-Specific Cell Survival, and Homologous Recombinational Repair. *Mol. Cell. Biol.* **26**, 1850–1864 (2006).

202. Singh, A. & Xu, Y.-J. The Cell Killing Mechanisms of Hydroxyurea. *Genes* **7**, 99 (2016).

203. Lieberman, H. B. *et al.* The role of RAD9 in tumorigenesis. *J. Mol. Cell Biol.* **3**, 39–43 (2011).

204. Parrilla-Castellar, E. R., Arlander, S. J. H. & Karnitz, L. Dial 9–1–1 for DNA damage: the Rad9–Hus1–Rad1 (9–1–1) clamp complex. *DNA Repair* **3**, 1009–1014 (2004).

205. He, W. *et al.* Rad9 plays an important role in DNA mismatch repair through physical interaction with MLH1. *Nucleic Acids Res.* **36**, 6406–6417 (2008).

206. Li, T. *et al.* Checkpoint protein Rad9 plays an important role in nucleotide excision repair. *DNA Repair* **12**, 284–292 (2013).

207. Stevens, C. & La Thangue, N. B. E2F and cell cycle control: a double-edged sword. *Arch. Biochem. Biophys.* **412**, 157–169 (2003).

208. Gamper, A. M. *et al.* Regulation of KLF4 Turnover Reveals an Unexpected Tissue-Specific Role of pVHL in Tumorigenesis. *Mol. Cell* **45**, 233–243 (2012).

209. Zhou, Q., Hong, Y., Zhan, Q., Shen, Y. & Liu, Z. Role for Kruppel-Like Factor 4 in Determining the Outcome of p53 Response to DNA Damage. *Cancer Res.* **69**, 8284–8292 (2009).

210. Hu, D., Zhou, Z., Davidson, N. E., Huang, Y. & Wan, Y. Novel Insight into KLF4 Proteolytic Regulation in Estrogen Receptor Signaling and Breast Carcinogenesis. *J. Biol. Chem.* **287**, 13584–13597 (2012).

211. Pommier, Y., Sun, Y., Huang, S. N. & Nitiss, J. L. Roles of eukaryotic topoisomerases in transcription, replication and genomic stability. *Nat. Rev. Mol. Cell Biol.* **17**, 703–721 (2016).

212. Das, B. B. *et al.* PARP1–TDP1 coupling for the repair of topoisomerase I–induced DNA damage. *Nucleic Acids Res.* **42**, 4435–4449 (2014).

213. Huang, S. -y. N. *et al.* TDP1 repairs nuclear and mitochondrial DNA damage induced by chain-terminating anticancer and antiviral nucleoside analogs. *Nucleic Acids Res.* **41**, 7793–7803 (2013).

214. El-Khamisy, S. F. & Caldecott, K. W. TDP1-dependent DNA single-strand break repair and neurodegeneration. *Mutagenesis* **21**, 219–224 (2006).

215. Yang, H. *et al.* PRMT5 competitively binds to CDK4 to promote G1-S transition upon glucose induction in hepatocellular carcinoma. *Oncotarget* **7**, 72131–72147 (2016).

216. Lim, J.-H. *et al.* PRMT5 is essential for the eIF4E-mediated 5′-cap dependent translation. *Biochem. Biophys. Res. Commun.* **452**, 1016–1021 (2014).

217. Pal, S., Vishwanath, S. N., Erdjument-Bromage, H., Tempst, P. & Sif, S. Human SWI/SNF-Associated PRMT5 Methylates Histone H3 Arginine 8 and Negatively Regulates Expression of ST7 and NM23 Tumor Suppressor Genes. *Mol. Cell. Biol.* **24**, 9630–9645 (2004).

218. Kumar, B. *et al.* Nuclear PRMT5, cyclin D1 and IL-6 are associated with poor outcome in oropharyngeal squamous cell carcinoma patients and is inversely associated with p16-status. *Oncotarget* **8**, (2017).

219. Jung, S. Y. *et al.* Complications in the Assignment of 14 and 28 Da Mass Shift Detected by Mass Spectrometry as in Vivo Methylation from Endogenous Proteins. *Anal. Chem.* **80**, 1721–1729 (2008).

220. Zhang, Y. *et al.* The impact of R213 mutation on p53-mediated p21 activity. *Biochimie* **99**, 215–218 (2014).

221. Hiroshi Tanaka *et al.* PRMT5, a Novel TRAIL Receptor-Binding Protein, Inhibits TRAIL-Induced Apoptosis via Nuclear Factor-κB Activation. *Mol. Cancer Res.* **7**, 557–569 (2009).

222. Wei, H. *et al.* PRMT5 dimethylates R30 of the p65 subunit to activate NF-κB. *PNAS* **110**, 13516–13521 (2013).

223. Chen, M. *et al.* Cross-talk between Arg methylation and Ser phosphorylation modulates apoptosis signal–regulating kinase 1 activation in endothelial cells. *Mol. Biol. Cell* **27**, 1358–1366 (2016).

224. H Kadowaki *et al.* Amyloid β induces neuronal cell death through ROS-mediated ASK1 activation. *Cell Death Differ.* **12**, 19–24.

225. Kim, A. H., Khursigara, G., Sun, X., Franke, T. F. & Chao, M. V. Akt Phosphorylates and Negatively Regulates Apoptosis Signal-Regulating Kinase 1. *Mol. Cell. Biol.* **21**, 893–901 (2001).

226. Powers, M. A., Fay, M. M., Factor, R. E., Welm, A. L. & Ullman, K. S. Protein Arginine Methyltransferase 5 Accelerates Tumor Growth by Arginine Methylation of the Tumor Suppressor Programmed Cell Death 4. *Cancer Res.* **71**, 5579–5587 (2011).

227. Eto, K., Goto, S., Nakashima, W., Ura, Y. & Abe, S.-I. Loss of programmed cell death 4 induces apoptosis by promoting the translation of procaspase-3 mRNA. *Cell Death Differ.* **19**, 573–581 (2012).

228. Yang, M. *et al.* Caenorhabditis elegans Protein Arginine Methyltransferase PRMT-5 Negatively Regulates DNA Damage-Induced Apoptosis. *PLoS Genet.* **5**, e1000514 (2009).

229. Schumacher, B. *et al.* Translational Repression of C. elegans p53 by GLD-1 Regulates DNA Damage-Induced Apoptosis. *Cell* **120**, 357–368 (2005).

230. Cid, V. J., Shulewitz, M. J., McDonald, K. L. & Thorner, J. Dynamic Localization of the Swe1 Regulator Hsl7 During the *Saccharomyces cerevisiae* Cell Cycle. *Mol. Biol. Cell* **12**, 1645–1669 (2001).

231. Theesfeld, C. L., Zyla, T. R., Bardes, E. G. S. & Lew, D. J. A Monitor for Bud Emergence in the Yeast Morphogenesis Checkpoint. *Mol. Biol. Cell* **14**, 3280–3291 (2003).

232. Yamada, A., Duffy, B., Perry, J. A. & Kornbluth, S. DNA replication checkpoint control of Wee1 stability by vertebrate Hsl7. *J. Cell Biol.* **167**, 841–849 (2004).

233. Yuan, H., Kamata, M., Xie, Y.-M. & Chen, I. S. Y. Increased Levels of Wee-1 Kinase in G2 Are Necessary for Vpr- and Gamma Irradiation-Induced G2 Arrest. *J. Virol.* **78**, 8183–8190 (2004).

234. Li, Q., Zhao, Y., Yue, M., Xue, Y. & Bao, S. The Protein Arginine Methylase 5 ( PRMT5/SKB1 ) Gene Is Required for the Maintenance of Root Stem Cells in Response to DNA Damage. *J. Genet. Genomics* **43**, 187–197 (2016).

235. Fulcher, N. & Sablowski, R. Hypersensitivity to DNA damage in plant stem cell niches. *Proc. Natl. Acad. Sci.* **106**, 20984–20988 (2009).

236. Nisa, M.-U., Huang, Y., Benhamed, M. & Raynaud, C. The Plant DNA Damage Response: Signaling Pathways Leading to Growth Inhibition and Putative Role in Response to Stress Conditions. *Front. Plant Sci.* **10**, (2019).

237. Lam, E. Controlled cell death, plant survival and development. *Nat. Rev. Mol. Cell Biol.* **5**, 305–315 (2004).

238. Lee, M.-Y. *et al.* Alkylating agent methyl methanesulfonate (MMS) induces a wave of global protein hyperacetylation: Implications in cancer cell death. *Biochem. Biophys. Res. Commun.* **360**, 483–489 (2007).

239. Yu, R. & Zhang, W. Molecule mechanism of stem cells in Arabidopsis thaliana. *Pharmacogn. Rev.* **8**, 105 (2014).

240. De Schutter, K. *et al. Arabidopsis* WEE1 Kinase Controls Cell Cycle Arrest in Response to Activation of the DNA Integrity Checkpoint. *Plant Cell* **19**, 211–225 (2007).

241. Lin, H. & Luengo, J. I. Nucleoside protein arginine methyltransferase 5 (PRMT5) inhibitors. *Bioorg. Med. Chem. Lett.* **29**, 1264–1269 (2019).

242. Lin, H. *et al.* Discovery of Potent and Selective Covalent Protein Arginine Methyltransferase 5 (PRMT5) Inhibitors. *ACS Med. Chem. Lett.* **10**, 1033–1038 (2019).

243. Wang, Y., Hu, W. & Yuan, Y. Protein Arginine Methyltransferase 5 (PRMT5) as an Anticancer Target and Its Inhibitor Discovery. *J. Med. Chem.* **61**, 9429–9441 (2018).

244. Mao, R. *et al.* Potent, Selective, and Cell Active Protein Arginine Methyltransferase 5 (PRMT5) Inhibitor Developed by Structure-Based Virtual Screening and Hit Optimization. *J. Med. Chem.* **60**, 6289–6304 (2017).

245. Sakamoto, K. M. *et al.* Protacs: Chimeric molecules that target proteins to the Skp1-Cullin-F box complex for ubiquitination and degradation. *Proc. Natl. Acad. Sci.* **98**, 8554–8559 (2001).

246. Rowe, S. P. *et al.* Prostate-Specific Membrane Antigen-Targeted Radiohalogenated PET and Therapeutic Agents for Prostate Cancer. *J. Nucl. Med.* **57**, 90S-96S (2016).

247. Khanna, K. K. & Jackson, S. P. DNA double-strand breaks: signaling, repair and the cancer connection. *Nat. Genet.* **27**, 247–254 (2001).

248. Heidenreich, A. *et al.* EAU Guidelines on Prostate Cancer. Part II: Treatment of Advanced, Relapsing, and Castration-Resistant Prostate Cancer. *Eur. Urol.* **65**, 467–479 (2014).

249. Alinari, L. *et al.* Selective inhibition of protein arginine methyltransferase 5 blocks initiation and maintenance of B-cell transformation. *Blood* **125**, 2530–2543 (2015).

250. Montecucco, A. & Biamonti, G. Cellular response to etoposide treatment. *Cancer Lett.* **252**, 9–18 (2007).

251. Treszezamsky, A. D. *et al.* BRCA1- and BRCA2-Deficient Cells Are Sensitive to Etoposide-Induced DNA Double-Strand Breaks via Topoisomerase II. *Cancer Res.* **67**, 7078–7081 (2007).

252. Furuta, T. *et al.* Phosphorylation of Histone H2AX and Activation of Mre11, Rad50, and Nbs1 in Response to Replication-dependent DNA Double-strand Breaks Induced by Mammalian DNA Topoisomerase I Cleavage Complexes. *J. Biol. Chem.* **278**, 20303–20312 (2003).

253. Saha, K., Adhikary, G. & Eckert, R. L. MEP50/PRMT5 Reduces Gene Expression by Histone Arginine Methylation and this Is Reversed by PKCδ/p38δ Signaling. *J. Invest. Dermatol.* **136**, 214–224 (2016).

254. The Cancer Genome Atlas Research Network *et al.* The Cancer Genome Atlas Pan-Cancer analysis project. *Nat. Genet.* **45**, 1113–1120 (2013).

255. Sun, Y., Jiang, X., Chen, S., Fernandes, N. & Price, B. D. A role for the Tip60 histone acetyltransferase in the acetylation and activation of ATM. *Proc. Natl. Acad. Sci.* **102**, 13182–13187 (2005).

256. Bhoumik, A., Singha, N., O'Connell, M. J. & Ronai, Z. A. Regulation of TIP60 by ATF2 Modulates ATM Activation. *J. Biol. Chem.* **283**, 17605–17614 (2008).

257. Burma, S., Chen, B. P., Murphy, M., Kurimasa, A. & Chen, D. J. ATM Phosphorylates Histone H2AX in Response to DNA Double-strand Breaks. *J. Biol. Chem.* **276**, 42462–42467 (2001).

258. Murr, R. *et al.* Histone acetylation by Trrap–Tip60 modulates loading of repair proteins and repair of DNA double-strand breaks. *Nat. Cell Biol.* **8**, 91–99 (2006).

259. Ikura, T. *et al.* Involvement of the TIP60 Histone Acetylase Complex in DNA Repair and Apoptosis. *Cell* **102**, 463–473 (2000).

260. Asim, M. *et al.* Synthetic lethality between androgen receptor signalling and the PARP pathway in prostate cancer. *Nat. Commun.* **8**, (2017).

261. Li, L. *et al.* Androgen receptor inhibitor–induced "BRCAness" and PARP inhibition are synthetically lethal for castration-resistant prostate cancer. *Sci. Signal.* **10**, 480 (2017).

262. Schild, D. & Wiese, C. Overexpression of RAD51 suppresses recombination defects: a possible mechanism to reverse genomic instability. *Nucleic Acids Res.* **38**, 1061–1070 (2010).

263. Petermann, E., Orta, M. L., Issaeva, N., Schultz, N. & Helleday, T. Hydroxyurea-Stalled Replication Forks Become Progressively Inactivated and Require Two Different RAD51-Mediated Pathways for Restart and Repair. *Mol. Cell* **37**, 492–502 (2010).

264. Hayman, T. J. *et al.* Translation Initiation Factor eIF4E Is a Target for Tumor Cell Radiosensitization. *Cancer Res.* **72**, 2362–2372 (2012).

265. Gavande, N. S. *et al.* DNA repair targeted therapy: The past or future of cancer treatment? *Pharmacol. Ther.* **160**, 65–83 (2016).

266. Hsu, C.-C. & Hu, C.-D. Transcriptional activity of c-Jun is critical for the suppression of AR function. *Mol. Cell. Endocrinol.* **372**, 12–22 (2013).

267. Wiederschain, D. *et al.* Single-vector inducible lentiviral RNAi system for oncology target validation. *Cell Cycle* **8**, 498–504 (2009).

268. Rapp, A. After double-strand break induction by UV-A, homologous recombination and nonhomologous end joining cooperate at the same DSB if both systems are available. *J. Cell Sci.* **117**, 4935–4945 (2004).

269. Slupianek, A., Nowicki, M. O., Koptyra, M. & Skorski, T. BCR/ABL modifies the kinetics and fidelity of DNA double-strand breaks repair in hematopoietic cells. *DNA Repair* **5**, 243–250 (2006).

270. Schneider, C. A., Rasband, W. S., Eliceiri, K. W. & others. NIH Image to ImageJ: 25 years of image analysis. *Nat Methods* **9**, 671–675 (2012).

271. Lee, J.-H. *et al.* ID3 regulates the MDC1-mediated DNA damage response in order to maintain genome stability. *Nat. Commun.* **8**, 903 (2017).

272. Nassour, J. *et al.* Defective DNA single-strand break repair is responsible for senescence and neoplastic escape of epithelial cells. *Nat. Commun.* **7**, 10399 (2016).

273. Higo, T. *et al.* DNA single-strand break-induced DNA damage response causes heart failure. *Nat. Commun.* **8**, 15104 (2017).

274. Mo, L.-J. *et al.* Exosome-packaged miR-1246 contributes to bystander DNA damage by targeting LIG4. *Br. J. Cancer* **119**, 492–502 (2018).

275. Xiao, X. *et al.* DNA-PK inhibition synergizes with oncolytic virus M1 by inhibiting antiviral response and potentiating DNA damage. *Nat. Commun.* **9**, (2018).

276. Dungrawala, H. *et al.* RADX Promotes Genome Stability and Modulates Chemosensitivity by Regulating RAD51 at Replication Forks. *Mol. Cell* **67**, 374-386.e5 (2017).

277. Liu, H. *et al.* Nuclear cGAS suppresses DNA repair and promotes tumorigenesis. *Nature* **563**, 131–136 (2018).

278. Dobin, A. *et al.* STAR: ultrafast universal RNA-seq aligner. *Bioinformatics* **29**, 15–21 (2013).

279. Liao, Y., Smyth, G. K. & Shi, W. featureCounts: an efficient general purpose program for assigning sequence reads to genomic features. *Bioinformatics* **30**, 923–930 (2014).

280. Robinson, M. D., McCarthy, D. J. & Smyth, G. K. edgeR: a Bioconductor package for differential expression analysis of digital gene expression data. *Bioinformatics* **26**, 139–140 (2010).

281. Huang, D. W. *et al.* The DAVID Gene Functional Classification Tool: a novel biological module-centric algorithm to functionally analyze large gene lists. *Genome Biol.* **8**, R183 (2007).

282. Huang, D. W., Sherman, B. T. & Lempicki, R. A. Systematic and integrative analysis of large gene lists using DAVID bioinformatics resources. *Nat. Protoc.* **4**, 44–57 (2009).

283. Chew, Y. C., Adhikary, G., Xu, W., Wilson, G. M. & Eckert, R. L. Protein Kinase C δ Increases Kruppel-like Factor 4 Protein, which Drives Involucrin Gene Transcription in Differentiating Keratinocytes. *J. Biol. Chem.* **288**, 17759–17768 (2013).

284. Fox, M. H. A model for the computer analysis of synchronous DNA distributions obtained by flow cytometry. *Cytometry A* **1**, 71–77 (1980).

285. Wilczek, C. *et al.* Protein Arginine Methyltransferase Prmt5-Mep50 Methylates Histones H2A and H4 and the Histone Chaperone Nucleoplasmin in *Xenopus laevis* Eggs. *J. Biol. Chem.* **286**, 42221–42231 (2011).

286. Zhang, H.-T. *et al.* The E3 ubiquitin ligase CHIP mediates ubiquitination and proteasomal degradation of PRMT5. *Biochim. Biophys. Acta BBA - Mol. Cell Res.* **1863**, 335–346 (2016).

287. Chari, A. *et al.* An Assembly Chaperone Collaborates with the SMN Complex to Generate Spliceosomal SnRNPs. *Cell* **135**, 497–509 (2008).

288. Paul, C., Sardet, C. & Fabbrizio, E. The Wnt-target gene Dlk-1 is regulated by the Prmt5-associated factor Copr5 during adipogenic conversion. *Biol. Open* **4**, 312–316 (2015).

289. Hu, C.-D., Chinenov, Y. & Kerppola, T. K. Visualization of Interactions among bZIP and Rel Family Proteins in Living Cells Using Bimolecular Fluorescence Complementation. *Mol. Cell* **9**, 789–798 (2002).

290. Kodama, Y. & Hu, C.-D. An improved bimolecular fluorescence complementation assay with a high signal-to-noise ratio. *BioTechniques* **49**, 793–805 (2010).

291. Kodama, Y. & Hu, C.-D. Bimolecular fluorescence complementation (BiFC): A 5-year update and future perspectives. *BioTechniques* **53**, 285–298 (2012).

292. Shyu, Y. J. & Hu, C.-D. Fluorescence complementation: an emerging tool for biological research. *Trends Biotechnol.* **26**, 622–630 (2008).

293. Pratt, E. P. S., Owens, J. L., Hockerman, G. H. & Hu, C.-D. Bimolecular Fluorescence Complementation (BiFC) Analysis of Protein–Protein Interactions and Assessment of Subcellular Localization in Live Cells. *Methods Mol. Biol.* **1474**, 153–170 (2016).

294. Ghufran, M. S., Ghosh, K. & Kanade, S. R. Aflatoxin B1 induced upregulation of protein arginine methyltransferase 5 in human cell lines. *Toxicon* **119**, 117–121 (2016).

295. Ghosh, K., Chatterjee, B., Behera, P. & Kanade, S. R. The carcinogen cadmium elevates CpG-demethylation and enrichment of NFYA and E2F1 in the promoter of oncogenic PRMT5 and EZH2 methyltransferases resulting in their elevated expression in vitro. *Chemosphere* **242**, 125186 (2020).

296. Chatterjee, B., Ghosh, K., Suresh, L. & Kanade, S. R. Curcumin ameliorates PRMT5-MEP50 arginine methyltransferase expression by decreasing the Sp1 and NF-YA transcription factors in the A549 and MCF-7 cells. *Mol. Cell. Biochem.* **455**, 73–90 (2019).

297. Bellutti, F. *et al.* CDK6 Antagonizes p53-Induced Responses during Tumorigenesis. *Cancer Discov.* **8**, 884–897 (2018).

298. Jin, S. *et al.* Transcription factors Oct-1 and NF-YA regulate the p53-independent induction of the GADD45 following DNA damage. *Oncogene* **20**, 2683–2690 (2001).

299. Skipper, A., Sims, J., Yedjou, C. & Tchounwou, P. Cadmium Chloride Induces DNA Damage and Apoptosis of Human Liver Carcinoma Cells via Oxidative Stress. *Int. J. Environ. Res. Public. Health* **13**, 88 (2016).

300. Wang, Y. & Taniguchi, T. MicroRNAs and DNA damage response: Implications for cancer therapy. *Cell Cycle* **12**, 32–42 (2013).

301. Li, B. *et al.* Down-regulation of microRNA 106b is involved in p21-mediated cell cycle arrest in response to radiation in prostate cancer cells. *The Prostate* **71**, 567–574 (2011).

302. Pal, S. *et al.* Low levels of miR-92b/96 induce PRMT5 translation and H3R8/H4R3 methylation in mantle cell lymphoma. *EMBO J.* **26**, 3558–3569 (2007).

303. Wang, Y., Huang, J.-W., Calses, P., Kemp, C. J. & Taniguchi, T. MiR-96 Downregulates REV1 and RAD51 to Promote Cellular Sensitivity to Cisplatin and PARP Inhibition. *Cancer Res.* **72**, 4037–4046 (2012).

304. Lindsay M. Webb *et al.* NF-κB/mTOR/MYC Axis DrivesPRMT5 Protein Induction After T CellActivation via Transcriptional andNon-transcriptional Mechanisms. *Front. Immunol.* **10**, (2019).

305. Rahman, M. *et al.* miR-15b/16-2 Regulates Factors That Promote p53 Phosphorylation and Augments the DNA Damage Response following Radiation in the Lung. *J. Biol. Chem.* **289**, 26406–26416 (2014).

306. Lee, J.-H. & Paull, T. T. ATM Activation by DNA Double-Strand Breaks Through the Mre11-Rad50-Nbs1 Complex. **308**, 6 (2005).

307. Fu, T., Lv, X., Kong, Q. & Yuan, C. A novel SHARPIN-PRMT5-H3R2me1 axis is essential for lung cancer cell invasion. *Oncotarget* **8**, (2017).

308. Yang, H. *et al.* SHARPIN Facilitates p53 Degradation in Breast Cancer Cells. *Neoplasia* **19**, 84–92 (2017).

309. Biswas, K. *et al.* The E3 Ligase CHIP Mediates p21 Degradation to Maintain Radioresistance. *Mol. Cancer Res.* **15**, 651–659 (2017).

310. Sarkar, S., Brautigan, D. L., Parsons, S. J. & Larner, J. M. Androgen receptor degradation by the E3 ligase CHIP modulates mitotic arrest in prostate cancer cells. *Oncogene* **33**, 26–33 (2014).

311. Ambrosio, S. *et al.* Cell cycle-dependent resolution of DNA double-strand breaks. *Oncotarget* **7**, 4949–4960 (2016).

312. Kyjacova, L. *et al.* Radiotherapy-induced plasticity of prostate cancer mobilizes stem-like non-adherent, Erk signaling-dependent cells. *Cell Death Differ.* **22**, 898–911 (2015).

313. Biran, A. *et al.* Quantitative identification of senescent cells in aging and disease. *Aging Cell* **16**, 661–671 (2017).

314. Zhang, Y. *et al.* Androgen deprivation promotes neuroendocrine differentiation and angiogenesis through CREB-EZH2-TSP1 pathway in prostate cancers. *Nat. Commun.* **9**, (2018).

315. Svensson, C. *et al.* REST mediates androgen receptor actions on gene repression and predicts early recurrence of prostate cancer. *Nucleic Acids Res.* **42**, 999–1015 (2014).

316. Jang, S. *et al.* Histone deacetylase inhibitor thailandepsin-A activates Notch signaling and suppresses neuroendocrine cancer cell growth *in vivo*. *Oncotarget* **8**, 70828–70840 (2017).

317. Knudsen, K. E., Arden, K. C. & Cavenee, W. K. Multiple G $_1$ Regulatory Elements Control the Androgen-dependent Proliferation of Prostatic Carcinoma Cells. *J. Biol. Chem.* **273**, 20213–20222 (1998).

318. Pernicová, Z. *et al.* The role of high cell density in the promotion of neuroendocrine transdifferentiation of prostate cancer cells. *Mol. Cancer* **13**, 113 (2014).

319. Michael E. Cox, Paul D. Deeble, Eric A. Bissonette & Sarah J. Parsons. Activated 3′,5′-Cyclic AMP-dependent Protein Kinase Is Sufficient to Induce Neuroendocrine-like Differentiation of the LNCaP Prostate Tumor Cell Line. *J. Biol. Chem.* **275**, 13812–13818 (2000).

320. Tsai, W.-W. *et al.* PRMT5 modulates the metabolic response to fasting signals. *Proc. Natl. Acad. Sci.* **110**, 8870–8875 (2013).

321. Xu, W. A Transcriptional Switch Mediated by Cofactor Methylation. *Science* **294**, 2507–2511 (2001).

322. Schroeder, A. *et al.* The RIN: an RNA integrity number for assigning integrity values to RNA measurements. *BMC Mol. Biol.* 14 (2006).

323. McCarthy, D. J., Chen, Y. & Smyth, G. K. Differential expression analysis of multifactor RNA-Seq experiments with respect to biological variation. *Nucleic Acids Res.* **40**, 4288–4297 (2012).

324. Neureiter, D. *et al.* Different capabilities of morphological pattern formation and its association with the expression of differentiation markers in a xenograft model of human pancreatic cancer cell lines. *Pancreatology* **5**, 387–397 (2005).

325. Wu, C. & Huang, J. Phosphatidylinositol 3-Kinase-AKT-Mammalian Target of Rapamycin Pathway Is Essential for Neuroendocrine Differentiation of Prostate Cancer. *J. Biol. Chem.* **282**, 3571–3583 (2006).

326. Ishii, J. *et al.* POU domain transcription factor BRN2 is crucial for expression of ASCL1, ND1 and neuroendocrine marker molecules and cell growth in small cell lung cancer: Functions of BRN2 in SCLC. *Pathol. Int.* **63**, 158–168 (2013).

327. Lattouf, H. *et al.* LKB1 regulates PRMT5 activity in breast cancer. *Int. J. Cancer* **144**, 595–606 (2019).

328. Wang, Y.-S. *et al.* LKB1 is a DNA damage response protein that regulates cellular sensitivity to PARP inhibitors. *Oncotarget* **7**, (2016).

329. Witze, E. S., Old, W. M., Resing, K. A. & Ahn, N. G. Mapping protein post-translational modifications with mass spectrometry. *Nat. Methods* **4**, 798–806 (2007).

330. Olsen, J. V. & Mann, M. Status of Large-scale Analysis of Post-translational Modifications by Mass Spectrometry. *Mol. Cell. Proteomics* **12**, 3444–3452 (2013).

331. Liu, B. & Qian, S.-B. Translational reprogramming in cellular stress response: Translational reprogramming in stress. *Wiley Interdiscip. Rev. RNA* **5**, 301–305 (2014).

332. Spriggs, K. A., Bushell, M. & Willis, A. E. Translational Regulation of Gene Expression during Conditions of Cell Stress. *Mol. Cell* **40**, 228–237 (2010).

333. Braunstein, S., Badura, M. L., Xi, Q., Formenti, S. C. & Schneider, R. J. Regulation of Protein Synthesis by Ionizing Radiation. *Mol. Cell. Biol.* **29**, 5645–5656 (2009).

334. Kim, E. J., Kang, S. & Lim, Y.-B. Ionizing radiation activates PERKeIF2αATF4 signaling via ER stress-independent pathway in human vascular endothelial cells. *Int. J. Radiat. Biol.* **90**, 306–312 (2014).

335. Kerridge, D. The effect of actidione and other antifungal agents on nucleic acid and protein synthesis in Saccharomyces carlsbergensis. *Microbiology* **19**, 497–506 (1958).

336. Lim, P. S., Hardy, K., Peng, K. & Shannon, F. M. Transcriptomic analysis of mouse EL4 T cells upon T cell activation and in response to protein synthesis inhibition via cycloheximide treatment. *Genomics Data* **7**, 148–151 (2016).

337. Fujita, T. & Fujii, H. Efficient isolation of specific genomic regions and identification of associated proteins by engineered DNA-binding molecule-mediated chromatin immunoprecipitation (enChIP) using CRISPR. *Biochem. Biophys. Res. Commun.* **439**, 132–136 (2013).

338. Fujii, H. & Fujita, T. Isolation of Specific Genomic Regions and Identification of Their Associated Molecules by Engineered DNA-Binding Molecule-Mediated Chromatin Immunoprecipitation (enChIP) Using the CRISPR System and TAL Proteins. *Int. J. Mol. Sci.* **16**, 21802–21812 (2015).

339. Peterson, L. X. *et al.* Modeling the assembly order of multimeric heteroprotein complexes. *PLOS Comput. Biol.* **14**, e1005937 (2018).

340. Skene, P. J. & Henikoff, S. An efficient targeted nuclease strategy for high-resolution mapping of DNA binding sites. *eLife* **6**, (2017).

341. Chan-Penebre, E. *et al.* A selective inhibitor of PRMT5 with in vivo and in vitro potency in MCL models. *Nat. Chem. Biol.* **11**, 432–437 (2015).

# VITA

EDUCATION

*Doctor of Philosophy – Purdue University*, West Lafayette, IN (August 2014 – June 2020)
- Medicinal Chemistry and Molecular Pharmacology (MCMP), GPA: 4.0
- Research focus - Investigating the response of cancer cells to radiation with a goal to enhance radiation therapy for cancer patients
- Writing in the Sciences - Certificate with honors, Stanford University

*Bachelor of Arts – Monmouth College*, Monmouth, IL (August 2010 – May 2014)
- *Summa Cum Laude* with Departmental Honors and Honors Program
- Biochemistry and Biology double major

ACCOMPLISHMENTS DURING PH.D. STUDY

*Publications*
- Owens and Hu, Oncogene, 2020. Invited review in preparation (1st author)
- Beketova *et al.*, Cancer research, 2020. In revision (2nd author)
- Beketova *et al.*, Oncogene, 2020. Invited review in preparation (2nd author)
- Kumari *et al*., Scientific Reports, 2020. In revision (3rd author)
- Owens *et al*., iScience, 2019 (1st author)
- Pratt *et al*., Methods in Molecular Biology, 2016 (2nd author)

*Poster and Oral Presentation Awards*
- Blue Ribbon Poster Award - Translational Science 2019
- 1st Place Poster Presentation Award - Indiana CTSI 2017
- 2nd Place Oral Presentation Award - IBUR 2017
- Lafayette Lions Club Cancer Research Award - Lafayette Lions Club 2017

*Research and Travel Awards*
- Jenkins-Knevel Award - Outstanding Research in College of Pharmacy, Purdue University
- Burroughs Wellcome Fund Trainee Travel Award - Presentation at ACTS 2019
- MCMP Travel Award - Present at SBUR 2019
- College of Pharmacy Travel Award – Presentation at SBUR 2018

*Fellowships*
- Bilsland Dissertation Fellowship - Purdue University
- Indiana CTSI Pre-Doctoral Fellowship - National Institutes of Health (NIH) and National Center for Advancing Translational Sciences (NCATS)
- Ross Award Graduate Student Fellowship - MCMP department, Purdue University

*Presentations*
- 7 external and 6 internal oral presentations as well as 9 journal club presentations
- 12 external and 11 internal poster presentations
- Guest lecturer for STAT598 bioinformatics course

COLLABORATIONS
- *Dr. Jun Wan (Indiana University School of Medicine):*
  Provide biological insight and clinical relevance for bioinformatics studies and work closely on figure design and manuscript edits (Owens et al., iScience, 2019)

- *Dr. Emily Dykhuizen (Purdue University):*
  Team-up on several presentations including departmental seminar, oral prelim, thesis committee meetings, and cancer center journal club
- *Angela Roberts (Senior Graphic Designer/Writer, Purdue University):*
  Initiate partnership with creative personnel to design the first draft of the graphical abstract used for publication (Owens et al., iScience, 2019)
- *Dr. James Forney (Purdue University, NSF coordinator):*
  Invite by Dr. Forney to mentor fellowship students on poster/oral presentations. Orchestrate workshop and guide individual meetings toward improving clarity, scientific precision, and visual quality
- *Dr. GuangJun Zhang (Purdue University):*
  Serve as subject matter expert of RT and DDR to provide clinical relevance and biological insight as well as perform radiation experiments for manuscript. Assist in figure design and writing for manuscript (Kumari et al., Scientific Reports, 2020. In revision)

## COMPETENCIES

*Project Management*

- Ensure high quality of scientific deliverables for lab members as well as professors
  - Provide creative input and editorial support on scientific content (e.g. slide decks, posters/presentations, travel award/fellowship applications, and PI grant applications)
  - Edit manuscripts for clarity, accuracy, and clinical relevance including several published articles and manuscripts in preparation (e.g. a review: Hu et al., *Frontiers of Oncology*, 2016 and a research article and graphical model: Zhang et al., *BBA*, 2016)
- Promote a positive and successful atmosphere using energy, enthusiasm, and intellect
  - Cooperate with lab members to meet project needs, deadlines, and deliverables
  - Form genuine relationships to foster a strong team-oriented workplace culture
  - Organize lab meetings, journal clubs, and team-building events with lab associates
- Facilitate discussions on potential actionable insights at lab meetings using detailed notes and summaries from both internal and external meetings and conferences
- Enable compliance with safety, legal, and regulatory requirements at Purdue University as the safety manager of the X-ray irradiator device
  - Train new users for proper use with 100% pass rate on safety exam
  - 100% compliance on safety inspections by Radiological & Environmental Management

*Subject Matter Expert and Tech Transfer*

- Subject matter expert for RT and X-ray irradiator, DNA damage response assays, qRT-PCR and Quant studio device, and imaging assays and fluorescence microscope
- Advise on experimental design and data interpretation for accuracy and clinical relevance
- Oversee the transfer of imaging assays and DNA damage response assays to other labs
- Train and support 30+ users of X-ray irradiator, qPCR device, and fluorescence microscope

*Proficiencies*: Adobe Illustrator, GraphPad Prism, FlowJo, Microsoft Office, Zotero

## TEACHING AND MENTORSHIP EXPERIENCES

- Guest lecturer as both a graduate student and undergrad
- Instructor for 2 sections of organic chemistry lab as a graduate student
- Teaching assistant for 6 courses as an undergrad
- Scientific mentor to 3 visiting scholars, 10 rotation students, and 2 undergrad students
- College of Pharmacy representative for Science in Schools External Outreach Program

## PROFESSIONAL AFFILIATIONS

- Association for Clinical and Translational Science (ACTS) (2017 – Current)
- Indiana Clinical and Translational Science Institute (CTSI) (2017 – Current)
- American Chemical Society (ACS) (2011-2015)

# PUBLICATIONS

Below is a list of all publications completed or in revision as of June 2020. Other manuscripts in preparation are not included. Links to publications are embedded when possible. Please see https://www.researchgate.net/profile/Jake_Owens for updated publications lists.

Beketova, E., **Owens, J. L.**, Asberry, A. M., & Hu, C. D. PRMT5: A putative oncogene and therapeutic target in prostate cancer. Oncogene (2020) (in revision)

Kumari R., Jiang G., **Owens, J.L.**, Hu C.D., Mittal, S., and Zhang G., Smarcad1a, a new tumor suppressor gene in zebrafish malignant peripheral nerve sheath tumors. Scientific reports (2020) (in revision)

Beketova, E., Fang, S., **Owens, J. L.**, Liu, S., Chen, X., Zhang, Q., Asberry, A. M., Deng, X., Malola, J., Huang, J., Li, C., Pili, R., Elzey, B.D., Ratliff, T.L., Wan, J., & Hu, C. D. Protein arginine methyltransferase 5 promotes androgen receptor transcription in a pICln-dependent manner in castration-resistant prostate cancer. Cancer research (2020) (in revision)

**Owens, J. L.**, Beketova, E., Liu, S., Tinsley, S. L., Asberry, A. M., Deng, X., Huang, J., Li, C., Wan, J., & Hu, C. D. PRMT5 Cooperates with pICln to Function as a Master Epigenetic Activator of DNA Double-Strand Break Repair Genes. iScience 23, 100750 (2020).

Pratt, E. P. S., **Owens, J. L.**, Hockerman, G. H., & Hu, C.-D. Bimolecular Fluorescence Complementation (BiFC) Analysis of Protein–Protein Interactions and Assessment of Subcellular Localization in Live Cells. Methods Mol. Biol. 1474, 153–170 (2016).